

UC San Diego

UC San Diego Electronic Theses and Dissertations

Title

The impact of meteorological conditions and variation in chemical composition of aerosols on regional cloud formation

Permalink

<https://escholarship.org/uc/item/504880vk>

Author

Creamean, Jessie Marie

Publication Date

2012

Peer reviewed|Thesis/dissertation

UNIVERSITY OF CALIFORNIA, SAN DIEGO

The Impact of Meteorological Conditions and Variation in Chemical Composition of
Aerosols on Regional Cloud Formation

A dissertation submitted in partial satisfaction of the requirements for the degree of
Doctor of Philosophy

in

Chemistry

by

Jessie Marie Creamean

Committee in charge:

Professor Kimberly Prather, Chair

Professor Joel Norris

Professor Michael Sailor

Professor Amitabha Sinha

Professor Mark Thiemens

2012

Copyright

Jessie Marie Creamean, 2012

All rights reserved.

The Dissertation of Jessie Marie Creamean is approved, and it is acceptable in quality and form for publication on microfilm and electronically:

Chair

University of California, San Diego

2012

DEDICATION

I would like to dedicate this dissertation to my parents Allen and Sharon Creamean, my brothers Allen and Alex Creamean, my boyfriend Nicholas Prola, and my close friends for all of their love and support throughout my doctoral research.

EPIGRAPH

Ideas are like rabbits. You get a couple and learn how to handle them, and pretty soon you have a dozen.

John Steinbeck

TABLE OF CONTENTS

SIGNATURE PAGE	iii
DEDICATION.....	iv
EPIGRAPH.....	v
TABLE OF CONTENTS.....	vi
LIST OF ABBREVIATIONS.....	xi
LIST OF FIGURES	xv
LIST OF TABLES.....	xxi
ACKNOWLEDGEMENTS.....	xxii
VITA.....	xxix
ABSTRACT OF THE DISSERTATION.....	xxxix
1. Introduction.....	1
1.1. Sources of Atmospheric Aerosols.....	1
1.2. Environmental Impacts of Atmospheric Aerosols.....	3
1.2.1. Effects on Health	3
1.2.2. Serving as Cloud Seeds.....	3
1.2.3. Broader Impacts on Precipitation and the Global Water Cycle.....	5
1.3. Variability in Aerosol Chemical Composition	6
1.3.1. Effects due to Transport Conditions	6
1.3.2. Effects due to Meteorology.....	8
1.4. Real-Time, Single-Particle Measurements of Chemical Composition.....	8
1.5. Key Outstanding Questions Regarding Distributions of Aerosols and Cloud Seeds	10
1.6. Synopsis and Goals of the Dissertation	11
1.7. Acknowledgements.....	12
1.8. Figures	13
1.9. References.....	14

2. Long-term Impacts of Source and Meteorology on Aerosol Chemical Mixing State in Riverside, CA	43
2.1. Introduction.....	43
2.2. Experimental.....	45
2.3. Results and Discussion	47
2.3.1. The Impact of Meteorology and Air Mass Sources on PM _{2.5}	47
2.4. Aerosol Chemical Composition.....	49
2.4.1. Single-particle Mixing State and Atmospheric Aging.....	51
2.5. Conclusions.....	54
2.6. Acknowledgements.....	55
2.7. Figures	56
2.8. Tables.....	60
2.9. References.....	61
3. Significant Changes in Urban Aerosol Chemistry and CCN Concentrations Induced by Tropical Cyclones	68
3.1. Introduction.....	68
3.2. Experimental.....	70
3.3. Results and Discussion	71
3.3.1. Meteorological changes in Atlanta during TCs	71
3.3.2. TC effects on aerosol size and chemical composition.....	72
3.3.3. Implications of TC influences on CCN activity in Atlanta	75
3.4. Conclusions.....	76
3.5. Acknowledgements.....	77
3.6. Figures	78
3.7. Tables.....	81
3.8. References.....	81
4. Measurements of Aerosol Chemistry during New Particle Formation Events at a Remote Rural Mountain Site	86

4.1.	Introduction.....	86
4.2.	Experimental.....	88
4.3.	Results and Discussion	90
4.3.1.	Ambient Conditions for NPF.....	90
4.3.2.	Growth of New Particles into CCN.....	91
4.3.3.	Single Particle Chemical Composition during NPF Events	93
4.3.4.	Potential Sources of Gas-Phase Species Involved in New Particle Formation	96
4.4.	Conclusions.....	98
4.5.	Acknowledgments	99
4.6.	Figures	100
4.7.	References.....	102
5.	Dust and Biological Aerosols from the Sahara and Asia Influence Precipitation in the Western U.S.	108
5.1.	Introduction.....	108
5.2.	Results and Discussion	110
5.3.	Conclusions.....	116
5.4.	Acknowledgments	117
5.5.	Figures	118
5.6.	References.....	121
6.	Inter-annual Evidence of Aerosols Affecting Orographic Precipitation in the Sierra Nevada.....	126
6.1.	Introduction.....	126
6.2.	Measurements	128
6.2.1.	The CalWater Phase I Field Campaign.....	128
6.2.2.	Meteorological Measurements at SPD and Offshore of California.....	128
6.2.3.	Satellite-Retrieved Cloud Properties	129
6.2.4.	Chemical Characterization of Insoluble Precipitation Residues.....	130

6.2.5.	Ice Nuclei Measurements.....	131
6.3.	Results and Discussion	131
6.3.1.	Overall Chemical Composition of Insoluble Precipitation Residues	131
6.3.2.	Inter-annual Precipitation Trends during <i>CalWater Phase I</i>	134
6.3.2.1.	Links between Residue Composition and Precipitation Properties	134
6.3.2.2.	Links between Residue Composition and Cloud Properties	137
6.3.3.	Elevation Dependent Trends: Further Insight into Relationships between Residue Composition and Cloud Properties.....	139
6.3.4.	Ice Forming Potential of Dust and Biological Precipitation Residues	140
6.3.5.	Insight into Precipitation Residue Sources	142
6.4.	Conclusions.....	143
6.5.	Acknowledgements.....	144
6.6.	Figures	145
6.7.	Tables.....	156
6.8.	References.....	157
7.	Conclusions and Future Work	165
7.1.	Synopsis.....	165
7.2.	Conclusions.....	165
7.2.1.	Sources and Chemical Composition of Aerosols as CCN at different Urban Locations.....	165
7.2.2.	Sources of CCN at a Remote Region.....	168
7.2.3.	Sources and Precipitation Effects of IN at a Remote Region	169
7.2.4.	Overall Conclusions.....	170
7.3.	Ongoing and Future Work	172
7.3.1.	Continuous Precipitation Measurements at SPD.....	172
7.3.2.	Source Determination of IN during <i>CalWater</i>	173
7.4.	Acknowledgements.....	175

7.5.	Figures	176
7.6.	References.....	183
8.	Appendix for Chapter 2	186
8.1.	Figures	186
9.	Appendix for Chapter 4	189
9.1.	Supplemental Methods	189
9.1.1.	Growth Rate Calculations.....	189
9.2.	Supplemental Results and Discussion	190
9.2.1.	Size and Number Distributions of NPF	190
9.2.2.	Black Carbon Measurements.....	191
9.2.3.	Classifications of Major Ambient Particle Types.....	191
9.2.4.	Size Distributions of Amine-OC Particle Types during NPF Events.....	192
9.2.5.	Increases in Amine Species on Ambient Particles.....	193
9.2.6.	Analysis of Absolute Peak Areas of Key Spectral Markers	193
9.2.7.	SO ₂ Source Determination.....	194
9.3.	Figures	197
9.4.	Tables.....	208
9.5.	References.....	209
10.	Appendix for Chapter 5	212
10.1.	Supplemental Materials and Methods.....	212
10.2.	Supplemental Results and Discussion	218
10.3.	Figures	221
10.4.	Tables.....	234
10.5.	Author Contributions	234
10.6.	References.....	234

LIST OF ABBREVIATIONS

%Dust+Bio	combined percentages of dust and biological precipitation residues
AMIGAS	August Mini-Intensive Gas and Aerosol Study
Amine-OC	amine-containing organic carbon
APS	aerodynamic particle sizer
AR	atmospheric river
ARA	Atmospheric Research & Analysis, Inc.
ART-2a	adaptive resonance theory, version 2a
ATOFMS	aerosol time-of-flight mass spectrometer
A-ATOFMS	aircraft aerosol time-of-flight mass spectrometer
BB	brightband
BC	black carbon
Bio	biological residues
BL	boundary layer
BP	Badger Pass
BVOC	biogenic volatile organic compounds
CALIPSO	Cloud-Aerosol Lidar and Infrared Pathfinder Satellite Observation
CARB	California Air Resources Board
CCN	cloud condensation nuclei
CCNc	cloud condensation nuclei counter
CF	Crane Flat

CN	condensation nuclei
Conv	convective precipitation
CPC	condensation particle counter
CV	Central Valley
DMS	dimethyl sulfide
Dust+Bio	number of dust and biological residues combined
EC	elemental carbon
ECOC	elemental carbon mixed with organic carbon
ESRL	Earth System Research Laboratory
f_{CCN}	fraction of CCN
GR	growth rate
<i>GOES-11</i>	Geostationary Operational Environmental Satellite (West)
HMT	Hydrometeorological Testbed
HYSPLIT	Hybrid Single Particle Lagrangian Integrated Trajectory Model
IN	ice nuclei
IWV	integrated water vapor
LA	Los Angeles
LSI	laser desorption/ionization
MODIS	Moderate Resolution Imager Spectroradiometer
NAAPS	Navy Aerosol Analysis and Prediction System
NBB	non-brightband

NOAA	National Oceanic and Atmospheric Administration
NPF	new particle formation
OC	organic carbon
OMI	Ozone Monitoring Instrument
PM	particulate matter
PMT	photomultiplier tube
PSL	polystyrene latex sphere
RH	relative humidity
S-PROF	S-band profiling radar
SEARCH	Southeastern Aerosol Research and Characterization
SINT	Shortwave-infrared Infrared Near-infrared Technique
SIST	Shortwave-infrared Infrared Split-window Technique
SMPS	scanning mobility particle sizer
SOA	secondary organic aerosol
SOAR	Study of Organic Aerosols at Riverside
SPD	Sugar Pine Dam
SSM/I	Special Sensor Microwave Imager
TC	tropical cyclone
TDCIMS	thermal desorption chemical ionization mass spectrometer
TM	Tuolumne Meadows
TOA	top-of-atmosphere

UCR	University of California, Riverside
UF-ATOFMS	ultrafine aerosol time-of-flight mass spectrometer
VISST	Visible Infrared Solar-infrared Split-Window Technique
VOC	volatile organic compounds
WD	wind direction
WNW	west northwest
WS	wind speed

LIST OF FIGURES

Figure 1.1 a) Schematic of the standard, nozzle inlet ATOFMS adapted from Gard et al., 1997 and b) schematic of the aerodynamic inlet UF-ATOFMS adapted from Su et al., 2004.....	13
Figure 1.2 Simplified top-view schematic of A-ATOFMS Z-shaped dual polarity mass spectrometer adapted from Pratt <i>et al.</i> , 2009.	14
Figure 2.1 Temporal profiles of hourly PM _{2.5} mass concentrations, wind direction (WD), temperature (T), and relative humidity (RH) from a) 2005, b) 2006, and c) 2007. The color of the WD represents the corresponding hourly WS measurement.	56
Figure 2.2 Google Earth images showing 24-hour air mass back trajectories calculated for each day during the summers of 2005, 2006, and 2007 over Riverside, CA. Trajectories end 100 m above Riverside and at 00:00 (dark blue) and 12:00 (red) daily. The green stars highlight major dairy farms in the Chino area.....	57
Figure 2.3 Hourly-resolved submicron (0.2-1.0 μm) chemical mixing state of individual particles as measured by ATOFMS for summer studies from 2005-2007.	58
Figure 2.4 Relative amount of major submicron particle types including OC, amine-OC, ECOC, dust, and sea salt, from 2005-2007 mixed with secondary species and relative abundance of each secondary species on each of the particle types. The bars show the percentage of each major type mixed.	59
Figure 3.1 Google Earth images including air mass back trajectories calculated with HYSPLIT for TCs a) Gustav and b) Hanna. Markers represent the storm paths in time (http://www.hurricane-tracking.co.uk/download.php). Markers and trajectories of same color occurred on the same date.	78
Figure 3.2 Wind speed (m/s) and direction (degrees) during AMIGAS. The green boxes correspond to time periods with “normal conditions,” i.e., time periods uninfluenced by TCs, and maroon boxes correspond to TC time periods or “TC conditions.”.....	79
Figure 3.3 Panel a) shows PM _{2.5} mass concentrations (μg/m ³), total number concentrations from the APS (cm ⁻³), and hourly submicron and supermicron particle counts from the ATOFMS. Panels b) and c) show the relative fractions of the submicron and supermicron particle chemistry, respectively.....	80
Figure 4.1 a) 5-minute temporally-resolved SMPS size distributions (nm) with superimposed 2-minute relative humidity (%) and temperature (°C), b) hourly precipitation (mm/h) and 2-minute solar radiation (W/m ²), and c) hourly gas-phase relative SO ₂ and O ₃ (ppm) concentrations and black carbon.....	100
Figure 4.2 SMPS plotted with $f_{CCN[0.3]}$. The inset is the strongest correlation of $f_{CCN[0.3]}$ with an NPF event (3/7-3/8). The markers superimposed over each NPF event are	

the estimated GRs for the event on that day. Blue and red markers represent GRs during P1 and P2, respectively.....	101
Figure 4.3 ATOFMS particle types in the 100-1000 nm size range measured during P1. Also pictured are the SMPS total particle number concentrations ($\#/cm^3$), SMPS mean sizes (nm), and number of ATOFMS sulfate-containing (m/z -97) particles during each sub-period. All of these values are averaged over the.	101
Figure 4.4 a) SMPS plotted with the fraction of amine-OC particles containing sulfate (out of the total number of particles) as a function of study date and time in color and the total number of particles. b) Correlation of the fraction of particles with sulfate (m/z -97) to fraction of particles with amines (m/z 86)	102
Figure 5.1. Precipitation characteristics during each sample collection dates of the 2011 CalWater study at SPD. Brown bars represent the percentages of dust and biological residues (%Dust+Bio) per sample collection dates at SPD in 2011. Percentages of cold rain, snow, and warm rain per sample	118
Figure 5.2 Dust source analysis including (A) 10-day back trajectories ending during the storms at SPD in 2011, with the boxes highlighting the four dust regions. Storms were investigated in order to achieve statistical significance. The percentages under each box represent the frequency that the trajectories	119
Figure 5.3 Dust tracking for days during the (A) Feb 14-16 and (B) Feb 24-26 storms. The 10-day air mass back trajectories ended at cloud top heights over SPD (shown by the star) on Feb 16 th (7390 m, MSL) and Feb 25 th (9340 m, MSL). Within each trajectory, the color scale represents	120
Figure 5.4 Vertical profiles of Dust+bio and sea salt cloud residues, the total number of residues, and temperature for the flight on (A) Feb 16 th ascent (17:01-18:29 UTC) and (B) Feb 16 th descent (18:29-20:19 UTC). Also shown are cloud particle residual IN concentrations as asterisks with the color representing.	121
Figure 6.1 Google Earth image of CalWater Phase I sites where meteorological measurements and/or precipitation samples were acquired, including Sugar Pine Dam (39.129°N, 120.801°W), Crane Flat (38.106°N, 119.844°W), Badger Pass (37.666°N, 119.654°W), and Tuolumne Meadows (37.870°N, 119.361°W).....	145
Figure 6.2 Representative mass spectra for ATOFMS precipitation residues. Examples include dust (panels a-c), biological (panels d and e), and OC residues (panels f-h). Positive and negative ion intensities vary by type.....	146
Figure 6.3 Panel (a) shows the total accumulated precipitation per storm (mm) and the maximum offshore IWV (cm) during each storm in 2009. Panel (b) shows the percentage of snow, BB rain, NBB rain, Conv, and Insuf estimated by S-PROF and the average surface air temperature (T_{surf} , °C) during each storm	148

Figure 6.4 Panel (a) shows the total accumulated precipitation per storm (mm) and the maximum offshore IWV (cm) during each storm in 2010. Panel (b) shows the percentage of snow, BB rain, mixed precipitation, NBB rain, Conv, and Insuf estimated by S-PROF and the average surface air temperature..... 149

Figure 6.5 Panel (a) shows the total accumulated precipitation per storm (mm) and the maximum offshore IWV (cm) during each storm in 2011. Panel (b) shows the percentage of snow, BB rain, mixed precipitation, NBB rain, Conv, and Insuf estimated by S-PROF and the average surface air temperature..... 150

Figure 6.6 Panel (a) shows precipitation rate (mm/h) at the surface at SPD and the percentage of dust, biological, and OC residues in each sample in 2009. The width of the bars reflect the duration of the sample collection. Panel (b) shows hourly liquid water path (LWP), ice water path (IWP), and the location. 151

Figure 6.7 Panel (a) shows precipitation rate (mm/h) at the surface at SPD and the percentage of dust, biological, and OC residues in each sample in 2010. The width of the bars reflect the duration of the sample collection. Panel (b) shows hourly liquid water path (LWP), ice water path (IWP), and the location. 152

Figure 6.8 Panel (a) shows precipitation rate (mm/h) at the surface at SPD and the percentage of dust, biological, and OC residues in each sample in 2011. The width of the bars reflect the duration of the sample collection. Panel (b) shows hourly liquid water path (LWP), ice water path (IWP), and the location 153

Figure 6.9 Bar graph showing the percentage of each residue type at SPD and each of the Yosemite sites in 2011. Also shown are the percentage of ice in cloud (%Ice), percentage of liquid in cloud (%Liq), and effective cloud temperatures (T_{eff} , °C) averaged during sample collection time periods combined..... 154

Figure 6.10 IN measurements for the dry Asian soil samples, S4 from 2011 (“dust precip sample”), S7 from 2011 (“bio 1 precip sample”), and S4 from 2010 (“bio 2 precip sample”). “Heated” represents samples that were heat treated for biological material and “Filtered” represents samples that were..... 155

Figure 7.1 Overall ambient aerosol chemical composition at Riverside during the summers of a) 2005, b) 2006, and c) 2007, at Atlanta during the summer of 2008, and at Sugar Pine Dam during the winter of 2009..... 176

Figure 7.2 Pie graphs representing the overall chemical composition of the aerosols as insoluble residues in precipitation samples collected from SPD in a) 2009, b) 2010, and c) 2011 and at sites of variable elevation in Yosemite National Park in 2011 only, including d) Badger Pass, e) Crane Flat, and..... 177

Figure 7.3 NOAA HMT-West sites in California. Site inventory list is provided at <http://www.esrl.noaa.gov/psd/data/obs/sites/>. The red marker shows the location of Sugar Pine Dam (SPD)..... 178

Figure 7.4 Air mass back trajectories calculated using HYSPLIT for every 3 hours during storm time periods within the a) 2009, b) 2010, and c) 2011 winter seasons of <i>CalWater</i> . The boxes highlight the major arid regions, including North Africa, the Middle East, the Taklimakan, and East Asia.	179
Figure 7.5 Simplified pie graphs of insoluble precipitation residues from the <i>CalWater</i> winter seasons. The bars represent the frequency of trajectories that traveled over each dust region presented in Chapter 5. The shaded portion of the bars represents the relative frequency of times a trajectory passed through a dust.	180
Figure 7.6 Geopotential height anomalies from Jan 1-Mar 31 during a) 2009, b) 2010, and c) 2011.	181
Figure 7.7 Mean wind speeds from Jan 1-Mar 31 during a) 2009, b) 2010, and c) 2011.	182
Figure 7.8 Mean precipitation rates from Jan 1-Mar 31 during a) 2009, b) 2010, and c) 2011.	183
Figure 8.1 Hourly PM _{2.5} mass concentrations ($\mu\text{g}/\text{m}^3$), gas-phase O ₃ concentrations (ppb), wind speed (WS, m/s), and particle number concentrations ($\#/\text{cm}^3$) from 0.523-10 μm , as measured by an aerodynamic particle sizer (APS), for the summers of 2005-2007 in Riverside, CA. Particle number.	186
Figure 8.2 Representative mass spectra of the ATOFMS particle types in Riverside during the summers of 2005-2007 from the average of a cluster of each particle type. The particle types shown are not always mixed with the same negative ion species; the negative spectra shown are for reference.	187
Figure 8.3 The ratio of the sum of peak areas m/z 43 ($\text{C}_2\text{H}_3\text{O}^+/\text{CHNO}^+$) to m/z 37 (C_3H^+) plotted as a function of O ₃ concentration (ppm) from 2005-2007. Also pictured is the temporal profile of PM _{2.5} mass concentrations ($\mu\text{g}/\text{m}^3$). The fact that this ratio is highest during the highest O ₃ concentration.	188
Figure 9.1 Particle mean diameters plotted from the event on 2/24. The fitted line is pictured and the slope of the equation for this line represents the estimated GR. The red circle highlights the discontinuity between the smallest and largest mean sizes.	197
Figure 9.2 SMPS size distribution of an NPF event (2/25 of the current study). The shading represents the number concentrations of particles for each size bin.	197
Figure 9.3 Representative mass spectra of the major UF-ATOFMS particle types present at Sugar Pine, which included: a) amine-OC, b) biomass, c) aged OC, d) ECOC, e) EC, and f) salt particle types.	198

Figure 9.4 UF-ATOFMS size distributions of amine-OC particle types from 100-600 nm during the NPF sub-periods. Values are given in number of amine-OC particle types per 10-nm size bin.	199
Figure 9.5 Digital color histograms from the NPF event on 2/24 from a) before the event at larger sizes (300-1000 nm), b) before the event at smaller sizes (100-300 nm), c) during the beginning of the event at all sizes (100 -1000 nm), and d) during the end of the event at all sizes.	200
Figure 9.6 The areas of m/z 86 and m/z -97 during each sub-period, which were averaged over the first NPF period.....	201
Figure 9.7 Back trajectories calculated using FLEXPART for each day corresponding to an NPF event. Trajectories plotted by release height for 500, 1000, 2000, and 4000 m plotted by altitude and latitude and longitude over time are shown in a), b), c), d), e), and f) for 2/24, 2/25, 2/26, 2/27, 3/6, and 3/7	201
Figure 9.8 OMI images during the days of SO ₂ transport including the day following P2, when SO ₂ returned to background levels. The black circles illustrate the evolution of the long-range trans-Pacific SO ₂ plume.....	205
Figure 10.1 Time-height cross sections (with time reversed per meteorological convention) of S-PROF radar-observed vertical profiles of precipitation above Sugar Pine Dam (SPD). The parameter shown is the signal-to-noise ratio (SNR), essentially the strength of the radar pulse scattered back.	221
Figure 10.2 Representative mass spectra for ATOFMS precipitation residues. Examples include dust (A)-(D) and biological residues (E) and (F). Positive and negative ion intensities vary by type.	222
Figure 10.3 Map showing the flight tracks for all 25 <i>CalWater</i> flights. McClellan Airfield is labeled in red.	223
Figure 10.4 Feb 16 th flight track colored by time on the left and by ascent or descent on the right. The size of the markers in the left panel represents altitude (m, MSL).	223
Figure 10.5 The Feb 25 th flight track colored by time with altitude (m, MSL) shown by the size of the markers.	224
Figure 10.6 Representative mass spectra for A-ATOFMS cloud residues. Examples include dust (A)-(C), biological residues (D)-(F), and sea salt (G). Positive and negative ion intensities vary by type.....	225
Figure 10.7 Representative 2D-S images including the classifications for 0-4.....	226
Figure 10.8 Example NAAPS time-height cross sections for (A) Sedebocker, (B) Solar Village, (C) Yinchuan, and (D) Beijing.....	226

Figure 10.9 Example NAAPS time-height cross sections for (A) Sedebocker, (B) Solar Village, (C) Yinchuan, and (D) Beijing..... 227

Figure 10.10 NAAPS time-height cross section data used to determine the maximum height of dust plumes at sites in each of the dust regions. The times of the dust plume heights correspond to times when trajectories passed through the dust regions. Also shown are the altitudes of these trajectories endpoints..... 228

Figure 10.11 CALIPSO images that correspond to the numbered markers in Figure 5.3 of Chapter 5. Latitude and longitude correspond to highlighted portion of satellite path in the map insets. N/A and panels 1-3 correspond to the trajectory ending on Feb 16th while panels 4-6 correspond to the trajectory ending. 229

Figure 10.12 TEM analysis of collected ice nuclei categorized as dust and biological. Includes: (A) image of dust IN, (B) spectrum for the dust IN shown in (A), (C) image of a biological IN, and (D) spectrum for the biological IN shown in (C).232

Figure 10.13 Vertical profiles of Dust+bio cloud residues, the total number of residues, and temperature for the flight on Feb 25th, 2011 (20:57 – 00:36 UTC). Also shown are cloud particle residual IN concentrations as asterisks with the color representing the temperature at which the measurement..... 233

LIST OF TABLES

Table 2.1 Averages of PM_{2.5}, relative humidity (RH), temperature (T), wind speed (WS), and gas-phase O₃ concentrations for the sampling periods during 2005-2007. Standard deviations (σ), medians, and measurement ranges are also listed. ‘Avg. Daily Maxima’ refers to the average time of the daily maximum. 60

Table 2.2 Descriptions of the major ATOFMS submicron particle types from 2005-2007. All particle types showed evidence of aging based on the presence of ammonium (¹⁸NH₄⁺), sulfate (⁹⁷HSO₄⁻), nitrate (⁴⁶NO₂⁻ and ⁶²NO₃⁻) and/or organics, including amines (⁸⁶C₅H₁₂N⁺) and oxidized OC (⁴³C₂H₃O⁺/CHNO⁺). 61

Table 3.1 Dates and maximum wind speed (WS) corresponding to “normal condition” time periods in green and “TC condition” time periods in maroon. Includes average SO₂ concentrations, $f_{CCN[0.2]}$, and CCN concentrations during each period. 81

Table 6.1 Statistics for precipitation sample collection from 2009-2011 at SPD, CF, BP, and TM. Includes start and end dates and times for sample collection and number of residues that were chemically analyzed. Storms are also labeled for corresponding samples. 156

Table 9.1 Mean sizes used to estimate GRs. Variables in the linear regression equation are mean size (y) in nm and time (x) per 5-minute SMPS scan. Time to 100 nm (h) is calculated from the linear regression equation and multiplied by 12 to give time in hours. 208

Table 9.2 Dates of P1 and P2 separated into before events, G1 (≤ 20 nm), G2 (20-25 nm), G3 (25-30 nm), G4 (≥ 30 nm at higher number concentrations), and end events (≥ 30 nm at lower number concentrations). The SMPS size distribution mean sizes (nm) and number concentrations ($\#/cm^3$) are averaged 209

Table 10.1 Statistics for precipitation sample collection during winter storms in 2011 at SPD. Includes start and end dates and times for sample collection and number of residues that were chemically analyzed. Storms are also labeled for corresponding samples. 234

ACKNOWLEDGEMENTS

First and foremost, I would like to thank my advisor, Prof. Kimberly Prather, for making the work in this dissertation possible. She has supported my research ideas throughout and has enabled me to assess environmental problems from different, unique angles. I enjoy her dedication when it comes to our line of work, and her enthusiasm has most certainly rubbed off on me. She has given me the opportunity to learn and grow as a scientist and has supported my research interests throughout graduate school. I am grateful for her providing me with her support, words of wisdom, and having faith in me achieving my goals over the years.

I would also like to thank my committee members: Prof. Mark Thiemens, Prof. Joel Norris, Prof. Amitabha Sinha, and Prof. Michael Sailor. Each of my committee members has dedicated time to helping me further my graduate and postgraduate career, through writing recommendation letters for my postdoctoral fellowships, providing valuable feedback on my research during my departmental and qualifying exams, and offering words of encouragement. I cannot thank them enough for their support. I have also had the opportunity to work with a wide array of collaborators throughout my graduate tenure. I would like to thank many of our collaborators at the National Oceanic and Atmospheric Administration's Earth System Research Laboratory (NOAA/ESRL) in Boulder, CO. In particular, I would like to thank Dr. Marty Ralph, who has provided unlimited advice and guidance for my projects involving CalWater. I value his commitment and genuine interest in solving complex problems associated with meteorology and aerosols and in interdisciplinary research. I am honored to be able to work with Marty as a postdoctoral fellow in his group following graduate school. Also from NOAA/ESRL, Dr. Allen White, Dr. Paul Neimann, Dr. Gary Wick, Dr. Christopher Williams, Dr. Ryan Spackman, Dr. Sergey Matrosov, Dr. David Kingsmill, and Dr. Chris Fairall, have generously provided their time and gracious help interpreting meteorological data that have supported my own work. Allen, Paul, Ryan, and Chris provided invaluable feedback and advice for my postdoctoral fellowship applications. They, in addition to everyone in Marty's group at NOAA/ESRL, are very kind,

welcoming, and eager to work together. I have greatly appreciated working with and look forward to working with all of them for years to come.

I have had the opportunity to work with many other collaborators, who I greatly appreciate having been acquainted with. Dr. Greg Roberts was a great help interpreting CCN data and a great (and patient) running partner in the beautiful backwoods of Foresthill, CA during the CalWater field campaign. I appreciate Greg taking the time to work through edits in person on my first publication. John Ten Hoeve and Prof. Mark Jacobson from Stanford University also contributed greatly to my first publication by discovering the source of a particularly important gas phase species and introducing me into the world of satellite data. Dr. Patrick Minnis from NASA Langley Research Center and Dr. Kirk Ayers and Dr. Rabindra Palikonda enabled me to expand beyond aerosol data by looking at cloud properties via satellite measurements. Without their assistance and hard work, I would not be as familiar with using satellite data as I am today. Patrick and Kirk in particular have graciously taken time to retrieve data from the GOES-11 satellite and interpret it in terms that I could understand, even without being funded to do so. Dr. Thomas Hill, Dr. Gary Franc, Prof. Paul DeMott, and Dr. Ryan Sullivan have readily provided ice nuclei measurements and I am very grateful for that. In particular, Tom would without question analyze samples for me and humor me with his witty emails. Paul has provided extremely valuable feedback on a few of my projects, especially when interpreting ice nuclei data. Another group of people, I call the “Yosemite Crew,” I am extremely grateful for due to their persistence in collecting, retrieving, and sending me snow samples from Yosemite National Park throughout multiple winter seasons. I applaud their dedication, enduring the rough winter storm conditions to collect samples for me. Kathy Warner has been my point person at Yosemite, and has been great with making sure those samples arrive at my office door still frozen. On the other side of the United States, Dr. Tyler Coplan and Bryan Buck have been invaluable collaborators, trusting me with their home-build automated precipitation samplers each winter season. Ty has gone above and beyond, explaining his isotope analysis to me one-on-one. He has taken the time to have numerous phone calls with me to make sure we had what we needed and even to inquire about my career. I am

greatly appreciative of his advice, understanding, and willingness to work together. I would also like to thank Prof. Daniel Rosenfeld, for traveling all the way from Israel to provide one-on-one input on my papers and improving them beyond belief. It was a pleasure to work with him and I value his feedback. He even inserts comical comments here and there, which put a smile on my face. Dr. Dan Cayan and Mary Tyree taught me how to use NCEP/NCAR reanalysis and were willing to do so at the drop of a hat. For all of my collaborators involved with CalWater, I am grateful to have had the opportunity to work with them and look forward to working with them once again for the future CalWater II project.

Although the majority of my graduate career involved CalWater, the first two projects I focused on involved the help of many people. I would like to thank Dr. Xueying (Sharon) Qin for work on the Riverside project and helping me interpret some of the ATOFMS results. For the AMIGAS study in Atlanta, GA, I would like to thank my collaborators at the Georgia Institute of Technology, including Richard Moore, Dr. Luz Padro-Martinez, and Prof. Anthanasios Nenes. I enjoyed conversing with them at the conferences I attended throughout graduate school. Also a part of AMIGAS, Jerry Brown was a great help at the Jefferson Street trailer and definitely was quite entertaining.

I also must thank the past and present members of the Prather group for their endless help with field study setup, data analysis, writing, and the list goes on. Although not a student, Joe Mayer is the best machinist I know and is great company on that 15 hour drive up to Sugar Pine. Joe can rig a setup that will protect our supplies on top of the trailer so fast that you would need a high speed camera to catch it. Dr. Andy Ault and Dr. Kerri Pratt I consider my “science parents.” They have been my mentors since the start; they took me in and helped shape me into the scientist I am today. I cannot even count how many hours they spent teaching me how to use a script, or how to fix a laser, or how to...leave things alone during a field study. Outside of lab, Kerri is a great hockey partner and Andy, given his faults of country music and Taco Bell, is a great running partner. Andy taught me the ins and outs of field work, which I am extremely appreciative of. I am so grateful for everything they have taught me and the friendships that have

developed with them. Dr. Cassandra Gaston has also been a great mentor and helped numerous times with instrument troubleshooting, writing, and data analysis. Cassie is not the greatest shuffleboard player, but she sure knows the literature like the back of her own hand. Lindsay Hatch would tear my drafts to shreds, but without her editing, they would be nowhere where they are today. She has been incredibly helpful with shaping up my papers and proposals, and has also introduced me into the wonderful worlds of running and veganism. Liz Fitzgerald is quite the hasher and hockey fanatic, but I am mostly grateful for her help with the IC. I had a blast with her during the 2010 CalWater study, however, will continue to tease her for being a Redwings fan. Dr. Melanie Zauscher is a computer and programming guru and has helped me multiple times with computer related issues. I will never forget our game of “Real or Fake.” Dr. Meaghan Moore taught me how to use certain scripts and how to calculate certain parameters with CCN data; it was a pleasure to have worked with her. Kaitlyn “Hot Hands” Suski is the aircraft wizard and I am happy to have had the opportunity to work with her, specifically on our Science paper. Doug Collins has been heavily involved with CalWater and even though we have had our moments, he has provided valuable input on my papers and has been great with field work. I will never forget that great photo of Doug, Liz, and I in our flannel shirts and puffy vests. We had to somehow fit into the backwoods of the Sierra Nevada somehow...didn't we? Although Jack Cahill, Mr. Meat and Potatoes, pokes fun of my veganism constantly, he has the Midwest kindness and constantly makes me laugh. He has solved many computer and Matlab issues for me and was such a great company during the 2011 CalWater study. I consider Dr. Alberto Cazorla the Matlab guru; he has helped me numerous times with my source analysis. I tell him I have all this data and I need to get ‘X’ out of it, and poof, he generates a script, plot, or spreadsheet that fits exactly my needs. Dr. Bob Moision was a postdoc when I first started and I have to say, I am quite impressed with his patience for teaching. He is an amazing teacher; taking the time to teach me simple electrical principles and even how to solder correctly. Bob was invaluable during the AMIGAS study and has quite the sense of humor. I would also like to thank Mallory Pickett and Chris Lee for running all those control experiments for me, I would have been tied to Laverne for weeks and not written anything if it weren't for

them. For the other/newer Prather Lab members who I did not get the chance to work with, including Matt Ruppel, Defend Zhao, Camille Sultana, and Tim Guasco, it was a pleasure to get to know them and I wish them all the best in the future.

I first decided to go to graduate school after I got a C+ in physiology and decided I probably should not be a doctor. Ha, just kidding. But the real reason is because of my undergraduate thesis advisor, Prof. Gregory Girolami. I worked in his laboratory for about a year and he was the kindest, most genuine guy. He would meet with me on a regular basis to see how my research was going. Greg also spent probably hours editing my bachelor's thesis to make sure it was just right and nominated me for the Proctor & Gamble Research Award, which I was indeed awarded my senior year. To this day, we talk via email every now and then. I hope to keep in touch with him in the future and am very grateful for his strong influence on my career choice.

Last, but certainly not least, I would like to thank my friends, family, and boyfriend. Through stressful times, they have all been there for me, lending an ear and always trying to make me feel better. My parents Allen and Sharon have endlessly supported me, whether it was to join dance as a child or to go to school to get my Ph.D. They have always been there for me, through the thick and thin, and I am eternally grateful for that. I could not have made it through graduate school without them! They tell me they are very proud of me and my accomplishments, but it is them who I am proud of, being such great parents throughout the years. My brothers, Allen (a.k.a. Alien) and Alex, have been the best brothers a sister could have. Although we are separated by thousands of miles, we contact each other when we can and they definitely make me laugh. I am happy to see them achieving so much in their own lives and cannot wait for them to come see me in Boulder, and then off to the ski slopes we go. My boyfriend, Nick Prola, has been there for me day after day. No one has endured more venting during stressful times than him; I am truly appreciative of him and his support. He always makes the most sense of situations and has the ability to always make me feel better. Unfortunately, we were separated over two years ago after he graduated law school and had to move back to Chicago, but he still encourages me to finish and fully supports my

career path in Boulder. I cannot express enough how much I love him and all of my family. I am so thankful they were there for me during graduate school; I truly could not have done it without them.

Chapter 2 is in preparation for submission to *Atmospheric Environment*: Creamean, J.M., K.A. Pratt, A.P. Ault, X.Y. Qin, C.J. Gaston, and K.A. Prather, Long-term Impacts of Sources and Meteorology on Aerosol Chemical Mixing State in Riverside, CA. The dissertation author was the primary investigator and author of this paper.

Chapter 3 is in preparation for submission to *Geophysical Research Letters*: Creamean, J.M., A.P. Ault, E. Edgerton, R.H. Moore, L.T. Padro, A. Nenes, and K.A. Prather, Significant Changes in Urban Aerosol Chemistry and CCN Concentrations Induced by Tropical Cyclones. The dissertation author was the primary investigator and author of this paper.

Chapter 4 is in reprinted with permission from Creamean, J.M., A.P. Ault, J.E. Ten Hoeve, M.Z. Jacobson, G.C. Roberts, and K.A. Prather, Measurements of Aerosol Chemistry during New Particle Formation Events at a Remote Rural Mountain Site, *Environmental Science & Technology*, 45 (19), 8208-8216, 2011. Copyright 2011 American Chemical Society. The dissertation author was the primary investigator and author of this paper.

Chapter 5 has been submitted to *Science*: Creamean, J.M., K.J. Suski, D. Rosenfeld, A. Cazorla, P.J. Demott, R.C. Sullivan, A.B. White, F.M. Ralph, and K.A. Prather, Dust and Biological Aerosols from the Sahara and Asia Influence Precipitation in the Western United States. The dissertation author was the primary investigator and author of this paper.

Chapter 6 is in preparation for submission to *Journal of Geophysical Research-Atmospheres*: Creamean, J.M., P. Minnis, J.K. Ayers, R. Palikonda, T.C. Hill, G.D. Franc, P.J. Demott, K.Y. Warner, P.J. Neiman, A.B. White, F.M. Ralph, D.B. Collins, J.F. Cahill, A.P. Ault, and K.A. Prather, Inter-annual Evidence of Aerosols Affecting

Orographic Precipitation in the Sierra Nevada. The dissertation author was the primary investigator and author of this paper.

VITA

- 2007 B.A.S. in Chemistry, University of Illinois, Urbana-Champaign
- 2007-2008 Teaching Assistant, Department of Chemistry and Biochemistry,
University of California, San Diego
- 2008-2012 Graduate Student Researcher, University of California, San Diego
- 2009 M.S. in Chemistry, University of California, San Diego
- 2012 Ph.D. in Chemistry, University of California, San Diego

PUBLICATIONS

- Creamean, J.M.,** A.P. Ault, J.E. Ten Hoeve, M.Z. Jacobson, G.C. Roberts, and K.A. Prather, Measurements of Aerosol Chemistry during New Particle Formation Events at a Remote Rural Mountain Site, *Environmental Science & Technology*, 45 (19), 8208-8216, 2011.
- Creamean, J.M.,** K.J. Suski, D. Rosenfeld, A. Cazorla, P.J. Demott, R.C. Sullivan, R. Spackman, A.B. White, F.M. Ralph, and K.A. Prather, Dust and Biological Aerosols from the Sahara and Asia Influence Precipitation in the Western United States, *Science*, under external review, 2012.
- Creamean, J.M.,** A.P. Ault, E. Edgerton, R.H. Moore, L.T. Padro, A. Nenes, and K.A. Prather, Significant Changes in Urban Aerosol Chemistry and CCN Concentrations Induced by Tropical Cyclones *Geophysical Research Letters*, in preparation, 2012.
- Creamean, J.M.,** A. Cazorla, F.M. Ralph, P. Minnis, J.K. Ayers, R. Palikonda, and K.A. Prather, Long-Term Variability of Dust Sources and Transport Mechanisms to the West Coast of the United States, *Journal of Geophysical Research-Atmospheres*, in preparation, 2012.
- Creamean, J.M.,** P. Minnis, J.K. Ayers, R. Palikonda, T.C. Hill, G.D. Franc, P.J. Demott, K.Y. Warner, P.J. Neiman, A.B. White, F.M. Ralph, D.B. Collins, J.F. Cahill, A.P. Ault, and K.A. Prather, Inter-annual Evidence of Aerosols Affecting Orographic Precipitation in the Sierra Nevada, *Journal of Geophysical Research-Atmospheres*, in preparation, 2012.
- Creamean, J.M.,** K.A. Pratt, A.P. Ault, X.Y. Qin, C.J. Gaston, and K.A. Prather, Long-term Impacts of Sources and Meteorology on Aerosol Chemical Mixing State in Riverside, CA, *Atmospheric Environment*, in preparation, 2012.

- Ault, A.P., C.R. Williams, A.B. White, P.J. Neiman, **J.M. Creamean**, C.J. Gaston, F.M. Ralph, and K.A. Prather, Detection of Asian dust in California orographic precipitation *Journal of Geophysical Research-Atmospheres*, 116 (D16205), doi:10.1029/2010JD015351, 2011.
- Ault, A.P., **J.M. Creamean**, and K.A. Prather. Mobile laboratory observations of spatial variability within the urban aerosol in a coastal environment, in preparation for *Atmospheric Environment*.
- Collins, D.B., D.E. Kingsmill, G.C. Roberts, **J.M. Creamean**, and K.A. Prather, Barrier Jet Transport of Cloud Condensation Nuclei to Regions of Orographic Precipitation Formation, *Geophysical Research Letters*, in preparation, 2012.
- Hatch, L.E., **J.M. Creamean**, A.P. Ault, J.D. Surratt, M.N. Chan, J.H. Seinfeld, E.S. Edgerton, Y.X. Su, and K.A. Prather, Measurements of Isoprene-Derived Organosulfates in Ambient Aerosols by Aerosol Time-of-Flight Mass Spectrometry - Part 1: Single Particle Atmospheric Observations in Atlanta, *Environmental Science & Technology*, 45 (12), 5105-5111, 2011.
- Hatch, L.E., **J.M. Creamean**, A.P. Ault, J.D. Surratt, M.N. Chan, J.H. Seinfeld, E.S. Edgerton, Y.X. Su, and K.A. Prather, Measurements of Isoprene-Derived Organosulfates in Ambient Aerosols by Aerosol Time-of-Flight Mass Spectrometry - Part 2: Temporal Variability & Formation Mechanisms, *Environmental Science & Technology*, 45 (20), 8648-8655, 2011.

FIELDS OF STUDY

Major Field: Chemistry

Studies in Atmospheric Chemistry

Professor Kimberly A. Prather

ABSTRACT OF THE DISSERTATION

The Impact of Meteorological Conditions and Variation in Chemical Composition of
Aerosols on Regional Cloud Formation

by

Jessie Marie Creamean

Doctor of Philosophy in Chemistry

University of California, San Diego, 2012

Professor Kimberly Prather, Chair

Atmospheric aerosols have significant implications for human health and climate. For instance, aerosols impact climate directly by scattering and absorbing solar and terrestrial radiation and indirectly by acting as cloud condensation nuclei (CCN) and ice nuclei (IN), which facilitate cloud droplet and ice crystal formation, respectively. Changes in chemistry, size, and number concentrations between different locations and over time alter how aerosols impact air quality and cloud formation, and can have broader implications on precipitation efficiency and phase. Further, aerosol composition largely depends on meteorology, which influences sources and chemical transformation in the atmosphere. Aerosol-cloud-precipitation interactions represent one of the largest sources of uncertainty in climate science; therefore, a better understanding of the aerosols that contribute to these effects is needed. To address this source of uncertainty, the chemical composition of individual ambient aerosols and aerosols as insoluble residues in precipitation samples was determined using aerosol time-of-flight mass spectrometry (ATOFMS) and provided insight into their potential to serve as cloud seeds at three different locations over time. A three-year summer study (2005-2007) in Riverside, CA afforded information on the inter-annual variability of the urban aerosol due to changes in aerosol transport and meteorological conditions. In the summer of 2008 in Atlanta, GA, tropical cyclones shifted the representative aged urban aerosol to a less-aged, less-CCN active aerosol population, having implications on regional cloud formation after extreme weather events. At a remote site in the Sierra Nevada Mountains in the winter of 2009, observations of newly-formed aerosols presented a new source of CCN. Inter-annual trends in precipitation at the same remote site showed how IN transported from the Sahara and Asia potentially influenced precipitation processes during three winter seasons (2009-2011). Investigating changes in cloud seeds represents a longer-term goal to reduce uncertainties associated with modeling aerosol-cloud-precipitation interactions. Larger spatial and temporal coverage is needed to better understand trends in cloud formation and precipitation and to provide more detail for regional and global model parameterization. The results presented herein represent a noteworthy advancement towards understanding variation in composition and sources of cloud seeds in different regions and in most cases long time periods.

1. Introduction

1.1. Sources of Atmospheric Aerosols

Aerosols are small liquid or solid particles suspended in a gas medium, such as the atmosphere. They are ubiquitous in the troposphere and vary considerably in terms of composition, size, source, and their resulting effects on air quality and climate [Poschl, 2005]. Aerosols originate from a multitude of natural and anthropogenic sources, and can be directly emitted (primary aerosol) or formed/transformed in the atmosphere through heterogeneous reactions and condensation of gas phase species (secondary aerosol).

Some of the main constituents to the global aerosol burden include crustal elements (i.e., dust), sea salt, sulfate, and organics [Poschl, 2005; Seinfeld and Pandis, 2006]. All of these aerosol types can originate from natural sources, although dust (i.e., road dust [Pagotto et al., 2001]), sulfate, and organics can be anthropogenic as well. Natural dust injected into the troposphere via Aeolian processes in arid regions is among the largest contributors to the global dust burden. One-third of the global land area is covered by dust-producing surfaces, made up of hyperarid regions like the Sahara that covers 0.9 billion ha, and drylands, which occupy 5.2 billion ha [Jickells et al., 2005; Prospero et al., 2002]. Biological aerosols, which can fall under the primary organic aerosol category [Heald and Spracklen, 2009], can be lofted with dust from arid regions [Hallar et al., 2011; Hua et al., 2007], but can also originate from a plethora of terrestrial, marine, urban, and rural sources [Despres et al., 2012; Schnell and Vali, 1976]. Biological aerosol encompasses microorganisms such as bacteria, fungi, pollen, and spores [Despres et al., 2012; Vali et al., 1976], in addition to fragments and excretions from decomposing vegetation [Schnell and Vali, 1972]. Sea salt is a primary aerosol injected into the atmosphere from mechanical processes such as wave breaking and bubble bursting [Bigg and Leck, 2008; Foltescu et al., 2005]. Sulfate can be emitted with sea salt, but can also form in the atmosphere from phytoplankton emissions via secondary heterogeneous reactions. Certain phytoplankton produce dimethyl sulfide

(DMS), which is released into the atmosphere, where it is oxidized to form sulfur dioxide (SO₂) gas [Charlson *et al.*, 1987]. SO₂ can be further oxidized leading to the production of sulfate in the particle phase [Finlayson-Pitts, 2000]. Primary organic aerosols can also originate from phytoplankton blooms and are ejected into the atmosphere through bubble bursting [Facchini *et al.*, 2008]. Other natural sources of sulfate and organics include aerosol formation and transformation over vegetation or boreal forests [Tunved *et al.*, 2006 and references therein]. Naturally-produced secondary organic aerosols (SOA) can be formed via oxidation followed by condensation of biogenic volatile organic compound (BVOC) emissions over boreal forests [Hoffmann *et al.*, 1997]. Further, new particle formation (NPF) is a process where organic and/or sulfate aerosols can be spontaneously formed *in situ* under specific conditions from gas phase precursors [Kulmala *et al.*, 2004], as discussed in more detail in Chapter 4.

Although natural sources largely contribute to the global sulfate and organic aerosol burden, anthropogenic sources have a significant influence [Kanakidou *et al.*, 2005]. Coal-fired power plants have been estimated to contribute up to 56% of global SO₂ emissions, which forms sulfate aerosol [Smith *et al.*, 2001]. Other anthropogenic SO₂ sources include petroleum oil combustion (24%), industrial processes (15%), and biomass burning (3%) [Smith *et al.*, 2001]. Primary organic aerosol emissions from meat cooking operations, automobiles, and heavy-duty diesel trucks can comprise up to 21% each of the primary fine organic carbon emissions in highly populated urban areas such as Los Angeles [Rogge *et al.*, 1993a; Rogge *et al.*, 1991]. Smaller contributions to urban organic aerosol emissions includes tire debris [Rogge *et al.*, 1993b], urban vegetation [Rogge *et al.*, 1993c], natural gas appliances [Rogge *et al.*, 1993d], hot asphalt [Rogge *et al.*, 1997a], distillate fuel oil [Rogge *et al.*, 1997b], and residential biomass burning [Rogge *et al.*, 1998]. Estimates obtained from apportionment studies indicate that the organic fraction in ambient aerosol is overwhelmingly secondary in nature in cities such as Riverside, CA [Docherty *et al.*, 2008]. Photochemical smog from urban pollution is a rich medium for the formation of SOA [Volkamer *et al.*, 2006], consisting of volatile organic compounds (VOCs) from automobile emissions and amines from agricultural

sources that photooxidize into condensable products [Malloy *et al.*, 2009; Pandis *et al.*, 1992; Silva *et al.*, 2008; Sorooshian *et al.*, 2008].

1.2. Environmental Impacts of Atmospheric Aerosols

1.2.1. Effects on Health

In particular, the variety and complexity of urban aerosol chemical composition renders numerous effects on air quality and therefore unlimited adverse health effects [Hidy *et al.*, 1975]. For instance, aerosols from urban air pollution have been linked to a wide array of adverse health effects, including but not limited to cardiovascular and pulmonary diseases [Latzin *et al.*, 2009; Nawrot *et al.*, 2011], allergies and asthma [Dockery *et al.*, 1996], and even increased mortality [Samet and Katsouyanni, 2006]. Although significant advancements have been made to improve the understanding of health effects of aerosols, better approximations based on measurements are needed to improve the representation of urban aerosols in models and pollution regulations [Vedal, 1997]. Understanding specific effects due to aerosol size and chemistry has been identified as critical to evaluating the overall causal relationship between aerosol exposure and adverse health effects [Brook *et al.*, 2010].

1.2.2. Serving as Cloud Seeds

Although future research on aerosol health effects is needed, the climatic effects of aerosols on cloud microphysics are even more poorly understood due to complexity in chemical composition, size, and number concentrations [IPCC, 2007]. Aerosols can directly scatter and absorb incoming solar and outgoing longwave radiation, and also indirectly impact climate by participating as “seeds” or nuclei for cloud droplet or ice crystal growth, which can subsequently mature into precipitation [Seinfeld and Pandis, 2006]. Aerosols can serve as sites for condensation of atmospheric water vapor either as cloud condensation nuclei (CCN) or as ice nuclei (IN), forming cloud droplets and ice crystals, respectively. Overall, CCN and IN have different physiochemical properties and thus have different effects on cloud microphysics.

The ability of aerosols to serve as CCN is dependent on the size and amount of soluble material as described by Köhler theory; it combines the Kelvin effect, which describes the change in saturation vapor pressure due to a curved surface, and Raoult's Law, which relates the saturation vapor pressure to the solute [Köhler, 1921]. Efficient CCN are typically composed of soluble or at least partially soluble material (i.e., sea salt) [Petters and Kreidenweis, 2007]. The CCN activation threshold is roughly between 0.04 and 0.2 μm in diameter, which is also where aerosol solute concentrations are most important [McFiggans et al., 2006]. However, aerosols $>0.2 \mu\text{m}$ can also serve as CCN based on their size. In high number concentrations and under constant water content, CCN create large populations of small-sized cloud droplets, subsequently enabling the cloud to become more reflective [Twomey, 1974]. Further, clouds with high CCN concentrations become thicker and have increased lifetimes [Albrecht, 1989; Pincus and Baker, 1994]. Cloud droplet nucleation and the resulting effects from CCN are thought to occur in the lower layers of clouds [Rosenfeld et al., 2008a; Yin et al., 2000].

The oceans are a large source of various types of aerosols that have been shown to effectively serve as CCN, including sea salt, sulfate aerosols, and organic aerosols [Boucher and Lohmann, 1995; Novakov and Penner, 1993; O'Dowd et al., 2004]. Rosenfeld et al. [2000; 2006] have shown that urban and industrial emissions contributed significant concentrations of CCN, which suppressed rain and snow in multiple regions worldwide. Further, NPF in urban and rural regions has been estimated to increase springtime boundary layer (BL) global mean CCN concentrations by up to 50% [Spracklen et al., 2008]. NPF events can produce a significant fraction of aerosols that grow to sizes as large as 100-200 nm within a few hours, and thus constitute an important source of CCN [Laaksonen et al., 2005].

On the other hand, IN are atmospheric particles that catalyze the freezing of water vapor and supercooled cloud droplets, producing ice crystals that could otherwise not form at mixed phase cloud temperatures (within a range of $\sim -38 \text{ }^\circ\text{C}$ to $0 \text{ }^\circ\text{C}$) [Isono et al., 1959]. Aerosols that serve as efficient IN are typically more insoluble, such as dust and some biological material [Christner et al., 2008; DeMott et al., 2003; Despres et al.,

2012; Wiacek *et al.*, 2010]. Soot—from incomplete combustion of hydrocarbon emissions from factories, engines, and forest fires [Graham *et al.*, 1975]—has the potential to serve as IN at very cold temperatures (≤ -40 °C), although is unlikely to significantly contribute to the global IN budget [Friedman *et al.*, 2011]. Formation of ice crystals from IN has been shown to occur at the tops of clouds [Meyers *et al.*, 1992]. In mixed phase clouds, ice formed from IN can gravitationally fall into regions where cloud droplets were formed by CCN, demonstrating the complex nature that could result within a single cloud system. The climate system has been shown to be highly sensitive to the concentration of IN in the atmosphere, however, the physical processes associated with IN are still poorly understood [DeMott *et al.*, 2010].

1.2.3. Broader Impacts on Precipitation and the Global Water Cycle

Clouds affected by CCN and IN tend to result in different precipitation processes. For instance, high concentrations of CCN, particularly from urban regions, are thought to suppress or delay the onset of precipitation [Rosenfeld, 2000]. Delaying the onset of precipitation allows invigoration of updrafts, causing intense thunderstorms and large hail [Andreae *et al.*, 2004]. Further, the invigorated storms release latent heat higher in the atmosphere, which could substantially affect the regional and global circulation systems and affect the water cycle by shifting the location and possibly intensity of precipitation [Andreae *et al.*, 2004]. Conversely, although only very few in number, large drops resulting from the activation of giant CCN (≥ 2 μm) are thought to enhance the collision coalescence process which leads to initiation of precipitation in an otherwise non-precipitating cloud [Kogan *et al.*, 2012; Posselt and Lohmann, 2008; Yin *et al.*, 2000]. Determining the net precipitation effect of CCN represents a significant challenge due to the dependence of precipitation forming processes on CCN size and chemistry, especially on a global scale.

Even in small concentrations, IN can strongly influence ice crystal concentrations in clouds [DeMott *et al.*, 2010]. After the initial IN activation of cloud ice, water vapor favors condensing on ice versus liquid droplets, thereby causing ice crystals to grow faster and larger into snowflakes [Bergeron, 1935]. Ice crystals also grow diffusively at

the expense of liquid droplets [Korolev, 2007], and can undergo accretion or aggregation to form graupel or snow [Hosler et al., 1957; Houze, 1993]. These ice processes impact precipitation mechanisms and potentially precipitation efficiency in regions where snowpack supplies copious amounts of water to reservoir networks [Guan et al., 2010]. However, with the projected increase in surface air temperature by the end of the century, a shift from snowfall to rainfall may occur [Guan et al., 2010]. A decrease in snowpack has significant implications with regard to the water cycle and reservoir demands; snowpack water storage is lost and increased flood risks may result [Guan et al., 2010; Leung and Qian, 2009b]. Additional complications involving IN precipitation effects arise in cases where temperatures are not cold enough for the IN to form ice; instead, these IN actually serve as giant CCN and in the absence of small, preexisting cloud droplets, can actually suppress precipitation [Posselt and Lohmann, 2008; Rosenfeld et al., 2001]. It is estimated that over 50% of precipitation globally is initiated in the ice phase [Lau and Wu, 2003], however, the overall effects of IN on precipitation processes are poorly understood [Dymarska et al., 2006].

These often conflicting effects of CCN and IN demonstrate the need to improve our understanding of aerosols that can serve as cloud seeds. One step towards improving the understanding of the effects of CCN and IN in a particular regions is determining their sources. Additional observations will enable the climate modeling community to better assess how regional climate may change due to the effects from aerosols. Improving our ability to model aerosol-cloud-precipitation interactions that suppress or produce precipitation will potentially lead to more efficient preparedness for flood and/or drought in the future.

1.3. Variability in Aerosol Chemical Composition

1.3.1. Effects due to Transport Conditions

After aerosols are emitted into the atmosphere from the various sources described above, the overall chemical composition of the aerosol population in a particular region is subject to alteration, due to certain processes that may be dependent on transport,

availability of secondary species, and meteorological conditions. Transport from different sources has large impacts on particle chemistry, number, and mass concentrations, even for urban locations [Finlayson-Pitts, 2000]. Winds can transport aerosols long distances from their sources [Liu et al., 2009a; Liu et al., 2009b]; for instance, dust from Asia has been shown to circle the globe within 13 days [Uno et al., 2009]. Further, tropospheric winds have been linked to outbreak cases of aerosolized microorganisms possibly containing Kawasaki Disease agents in Japan and California [Rodo et al., 2011]. During transport, aerosols can become chemically “aged” by undergoing heterogeneous reactions with trace gases and gas-to-particle partitioning of secondary species, developing coatings of nitrate [Hughes et al., 2000], sulfate [Hughes et al., 2000; Ying and Kleeman, 2006], ammonium [Hughes et al., 2000; Russell et al., 1986], amines [Pratt et al., 2009b], and/or oxidized organics [Docherty et al., 2008]. The resulting aging of aerosols with different secondary species can have variable effects air quality and climate. For instance, a sulfate coating has been shown to increase the toxicity of a particular aerosol and has previously been linked to increased cardiopulmonary mortality rates [Pope et al., 1995]. Further, a coating of sulfate on soot particles can actually amplify their light absorption and enable the soot to become hygroscopic, resulting in a CCN-active soot aerosol [Adachi and Buseck, 2008].

Aerosols from one source region can experience transport to multiple regions. Consider an example of Saharan dust injected into the atmosphere, where the dust can be lofted at various altitudes and travel to multiple regions. The dust can be transported into anthropogenic pollution plumes over Europe [Birmili et al., 2008], where it may develop a coating of secondary sulfate and/or nitrate. Not only does this complicate the chemical composition and the resulting effects on air quality, it also influences the cloud seeding effects of the dust; chemical aging with nitrate has been shown to limit the IN and enhance the CCN capabilities of dust [Sullivan et al., 2009a]. The dust could also travel at higher altitudes into the Atlantic Ocean, reaching the eastern coasts of North and South America [Prospero, 1999; Prospero et al., 1981], or is potentially lofted high enough for the jet stream to capture the dust plumes, transporting the dust to the west clear across the Pacific Ocean and reaching North America [McKendry et al., 2007]. This example

illustrates how transport and chemical aging have implications for cloud formation in regions other than the source region. On the other hand, one region is typically influenced by multiple sources, even those that are far from the proximity of the source (i.e., remote locations away from roads). For instance, Chapters 3-6 describe *in situ* sources, regional transport, and long-range transport of aerosols to one remote site in the Sierra Nevada Mountains and the resulting implications for cloud formation in that region.

1.3.2. Effects due to Meteorology

Transport also depends on meteorology; microscale (<1 km horizontal resolution), mesoscale (5 to several hundred km), and even synoptic scale (thousands of km) weather patterns can affect aerosol transport. These dynamical systems include diverse phenomena as thunderstorms, tornadoes, tropical cyclones (TCs; includes tropical storms and hurricanes), extratropical cyclones, jet streams, and global-scale circulations. For instance, synoptic scale dynamics over the Pacific Ocean create ideal conditions for trans-Pacific transport of dust and pollutants from over Asia into clouds over the western United States as discussed in Chapters 4 and 5. Aerosols can also be transported via mesoscale TCs as discussed in Chapter 3 and can also depend on microscale prefrontal storm conditions where wind speed is strongest [Noble and Prather, 1997].

Further, partitioning of gas phase precursors not only depends on the availability of secondary species, but also on local meteorological conditions as discussed in Chapter 2. Relative humidity has been shown to enable the condensation of gas phase amines into the particle phase [Angelino *et al.*, 2001b]. Overall, aerosol chemical composition in a particular region can be quite complex due to variability in sources, transport, meteorology, and gas phase precursors for chemical aging. It can also change at one location between seasons and from year-to-year. Thus, it is important to investigate aerosol chemistry at multiple regions and during multiple time periods to gain a larger, more detailed picture of aerosol variability.

1.4. Real-Time, Single-Particle Measurements of Chemical Composition

Analyzing aerosol chemical composition represents a significant challenge due to their ever-changing physicochemical behavior [Hoffmann *et al.*, 2011]. Several techniques are currently used to address these challenges, including bulk phase, single-particle, off-line, and on-line measurements [Pratt and Prather, 2011a; Pratt and Prather, 2011b]. The technique used throughout this dissertation involves on-line, single-particle measurements using the aerosol time-of-flight mass spectrometer (ATOFMS).

The ATOFMS analyzes the size and chemical composition of individual aerosols between 0.2-3.0 μm vacuum aerodynamic diameter (D_{va}) in real-time [Gard *et al.*, 1997b]. Figure 1.1a shows a schematic of the ATOFMS. Aerosols first enter the ATOFMS through a converging nozzle inlet into a differentially pumped vacuum chamber, which causes the particles to supersonically expand and accelerate to their size-dependent terminal velocities. Particles then traverse two orthogonal, continuous wave scattering lasers (532 nm) beams spaced 6 cm apart. The scattering signals are detected using two photomultiplier tubes; the time between the scattering signals is used to determine each particle's velocity. Particle D_{va} is calculated based on particle velocity and a size calibration with polystyrene latex spheres of known sizes. The scattering signal from the second continuous wave laser is also used to fire a third Q-switched Nd:YAG laser (266 nm), in which the particle is simultaneously desorbed and ionized. The ions produced from the third laser are then guided through the dual-polarity reflectron time-of-flight mass spectrometer using a series of high voltages; ultimately reaching two separate detectors used to chemically analyze the positive and negative ions produced from each individual particle. Positive ions provide information on the source of the particle (e.g., ocean versus coal combustion), while negative ions provide insight into secondary species acquired during atmospheric processing [Guazzotti *et al.*, 2003; Noble and Prather, 1997].

The standard ATOFMS was used for chemical analysis in Chapters 2-3, and 5-6. Modified versions called the ultrafine (UF)-ATOFMS and aircraft (A)-ATOFMS were also used in Chapters 4 and 5, respectively. The UF-ATOFMS, shown in Figure 1.1b, measures aerosols between 0.1-1.0 μm using an aerodynamic lens inlet [Liu *et al.*, 1995;

Su et al., 2004]. The A-ATOFMS is a compact version of the ATOFMS, packaged to fit on a double wide aircraft rack [*Pratt et al., 2009d*]. The inlet and sizing regions are similar to the UF-ATOFMS, with the major difference being the compact Z-shaped dual-polarity mass spectrometer and optically decoupled detectors for better mass resolution, as shown in Figure 1.2. The A-ATOFMS also utilizes an aerodynamic lens inlet, but focuses particles from 0.1-2.5 μm . Mass spectra acquired for each individual particle were imported into YAADA (www.yaada.org), a software toolkit for analysis using Matlab (The Mathworks, Inc.). Individual particle mass spectra were classified into separate clusters depending on the presence and intensity of ion peaks. For the smaller datasets in Chapters 5 and 6, mass spectra were manually classified into similar classifications. For the larger datasets, an adaptive resonance theory-based clustering method (ART-2a) [*Song et al., 1999a*] was used to classify and group single-particle mass spectra with a vigilance factor of 0.80, learning rate of 0.05, and 20 iterations followed by regrouping with a vigilance factor of 0.85. The most populated 50-100 clusters accounted for >90% of the total ART-2a classified particles and are thus representative of the overall aerosol composition during each study presented herein. Peak identifications in this dissertation correspond to the most probable ions for a given m/z ratio based on previous lab and field studies.

1.5. Key Outstanding Questions Regarding Distributions of Aerosols and Cloud Seeds

Although substantial progress has been made to understand the chemical composition and properties of aerosols and how they may impact human health and serve as cloud seeds, previous observational work has predominantly focused on either one intensive study or inter-seasonal measurements at one location [e.g., *Ham and Kleeman, 2011*]. For instance, transport of dust to the west coast of the United States from Asia is typically the most frequent in April, and is therefore the time period of focus for many dust transport studies [e.g., *Husar et al., 2001*; *Uno et al., 2011*]. However, dust transport can occur earlier in the winter and the frequency, timing, transport patterns, and sources may change on a yearly basis. Previous work on the spatial and temporal distributions of

aerosols primarily focuses on health effects [e.g., *Pope III et al.*, 2009], while distributions of CCN and IN are limited except for modeling studies [e.g., *Aquila et al.*, 2010; *Yu and Luo*, 2009], which still have several uncertainties associated with them. The main questions to address regarding distributions of aerosols and cloud seeds in different regions include:

1. What types of aerosols affect air quality and serve as CCN or IN at similar sites and how do they compare to each other?
2. The ultimate fate of CCN and IN effects is dependent on size and chemical composition. Can this change abruptly on a given spatial and temporal scale, even in one location?
3. How do aerosol properties and sources change on a yearly basis at particular sites, including at remote and urban sites?
4. What are the different transport mechanisms (i.e., microscale, mesoscale, and synoptic scale dynamics) that affect these specific remote and urban sites?
5. Can a larger scale distribution or even a global picture of these cloud seeds, and hence resulting precipitation effects, be developed based on studies similar to those presented in this dissertation?

1.6. Synopsis and Goals of the Dissertation

The goals of this dissertation are to address these questions by investigating the physicochemical properties of aerosols at various locations and in most cases for long time periods. Chapter 2 investigates the changes in chemical composition of aerosols in a highly populated urban area of Riverside, CA during three consecutive summers. Aerosol chemistry was vastly different during all three summers namely due to differences in meteorological conditions, which impacted the dominant sources and chemical mixing states. Chapter 3 also focuses on an urban area, Atlanta, GA, but investigated the vast changes on typical urban aerosol composition due to influences from TCs. Precipitation during the TCs removed the CCN-active, aged organic aerosols present before TCs while

the fast winds transported fresh sea-spray to the sampling site. The overall decrease in CCN concentrations from before, during, and after the TCs potentially impacted regional cloud formation by removing the seeds that cloud droplets form upon. Chapter 4 transitions to a remote site, Sugar Pine Dam (SPD), in the California Sierra Nevada Mountains by investigating the source of CCN formed *in situ* from gas phase amines and SO₂ during the 2009 winter season. Interestingly, long-range transport of SO₂ from Asia appeared to potentially play a role in NPF during faster particle growth. Chapter 5 continues the examination of the sources of cloud seeds in the Sierra Nevada by investigating the chemical composition of aerosols as insoluble residues in precipitation samples and in cloud residues via aircraft measurements during the 2011 winter season. Dust and biological aerosols, transported from as far as the Sahara, appeared as cloud residues in high altitude clouds coincident with elevated IN concentrations and precipitation initiated in the ice phase. Chapter 6 presents an inter-annual comparison of insoluble precipitation residues during the 2009-2011 winter seasons at SPD. The chemical composition of the precipitation residues was linked with trends in precipitation type and quantity, and cloud microphysical properties during the three consecutive winters and at multiple remote sites in addition to SPD in the Sierra Nevada. Overall, the work presented in this dissertation is an attempt to develop a more detailed picture of CCN and IN over time and on a large spatial scale. However, future observations involving more locations and over longer periods of time are needed, as discussed in Chapter 7.

1.7. Acknowledgements

Melanie Zauscher is acknowledged for helping edit this chapter.

1.8. Figures

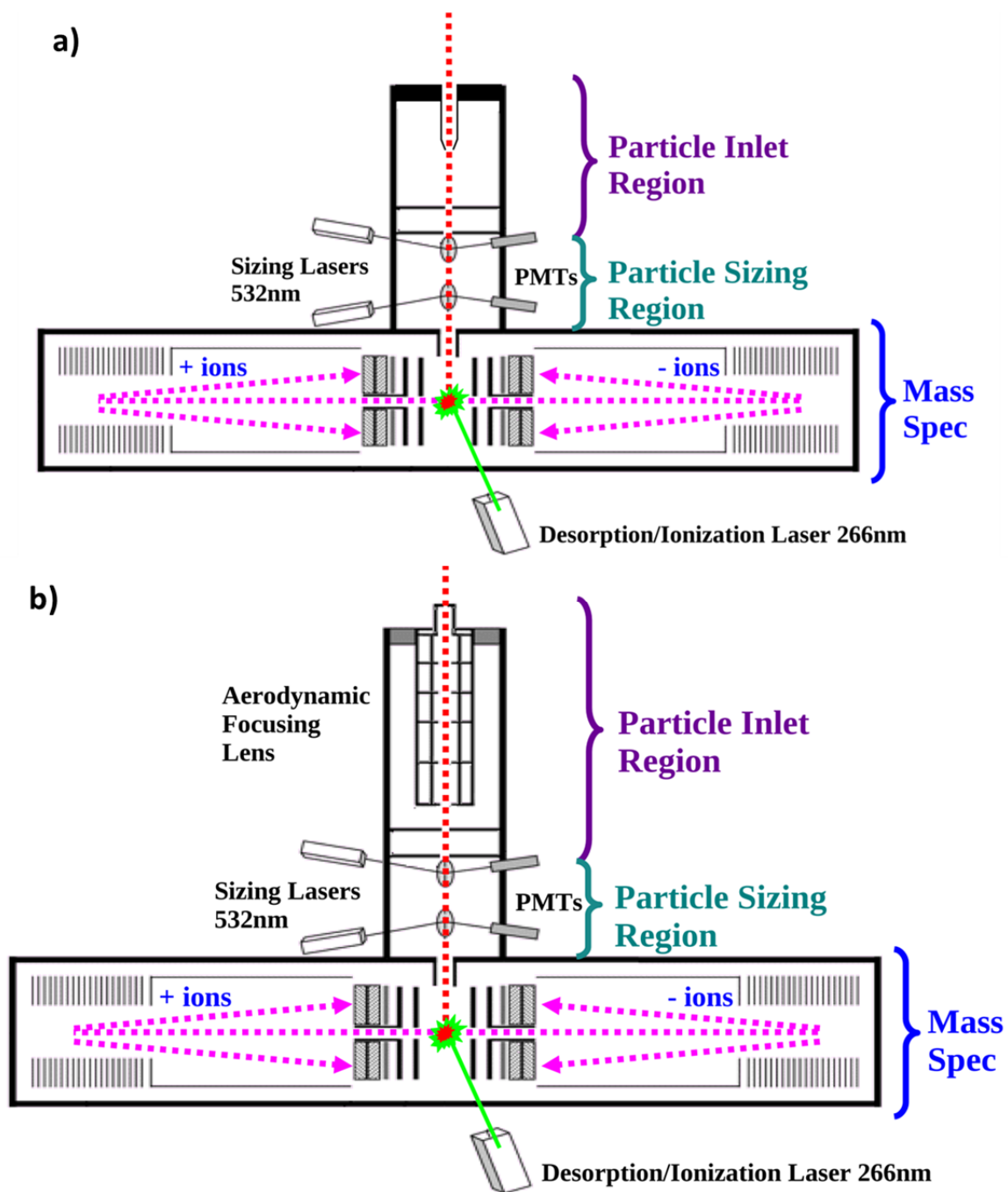


Figure 1.1 a) Schematic of the standard, nozzle inlet ATOFMS adapted from Gard et al., 1997 and b) schematic of the aerodynamic inlet UF-ATOFMS adapted from Su et al., 2004.

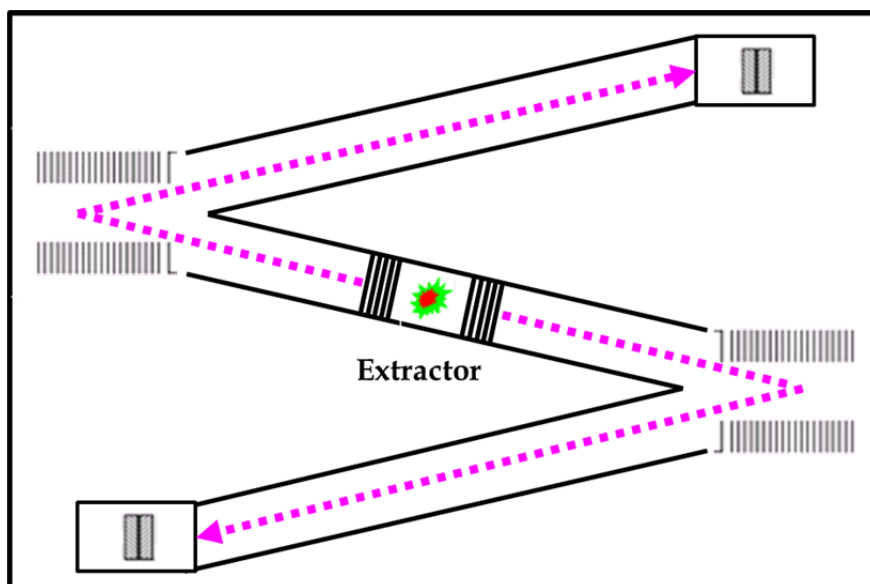


Figure 1.2 Simplified top-view schematic of A-ATOFMS Z-shaped dual polarity mass spectrometer adapted from Pratt *et al.*, 2009.

1.9. References

- Adachi, K., and P.R. Buseck, Internally mixed soot, sulfates, and organic matter in aerosol particles from Mexico City, *Atmospheric Chemistry and Physics*, 8 (21), 6469-6481, 2008.
- Albrecht, B.A., Aerosols, cloud microphysics, and fractional cloudiness, *Science*, 245 (4923), 1227-1230, 1989.
- Allen, J.O., Quantitative Analysis of Aerosol Time-of-Flight Mass Spectrometry Data using YAADA, Arizona State University, Tempe, 2004.
- Alston, E.J., I.N. Sokolik, and B.G. Doddridge, Investigation into the Use of Satellite Data in Aiding Characterization of Particulate Air Quality in the Atlanta, Georgia Metropolitan Area, *Journal of the Air & Waste Management Association*, 61 (2), 211-225, 2011.
- Amato, P., M. Parazols, M. Sancelme, G. Mailhot, P. Laj, and A.-M. Delort, An important oceanic source of micro-organisms for cloud water at the puy de Dôme (France), *Atmos. Environ.*, 41, 8253–8263, 2007.
- Andreae, M.O., and D. Rosenfeld, Aerosol-cloud-precipitation interactions. Part 1. The nature and sources of cloud-active aerosols, *Earth-Science Reviews*, 89 (1-2), 13-41, 2008.

- Andreae, M.O., D. Rosenfeld, P. Artaxo, A.A. Costa, G.P. Frank, K.M. Longo, and M.A.F. Silva-Dias, Smoking rain clouds over the Amazon, *Science*, 303 (5662), 1337-1342, 2004.
- Andreas, E.L., and K.A. Emanuel, Effects of sea spray on tropical cyclone intensity, *Journal of the Atmospheric Sciences*, 58 (24), 3741-3751, 2001.
- Angelino, S., D.T. Suess, and K.A. Prather, Formation of aerosol particles from reactions of secondary and tertiary alkylamines: Characterization by aerosol time-of-flight mass spectrometry, *Environmental Science & Technology*, 35 (15), 3130-3138, 2001a.
- Angelino, S., D.T. Suess, and K.A. Prather, Formation of aerosol particles from reactions of secondary and tertiary alkylamines: Characterization by aerosol time-of-flight mass spectrometry, *Environ. Sci. Technol.*, 35 (15), 3130-3138, 2001b.
- Appel, B.R., E.L. Kothny, E.M. Hoffer, G.M. Hidy, and J.J. Wesolowski, Sulfate and Nitrate Data from California Aerosol Characterization Experiment (Achex), *Environmental Science & Technology*, 12 (4), 418-425, 1978.
- Aquila, V., J. Hendricks, A. Lauer, N. Riemer, H. Vogel, D. Baumgardner, J.P. Schwartz, J.R. Spackman, B. Weinzierl, M. Righi, and M. Dall'Amico, MADE-IN: a new aerosol microphysics submodel for global simulation of potential atmospheric ice nuclei, *Geosci. Model Dev. Discuss.*, 3, 2221-2290, 2010.
- Ault, A.P., C.R. Williams, A.B. White, P.J. Neiman, J.M. Creamean, C.J. Gaston, F.M. Ralph, and K.A. Prather, Detection of Asian dust in California orographic precipitation *Journal of Geophysical Research-Atmospheres*, 116 (D16205), doi:10.1029/2010JD015351, 2011a.
- Ault, A.P., C.R. Williams, A.B. White, P.J. Neiman, J.M. Creamean, C.J. Gaston, F.M. Ralph, and K.A. Prather, Detection of Asian dust in California orographic precipitation, *Journal of Geophysical Research-Atmospheres*, 116, 2011b.
- Aylor, D.E., A Framework for Examining Interregional Aerial Transport of Fungal Spores, *Agricultural and Forest Meteorology*, 38 (4), 263-288, 1986.
- Baltensperger, U., N. Streit, E. Weingartner, S. Nyeki, A.S.H. Prevot, R. Van Dingenen, A. Virkkula, J.P. Putaud, A. Even, H. ten Brink, A. Blatter, A. Neftel, and H.W. Gaggeler, Urban and rural aerosol characterization of summer smog events during the PIPAPO field campaign in Milan, Italy, *Journal of Geophysical Research-Atmospheres*, 107 (D22), 2002.
- Bao, J.W., S.A. Michelson, P.O.G. Persson, I.V. Djalalova, and J.M. Wilczak, Observed and WRF-simulated low-level winds in a high-ozone episode during the Central California Ozone Study, *J. Appl. Meteorol. Clim.*, 47 (9), 2372-2394, 2008.

- Barsanti, K.C., P.H. McMurry, and J.N. Smith, The potential contribution of organic salts to new particle growth, *Atmos. Chem. Phys. Discuss.*, 9 (9), 2949-2957, 2009.
- Bauer, H., A. Kasper-Giebl, M. Loflund, H. Giebl, R. Hitzemberger, F. Zibuschka, and H. Puxbaum, The contribution of bacteria and fungal spores to the organic carbon content of cloud water, precipitation and aerosols, *Atmospheric Research*, 64 (1-4), 109-119, 2002.
- Bergeron, T., On the physics of cloud and precipitation, in 5th Assembly of the U.G.G.I., pp. 156-178, Paul Dupont, Paris, 1935.
- Berndt, T., F. Stratmann, M. Sipila, J. Vanhanen, T. Petaja, J. Mikkila, A. Gruner, G. Spindler, R.L. Mauldin III, J. Curtius, M. Kulmala, and J. Heintzenberg, Laboratory study on new particle formation from reaction OH + SO₂: influence of experimental conditions, H₂O vapour, NH₃ and the amine tert-butylamine on the overall process, *Atmos. Chem. Phys.*, 10, 6447-6484, 2010.
- Beven II, J.L., and T.B. Kimberlain, Tropical Cyclone Report Hurricane Gustav, pp. 1-38, NOAA National Hurricane Center, 2009.
- Bhave, P.V., J.O. Allen, B.D. Morrical, D.P. Fergenson, G.R. Cass, and K.A. Prather, A field-based approach for determining ATOFMS instrument sensitivities to ammonium and nitrate, *Environmental Science & Technology*, 36 (22), 4868-4879, 2002a.
- Bhave, P.V., J.O. Allen, B.D. Morrical, D.P. Fergenson, G.R. Cass, and K.A. Prather, A field-based approach for determining ATOFMS instrument sensitivities to ammonium and nitrate, *Environ. Sci. Technol.*, 36 (22), 4868-4879, 2002b.
- Bigg, E.K., and C. Leck, The composition of fragments of bubbles bursting at the ocean surface, *Journal of Geophysical Research-Atmospheres*, 113 (D11), 2008.
- Birmili, W., K. Schepanski, A. Ansmann, G. Spindler, I. Tegen, B. Wehner, A. Nowak, E. Reimer, I. Mattis, K. Muller, E. Brüggemann, T. Gnauk, H. Herrmann, A. Wiedensohler, D. Althausen, A. Schladitz, T. Tuch, and G. Loschau, A case of extreme particulate matter concentrations over Central Europe caused by dust emitted over the southern Ukraine, *Atmospheric Chemistry and Physics*, 8 (4), 997-1016, 2008.
- Blanchard, C.L., G.M. Hidy, S. Tanenbaum, and E.S. Edgerton, NMOC, ozone, and organic aerosol in the southeastern United States, 1999-2007: 3. Origins of organic aerosol in Atlanta, Georgia, and surrounding areas, *Atmospheric Environment*, 45 (6), 1291-1302, 2011.
- Borys, R.D., D.H. Lowenthal, and D.L. Mitchell, The relationships among cloud microphysics, chemistry, and precipitation rate in cold mountain clouds, *Atmospheric Environment*, 34 (16), 2593-2602, 2000.

- Boucher, O., and U. Lohmann, The Sulfate-CCN-Cloud Albedo Effect - a Sensitivity Study with 2 General-Circulation Models, *Tellus Series B-Chemical and Physical Meteorology*, 47 (3), 281-300, 1995.
- Brook, R.D., S. Rajagopalan, C.A. Pope, J.R. Brook, A. Bhatnagar, A.V. Diez-Roux, F. Holguin, Y.L. Hong, R.V. Luepker, M.A. Mittleman, A. Peters, D. Siscovick, S.C. Smith, L. Whitsel, J.D. Kaufman, A.H.A.C. Epidemiol, C.K.C. Dis, and C.N.P.A. Metab, Particulate Matter Air Pollution and Cardiovascular Disease An Update to the Scientific Statement From the American Heart Association, *Circulation*, 121 (21), 2331-2378, 2010.
- Brown, D.P., and T.B. Kimberlain, Tropical Cyclone Report Hurricane Hanna, pp. 1-36, NOAA National Hurricane Center, 2008.
- Bukowiecki, N., D.B. Kittelson, W.F. Watts, H. Burtscher, E. Weingartner, and U. Baltensperger, Real-time characterization of ultrafine and accumulation mode particles in ambient combustion aerosols, *J. Aerosol Sci.*, 33 (8), 1139-1154, 2002.
- Burge, H.A., and W.R. Solomon, Sampling and Analysis of Biological Aerosols, *Atmospheric Environment*, 21 (2), 451-456, 1987.
- Bzdek, B.R., D.P. Ridge, and M.V. Johnston, Size-dependent reactions of ammonium bisulphate clusters with dimethylamine, *J. Phys. Chem. A*, 114 (43), 11638-11644, 2010.
- Carroll, J.J., and A.J. Dixon, Regional scale transport over complex terrain, a case study: tracing the Sacramento plume in the Sierra Nevada of California, *Atmospheric Environment*, 36 (23), 3745-3758, 2002.
- Chang, L.S., S.E. Schwartz, R. McGraw, and E.R. Lewis, Sensitivity of aerosol properties to new particle formation mechanism and to primary emissions in a continental-scale chemical transport model, *J. Geophys. Res.*, 114, D07203, doi:10.1029/2008JD011019, 2009.
- Chang, L.T.C., J.H. Tsai, J.M. Lin, Y.S. Huang, and H.L. Chiang, Particulate matter and gaseous pollutants during a tropical storm and air pollution episode in Southern Taiwan, *Atmospheric Research*, 99 (1), 67-79, 2011.
- Charlson, R.J., J.E. Lovelock, M.O. Andreae, and S.G. Warren, Oceanic Phytoplankton, Atmospheric Sulfur, Cloud Albedo and Climate, *Nature*, 326 (6114), 655-661, 1987.
- Choi, Y.S., R.S. Lindzen, C.H. Ho, and J. Kim, Space observations of cold-cloud phase change, *Proceedings of the National Academy of Sciences of the United States of America*, 107 (25), 11211-11216, 2010.

- Choulaton, T.W., and S.J. Perry, A Model of the Orographic Enhancement of Snowfall by the Seeder-Feeder Mechanism, *Quarterly Journal of the Royal Meteorological Society*, 112 (472), 335-345, 1986.
- Chow, J.C., J.G. Watson, E.M. Fujita, Z.Q. Lu, D.R. Lawson, and L.L. Ashbaugh, Temporal and Spatial Variations of Pm(2.5) and Pm(10) Aerosol in the Southern California Air-Quality Study, *Atmospheric Environment*, 28 (12), 2061-2080, 1994.
- Christner, B.C., C.E. Morris, C.M. Foreman, R.M. Cai, and D.C. Sands, Ubiquity of biological ice nucleators in snowfall, *Science*, 319 (5867), 1214-1214, 2008.
- Chubarova, N.Y., M.A. Sviridenkov, A. Smirnov, and B.N. Holben, Assessments of urban aerosol pollution in Moscow and its radiative effects, *Atmospheric Measurement Techniques*, 4 (2), 367-378, 2011.
- Churchill, D.D., and R.A. Houze, Mesoscale Updraft Magnitude and Cloud-Ice Content Deduced from the Ice Budget of the Stratiform Region of a Tropical Cloud Cluster, *Journal of the Atmospheric Sciences*, 41 (10), 1717-1725, 1984.
- Cione, J.J., and E.W. Uhlhorn, Sea surface temperature variability in hurricanes: Implications with respect to intensity change, *Monthly Weather Review*, 131 (8), 1783-1796, 2003.
- Clement, C.F., I.J. Ford, C.H. Twohy, A. Weinheimer, and T. Campos, Particle production in the outflow of a midlatitude storm, *J. Geophys. Res.*, 107 (D21), 4559, doi:10.1029/2001JD001352, 2002.
- Colle, B.A., and Y.G. Zeng, Bulk microphysical sensitivities within the MM5 for orographic precipitation. Part I: The Sierra 1986 event, *Monthly Weather Review*, 132 (12), 2780-2801, 2004.
- Collett, J.L., B.C. Daube, D. Gunz, and M.R. Hoffmann, Intensive Studies of Sierra-Nevada Cloudwater Chemistry and Its Relationship to Precursor Aerosol and Gas Concentrations, *Atmospheric Environment Part a-General Topics*, 24 (7), 1741-1757, 1990a.
- Collett, J.L., B.C. Daube, D. Gunz, and M.R. Hoffmann, Intensive studies of Sierra-Nevada cloudwater chemistry and its relationship to precursor aerosol and gas concentrations, *Atmos. Environ. a-Gen.*, 24 (7), 1741-1757, 1990b.
- Conen, F., C.E. Morris, J. Leifeld, M.V. Yakutin, and C. Alewell, Biological residues define the ice nucleation properties of soil dust, *Atmospheric Chemistry and Physics*, 11 (18), 9643-9648, 2011.
- Covert, D.S., V.N. Kapustin, P.K. Quinn, and T.S. Bates, New particle formation in the marine boundary-layer, *J. Geophys. Res.*, 97 (D18), 20581-20589, 1992.

- Creamean, J.M., A.P. Ault, J.E. Ten Hoeve, M.Z. Jacobson, G.C. Roberts, and K.A. Prather, Measurements of Aerosol Chemistry during New Particle Formation Events at a Remote Rural Mountain Site, *Environmental Science & Technology*, 45 (19), 8208-8216, 2011.
- Creamean, J.M., K.J. Suski, A. Carzola, D.B. Collins, A.B. White, F.M. Ralph, P. Minnis, J.K. Ayers, R. Palikonda, D. Rosenfeld, and K.A. Prather, Long Range Transported Dust and Biological Aerosols Impact Precipitation during Multiple Winters in the Sierra Nevada, *Science*, in prep., 2012.
- Czerwieniec, G.A., S.C. Russell, H.J. Tobias, M.E. Pitesky, D.P. Fergenson, P. Steele, A. Srivastava, J.M. Horn, M. Frank, E.E. Gard, and C.B. Lebrilla, Stable isotope labeling of entire *Bacillus atrophaeus* spores and vegetative cells using bioaerosol mass spectrometry, *Analytical Chemistry*, 77 (4), 1081-1087, 2005.
- Dal Maso, M., M. Kulmala, K.E.J. Lehtinen, J.M. Mäkelä, P. Aalto, and C.D. O'Dowd, Condensation and coagulation sinks and formation of nucleation mode particles in coastal and boreal forest boundary layers, *J. Geophys. Res.*, 107 (D15), 8097, doi:10.1029/2001JD001053, 2002.
- DeMott, P.J., A.J. Prenni, X. Liu, S.M. Kreidenweis, M.D. Petters, C.H. Twohy, M.S. Richardson, T. Eidhammer, and D.C. Rogers, Predicting global atmospheric ice nuclei distributions and their impacts on climate, *Proceedings of the National Academy of Sciences of the United States of America*, 107 (25), 11217-11222, 2010.
- DeMott, P.J., K. Sassen, M.R. Poellot, D. Baumgardner, D.C. Rogers, S.D. Brooks, A.J. Prenni, and S.M. Kreidenweis, African dust aerosols as atmospheric ice nuclei, *Geophysical Research Letters*, 30 (14), 2003.
- Deshler, T., and D.W. Reynolds, Physical Response of Winter Orographic Clouds over the Sierra-Nevada to Airborne Seeding Using Dry Ice or Silver-Iodide, *Journal of Applied Meteorology*, 29 (4), 288-330, 1990.
- Despres, V.R., J.A. Huffman, S.M. Burrows, C. Hoose, A.S. Safatov, G. Buryak, J. Frohlich-Nowoisky, W. Elbert, M.O. Andreae, U. Poschl, and R. Jaenicke, Primary biological aerosol particles in the atmosphere: a review, *Tellus Series B-Chemical and Physical Meteorology*, 64 (015598), DOI: 10.3402/tellusb.v64i0.15598, 2012.
- Dettinger, M., F.M. Ralph, T. Das, P.J. Neiman, and D.R. Cayan, Atmospheric Rivers, Floods and the Water Resources of California, *Water*, 3, 445-478; doi:10.3390/w3020445, 2011.
- Docherty, K.S., A.C. Aiken, J.A. Huffman, I.M. Ulbrich, P.F. DeCarlo, D. Sueper, D.R. Worsnop, D.C. Snyder, B.D. Grover, D.J. Eatough, A.H. Goldstein, P.J. Ziemann, and J.L. Jimenez, The 2005 Study of Organic Aerosols at Riverside (SOAR-1):

- instrumental intercomparisons and fine particle composition, *Atmos. Chem. Phys. Discuss.*, 11, 6301–6362, 2011.
- Docherty, K.S., E.A. Stone, I.M. Ulbrich, P.F. DeCarlo, D.C. Snyder, J.J. Schauer, R.E. Peltier, R.J. Weber, S.M. Murphy, J.H. Seinfeld, B.D. Grover, D.J. Eatough, and J.L. Jimenez, Apportionment of Primary and Secondary Organic Aerosols in Southern California during the 2005 Study of Organic Aerosols in Riverside (SOAR-1), *Environmental Science & Technology*, 42 (20), 7655-7662, 2008.
- Dockery, D.W., J. Cunningham, A.I. Damokosh, L.M. Neas, J.D. Spengler, P. Koutrakis, J.H. Ware, M. Raizenne, and F.E. Speizer, Health effects of acid aerosols on North American children: Respiratory symptoms, *Environmental Health Perspectives*, 104 (5), 500-505, 1996.
- Dore, A.J., M. Sobik, and K. Migala, Patterns of precipitation and pollutant deposition in the western Sudete mountains, Poland, *Atmospheric Environment*, 33 (20), 3301-3312, 1999.
- Draxler, R.R., and G.D. Rolph, HYSPLIT (HYbrid Single Particle Lagrangian Integrated Trajectory) v. 4.8 Model access via NOAA ARL READY Website (<http://www.arl.noaa.gov/ready/hysplit4.html>), NOAA Air Resources Laboratory, Silver Spring, MD, 2003.
- Draxler, R.R., and G.D. Rolph, HYSPLIT (HYbrid Single-Particle Lagrangian Integrated Trajectory) Model access via NOAA ARL READY Website (<http://ready.arl.noaa.gov/HYSPLIT.php>), NOAA Air Resources Laboratory, Silver Spring, MD, 2011a.
- HYSPLIT (HYbrid Single-Particle Lagrangian Integrated Trajectory) Model access via NOAA ARL READY Website (<http://ready.arl.noaa.gov/HYSPLIT.php>), NOAA Air Resources Laboratory, Silver Spring, MD. 2011b.
- Dymarska, M., B.J. Murray, L.M. Sun, M.L. Eastwood, D.A. Knopf, and A.K. Bertram, Deposition ice nucleation on soot at temperatures relevant for the lower troposphere, *Journal of Geophysical Research-Atmospheres*, 111 (D4), 2006.
- Edinger, J.G., Modification of the Marine Layer over Coastal Southern California, *Journal of Applied Meteorology*, 2 (6), 706-712, 1963.
- Ehn, M., H. Vuollekoski, T. Petäjä, V.M. Kerminen, M. Vana, P. Aalto, G. de Leeuw, D. Ceburnis, R. Dupuy, C.D. O'Dowd, and M. Kulmala, Growth rates during coastal and marine new particle formation in western Ireland, *J. Geophys. Res.*, 115, D18218, doi:10.1029/2010JD014292, 2010.
- Elbert, W., P.E. Taylor, M.O. Andreae, and U. Poschl, Contribution of fungi to primary biogenic aerosols in the atmosphere: wet and dry discharged spores, carbohydrates, and inorganic ions, *Atmospheric Chemistry and Physics*, 7 (17), 4569-4588, 2007.

- Facchini, M.C., M. Rinaldi, S. Decesari, C. Carbone, E. Finessi, M. Mircea, S. Fuzzi, D. Ceburnis, R. Flanagan, E.D. Nilsson, G. de Leeuw, M. Martino, J. Woeltjen, and C.D. O'Dowd, Primary submicron marine aerosol dominated by insoluble organic colloids and aggregates, *Geophysical Research Letters*, 35 (17), 2008.
- Feng, Y.R., A.Y. Wang, D. Wu, and X.D. Xu, The influence of tropical cyclone Melor on PM10 concentrations during an aerosol episode over the Pearl River Delta region of China: Numerical modeling versus observational analysis, *Atmospheric Environment*, 41 (21), 4349-4365, 2007.
- Ferguson, D.P., M.E. Pitesky, H.J. Tobias, P.T. Steele, G.A. Czerwieniec, S.C. Russell, C.B. Lebrilla, J.M. Horn, K.R. Coffee, A. Srivastava, S.P. Pillai, M.-T.P. Shih, H.L. Hall, A.J. Ramponi, J.T. Chang, R.G. Langlois, P.L. Estacio, R.T. Hadley, M. Frank, and E.E. Gard, Reagentless Detection and Classification of Individual Bioaerosol Particles in Seconds, *Analytical Chemistry*, 76 (2), 373-378, 2003.
- Ferguson, D.P., M.E. Pitesky, H.J. Tobias, P.T. Steele, G.A. Czerwieniec, S.C. Russell, C.B. Lebrilla, J.M. Horn, K.R. Coffee, A. Srivastava, S.P. Pillai, M.T.P. Shih, H.L. Hall, A.J. Ramponi, J.T. Chang, R.G. Langlois, P.L. Estacio, R.T. Hadley, M. Frank, and E.E. Gard, Reagentless detection and classification of individual bioaerosol particles in seconds, *Analytical Chemistry*, 76 (2), 373-378, 2004.
- Field, P.R., O. Mohler, P. Connolly, M. Kramer, R. Cotton, A.J. Heymsfield, H. Saathoff, and M. Schnaiter, Some ice nucleation characteristics of Asian and Saharan desert dust, *Atmospheric Chemistry and Physics*, 6, 2991-3006, 2006.
- Fine, P.M., B. Chakrabarti, M. Krudysz, J.J. Schauer, and C. Sioutas, Diurnal variations of individual organic compound constituents of ultrafine and accumulation mode particulate matter in the Los Angeles basin, *Environmental Science & Technology*, 38 (5), 1296-1304, 2004.
- Finlayson-Pitts, B.J., Pitts, J. N., *Chemistry of the Upper and Lower Atmosphere*, Academic Press, San Diego, 2000.
- Fisher, J.A., D.J. Jacob, M.T. Purdy, M. Kopacz, P. Le Sager, C. Carouge, C.D. Holmes, R.M. Yantosca, R.L. Batchelor, K. Strong, G.S. Diskin, H.E. Fuelberg, J.S. Holloway, E.J. Hyer, W.W. McMillan, J. Warner, D.G. Streets, Q. Zhang, Y. Wang, and S. Wu, Source attribution and interannual variability of Arctic pollution in spring constrained by aircraft (ARCTAS, ARCPAC) and satellite (AIRS) observations of carbon monoxide, *Atmospheric Chemistry and Physics*, 10 (3), 977-996, 2010.
- Foltescu, V.L., S.C. Pryor, and C. Bennet, Sea salt generation, dispersion and removal on the regional scale, *Atmospheric Environment*, 39 (11), 2123-2133, 2005.
- Fowler, D., I.D. Leith, J. Binnie, A. Crossley, D.W.F. Inglis, T.W. Choularton, M. Gay, J.W.S. Longhurst, and D.E. Conland, Orographic enhancement of wet deposition

in the United Kingdom: Continuous monitoring, *Water Air and Soil Pollution*, 85 (4), 2107-2112, 1995.

- Friedman, B., H. Herich, L. Kammermann, D.S. Gross, A. Arneth, T. Holst, and D.J. Cziczo, Subarctic atmospheric aerosol composition: 1. Ambient aerosol characterization, *J. Geophys. Res.*, 114, D13203, doi:10.1029/2009JD011772, 2009.
- Friedman, B., G. Kulkarni, J. Beranek, A. Zelenyuk, J.A. Thornton, and D.J. Cziczo, Ice nucleation and droplet formation by bare and coated soot particles, *Journal of Geophysical Research-Atmospheres*, 116, 2011.
- Gard, E., J.E. Mayer, B.D. Morrical, T. Dienes, D.P. Fergenson, and K.A. Prather, Real-time analysis of individual atmospheric aerosol particles: Design and performance of a portable ATOFMS, *Anal. Chem.*, 69 (20), 4083-4091, 1997a.
- Gard, E., J.E. Mayer, B.D. Morrical, T. Dienes, D.P. Fergenson, and K.A. Prather, Real-time analysis of individual atmospheric aerosol particles: Design and performance of a portable ATOFMS, *Analytical Chemistry*, 69 (20), 4083-4091, 1997b.
- Gard, E.E., M.J. Kleeman, D.S. Gross, L.S. Hughes, J.O. Allen, B.D. Morrical, D.P. Fergenson, T. Dienes, M.E. Galli, R.J. Johnson, G.R. Cass, and K.A. Prather, Direct observation of heterogeneous chemistry in the atmosphere, *Science*, 279 (5354), 1184-1187, 1998.
- Gaston, C.J., H. Furutani, S.A. Guazzotti, K.R. Coffee, T.S. Bates, P.K. Quinn, L.I. Aluwihare, B.G. Mitchell, and K.A. Prather, Unique ocean-derived particles serve as a proxy for changes in ocean chemistry, *Journal of Geophysical Research-Atmospheres*, 116, 2011.
- Geller, M.D., P.M. Fine, and C. Sioutas, The relationship between real-time and time-integrated coarse (2.5-10 μm), intermodal (1-2.5 μm), and fine (< 2.5 μm) particulate matter in the Los Angeles Basin, *Journal of the Air & Waste Management Association*, 54 (9), 1029-1039, 2004.
- Givati, A., and D. Rosenfeld, Quantifying precipitation suppression due to air pollution, *Journal of Applied Meteorology*, 43 (7), 1038-1056, 2004.
- Graham, S.C., J.B. Homer, and J.L.J. Rosenfeld, The Formation and Coagulation of Soot Aerosols Generated by the Pyrolysis of Aromatic Hydrocarbons, *Proc. R. Soc. Lond. A.*, 344, 259-285, 1975.
- Greene, N.A., V.R. Morris, A. Aikin, W. Hoegy, and D. Silberman, Use of the electrostatic classification method to investigate the size distribution of aerosols near Hurricane Erika, in *5th Conference on Atmospheric Chemistry: Gases, Aerosols, and Clouds*, Long Beach, CA, 2003.

- Griffin, D.W., C.A. Kellogg, V.H. Garrison, and E.A. Shinn, The global transport of dust - An intercontinental river of dust, microorganisms and toxic chemicals flows through the Earth's atmosphere, *American Scientist*, 90 (3), 228-235, 2002.
- Guan, B., N.P. Molotch, D.E. Waliser, E.J. Fetzer, and P.J. Neiman, Extreme snowfall events linked to atmospheric rivers and surface air temperature via satellite measurements, *Geophysical Research Letters*, 37, 2010.
- Guazzotti, S.A., D.T. Suess, K.R. Coffee, P.K. Quinn, T.S. Bates, A. Wisthaler, A. Hansel, W.P. Ball, R.R. Dickerson, C. Neususs, P.J. Crutzen, and K.A. Prather, Characterization of carbonaceous aerosols outflow from India and Arabia: Biomass/biofuel burning and fossil fuel combustion, *Journal of Geophysical Research-Atmospheres*, 108 (D15), 2003.
- Hallar, A.G., G. Chirokova, I. McCubbin, T.H. Painter, C. Wiedinmyer, and C. Dodson, Atmospheric bioaerosols transported via dust storms in the western United States, *Geophysical Research Letters*, 38, 2011.
- Ham, W.A., and M.J. Kleeman, Size-resolved source apportionment of carbonaceous particulate matter in urban and rural sites in central California, *Atmospheric Environment*, 45, 3988-3995, 2011.
- Hansen, A.D.A., and H. Rosen, Horizontal Inhomogeneities in the Particulate Carbon Component of the Arctic Haze, *Atmos. Environ.*, 19 (12), 2175-2180, 1985.
- Harrison, R.M., and J.X. Yin, Particulate matter in the atmosphere: which particle properties are important for its effects on health?, *Science of the Total Environment*, 249 (1-3), 85-101, 2000.
- Hatch, L.E., J.M. Creamean, A.P. Ault, J.D. Surratt, M.N. Chan, J.H. Seinfeld, E.S. Edgerton, Y.X. Su, and K.A. Prather, Measurements of Isoprene-Derived Organosulfates in Ambient Aerosols by Aerosol Time-of-Flight Mass Spectrometry - Part 1: Single Particle Atmospheric Observations in Atlanta, *Environmental Science & Technology*, 45 (12), 5105-5111, 2011a.
- Hatch, L.E., J.M. Creamean, A.P. Ault, J.D. Surratt, M.N. Chan, J.H. Seinfeld, E.S. Edgerton, Y.X. Su, and K.A. Prather, Measurements of Isoprene-Derived Organosulfates in Ambient Aerosols by Aerosol Time-of-Flight Mass Spectrometry - Part 2: Temporal Variability & Formation Mechanisms, *Environmental Science & Technology*, Submitted., 2011b.
- Heald, C.L., and D.V. Spracklen, Atmospheric budget of primary biological aerosol particles from fungal spores, *Geophysical Research Letters*, 36, 2009.
- Hennigan, C.J., A.P. Sullivan, C.I. Fountoukis, A. Nenes, A. Hecobian, O. Vargas, R.E. Peltier, A.T.C. Hanks, L.G. Huey, B.L. Lefer, A.G. Russell, and R.J. Weber, On the volatility and production mechanisms of newly formed nitrate and water

- soluble organic aerosol in Mexico City, *Atmospheric Chemistry and Physics*, 8 (14), 3761-3768, 2008.
- Hidy, G.M., B.R. Appel, R.J. Charlson, W.E. Clark, S.K. Friedlander, D.H. Hutchinson, T.B. Smith, J. Suder, J.J. Wesolowski, and K.T. Whitby, Summary of the California Aerosol Characterization Experiment, *Journal of the Air Pollution Control Association*, 25 (11), 1106-1114, 1975.
- Hitzenberger, R., and S. Tohno, Comparison of black carbon (BC) aerosols in two urban areas - concentrations and size distributions, *Atmos. Environ.*, 35 (12), 2153-2167, 2001.
- Hoffmann, T., R.J. Huang, and M. Kalberer, *Atmospheric Analytical Chemistry*, *Analytical Chemistry*, 83 (12), 4649-4664, 2011.
- Hoffmann, T., J.R. Odum, F. Bowman, D. Collins, D. Klockow, R.C. Flagan, and J.H. Seinfeld, Formation of organic aerosols from the oxidation of biogenic hydrocarbons, *Journal of Atmospheric Chemistry*, 26 (2), 189-222, 1997.
- Hogan, T.F., and L.R. Brody, Sensitivity Studies of the Navy Global Forecast Model Parameterizations and Evaluation of Improvements to Nogaps, *Monthly Weather Review*, 121 (8), 2373-2395, 1993.
- Hogan, T.F., and T.E. Rosmond, The Description of the Navy Operational Global Atmospheric Prediction Systems Spectral Forecast Model, *Monthly Weather Review*, 119 (8), 1786-1815, 1991.
- Holecek, J.C., M.T. Spencer, and K.A. Prather, Analysis of rainwater samples: Comparison of single particle residues with ambient particle chemistry from the northeast Pacific and Indian oceans, *Journal of Geophysical Research-Atmospheres*, 112 (D22), 2007.
- Hosler, C.L., D.C. Jensen, and L. Goldshlak, On the Aggregation of Ice Crystals to Form Snow, *Journal of Meteorology*, 14 (5), 415-420, 1957.
- Houze, R.A., *Cloud dynamics*, Academic Press, San Diego, USA, 1993.
- Hsu, S.-C., C.-A. Huh, C.-Y. Lin, W.-N. Chen, N.M. Mahowald, S.-C. Liu, C.C.K. Chou, M.-C. Liang, C.-J. Tsai, F.-J. Lin, J.-P. Chen, and Y.-T. Huang, Dust transport from non-East Asian sources to the North Pacific, *Geophys. Res. Lett.*, 39 (12), L12804, 2012.
- Hua, N.P., F. Kobayashi, Y. Iwasaka, G.Y. Shi, and T. Naganuma, Detailed identification of desert-originated bacteria carried by Asian dust storms to Japan, *Aerobiologia*, 23 (4), 291-298, 2007.
- Hughes, L.S., J.O. Allen, P. Bhave, M.J. Kleeman, G.R. Cass, D.Y. Liu, D.F. Fergenson, B.D. Morrical, and K.A. Prather, Evolution of atmospheric particles along

- trajectories crossing the Los Angeles basin, *Environmental Science & Technology*, 34 (15), 3058-3068, 2000.
- Hughes, L.S., J.O. Allen, L.G. Salmon, P.R. Mayo, R.J. Johnson, and G.R. Cass, Evolution of nitrogen species air pollutants along trajectories crossing the Los Angeles area, *Environmental Science & Technology*, 36 (18), 3928-3935, 2002.
- Husar, R.B., D.M. Tratt, B.A. Schichtel, S.R. Falke, F. Li, D. Jaffe, S. Gasso, T. Gill, N.S. Laulainen, F. Lu, M.C. Reheis, Y. Chun, D. Westphal, B.N. Holben, C. Gueymard, I. McKendry, N. Kuring, G.C. Feldman, C. McClain, R.J. Frouin, J. Merrill, D. DuBois, F. Vignola, T. Murayama, S. Nickovic, W.E. Wilson, K. Sassen, N. Sugimoto, and W.C. Malm, Asian dust events of April 1998, *Journal of Geophysical Research-Atmospheres*, 106 (D16), 18317-18330, 2001.
- IPCC, *Climate Change 2007: The Physical Science Basis. Contribution of Working Group I to the Fourth Assessment Report of the Intergovernmental Panel on Climate Change*, [Solomon, S., D. Qin, M. Manning, Z. Chen, M. Marquis, K.B. Averyt, M. Tignor and H.L. Miller (eds.)] Cambridge University Press, Cambridge, United Kingdom and New York, NY, USA, 2007.
- Isono, K., M. Komabayasi, and A. Ono, The nature and origin of ice nuclei in the atmosphere, *J. Meteorol. Soc. Japan*, 37, 211-233, 1959.
- Jacobson, M.Z., *Fundamentals of Atmospheric Modeling*, Cambridge University Press, New York, 2005.
- Jickells, T.D., Z.S. An, K.K. Andersen, A.R. Baker, G. Bergametti, N. Brooks, J.J. Cao, P.W. Boyd, R.A. Duce, K.A. Hunter, H. Kawahata, N. Kubilay, J. laRoche, P.S. Liss, N. Mahowald, J.M. Prospero, A.J. Ridgwell, I. Tegen, and R. Torres, Global iron connections between desert dust, ocean biogeochemistry, and climate, *Science*, 308 (5718), 67-71, 2005.
- Kanakidou, M., J.H. Seinfeld, S.N. Pandis, I. Barnes, F.J. Dentener, M.C. Facchini, R. Van Dingenen, B. Ervens, A. Nenes, C.J. Nielsen, E. Swietlicki, J.P. Putaud, Y. Balkanski, S. Fuzzi, J. Horth, G.K. Moortgat, R. Winterhalter, C.E.L. Myhre, K. Tsigaridis, E. Vignati, E.G. Stephanou, and J. Wilson, Organic aerosol and global climate modelling: a review, *Atmospheric Chemistry and Physics*, 5, 1053-1123, 2005.
- Kerminen, V.M., H. Lihavainen, M. Komppula, Y. Viisanen, and M. Kulmala, Direct observational evidence linking atmospheric aerosol formation and cloud droplet activation, *Geophys. Res. Lett.*, 32, L14803, doi:10.1029/2005GL02313, 2005.
- Kim, B.M., S. Teffera, and M.D. Zeldin, Characterization of PM_{2.5} and PM₁₀ in the South Coast Air Basin of southern California: Part 1 - Spatial variations, *Journal of the Air & Waste Management Association*, 50 (12), 2034-2044, 2000a.

- Kim, B.M., S. Teffera, and M.D. Zeldin, Characterization of PM_{2.5} and PM₁₀ in the South Coast Air Basin of southern California: Part 2 - Temporal variations, *Journal of the Air & Waste Management Association*, 50 (12), 2045-2059, 2000b.
- Kim, E., P.K. Hopke, and E.S. Edgerton, Improving source identification of Atlanta aerosol using temperature resolved carbon fractions in positive matrix factorization, *Atmospheric Environment*, 38 (20), 3349-3362, 2004.
- Kleeman, M.J., L.S. Hughes, J.O. Allen, and G.R. Cass, Source contributions to the size and composition distribution of atmospheric particles: Southern California in September 1996, *Environmental Science & Technology*, 33 (23), 4331-4341, 1999.
- Kogan, Y.L., D.B. Mechem, and K. Choi, Effects of Sea-Salt Aerosols on Precipitation in Simulations of Shallow Cumulus, *Journal of the Atmospheric Sciences*, 69 (2), 463-483, 2012.
- Kohler, A., Zur kondensation des wasserdampfe in der atmosphre, *Geophys. Publ.*, 2, 3-15, 1921.
- Korolev, A., Limitations of the wegener-bergeron-findeisen mechanism in the evolution of mixed-phase clouds, *Journal of the Atmospheric Sciences*, 64 (9), 3372-3375, 2007.
- Krotkov, M.A., B. McClure, R.R. Dickerson, S.A. Carn, C. Li, P.K. Bhartia, K. Yang, A.J. Krueger, Z. Li, P. Levelt, H. Chen, P. Wang, and D.R. Lu, Validation of SO₂ retrievals from the Ozone Monitoring Instrument (OMI) over NE China, *J. Geophys. Res.*, 113, D16S40, doi:10.1029/2007JD008818, 2008.
- Krotkov, N.A., S.A. Carn, A.J. Krueger, P.K. Bhartia, and K. Yang, Band residual difference algorithm for retrieval of SO₂ from the Aura Ozone Monitoring Instrument (OMI), *IEEE Trans. Geosci. Remote Sensing, AURA Special Issue*, 44 (5), 1259-1266, 2006.
- Kuang, C., P.H. McMurry, and A.V. McCormick, Determination of cloud condensation nuclei production from measured new particle formation events, *Geophys. Res. Lett.*, 36, L09822, doi:10.1029/2009GL037584, 2009.
- Kulmala, M., V.M. Kerminen, and A. Laaksonen, Simulations on the effect of sulphuric acid formation on atmospheric aerosol concentrations, *Atmos. Environ.*, 29 (3), 377-382, 1995.
- Kulmala, M., U. Pirjola, and J.M. Makela, Stable sulphate clusters as a source of new atmospheric particles, *Nature*, 404 (6773), 66-69, 2000.
- Kulmala, M., H. Vehkamaki, T. Petaja, M. Dal Maso, A. Lauri, V.M. Kerminen, W. Birmili, and P.H. McMurry, Formation and growth rates of ultrafine atmospheric particles: a review of observations, *J. Aerosol Sci.*, 35 (2), 143-176, 2004.

- Laaksonen, A., A. Hamed, J. Joutsensaari, L. Hiltunen, F. Cavalli, W. Junkermann, A. Asmi, S. Fuzzi, and M.C. Facchini, Cloud condensation nucleus production from nucleation events at a highly polluted region, *Geophysical Research Letters*, 32 (6), 2005.
- Latzin, P., M. Roosli, A. Huss, C.E. Kuehni, and U. Frey, Air pollution during pregnancy and lung function in newborns: a birth cohort study, *European Respiratory Journal*, 33 (3), 594-603, 2009.
- Lau, K.M., and H.T. Wu, Warm rain processes over tropical oceans and climate implications, *Geophysical Research Letters*, 30 (24), 2003.
- Leung, L.R., and Y. Qian, Atmospheric rivers induced heavy precipitation and flooding in the western US simulated by the WRF regional climate model, *Geophysical Research Letters*, 36, 2009a.
- Leung, L.R., and Y. Qian, Atmospheric rivers induced heavy precipitation and flooding in the western US simulated by the WRF regional climate model, *Geophysical Research Letters*, 36, doi 10.1029/2008gl036445, 2009b.
- Li, C.S., W.H. Lin, and F.T. Jenq, Characterization of Outdoor Submicron Particles and Selected Combustion Sources of Indoor Particles, *Atmospheric Environment Part B-Urban Atmosphere*, 27 (4), 413-424, 1993.
- Li, D.W., and B. Kendrick, A Year-Round Study on Functional-Relationships of Airborne Fungi with Meteorological Factors, *International Journal of Biometeorology*, 39 (2), 74-80, 1995.
- Liu, D.Y., R.J. Wenzel, and K.A. Prather, Aerosol time-of-flight mass spectrometry during the Atlanta Supersite Experiment: 1. Measurements, *Journal of Geophysical Research-Atmospheres*, 108 (D7), -, 2003.
- Liu, J.F., D.L. Mauzerall, and L.W. Horowitz, Evaluating inter-continental transport of fine aerosols:(2) Global health impact, *Atmospheric Environment*, 43 (28), 4339-4347, 2009a.
- Liu, J.F., D.L. Mauzerall, L.W. Horowitz, P. Ginoux, and A.M. Fiore, Evaluating inter-continental transport of fine aerosols: (1) Methodology, global aerosol distribution and optical depth, *Atmospheric Environment*, 43 (28), 4327-4338, 2009b.
- Liu, P., P.J. Ziemann, D.B. Kittelson, and P.H. McMurry, Generating Particle Beams of Controlled Dimensions and Divergence .1. Theory of Particle Motion in Aerodynamic Lenses and Nozzle Expansions, *Aerosol Science and Technology*, 22 (3), 293-313, 1995.
- Lunden, M.M., D.R. Black, M. McKay, K.L. Revzan, A.H. Goldstein, and N.J. Brown, Characteristics of fine particle growth events observed above a forested

- ecosystem in the Sierra Nevada Mountains of California, *Aerosol Science and Technology*, 40 (5), 373-388, 2006a.
- Lunden, M.M., D.R. Black, M. McKay, K.L. Revzan, A.H. Goldstein, and N.J. Brown, Characteristics of fine particle growth events observed above a forested ecosystem in the Sierra Nevada Mountains of California, *Aerosol Sci. Tech.*, 40 (5), 373-388, 2006b.
- Mäkelä, J.M., S. Yli-Koivisto, V. Hiltunen, W. Seidl, E. Swietlicki, K. Teinila, M. Sillanpää, I.K. Koponen, J. Paatero, K. Rosman, and K. Hameri, Chemical composition of aerosol during particle formation events in boreal forest, *Tellus Series B-Chemical and Physical Meteorology*, 53 (4), 380-393, 2001.
- Maki, L.R., E.L. Galyan, Changchi.Mm, and D.R. Caldwell, Ice Nucleation Induced by *Pseudomonas-Syringae*, *Applied Microbiology*, 28 (3), 456-459, 1974.
- Malloy, Q.G.J., L. Qi, B. Warren, D.R. Cocker, M.E. Erupe, and P.J. Silva, Secondary organic aerosol formation from primary aliphatic amines with NO₃ radical, *Atmospheric Chemistry and Physics*, 9 (6), 2051-2060, 2009.
- Mamane, Y., and J. Gottlieb, Nitrate Formation on Sea-Salt and Mineral Particles - a Single-Particle Approach, *Atmospheric Environment Part a-General Topics*, 26 (9), 1763-1769, 1992.
- Mann, M.E., and K.A. Emanuel, Atlantic Hurricane Trends Linked to Climate Change, *Eos Trans. Am. Geophys. Union*, 87 (24), 223-244, 2006.
- Marculli, C., S. Gedamke, T. Peter, and B. Zobrist, Efficiency of immersion mode ice nucleation on surrogates of mineral dust, *Atmospheric Chemistry and Physics*, 7 (19), 5081-5091, 2007.
- Mauderly, J.L., and J.C. Chow, Health effects of organic aerosols, *Inhalation Toxicology*, 20 (3), 257-288, 2008.
- McFiggans, G., P. Artaxo, U. Baltensperger, H. Coe, M.C. Facchini, G. Feingold, S. Fuzzi, M. Gysel, A. Laaksonen, U. Lohmann, T.F. Mentel, D.M. Murphy, C.D. O'Dowd, J.R. Snider, and E. Weingartner, The effect of physical and chemical aerosol properties on warm cloud droplet activation, *Atmospheric Chemistry and Physics*, 6, 2593-2649, 2006.
- McKendry, I.G., K.B. Strawbridge, N.T. O'Neill, A.M. Macdonald, P.S.K. Liu, W.R. Leitch, K.G. Anlauf, L. Jaegle, T.D. Fairlie, and D.L. Westphal, Trans-Pacific transport of Saharan dust to western North America: A case study, *Journal of Geophysical Research-Atmospheres*, 112 (D1), 2007.
- McMurry, P.H., M. Fink, H. Sakurai, M.R. Stolzenburg, R.L. Mauldin, J. Smith, F. Eisele, K. Moore, S. Sjostedt, D. Tanner, L.G. Huey, J.B. Nowak, E. Edgerton,

- and D. Voisin, A criterion for new particle formation in the sulfur-rich Atlanta atmosphere, *J. Geophys. Res.*, 110, D22S02, doi:10.1029/2005JD005901, 2005.
- Meng, Z., D. Dabdub, and J.H. Seinfeld, Chemical coupling between atmospheric ozone and particulate matter, *Science*, 277 (5322), 116-119, 1997.
- Merikanto, J., D.V. Spracklen, G.W. Mann, S.J. Pickering, and K.S. Carslaw, Impact of nucleation on global CCN, *Atmos. Chem. Phys. Discuss.*, 9, 12999–13037, 2009.
- Meyers, M.P., P.J. Demott, and W.R. Cotton, New Primary Ice-Nucleation Parameterizations in an Explicit Cloud Model, *Journal of Applied Meteorology*, 31 (7), 708-721, 1992.
- Minnis, P., L. Nguyen, D.R. Doelling, D.F. Young, W.F. Miller, and D.P. Kratz, Rapid calibration of operational and research meteorological satellite imagers. Part I: Evaluation of research satellite visible channels as references, *Journal of Atmospheric and Oceanic Technology*, 19 (9), 1233-1249, 2002.
- Minnis, P., S. Sun-Mack, D.F. Young, P.W. Heck, D.P. Garber, Y. Chen, D.A. Spangenberg, R.F. Arduini, Q.Z. Trepte, W.L.S. Jr., J.K. Ayers, S.C. Gibson, W.F. Miller, V. Chakrapani, Y. Takano, K.-N. Liou, Y. Xie, and P. Yang, CERES Edition-2 cloud property retrievals using TRMM VIRS and Terra and Aqua MODIS data, Part I: Algorithms, *Ieee Transactions on Geoscience and Remote Sensing*, 49 (11), doi: 10.1109/TGRS.2011.2144601, 2011.
- Minnis, P., Q.Z. Trepte, S. Sun-Mack, Y. Chen, D.R. Doelling, D.F. Young, D.A. Spangenberg, W.F. Miller, B.A. Wielicki, R.R. Brown, S.C. Gibson, and E.B. Geier, Cloud Detection in Nonpolar Regions for CERES Using TRMM VIRS and Terra and Aqua MODIS Data, *Ieee Transactions on Geoscience and Remote Sensing*, 46 (11), 3857-3884, 2008.
- Modini, R.L., Z.D. Ristovski, G.R. Johnson, C. He, N. Surawski, L. Morawska, T. Suni, and M. Kulmala, New particle formation and growth at a remote, sub-tropical coastal location, *Atmos. Chem. Phys.*, 9 (19), 7607-7621, 2009.
- Moffet, R.C., B. de Foy, L.T. Molina, M.J. Molina, and K.A. Prather, Measurement of ambient aerosols in northern Mexico City by single particle mass spectrometry, *Atmos. Chem. Phys.*, 8 (16), 4499-4516, 2008.
- Morris, C.E., D.G. Georgakopoulos, and D.C. Sands, Ice nucleation active bacteria and their potential role in precipitation, *Journal De Physique Iv*, 121, 87-103, 2004.
- Murphy, D.M., D.J. Cziczo, K.D. Froyd, P.K. Hudson, B.M. Matthew, A.M. Middlebrook, R.E. Peltier, A. Sullivan, D.S. Thomson, and R.J. Weber, Single-particle mass spectrometry of tropospheric aerosol particles, *Journal of Geophysical Research-Atmospheres*, 111 (D23), 2006.

- Murphy, S.M., A. Sorooshian, J.H. Kroll, N.L. Ng, P. Chhabra, C. Tong, J.D. Surratt, E. Knipping, R.C. Flagan, and J.H. Seinfeld, Secondary aerosol formation from atmospheric reactions of aliphatic amines, *Atmos. Chem. Phys.*, 7 (9), 2313-2337, 2007a.
- Murphy, S.M., A. Sorooshian, J.H. Kroll, N.L. Ng, P. Chhabra, C. Tong, J.D. Surratt, E. Knipping, R.C. Flagan, and J.H. Seinfeld, Secondary aerosol formation from atmospheric reactions of aliphatic amines, *Atmospheric Chemistry and Physics*, 7 (9), 2313-2337, 2007b.
- Nawrot, T.S., L. Perez, N. Kunzli, E. Munters, and B. Nemery, Public health importance of triggers of myocardial infarction: a comparative risk assessment, *Lancet*, 377 (9767), 732-740, 2011.
- Neff, J.C., E.A. Holland, F.J. Dentener, W.H. McDowell, and K.M. Russell, The origin, composition and rates of organic nitrogen deposition: A missing piece of the nitrogen cycle?, *Biogeochemistry*, 57 (1), 99-136, 2002.
- Nilsson, E.D., U. Rannik, M. Kulmala, G. Buzorius, and C.D. O'Dowd, Effects of continental boundary layer evolution, convection, turbulence and entrainment, on aerosol formation, *Tellus Series B-Chemical and Physical Meteorology*, 53 (4), 441-461, 2001.
- Noble, C.A., and K.A. Prather, Real-time single particle monitoring of a relative increase in marine aerosol concentration during winter rainstorms, *Geophysical Research Letters*, 24 (22), 2753-2756, 1997.
- Novakov, T., and J.E. Penner, Large Contribution of Organic Aerosols to Cloud-Condensation-Nuclei Concentrations, *Nature*, 365 (6449), 823-826, 1993.
- O'Dowd, C.D., M.C. Facchini, F. Cavalli, D. Ceburnis, M. Mircea, S. Decesari, S. Fuzzi, Y.J. Yoon, and J.P. Putaud, Biogenically driven organic contribution to marine aerosol, *Nature*, 431 (7009), 676-680, 2004.
- O'Halloran, T.L., J.D. Fuentes, D.R. Collins, M.J. Cleveland, and W.C. Keene, Influence of air mass source region on nanoparticle events and hygroscopicity in central Virginia, US, *Atmos. Environ.*, 43 (22-23), 3586-3595, 2009.
- Ogren, J.A., J. Heintzenberg, and R.J. Charlson, Insitu Sampling of Clouds with a Droplet to Aerosol Converter, *Geophysical Research Letters*, 12 (3), 121-124, 1985.
- Ortega, I.K., T. Kurten, H. Vehkamaki, and M. Kulmala, The role of ammonia in sulfuric acid ion induced nucleation, *Atmos. Chem. Phys.*, 8 (11), 2859-2867, 2008.
- Ospital, J., J. Cassmassi, and T. Chico, Multiple Air Toxics Exposure Study in the South Coast Air Basin (MATES III) Final Report, South Coast Air Quality Management District, Diamond Bar, 2008.

- Pagotto, C., N. Remy, M. Legret, and P. Le Cloirec, Heavy metal pollution of road dust and roadside soil near a major rural highway, *Environmental Technology*, 22 (3), 307-319, 2001.
- Pandey, G.R., D.R. Cayan, and K.P. Georgakakos, Precipitation structure in the Sierra Nevada of California during winter, *Journal of Geophysical Research-Atmospheres*, 104 (D10), 12019-12030, 1999.
- Pandis, S.N., R.A. Harley, G.R. Cass, and J.H. Seinfeld, Secondary Organic Aerosol Formation and Transport, *Atmospheric Environment Part a-General Topics*, 26 (13), 2269-2282, 1992.
- Parish, T.R., Barrier Winds Along the Sierra-Nevada Mountains, *Journal of Applied Meteorology*, 21 (7), 925-930, 1982.
- Pastor, S.H., J.O. Allen, L.S. Hughes, P. Bhave, G.R. Cass, and K.A. Prather, Ambient single particle analysis in Riverside, California by aerosol time-of-flight mass spectrometry during the SCOS97-NARSTO, *Atmospheric Environment*, 37, S239-S258, 2003.
- Petters, M.D., C.M. Carrico, S.M. Kreidenweis, A.J. Prenni, P.J. DeMott, J.L. Collett, and H. Moosmuller, Cloud condensation nucleation activity of biomass burning aerosol, *Journal of Geophysical Research-Atmospheres*, 114, 2009.
- Petters, M.D., and S.M. Kreidenweis, A single parameter representation of hygroscopic growth and cloud condensation nucleus activity, *Atmos. Chem. Phys.*, 7 (8), 1961-1971, 2007.
- Pey, J., A. Alastuey, X. Querol, N. Perez, and M. Cusack, A simplified approach to the indirect evaluation of the chemical composition of atmospheric aerosols from PM mass concentrations, *Atmospheric Environment*, 44 (39), 5112-5121, 2010.
- Phillips, V.T.J., C. Andronache, B. Christner, C.E. Morris, D.C. Sands, A. Bansemer, A. Lauer, C. McNaughton, and C. Seman, Potential impacts from biological aerosols on ensembles of continental clouds simulated numerically, *Biogeosciences*, 6 (6), 987-1014, 2009.
- Phillips, V.T.J., P.J. DeMott, and C. Andronache, An empirical parameterization of heterogeneous ice nucleation for multiple chemical species of aerosol, *Journal of the Atmospheric Sciences*, 65 (9), 2757-2783, 2008.
- Pierce, J.R., and P.J. Adams, Global evaluation of CCN formation by direct emission of sea salt and growth of ultrafine sea salt, *Journal of Geophysical Research-Atmospheres*, 111 (D6), -, 2006.
- Pierce, J.R., and P.J. Adams, Efficiency of cloud condensation nuclei formation from ultrafine particles, *Atmos. Chem. Phys.*, 7, 1367-1379, 2007.

- Pincus, R., and M.B. Baker, Effect of Precipitation on the Albedo Susceptibility of Clouds in the Marine Boundary-Layer, *Nature*, 372 (6503), 250-252, 1994.
- Pinsky, M., A. Khain, D. Rosenfeld, and A. Pokrovsky, Comparison of collision velocity differences of drops and graupel particles in a very turbulent cloud, *Atmospheric Research*, 49 (2), 99-113, 1998.
- Pope, C.A., and D.W. Dockery, Health effects of fine particulate air pollution: Lines that connect, *Journal of the Air & Waste Management Association*, 56 (6), 709-742, 2006.
- Pope, C.A., M.J. Thun, M.M. Namboodiri, D.W. Dockery, J.S. Evans, F.E. Speizer, and C.W. Heath, Particulate Air-Pollution as a Predictor of Mortality in a Prospective-Study of Us Adults, *American Journal of Respiratory and Critical Care Medicine*, 151 (3), 669-674, 1995.
- Pope III, C.A., M. Ezzati, and D.W. Dockery, Fine-Particulate Air Pollution and Life Expectancy in the United States, *The New England Journal of Medicine*, 360, 376-386, 2009.
- Poschl, U., Atmospheric aerosols: Composition, transformation, climate and health effects, *Angewandte Chemie-International Edition*, 44 (46), 7520-7540, 2005.
- Posfai, M., A. Gelencser, R. Simonics, K. Arato, J. Li, P.V. Hobbs, and P.R. Buseck, Atmospheric tar balls: Particles from biomass and biofuel burning, *Journal of Geophysical Research-Atmospheres*, 109 (D6), 2004.
- Posselt, R., and U. Lohmann, Influence of giant CCN on warm rain processes in the ECHAM5 GCM, *Atmospheric Chemistry and Physics*, 8 (14), 3769-3788, 2008.
- Pratt, K.A., New Insights into Single-Particle Mixing State using Aircraft Aerosol Time-of-Flight Mass Spectrometry, University of California, San Diego, La Jolla, 2009.
- Pratt, K.A., P.J. DeMott, J.R. French, Z. Wang, D.L. Westphal, A.J. Heymsfield, C.H. Twohy, A.J. Prenni, and K.A. Prather, In situ detection of biological particles in cloud ice-crystals, *Nature Geoscience*, 2 (6), 397-400, 2009a.
- Pratt, K.A., L.E. Hatch, and K.A. Prather, Seasonal volatility dependence of ambient particle phase amines, *Environ. Sci. Technol.*, 43 (14), 5276-5281, 2009b.
- Pratt, K.A., L.E. Hatch, and K.A. Prather, Seasonal Volatility Dependence of Ambient Particle Phase Amines, *Environmental Science & Technology*, 43, 5276-5281, 2009c.
- Pratt, K.A., J.E. Mayer, J.C. Holecek, R.C. Moffet, R.O. Sanchez, T.P. Rebotier, H. Furutani, M. Gonin, K. Fuhrer, Y.X. Su, S. Guazzotti, and K.A. Prather, Development and Characterization of an Aircraft Aerosol Time-of-Flight Mass Spectrometer, *Analytical Chemistry*, 81 (5), 1792-1800, 2009d.

- Pratt, K.A., and K.A. Prather, Real-Time, Single-Particle Volatility, Size, and Chemical Composition Measurements of Aged Urban Aerosols, *Environmental Science & Technology*, 43 (21), 8276-8282, 2009.
- Pratt, K.A., and K.A. Prather, Mass Spectrometry of Atmospheric Aerosols—Recent Developments and Applications. Part I: Off-line Mass Spectrometry Techniques, *Mass Spectrometry Reviews*, 31 (1), 1-16, 2011a.
- Pratt, K.A., and K.A. Prather, Mass Spectrometry of Atmospheric Aerosols—Recent Developments and Applications. Part II: On-line Mass Spectrometry Techniques, *Mass Spectrometry Reviews*, 31 (1), 17-48, 2011b.
- Pratt, K.A., and K.A. Prather, Mass spectrometry of atmospheric aerosols—Recent developments and applications. Part II: On-line mass spectrometry techniques, *Mass Spectrometry Reviews*, 31 (1), 17-48, 2012.
- Prospero, J.M., Long-term measurements of the transport of African mineral dust to the southeastern United States: Implications for regional air quality, *Journal of Geophysical Research-Atmospheres*, 104 (D13), 15917-15927, 1999.
- Prospero, J.M., P. Ginoux, O. Torres, S.E. Nicholson, and T.E. Gill, Environmental characterization of global sources of atmospheric soil dust identified with the Nimbus 7 Total Ozone Mapping Spectrometer (TOMS) absorbing aerosol product, *Reviews of Geophysics*, 40 (1), 2002.
- Prospero, J.M., R.A. Glaccum, and R.T. Nees, Atmospheric Transport of Soil Dust from Africa to South-America, *Nature*, 289 (5798), 570-572, 1981.
- Qian, S., Continuous measurements of 3 nm to 10 μ m aerosol size distributions, University of Minnesota, St. Louis, MN, 2003.
- Qin, X.Y., and K.A. Prather, Impact of biomass emissions on particle chemistry during the California Regional Particulate Air Quality Study, *International Journal of Mass Spectrometry*, 258 (1-3), 142-150, 2006a.
- Qin, X.Y., and K.A. Prather, Impact of biomass emissions on particle chemistry during the California Regional Particulate Air Quality Study, *Int. J. Mass Spectrom.*, 258 (1-3), 142-150, 2006b.
- Qin, X.Y., L.G. Shields, S.M. Toner, K.A. Pratt, and K.A. Prather, Seasonal Comparisons of Single-Particle Chemical Mixing State in Riverside, CA, accepted, 2012.
- Ralph, F.M., P.J. Neiman, and G.A. Wick, Satellite and CALJET aircraft observations of atmospheric rivers over the eastern north pacific ocean during the winter of 1997/98, *Monthly Weather Review*, 132 (7), 1721-1745, 2004.
- Ralph, F.M., R.M. Rauber, B.F. Jewett, D.E. Kingsmill, P. Pisano, P. Pugner, R.M. Rasmussen, D.W. Reynolds, T.W. Schlatter, R.E. Stewart, S. Tracton, and J.S.

- Waldstreicher, Improving short-term (0-48 h) cool-season quantitative precipitation forecasting - Recommendations from a USWRP workshop, *Bulletin of the American Meteorological Society*, 86 (11), 1619+, 2005.
- Ramsay, T.O., R.T. Burnett, and D. Krewski, The effect of concavity in generalized additive models linking mortality to ambient particulate matter, *Epidemiology*, 14 (1), 18-23, 2003.
- Reinking, R.F., J.B. Snider, and J.L. Coen, Influences of Storm-Embedded Orographic Gravity Waves on Cloud Liquid Water and Precipitation, *Journal of Applied Meteorology*, 39 (6), 733-759, 2000.
- Reynolds, D.W., and A.S. Dennis, A Review of the Sierra Cooperative Pilot Project, *Bulletin of the American Meteorological Society*, 67 (5), 513-523, 1986.
- Ristovski, Z.D., T. Suni, M. Kulmala, M. Boy, N.K. Meyer, J. Duplissy, A. Turnipseed, L. Morawska, and U. Baltensperger, The role of sulphates and organic vapours in growth of newly formed particles in a eucalyptus forest, *Atmos. Chem. Phys.*, 10, 2919-2926, 2010.
- Roberts, G.C., and A. Nenes, A continuous-flow streamwise thermal-gradient CCN chamber for atmospheric measurements, *Aerosol Sci. Tech.*, 39 (3), 206-221, 2005a.
- Roberts, G.C., and A. Nenes, A continuous-flow streamwise thermal-gradient CCN chamber for atmospheric measurements, *Aerosol Science and Technology*, 39 (3), 206-221, 2005b.
- Rodo, X., J. Ballester, D. Cayan, M.E. Melish, Y. Nakamura, R. Uehara, and J.C. Burns, Association of Kawasaki disease with tropospheric wind patterns, *Scientific Reports*, 1, 2011.
- Rogers, D.C., P.J. DeMott, S.M. Kreidenweis, and Y.L. Chen, A continuous-flow diffusion chamber for airborne measurements of ice nuclei, *Journal of Atmospheric and Oceanic Technology*, 18 (5), 725-741, 2001.
- Rogge, W.F., L.M. Hildemann, M.A. Mazurek, G.R. Cass, and B.R.T. Simoneit, Sources of Fine Organic Aerosol .2. Noncatalyst and Catalyst-Equipped Automobiles and Heavy-Duty Diesel Trucks, *Environmental Science & Technology*, 27 (4), 636-651, 1993a.
- Rogge, W.F., L.M. Hildemann, M.A. Mazurek, G.R. Cass, and B.R.T. Simoneit, Sources of Fine Organic Aerosol .3. Road Dust, Tire Debris, and Organometallic Brake Lining Dust - Roads as Sources and Sinks, *Environmental Science & Technology*, 27 (9), 1892-1904, 1993b.

- Rogge, W.F., L.M. Hildemann, M.A. Mazurek, G.R. Cass, and B.R.T. Simoneit, Sources of Fine Organic Aerosol .4. Particulate Abrasion Products from Leaf Surfaces of Urban Plants, *Environmental Science & Technology*, 27 (13), 2700-2711, 1993c.
- Rogge, W.F., L.M. Hildemann, M.A. Mazurek, G.R. Cass, and B.R.T. Simoneit, Sources of Fine Organic Aerosol .5. Natural-Gas Home Appliances, *Environmental Science & Technology*, 27 (13), 2736-2744, 1993d.
- Rogge, W.F., L.M. Hildemann, M.A. Mazurek, G.R. Cass, and B.R.T. Simoneit, Sources of fine organic aerosol .7. Hot asphalt roofing tar pot fumes, *Environmental Science & Technology*, 31 (10), 2726-2730, 1997a.
- Rogge, W.F., L.M. Hildemann, M.A. Mazurek, G.R. Cass, and B.R.T. Simoneit, Sources of fine organic aerosol .8. Boilers burning No. 2 distillate fuel oil, *Environmental Science & Technology*, 31 (10), 2731-2737, 1997b.
- Rogge, W.F., L.M. Hildemann, M.A. Mazurek, G.R. Cass, and B.R.T. Simoneit, Sources of fine organic aerosol .9. Pine, oak and synthetic log combustion in residential fireplaces, *Environmental Science & Technology*, 32 (1), 13-22, 1998.
- Rogge, W.F., L.M. Hildemann, M.A. Mazurek, G.R. Cass, and B.R.T. Simoneit, Sources of Fine Organic Aerosol .1. Charbroilers and Meat Cooking Operations, *Environmental Science & Technology*, 25 (6), 1112-1125, 1991.
- Rosenfeld, D., Suppression of rain and snow by urban and industrial air pollution, *Science*, 287 (5459), 1793-1796, 2000.
- Rosenfeld, D., and A. Givati, Evidence of orographic precipitation suppression by air pollution-induced aerosols in the western United States, *Journal of Applied Meteorology and Climatology*, 45 (7), 893-911, 2006.
- Rosenfeld, D., R. Lahav, A. Khain, and M. Pinsky, The role of sea spray in cleansing air pollution over ocean via cloud processes, *Science*, 297 (5587), 1667-1670, 2002.
- Rosenfeld, D., U. Lohmann, G.B. Raga, C.D. O'Dowd, M. Kulmala, S. Fuzzi, A. Reissell, and M.O. Andreae, Flood or drought: How do aerosols affect precipitation?, *Science*, 321 (5894), 1309-1313, 2008a.
- Rosenfeld, D., Y. Rudich, and R. Lahav, Desert dust suppressing precipitation: A possible desertification feedback loop, *Proceedings of the National Academy of Sciences of the United States of America*, 98 (11), 5975-5980, 2001.
- Rosenfeld, D., W.L. Woodley, D. Axisa, E. Freud, J.G. Hudson, and A. Givati, Aircraft measurements of the impacts of pollution aerosols on clouds and precipitation over the Sierra Nevada, *Journal of Geophysical Research-Atmospheres*, 113 (D15), 2008b.

- Rosenfeld, D., W.L. Woodley, D. Axisa, E. Freud, J.G. Hudson, and A. Givati, Aircraft measurements of the impacts of pollution aerosols on clouds and precipitation over the Sierra Nevada, *J. Geophys. Res.*, 113 (), D15203, doi:10.1029/2007JD00954, 2008c.
- Rosenfeld, D., X. Yu, G.H. Liu, X.H. Xu, Y.N. Zhu, Z.G. Yue, J. Dai, Z.P. Dong, Y. Dong, and Y. Peng, Glaciation temperatures of convective clouds ingesting desert dust, air pollution and smoke from forest fires, *Geophysical Research Letters*, 38, 2011.
- Rubasinghege, G., R.W. Lentz, M.M. Scherer, and V.H. Grassian, Simulated atmospheric processing of iron oxyhydroxide minerals at low pH: Roles of particle size and acid anion in iron dissolution, *Proceedings of the National Academy of Sciences of the United States of America*, 107 (15), 6628-6633, 2010.
- Russell, A.G., G.R. Cass, and J.H. Seinfeld, On Some Aspects of Nighttime Atmospheric Chemistry, *Environmental Science & Technology*, 20 (11), 1167-1172, 1986.
- Russell, S.C., Microorganism characterization by single particle mass spectrometry, *Mass Spectrometry Reviews*, 28 (2), 376-387, 2009.
- Ryoo, J.-M., D.E. Waliser, and E.J. Fetzer, Trajectory analysis on the origin of air mass and moisture associated with Atmospheric Rivers over the west coast of the United States, *Atmos. Chem. Phys. Discuss.*, 11, 11109-11142, 2011.
- Saleeby, S.M., W.R. Cotton, D. Lowenthal, R.D. Borys, and M.A. Wetzel, Influence of Cloud Condensation Nuclei on Orographic Snowfall, *Journal of Applied Meteorology and Climatology*, 48 (5), 903-922, 2009.
- Samet, J.M., and K. Katsouyanni, Air pollution and health: A combined European and North American Approach (APHENA), *Epidemiology*, 17 (6), S19-S20, 2006.
- Saul, T.D., M.P. Tolocka, and M.V. Johnston, Reactive uptake of nitric acid onto sodium chloride aerosols across a wide range of relative humidities, *Journal of Physical Chemistry A*, 110 (24), 7614-7620, 2006.
- Schluessel, P., and W.J. Emery, Atmospheric Water-Vapor Over Oceans From SSM/I Measurements, *International Journal of Remote Sensing*, 11 (5), 753-766, 1990.
- Schnell, R.C., and G. Vali, Atmospheric Ice Nuclei from Decomposing Vegetation, *Nature*, 236 (5343), 163-&, 1972.
- Schnell, R.C., and G. Vali, Biogenic Ice Nuclei .1. Terrestrial and Marine Sources, *Journal of the Atmospheric Sciences*, 33 (8), 1554-1564, 1976.
- Seaton, A., W. Macnee, K. Donaldson, and D. Godden, Particulate Air-Pollution and Acute Health-Effects, *Lancet*, 345 (8943), 176-178, 1995.

- Seinfeld, J.H., and S.N. Pandis, *Atmospheric Chemistry and Physics*, John Wiley & Sons, Inc., 2006.
- Sharkey, T.D., and F. Loreto, Water-Stress, Temperature, and Light Effects on the Capacity for Isoprene Emission and Photosynthesis of Kudzu Leaves, *Oecologia*, 95 (3), 328-333, 1993.
- Sihto, S.-L., J. Mikkilä, J. Vanhansen, M. Ehn, L. Liao, K. Lehtipalo, P.P. Aalto, J. Duplissy, T. Petaja, V.M. Kerminen, M. Boy, and M. Kulmala, Seasonal variation of CCN concentrations and aerosol activation properties in boreal forest, *Atmos. Chem. Phys. Discuss.*, 10, 28231-28272, 2010.
- Silva, P.J., *Source Profiling and Apportionment of Airborne Particles: A New Approach Using Aerosol Time-of-Flight Mass Spectrometry*, University of California, Riverside, Riverside, 2000.
- Silva, P.J., R.A. Carlin, and K.A. Prather, Single particle analysis of suspended soil dust from Southern California, *Atmospheric Environment*, 34 (11), 1811-1820, 2000.
- Silva, P.J., M.E. Erupe, D. Price, J. Elias, Q.G.J. Malloy, Q. Li, B. Warren, and D.R. Cocker, Trimethylamine as precursor to secondary organic aerosol formation via nitrate radical reaction in the atmosphere, *Environmental Science & Technology*, 42 (13), 4689-4696, 2008.
- Singh, M., P.A. Jaques, and C. Sioutas, Size distribution and diurnal characteristics of particle-bound metals in source and receptor sites of the Los Angeles Basin, *Atmospheric Environment*, 36 (10), 1675-1689, 2002.
- Smith, J.N., K.C. Barsanti, H.R. Friedli, M. Ehn, M. Kulmala, D.R. Collins, J.H. Scheckman, B.J. Williams, and P.H. McMurry, Observations of ammonium salts in atmospheric nanoparticles and possible climatic implications, *PNAS*, 107 (15), 6634-6639, 2009.
- Smith, J.N., K.F. Moore, P.H. McMurry, and F.L. Eisele, Atmospheric measurements of sub-20 nm diameter particle chemical composition by thermal desorption chemical ionization mass spectrometry, *Aerosol. Sci. Tech.*, 38 (2), 100-110, 2004.
- Smith, S.J., H. Pitcher, and T.M.L. Wigley, Global and regional anthropogenic sulfur dioxide emissions, *Global and Planetary Change*, 29 (1-2), 99-119, 2001.
- Sodeman, D.A., *Characterization of ambient, automobile, and diesel aerosols utilizing Aerosol Time of Flight Mass Spectrometry*, University of California, San Diego, La Jolla, 2004.
- Solomon, P.A., W. Chameides, R. Weber, A. Middlebrook, C.S. Kiang, A.G. Russell, A. Butler, B. Turpin, D. Mikel, R. Scheffe, E. Cowling, E. Edgerton, J. St John, J. Jansen, P. McMurry, S. Hering, and T. Bahadori, Overview of the 1999 Atlanta

- Supersite Project, *Journal of Geophysical Research-Atmospheres*, 108 (D7), -, 2003.
- Solomon, S., D. Qin, M. Manning, Z. Chen, M. Marquis, K.B. Averyt, and M. Tignor, *Climate Change 2007: The Physical Science Basis, Contribution of Working Group I to the Fourth Assessment Report of the Intergovernmental Panel on Climate Change*, Cambridge Univ. Press, Cambridge, U. K., 2007.
- Song, X.H., P.K. Hopke, D.P. Fergenson, and K.A. Prather, Classification of single particles analyzed by ATOFMS using an artificial neural network, *ART-2A, Anal. Chem.*, 71 (4), 860-865, 1999a.
- Song, X.H., P.K. Hopke, D.P. Fergenson, and K.A. Prather, Classification of single particles analyzed by ATOFMS using an artificial neural network, *ART-2A, Analytical Chemistry*, 71 (4), 860-865, 1999b.
- Sorooshian, A., S.N. Murphy, S. Hersey, H. Gates, L.T. Padro, A. Nenes, F.J. Brechtel, H. Jonsson, R.C. Flagan, and J.H. Seinfeld, Comprehensive airborne characterization of aerosol from a major bovine source, *Atmospheric Chemistry and Physics*, 8 (17), 5489-5520, 2008.
- Spencer, M.T., J.C. Holecek, C.E. Corrigan, V. Ramanathan, and K.A. Prather, Size-resolved chemical composition of aerosol particles during a monsoonal transition period over the Indian Ocean, *Journal of Geophysical Research-Atmospheres*, 113 (D16), 2008.
- Spencer, M.T., and K.A. Prather, Using ATOFMS to determine OC/EC mass fractions in particles, *Aerosol Sci. Tech.*, 40 (8), 585-594, 2006.
- Spracklen, D.V., K.S. Carslaw, M. Kulmala, V.M. Kerminen, S.L. Sihto, I. Riipinen, J. Merikanto, G.W. Mann, M.P. Chipperfield, A. Wiedensohler, W. Birmili, and H. Lihavainen, Contribution of particle formation to global cloud condensation nuclei concentrations, *Geophysical Research Letters*, 35 (6), 2008.
- Spracklen, D.V., K.S. Carslaw, U. Poschl, A. Rap, and P.M. Forster, Global cloud condensation nuclei influenced by carbonaceous combustion aerosol, *Atmospheric Chemistry and Physics*, 11 (17), 9067-9087, 2011.
- Steele, P.T., A. Srivastava, M.E. Pitesky, D.P. Fergenson, H.J. Tobias, E.E. Gard, and M. Frank, Desorption/ionization fluence thresholds and improved mass spectral consistency measured using a flat-top laser profile in the bioaerosol mass spectrometry of single *Bacillus endospores*, *Analytical Chemistry*, 77 (22), 7448-7454, 2005.
- Stephens, E.R., Marine Layer and Its Relation to a Smog Episode in Riverside California, *Atmospheric Environment*, 2 (4), 393-&, 1968.

- Stohl, A., C. Forster, A. Frank, P. Seibert, and G. Wotawa, Technical note: The Lagrangian particle dispersion model FLEXPART version 6.2, *Atmos. Chem. Phys.*, 5, 2461-2474, 2005.
- Stohl, A., M. Hittenberger, and G. Wotawa, Validation of the Lagrangian particle dispersion model FLEXPART against large-scale tracer experiment data, *Atmos. Environ.*, 32 (24), 4245-4264, 1998.
- Streets, D.G., K.F. Yarber, J.H. Woo, and G.R. Carmichael, Biomass burning in Asia: Annual and seasonal estimates and atmospheric emissions, *Global Biogeochemical Cycles*, 17 (4), -, 2003.
- Su, Y.X., M.F. Sipin, H. Furutani, and K.A. Prather, Development and characterization of an aerosol time-of-flight mass spectrometer with increased detection efficiency, *Anal. Chem.*, 76 (3), 712-719, 2004.
- Sullivan, R.C., M.J.K. Moore, M.D. Petters, S.M. Kreidenweis, G.C. Roberts, and K.A. Prather, Effect of chemical mixing state on the hygroscopicity and cloud nucleation properties of calcium mineral dust particles, *Atmospheric Chemistry and Physics*, 9 (10), 3303-3316, 2009a.
- Sullivan, R.C., M.J.K. Moore, M.D. Petters, S.M. Kreidenweis, G.C. Roberts, and K.A. Prather, Timescale for hygroscopic conversion of calcite mineral particles through heterogeneous reaction with nitric acid, *Physical Chemistry Chemical Physics*, 11 (36), 7826-7837, 2009b.
- Sun, J.M., M.Y. Zhang, and T.S. Liu, Spatial and temporal characteristics of dust storms in China and its surrounding regions, 1960-1999: Relations to source area and climate, *Journal of Geophysical Research-Atmospheres*, 106 (D10), 10325-10333, 2001.
- Tang, M.J., J. Thieser, G. Schuster, and J.N. Crowley, Uptake of NO₃ and N₂O₅ to Saharan dust, ambient urban aerosol and soot: a relative rate study, *Atmospheric Chemistry and Physics*, 10 (6), 2965-2974, 2010.
- Teller, A., and Z. Levin, The effects of aerosols on precipitation and dimensions of subtropical clouds: a sensitivity study using a numerical cloud model, *Atmospheric Chemistry and Physics*, 6, 67-80, 2006.
- Toner, S.M., L.G. Shields, D.A. Sodeman, and K.A. Prather, Using mass spectral source signatures to apportion exhaust particles from gasoline and diesel powered vehicles in a freeway study., *Abstracts of Papers of the American Chemical Society*, 229, U127-U127, 2005.
- Tu, F.H., D.C. Thornton, A.R. Bandy, G.R. Carmichael, Y.H. Tang, K.L. Thornhill, G.W. Sachse, and D.R. Blake, Long-range transport of sulfur dioxide in the central Pacific, *J. Geophys. Res.*, 109, D15S08, doi:10.1029/2003JD004309, 2004.

- Tunved, P., H.C. Hansson, V.M. Kerminen, J. Strom, M. Dal Maso, H. Lihavainen, Y. Viisanen, P.P. Aalto, M. Komppula, and M. Kulmala, High natural aerosol loading over boreal forests, *Science*, 312 (5771), 261-263, 2006.
- Turpin, B.J., and H.J. Lim, Origins of primary and secondary organic aerosol in Atlanta: Results' of time-resolved measurements during the Atlanta supersite experiment, *Environmental Science & Technology*, 36 (21), 4489-4496, 2002.
- Twomey, S., Pollution and Planetary Albedo, *Atmospheric Environment*, 8 (12), 1251-1256, 1974.
- Twomey, S., Influence of Pollution on Shortwave Albedo of Clouds, *J. Atmos. Sci.*, 34 (7), 1149-1152, 1977.
- Uno, I., K. Eguchi, K. Yumimoto, Z. Liu, Y. Hara, N. Sugimoto, A. Shimizu, and T. Takemura, Large Asian dust layers continuously reached North America in April 2010, *Atmospheric Chemistry and Physics*, 11 (14), 7333-7341, 2011.
- Uno, I., K. Eguchi, K. Yumimoto, T. Takemura, A. Shimizu, M. Uematsu, Z.Y. Liu, Z.F. Wang, Y. Hara, and N. Sugimoto, Asian dust transported one full circuit around the globe, *Nature Geoscience*, 2 (8), 557-560, 2009.
- Vali, G., M. Christensen, R.W. Fresh, E.L. Galyan, L.R. Maki, and R.C. Schnell, Biogenic Ice Nuclei .2. Bacterial Sources, *Journal of the Atmospheric Sciences*, 33 (8), 1565-1570, 1976.
- Vedal, S., Ambient particles and health: Lines that divide, *Journal of the Air & Waste Management Association*, 47 (5), 551-581, 1997.
- Volkamer, R., J.L. Jimenez, F. San Martini, K. Dzepina, Q. Zhang, D. Salcedo, L.T. Molina, D.R. Worsnop, and M.J. Molina, Secondary organic aerosol formation from anthropogenic air pollution: Rapid and higher than expected, *Geophysical Research Letters*, 33 (17), 2006.
- Wang, L., A.F. Khalizov, J. Zheng, W. Xu, Y. Ma, V. Lal, and R. Zhang, Atmospheric nanoparticles formed from heterogeneous reactions of organics, *Nature Geoscience*, 3, 238-242, 2010a.
- Wang, L., V. Lal, A.F. Khalizov, and R. Zhang, Heterogeneous chemistry of alkylamines with sulfuric acid: Implications for atmospheric formation of alkylammonium sulfates, *Environ. Sci. Technol.*, 44 (7), 2461-2465, 2010b.
- Warburton, J.A., L.G. Young, and R.H. Stone, Assessment of Seeding Effects in Snowpack Augmentation Programs - Ice Nucleation and Scavenging of Seeding Aerosols, *Journal of Applied Meteorology*, 34 (1), 121-130, 1995.

- Weaver, J.F., J.A. Knaff, D. Bikos, G.S. Wade, and J.M. Daniels, Satellite observations of a severe supercell thunderstorm on 24 July 2000 made during the GOES-11 science test, *Weather and Forecasting*, 17 (1), 124-138, 2002.
- Wehner, B., T. Petaja, M. Boy, C. Engler, W. Birmili, T. Tuch, A. Wiedensohler, and M. Kulmala, The contribution of sulfuric acid and non-volatile compounds on the growth of freshly formed atmospheric aerosols, *Geophys. Res. Lett.*, 32 (17), L17810, doi:10.1029/2005GL023827, 2005.
- Westphal, D.L., O.B. Toon, and T.N. Carlson, A Case-Study of Mobilization and Transport of Saharan Dust, *Journal of the Atmospheric Sciences*, 45 (15), 2145-2175, 1988.
- White, A.B., D.J. Gottas, A.F. Henkel, P.J. Neiman, F.M. Ralph, and S.I. Gutman, Developing a Performance Measure for Snow-Level Forecasts, *Journal of Hydrometeorology*, 11 (3), 739-753, 2010.
- White, A.B., D.J. Gottas, E.T. Strem, F.M. Ralph, and P.J. Neiman, An automated brightband height detection algorithm for use with Doppler radar spectral moments, *Journal of Atmospheric and Oceanic Technology*, 19 (5), 687-697, 2002.
- White, A.B., J.R. Jordan, B.E. Martner, F.M. Ralph, and B.W. Bartram, Extending the dynamic range of an S-band radar for cloud and precipitation studies, *Journal of Atmospheric and Oceanic Technology*, 17 (9), 1226-1234, 2000.
- White, A.B., P.J. Neiman, F.M. Ralph, D.E. Kingsmill, and P.O.G. Persson, Coastal orographic rainfall processes observed by radar during the California land-falling jets experiment, *Journal of Hydrometeorology*, 4 (2), 264-282, 2003.
- Wiacek, A., T. Peter, and U. Lohmann, The potential influence of Asian and African mineral dust on ice, mixed-phase and liquid water clouds, *Atmospheric Chemistry and Physics*, 10 (18), 8649-8667, 2010.
- Winker, D.M., J. Pelon, J.A. Coakley, S.A. Ackerman, R.J. Charlson, P.R. Colarco, P. Flamant, Q. Fu, R.M. Hoff, C. Kittaka, T.L. Kubar, H. Le Treut, M.P. McCormick, G. Megie, L. Poole, K. Powell, C. Trepte, M.A. Vaughan, and B.A. Wielicki, THE CALIPSO MISSION A Global 3D View of Aerosols and Clouds, *Bulletin of the American Meteorological Society*, 91 (9), 1211-1229, 2010.
- Xie, S.P., C. Deser, G.A. Vecchi, J. Ma, H.Y. Teng, and A.T. Wittenberg, Global Warming Pattern Formation: Sea Surface Temperature and Rainfall, *Journal of Climate*, 23 (4), 966-986, 2010.
- Yin, Y., Z. Levin, T.G. Reisin, and S. Tzivion, The effects of giant cloud condensation nuclei on the development of precipitation in convective clouds - a numerical study, *Atmospheric Research*, 53 (1-3), 91-116, 2000.

- Ying, Q., and M.J. Kleeman, Source contributions to the regional distribution of secondary particulate matter in California, *Atmospheric Environment*, 40 (4), 736-752, 2006.
- Yu, F., and G. Luo, Simulation of particle size distribution with a global aerosol model: contribution of nucleation to aerosol and CCN number concentrations, *Atmos. Chem. Phys. Discuss.*, 9, 10597-10645, 2009.
- Yuter, S.E., and R.A. Houze, Microphysical modes of precipitation growth determined by S-band vertically pointing radar in orographic precipitation during MAP, *Quarterly Journal of the Royal Meteorological Society*, 129 (588), 455-476, 2003.
- Zhang, Q., D.R. Worsnop, M.R. Canagaratna, and J.L. Jimenez, Hydrocarbon-like and oxygenated organic aerosols in Pittsburgh: insights into sources and processes of organic aerosols, *Atmospheric Chemistry and Physics*, 5, 3289-3311, 2005.
- Ziemba, L.D., J.E. Dibb, R.J. Griffin, L.G. Huey, and P. Beckman, Observations of particle growth at a remote, Arctic site, *Atmos. Environ.*, 44, 1649-1657, 2010.

2. Long-term Impacts of Source and Meteorology on Aerosol Chemical Mixing State in Riverside, CA

2.1. Introduction

Atmospheric particles are known to cause severe adverse health effects [Poschl, 2005; Seaton et al., 1995]. In particular, fine particulate matter (PM_{2.5}, particles $\leq 2.5 \mu\text{m}$ in diameter) has been linked to increases in cardiovascular and pulmonary diseases [Latzin et al., 2009; Nawrot et al., 2011], leading to elevated mortality and morbidity [Pope and Dockery, 2006]. Further, submicron particles (diameters $< 1 \mu\text{m}$) have higher deposition probabilities in the respiratory tract than larger particles, potentially leading to more severe health effects [Li et al., 1993]. Epidemiological studies have applied generalized additive models to time series data to estimate associations between PM_{2.5} exposure and human health [Ramsay et al., 2003]. Improvement of these models based on PM_{2.5} temporal changes is important for pollution regulations designed to minimize the health effects of particulate matter. Urban aerosols resulting from motor vehicle and industrial sources represent a significant fraction of PM_{2.5} mass concentrations in areas of the greatest human exposure [Chow et al., 1994]. However, better approximations based on measurements are needed to improve the representation of urban aerosols in models and pollution regulations [Vedal, 1997]. Understanding specific effects due to aerosol size and chemistry has been identified as critical to evaluating the overall causal relationship between PM_{2.5} exposure and negative health effects such as cardiovascular morbidity and mortality [Brook et al., 2010].

The Southern California Basin is recognized as having some of the highest levels of urban particulate pollution in the United States, especially the city of Riverside, which is ~50 miles east of downtown Los Angeles (LA) [CARB, 2010]. Prevailing westerly winds transport emissions from LA to Riverside, where air masses can stagnate due to the surrounding topography and inversion layer, increasing PM_{2.5} concentrations [Edinger, 1963; Stephens, 1968]. During transport heterogeneous reactions of particles with trace

gases and gas-to-particle partitioning of secondary species, such as nitrate [Hughes *et al.*, 2000], sulfate [Hughes *et al.*, 2000; Ying and Kleeman, 2006], ammonium [Hughes *et al.*, 2000; Russell *et al.*, 1986], amines [Pratt *et al.*, 2009b], and oxidized organics [Docherty *et al.*, 2008] result in major changes in particle size and chemistry compared to the physicochemical properties of particles emitted in LA [Finlayson-Pitts, 2000; Poschl, 2005]. Particles containing these secondary species may become more toxic [Pope and Dockery, 2006]. For instance, cardiopulmonary mortality rates have been related to airborne concentrations of sulfate [Pope *et al.*, 1995], while organics including amines can cause respiratory and cardiovascular problems [Brook *et al.*, 2010; Mauderly and Chow, 2008]. Secondary nitrate and sulfate formed from their acidic counterparts can lead to dissolution of metals such as iron in mineral dust and from industrial sources [Rubasinghege *et al.*, 2010], which increase particle toxicity and cause oxidative stress and inflammation [Brook *et al.*, 2010]. Overall, secondary species can constitute a large fraction of PM_{2.5} in urban areas of the Western U.S., with organics, nitrate, sulfate, and ammonium representing ~70% of the total PM_{2.5} mass [Harrison and Yin, 2000]. Therefore, the extent of particle aging may play a significant role in determining how harmful particulate matter is to human health.

Transport from different sources and local meteorology have large impacts on particle chemistry, number, and mass concentrations, even for urban locations [Finlayson-Pitts, 2000]. The relationship between sources, meteorology, and PM_{2.5} should be taken into account in models evaluating the connections between particulate matter and adverse health effects. Pey *et al.* [2010] have previously predicted PM chemistry based on meteorological trends for two sites in the Mediterranean. In Riverside, several previous studies have linked meteorology and gas-phase concentrations of precursor species with observed particle chemistry [Pastor *et al.*, 2003] and have monitored the seasonal variation of particulate mass concentrations [Chow *et al.*, 1994; Fine *et al.*, 2004; Geller *et al.*, 2004; Kim *et al.*, 2000a; Kim *et al.*, 2000b]. Pastor *et al.* [2003] observed increases in organic carbon particles during elevated O₃ levels in the afternoons during a 40-day summer study in Riverside. Fine *et al.* [2004] and Geller *et al.* [2004] found the highest PM_{2.5} in the summer months; in contrast, Chow

et al. [1994] and *Kim et al. [2000b]* found higher $PM_{2.5}$ in the winter months. These field studies highlight “snapshot” observations during short time periods, typically during 1-2 seasons of a particular year, which may capture episodic events and thus provide a different picture of the typical particulate concentrations in terms of long-term variability. In order to improve model results, longer term observations, preferably during multiple years encompassing varying meteorological conditions, are needed to unravel the impacts of variable sources and meteorology on particle chemistry.

Most long-term studies of variations in particle chemistry in the eastern LA basin have utilized off-line bulk filter measurements [*Ospital et al., 2008; Singh et al., 2002*]; however, in the current study, real-time, single-particle mass spectrometry was used. This technique provides information about particle mixing state with high time-resolution, providing detailed insight into the influence of particulate chemistry on $PM_{2.5}$ concentration trends. Chemical composition analysis of individual particles allows the identification of distinct mass spectral fingerprints indicative of different particle sources and an assessment of particle aging processes [*Pratt and Prather, 2012*]. Here, we examined the role of meteorology (temperature, relative humidity, wind speed, and air mass history) and O_3 as a proxy for photochemical aging on changes in $PM_{2.5}$ mass concentrations and measured submicron single-particle chemistry in Riverside for three consecutive summers (2005-2007). The goal of this work is to improve our understanding of long-term drivers for controlling $PM_{2.5}$ concentrations over multiple years.

2.2. Experimental

Single-particle mass spectrometry measurements were conducted during the summers of 2005-2007 at the University of California, Riverside (UCR). Measurements were made during the Study of Organic Aerosols in Riverside (SOAR) campaign from July 31 – August 14, 2005; subsequent studies included measurements on August 10 – 21, 2006 and August 30 – September 7, 2007. All data are given in Pacific Standard Time (PST), 1 hour later than local time. O_3 , $PM_{2.5}$ mass concentrations, and meteorological measurements, including wind speed, relative humidity, and temperature, were acquired from the California Air Resources Board (CARB) Riverside-Rubidoux sampling site,

located ~9 miles northwest of UCR in 2006-2007. In 2005, PM_{2.5} mass and O₃ concentrations were acquired from the CARB site, while meteorological data were measured at the UCR site. In 2005 and 2007, aerosol size distributions and number concentrations were measured between 0.523 – 10 μm using an aerodynamic particle sizer (APS) (Model 3321, TSI Inc.).

The size-resolved chemical composition of individual particles was measured using aerosol time-of-flight mass spectrometry (ATOFMS). A converging nozzle-inlet ATOFMS instrument, measuring particles with vacuum aerodynamic diameter (D_{va}) of 0.2-3.0 μm, was operated in the summers of 2005 and 2007, and the ground-based prototype of the aircraft (A)-ATOFMS instrument, measuring D_{va} of 0.07-1.2 μm with an aerodynamic lens inlet, was utilized in 2006. The overlap between the ATOFMS and A-ATOFMS is roughly between 0.2-1.0 μm; therefore, particles chemistry within this size range is presented herein. The co-located measurements made by these two instruments have been shown to agree in terms of their size-resolved submicron particle chemistry [Pratt, 2009]. These instruments are described in detail elsewhere [Gard *et al.*, 1997b; Pratt *et al.*, 2009d]. Briefly, particles traverse two 532 nm continuous wave lasers located 6 cm apart, in which the speeds are used to determine aerodynamic size by calibration with polystyrene latex spheres of known size. Individual particles are subsequently desorbed and ionized by a pulsed 266-nm Nd:YAG laser, creating positive and negative ions, which are detected within the dual-polarity time-of-flight mass spectrometer. Within the measured size range (0.2-1.0 μm), the ATOFMS chemically analyzed 374,119 particles during the summer of 2005, during 2006 the A-ATOFMS analyzed 855,585 particles, and during 2007 the ATOFMS analyzed 44,180 particles.

Mass spectra were imported into YAADA (www.yaada.org), a software toolkit for analysis using Matlab (The Mathworks, Inc.). An adaptive resonance theory-based clustering method (ART-2a) [Song *et al.*, 1999a] was then used to classify and group single-particle mass spectra with a vigilance factor of 0.80, learning rate of 0.05, and 20 iterations followed by regrouping with a vigilance factor of 0.85. ART-2a classifies individual particle mass spectra into separate clusters depending on the presence and

intensity of ion peaks. For the three studies presented, the most populated 50 clusters accounted for >90% of the total ART-2a classified particles and are representative of the overall submicron aerosol composition. Peak identifications in this paper correspond to the most probable ions for a given m/z ratio based on previous lab and field studies.

2.3. Results and Discussion

2.3.1. The Impact of Meteorology and Air Mass Sources on $PM_{2.5}$

Figure 2.1 shows temporal meteorological data including temperature, relative humidity (RH), and wind direction (WD) in addition to $PM_{2.5}$ mass concentrations during the summers of 2005-2007 (a-c, respectively). WD is colored by wind speed (WS), with blue representing the highest WS and red representing stagnant periods (WS \sim 0 m/s). Table 2.1 provides a summary of temperature, RH, WS, and $PM_{2.5}$ mass concentrations during the sampling periods for each of the summers. Air mass back trajectories (24-h) were calculated using HYSPLIT [Draxler and Rolph, 2011a]. Trajectories ending at 00:00 and 12:00 daily 100 m above the site for the three summers are shown in the Figure 2.2. Generally, winds transported air masses from similar source regions during the summers of 2005 and 2006, whereas winds, and thus, sources during the summer of 2007 were highly variable. As shown in Figure 2.1 and Figure 2.2, winds during the summers of 2005 and 2006 typically originated from 290-300° (west-northwest, WNW), were highest around noon when temperatures were also at their peak, and traveled over relatively flat terrain through the highly populated metropolitan area of LA and dairy farms in the Chino area. The main difference between 2005 and 2006 is the periods of overnight stagnation that occurred in 2006 (as shown by the red markers in Figure 2.1b) when temperatures became their lowest (16-22°C). In addition, RH was much higher during the summer of 2006, reaching 100% daily for up to 6 hours before sunrise. The temporal trends of RH in the summer of 2005 were similar to 2006, but did not reach and/or maintain 100% for as long each day (Figure 2.1a). During these two summers, $PM_{2.5}$ mass concentrations showed diurnal patterns, increasing during time periods of highest RH at night and peaking between 9:00 and 10:00 before temperatures and winds from the LA and Chino areas increased (\sim 8-10 m/s). This pattern suggests transport of

new, daily air masses from LA and Chino, which likely contained particles as well as species that underwent secondary conversion, such as organic species from urban pollution or ammonium nitrate from agriculture [Docherty *et al.*, 2008; Hughes *et al.*, 2002]. Under the humid nighttime conditions when wind speeds were low (~0-4 m/s), secondary species condensed onto the preexisting particles, causing particle mass concentrations to increase, particularly in the summer of 2006. As conditions became hotter and drier midday, particle mass, particularly contributions from ammonium nitrate, decreased due to volatilization [Hennigan *et al.*, 2008; Pratt and Prather, 2009; Qin *et al.*, 2012]. These findings are consistent with Fine *et al.* [2004] who also observed midday decreases in PM_{2.5} after the morning peak in the summer of 2002 in Riverside.

A completely different scenario existed in the summer of 2007 as shown in Figure 2.1c and Figure 2.2; the wind speed and direction were highly variable and air masses traveled over less populated mountain regions north, east, and south of Riverside as opposed to over the LA and Chino regions. PM_{2.5} did not show any diurnal trends, instead more variability occurred both in maximum values and peak times due to the variability in winds. Less transport from the LA and Chino areas introduced lower concentrations of preexisting aerosols and secondary species. Preexisting “seed” aerosols are necessary for heterogeneous reactions and condensation of secondary species. Further, higher temperatures in the summer of 2007 likely limited the condensation of secondary species on preexisting seed aerosols. These observations explain the low PM_{2.5} and particle number (APS) concentrations shown in Figure 2.1c and Figure 8.1, respectively.

Overall, the summer of 2007 was relatively hot and much drier (28°C, 56%) than the summers of 2005 (26°C, 71%) and 2006 (23°C, 75%) as revealed in Table 2.1. Interestingly, the average PM_{2.5} was lowest (22 µg/m³) during the hot and dry summer of 2007 and highest (32 µg/m³) during the cool and humid summer of 2006. In the summer of 2005, average PM_{2.5} (30 µg/m³) fell between 2006 and 2007 summer concentrations. These trends further show the importance of secondary species in leading to high values of PM_{2.5}, as previously shown by Mysliwiec and Kleeman [2002] in Riverside. By

comparing the three summers, the relative effects of gas-to-particle partitioning due to different meteorology (2005 versus 2006) and different source regions (2007 versus 2005 and 2006) on $PM_{2.5}$ can be investigated. However, in order to fully understand the differences in $PM_{2.5}$, we compare aerosol chemical composition to distinguish impacts due to partitioning of secondary species versus variable sources herein.

2.4. Aerosol Chemical Composition

Detailed analysis of individual particle chemistry provides insight into the main species that induced changes in $PM_{2.5}$ each summer. The mass spectral signatures of the ATOFMS particle types provided in Table 2.2 are similar to those described by Pastor *et al.* [2003] and Qin *et al.* [2012] in Riverside. The major submicron particle types present during the three summer studies were organic carbon (OC), amine-containing OC (amine-OC), elemental carbon (EC), EC mixed with OC (ECOC), biomass burning, sea salt dust, and vanadium-containing. Other minor types comprised <10% of the total number concentration for submicron sizes. Representative mass spectra for these particle types are shown in Figure 8.2. Figure 2.3 illustrates the time series of the number fraction of each ATOFMS submicron particle type. Immediately apparent are the major differences and common features of the overall chemical composition between the three summers. The highest average number fraction of OC particles was observed in the summer of 2005 (43%) compared to 2006 (8%) and 2007 (6%), which can be explained by the higher O_3 concentrations (average and maximum = 46.4 ppb and 155 ppb, respectively) compared to 2006 (38.8 ppb and 106 ppb) and 2007 (39.5 ppb and 131 ppb) as revealed in Table 2.1. O_3 is commonly used as a photochemical tracer and is critical for secondary organic aerosol (SOA) formation, indicating the OC was formed via secondary aging processes during transport from the LA area in the summer of 2005 [Docherty *et al.*, 2008; Meng *et al.*, 1997; Qin *et al.*, 2012]. The “aged” nature of OC is discussed in the following section. Our results are consistent with Docherty *et al.* [2008], who found organics to comprise 70-90% of PM_1 mass during the summer of 2005 using aerosol mass spectrometry (AMS).

Overall, organic-containing particles from anthropogenic sources (e.g. OC + amine-OC + ECOC) were comparable during the summers of 2005 and 2006 (79% and 80% of total particle number) likely due to the similar air mass transport as shown in Figure 2.2. However, amine-OC particles were dominant (86%) compared to the summers of 2005 and 2007 (3% and 5%, respectively). The presence of amine-OC particles during the summer of 2006 is attributed to the high RH (80% versus 71% and 50% during 2005 and 2007, respectively). In addition, winds were more stagnant in the summer of 2006, enabling time for amines from the Chino dairy farms to condense on the particles [Sorooshian *et al.*, 2008]. While amines represent a small fraction of the total particle mass, these species are indicators of increased gas-to-particle partitioning of secondary alkylamines [Pratt *et al.*, 2009b]. During previous measurements in Riverside, the detection of particle-phase amines was found to be incredibly sensitive to meteorological conditions, showing an increase with increasing RH and decreasing temperature [Angelino *et al.*, 2001b]. It is likely that OC particles were present similar to the summer of 2005, however due to the meteorological conditions in the summer of 2006, the OC was heavily coated with secondary amine species (discussed in further detail in the following section).

In contrast, transport from LA and Chino was less frequent in the summer of 2007 and meteorological conditions were unfavorable for gas-to-particle partitioning, i.e., the temperature was high (28°C) and RH was very low relative to 2005 and 2006, explaining the lower fraction of organic-containing particles (40%). Previous studies have shown that higher temperatures yield lower SOA concentrations [Takekawa *et al.*, 2003]. Not only were less secondary aerosols present (only 6% OC and 5% amine-OC), but the number of preexisting seed aerosols for secondary species to condense upon was low: ATOFMS submicron counts per day were ~5:1 for 2005 to 2007 and ~16:1 for 2006 to 2007. Aerosols that were present were sea salt and dust (23% and 10%, respectively), compared to the summers of 2005 (2% and 0.4%) and 2006 (1% and 0.1%) due to transport from over the Pacific Ocean then through less populated mountain regions south of Riverside (blue trajectories highlighted in Figure 2.2) and through the Mojave Desert (yellow trajectory in Figure 2.2). The ATOFMS supermicron particles (not shown) were

highest in number during the summer of 2007 compared to 2005 (16:1, 2007 to 2005) and were composed of predominantly sea salt (78%) and dust (15%), whereas supermicron sea salt (27%) and dust (9%) were relatively low during 2005 (supermicron analysis not available for 2006). This can be explained by: 1) different sources during 2007 and 2) the fact that sea salt and dust are typically larger than organic aerosols [Finlayson-Pitts, 2000; Liu et al., 2000; Wenzel et al., 2003].

Observations from the three summer studies demonstrate how meteorology not only determines the sources of primary emissions (soot, sea salt, dust), but also the extent of atmospheric processing from secondary species such as organics and amines. Although the summers of 2005 and 2006 had similar sources, high O₃ concentrations led to highly-aged SOA in 2005, while high RH during 2006 enabled condensation of secondary amines. Variable winds during the summer of 2007 introduced different sources while the combination of hot temperatures and deficiency of primary seed aerosols inhibited condensation of secondary species. Overall, meteorological factors including temperature, RH, and wind were the dominant mechanisms in controlling primary and secondary contributions to aerosol composition at Riverside.

2.4.1. Single-particle Mixing State and Atmospheric Aging

It is important to consider the relative amount of secondary species in individual particles because it can lead to more specific insight on how a particle is “aged” after emission into the atmosphere, and thus, what sort of adverse health effects are associated with it. The particles that exhibited the most inter-annual variation during the summers of 2005-2007 included OC, amine-OC, ECOC, dust, and sea salt, and showed evidence of aging based on ammonium (¹⁸NH₄⁺), sulfate (⁹⁷HSO₄⁻), nitrate (⁶²NO₃⁻) and organics, including amines (⁸⁶C₅H₁₂N⁺) and oxidized OC (⁴³C₂H₃O⁺/CHNO⁺). Figure 2.4 illustrates the relative number of OC, amine-OC, ECOC, dust, and sea salt particles internally mixed with these secondary species during the 2005-2007 summers (bars) in addition to the relative abundance (average relative ion peak areas) of each secondary species on each particle type (markers). As seen by the bars in Figure 2.4a, all particles were highly aged with oxidized OC during the summer of 2005 (44-83% of each major type)

compared to 2006 (31-72%) and 2007 (6-51%). In addition, the relative abundance of oxidized OC was highest during the summer of 2005, and preferentially partitioned more to organic-containing particles (i.e., higher average relative ion peak areas of m/z 43 in OC, amines-OC, and ECOC) as seen by the markers in Figure 2.4a. These observations are attributed to more photooxidation indicated by the higher O_3 concentrations and more frequent transport from polluted urban areas. The extent of particle aging by oxidized OC was further examined by comparing the ratio of m/z 43 to a less-oxidized marker (m/z +37, C_3H^+) and its relationship to O_3 as shown in Figure 8.3. The m/z +37 marker has been observed previously for fresh particle emissions from light duty vehicles [Toner *et al.*, 2005]. This method is similar to that of Qin *et al.* [2012] who discovered a trend between m/z 43 and O_3 , however here we extend the analysis to more than one year and by comparing to a less-oxidized marker. During the summers of 2005 and 2006, the ratio of m/z 43:37 peaked during the afternoons and was highest during the peak O_3 concentrations in 2005. These results agree with Docherty *et al.* [2011] who observed a high O/C ratio in 2005 (up to 0.42 during the afternoon), suggesting organics were highly oxidized and that SOA is the single largest component by mass of submicron particulate matter in Riverside. There was no trend with m/z 43:37 and O_3 in the summer of 2007 even though O_3 was diurnal, likely due to the low fraction of organic-containing particles present, deficiency in seed aerosol, and variable conditions.

Particles containing secondary amines were abundant in the summer of 2006 due to the influence of the Chino dairies and high RH. In particular, amines were present within all particle types (green markers in Figure 2.4b) predominantly as aminium sulfate during the summer of 2006 (dark pink bars in Figure 2.4b). Sulfate can be introduced into the particle phase by uptake of sulfuric acid, subsequently forming a salt in the presence of a strong base [Finlayson-Pitts, 2000; Pratt *et al.*, 2009b]. Aminium sulfate forms in the presence of high precursor concentrations [Murphy *et al.*, 2007a] and under high RH conditions [Hatch *et al.*, 2011a; Pratt *et al.*, 2009b], therefore the high RH during the summer of 2006 can explain the abundance of aminium sulfate. Pratt *et al.* [2009b] have previously shown aminium sulfate to preferentially form in Riverside during the summer. Throughout all of the summers, aminium sulfate and secondary amines tended to

preferentially partition to organic-containing particles as seen by the dark pink bars and green markers in Figure 2.4b, respectively, likely due to the similarity and proximity of the sources (i.e., organics and amines from LA and Chino). However, during the summers of 2005 and 2007, sulfate was not predominantly in the aminium salt form (light pink bars in Figure 2.4b) likely due to the deficiency in the strongly basic secondary amine species in the particle phase (green bars and markers in Figure 2.4b). It is possible sulfuric acid condensed onto the preexisting seed particles, but due to the deprivation of amine species, salts did not form. This is also evident by the absence of sulfate (light pink bars)/presence of aminium sulfate (dark pink bars) on amine-OC particles all three summers.

Although all particle types were aged with nitrate all three summers, nitrate appeared to partition more to particle types such as dust and sea salt likely through heterogeneous reactions (royal blue bars in Figure 2.4c) and partitioning of ammonium nitrate (dark blue bars in Figure 2.4c). High nitrate levels have been previously modeled and observed in Riverside due to strong influences from urban and agricultural sources [Chow *et al.*, 1994; Hughes *et al.*, 2000; Kleeman *et al.*, 1999]. Mineral dust and sea salt aerosols are known to react with $\text{N}_2\text{O}_5(\text{g})$, $\text{NO}_2(\text{g})$, and $\text{HNO}_3(\text{g})$ from the atmosphere leading to the formation of particulate nitrate [Gard *et al.*, 1998; Mamane and Gottlieb, 1992; Saul *et al.*, 2006; Sullivan *et al.*, 2009b; Tang *et al.*, 2010]. Aerosols can also acquire nitrate by uptake of ammonium nitrate associated with agricultural emissions during high RH and low temperature conditions [Appel *et al.*, 1978]. Across all the major particle types, more particles contained ammonium nitrate in the summers of 2005 and 2006 compared to the summer of 2007 due to transport from similar sources and cooler/more humid conditions. Qin *et al.* [2012] observed a buildup of ammonium and nitrate during cooler, more stagnant conditions during a 2005 seasonal comparison in Riverside. In addition, less transport from Chino occurred during the hottest and driest summer of 2007 when we observed the least amount of particles mixed with ammonium nitrate, therefore, it is likely the nitrate on dust and sea salt was formed through heterogeneous reactions.

Overall, oxidized OC and ammonium sulfate preferentially partitioned to submicron organic-containing particles, which can be attributed to the similarities in sources (i.e., urban and agricultural pollution), while dust and sea salt contained mostly heterogeneously-formed nitrate. Ammonium nitrate was present within all particle types, particularly during the summers of 2005 and 2006. Organics were found to be highly oxidized and more likely from secondary rather than primary sources during the summer of 2005, while particles contained ammonium sulfate in the cool and humid summer of 2006. The summer of 2007 was classified by the least “aged” particles as seen by the lower percentages of particles containing secondary species and lower relative ion peak areas of those secondary species (Figure 2.4c); due to transport from more pristine environments.

2.5. Conclusions

During a consecutive three summer study in Riverside, CA, the meteorological conditions (temperature, RH, and wind) were highly variable, thus influencing sources of primary aerosol seeds and aging mechanisms that contributed to particle mass. The sources during summers of 2005 and 2006 were very similar and the overall chemical composition exhibited a highly-aged atmosphere; however the summer of 2005 was classified as a highly oxidized organic atmosphere due to enhanced photochemistry, whereas the aerosol composition during the summer of 2006 was controlled by the more stagnant and humid conditions enabling condensation of secondary species—particularly amines from agricultural sources and sulfate—to the particle phase. The summer of 2007 was anomalous compared to the previous summers as dust and sea salt were transported from more rural regions, thus fewer carbonaceous particles and overall less primary seed aerosols were observed. Without preexisting seed aerosols, secondary species and trace gases did not have surfaces to react or condense upon. This, in combination with the hot and dry conditions, led to a cleaner atmosphere with less-aged particles.

This study extends previous work by Qin *et al.* [2012], who compared seasonal single-particle chemistry during 2005 in Riverside. They discovered that even though PM_{2.5} was similar between the summer and fall, the single-particle chemistry was quite

different. In the summer, photochemical production of highly-aged aerosols containing organics and sulfate contributed to particle mass, whereas in the fall, periods with cooler and more stagnant conditions enabled the buildup of organics and ammonium nitrate and periods with strong easterly winds introduced large relative amounts of dust [Qin *et al.*, 2012]. Results presented herein and by Qin *et al.* [2012] demonstrate how variable meteorological conditions largely influence aerosol chemical composition during different time periods. Thus, understanding how single particles can undergo aging processes cannot be based on one major study to represent all years. Observations such as these can be used as proxies for model parameterization; for instance, the summers of 2005, 2006, and 2007 were classified as a photochemically-active environment, condensational aging environment (higher RH, lower temperature), and a cleaner environment (less primary aerosol seeds and low influence from secondary species), respectively. Meteorological parameters such as temperature, RH, and winds result in these proxies and can be used to predict the relative roles of heterogeneous chemistry and sources on particle chemistry. The resulting improved output from using these metrics could be used as a first approximation as to what the detailed chemical composition of PM_{2.5} may be and therefore motivate stricter pollution regulations that are targeted to specific sources based on better-defined health effects models.

2.6. Acknowledgements

We acknowledge Paul Ziemann (UCR), the UCR Air Pollution Research Center, and the Prather group, particularly Laura Shields and Hiroshi Furutani for support during SOAR. We thank Megan McKay and the Goldstein group (UC-Berkeley) for the meteorological measurements in 2005. The authors gratefully acknowledge the NOAA Air Resources Laboratory (ARL) for the provision of the HYSPLIT transport and dispersion model and/or READY website (<http://www.arl.noaa.gov/ready.php>) used in this publication. This work was supported by the California Air Resources Board (CARB 04-336) and the National Science Foundation (NSF ATM-0321362). Kerri Pratt has been supported by a NSF Graduate Research Fellowship and in part by an EPA STAR Graduate Fellowship (2006-2009); the EPA has not officially endorsed this publication,

and the views expressed herein may not reflect the views of the EPA. Andrew Ault has been supported by a Department of Energy Global Change Education Program graduate research environmental fellowship. Cassandra Gaston received funding through a San Diego Fellowship.

2.7. Figures

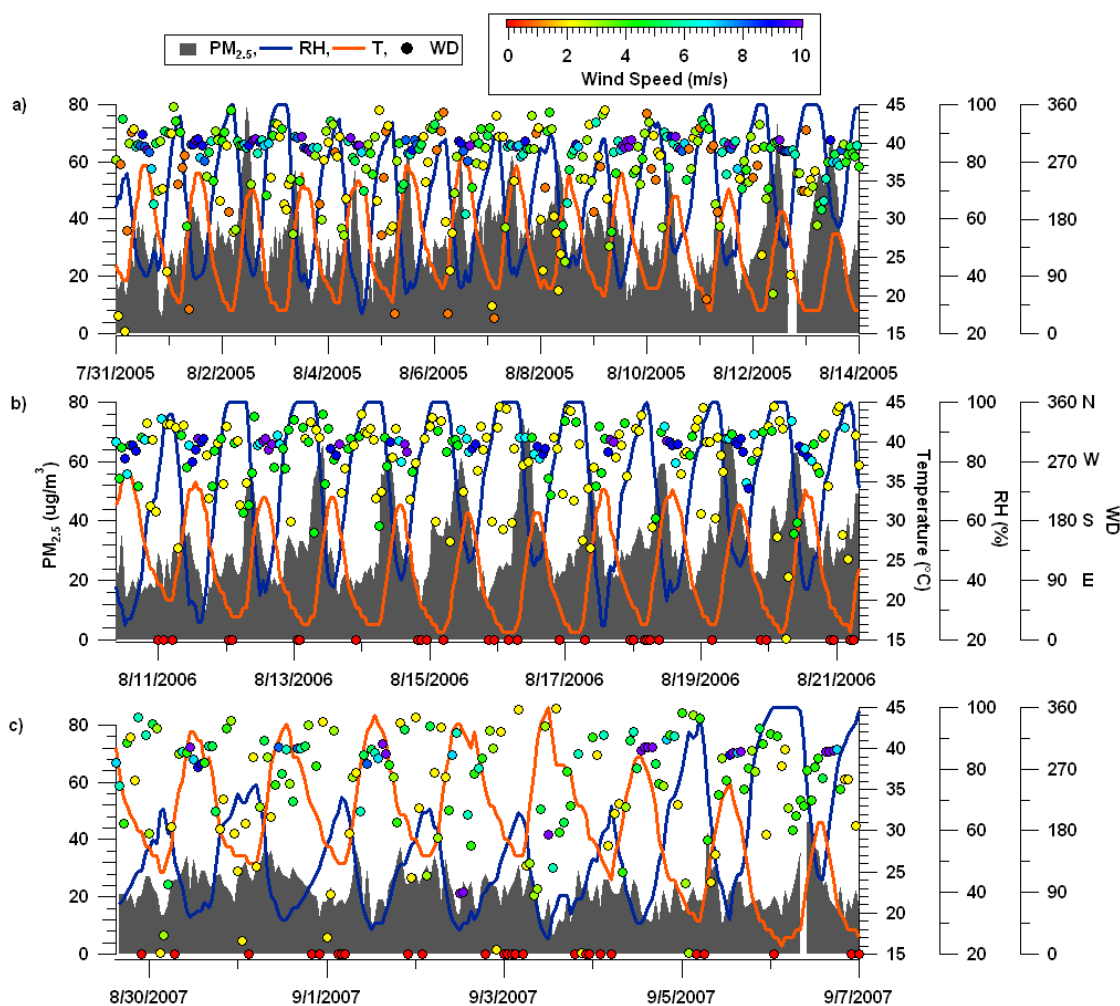


Figure 2.1 Temporal profiles of hourly $PM_{2.5}$ mass concentrations, wind direction (WD), temperature (T), and relative humidity (RH) from a) 2005, b) 2006, and c) 2007. The color of the WD represents the corresponding hourly WS measurement.

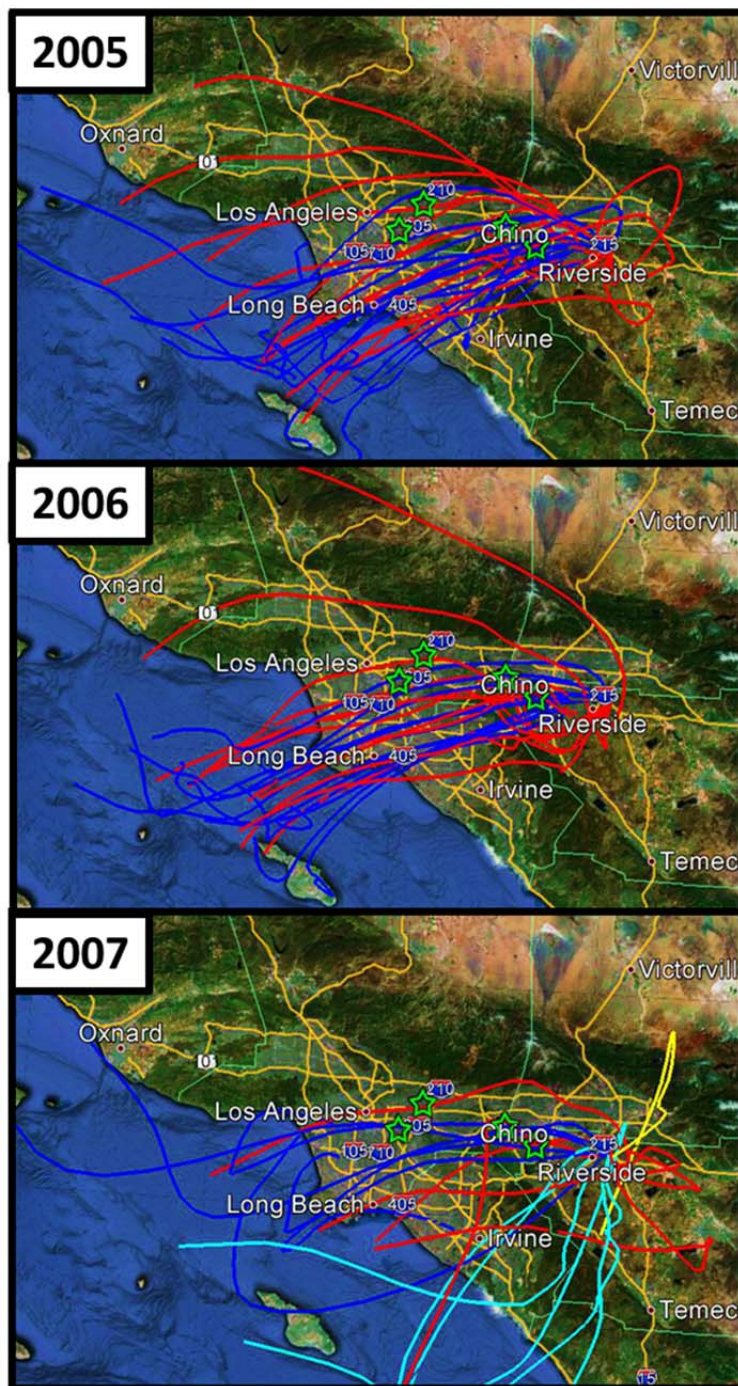


Figure 2.2 Google Earth images showing 24-hour air mass back trajectories calculated for each day during the summers of 2005, 2006, and 2007 over Riverside, CA. Trajectories end 100 m above Riverside and at 00:00 (dark blue) and 12:00 (red) daily. The green stars highlight major dairy farms in the Chino area.

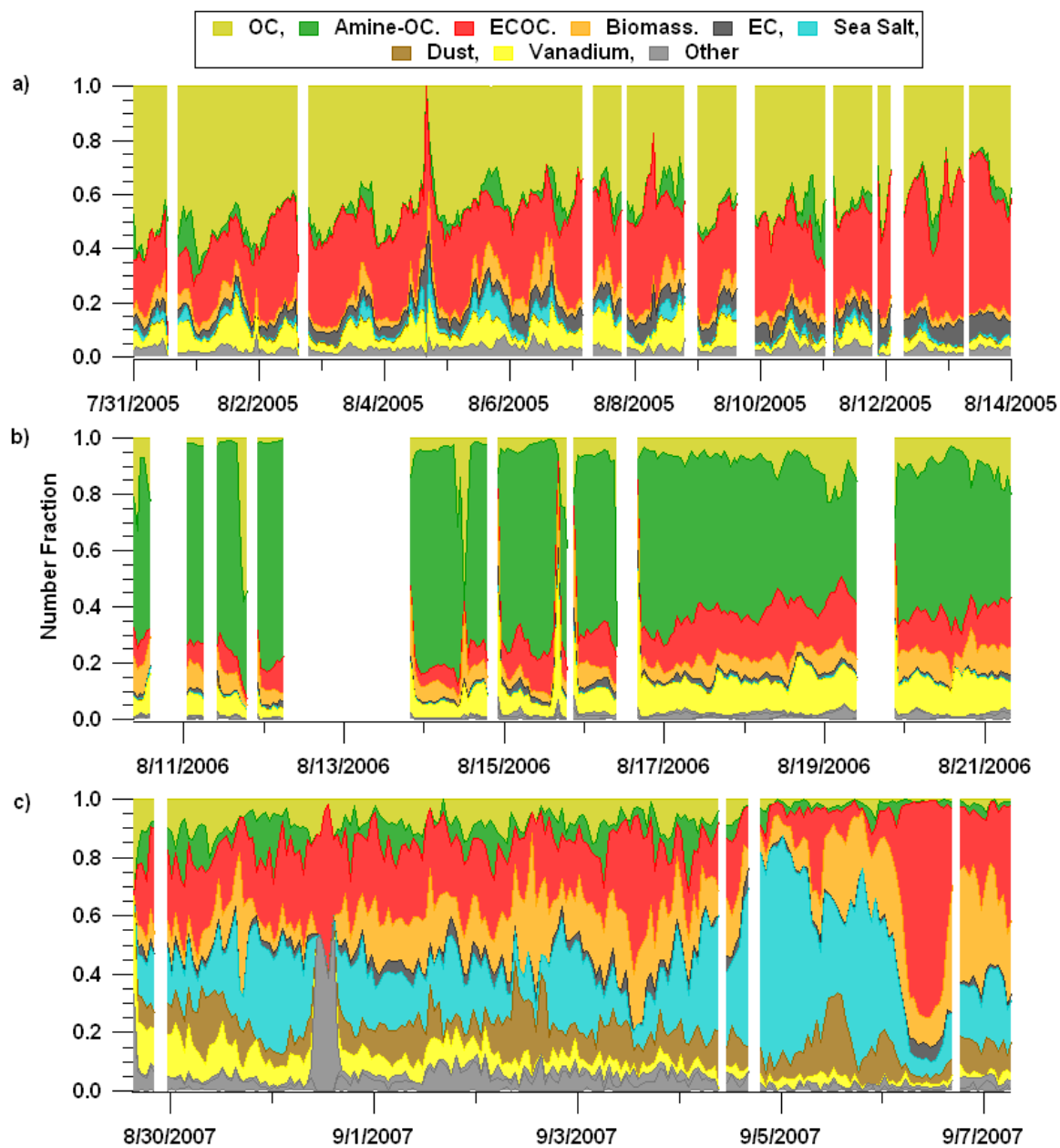


Figure 2.3 Hourly-resolved submicron (0.2-1.0 μm) chemical mixing state of individual particles as measured by ATOFMS for summer studies from 2005-2007.

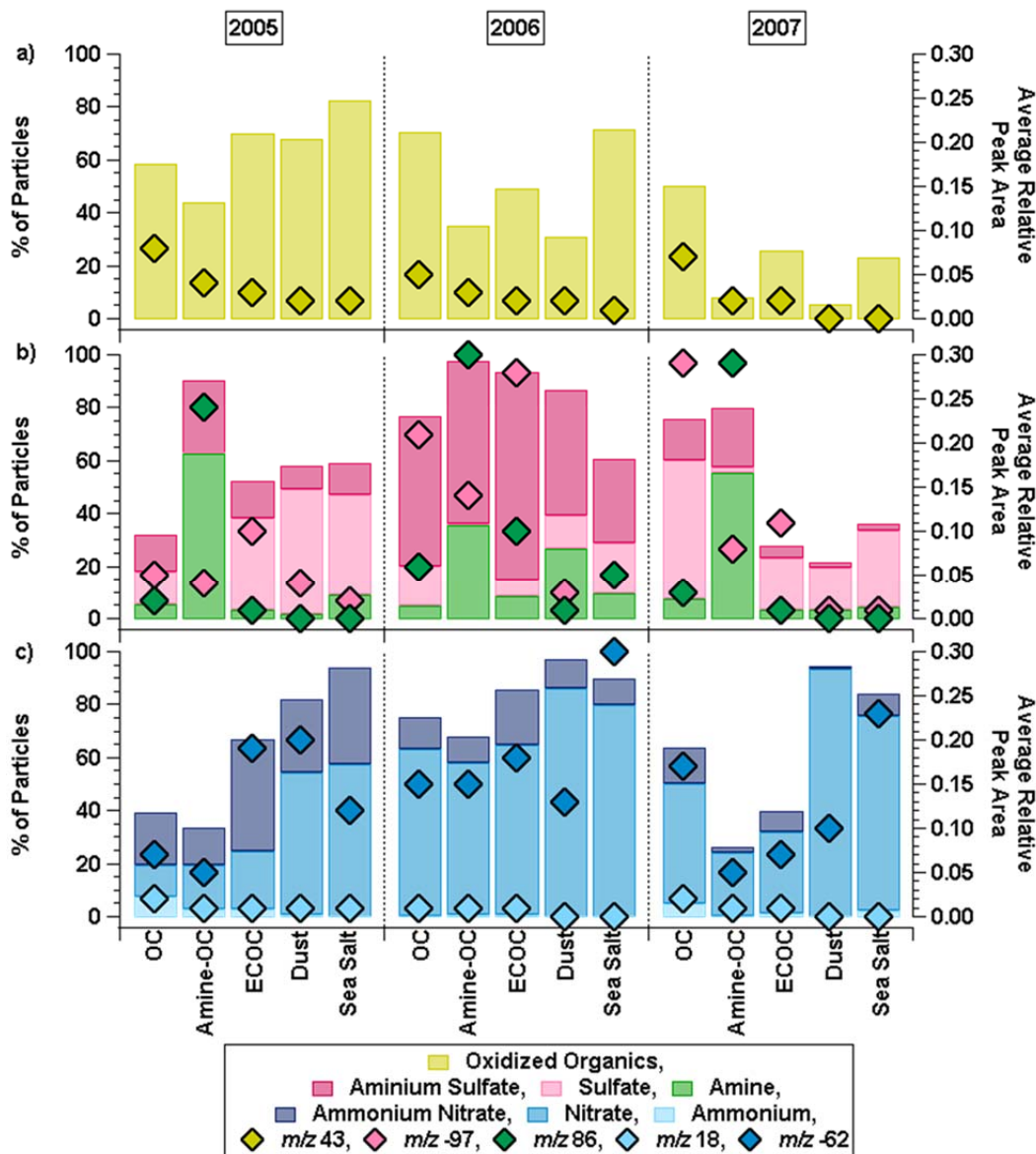


Figure 2.4 Relative amount of major submicron particle types including OC, amine-OC, ECOC, dust, and sea salt, from 2005-2007 mixed with secondary species and relative abundance of each secondary species on each of the particle types. The bars show the percentage of each major type mixed with a) secondary oxidized OC (containing m/z 43), b) aminium sulfate (containing m/z 86 and -97), sulfate (containing m/z -97 without m/z 86), and amine (containing m/z 86 without m/z -97), and c) ammonium nitrate (containing m/z 18 and -62), nitrate (containing m/z -62 without m/z 18), and ammonium (containing m/z 18 without m/z -62). The markers show the relative abundance, or average relative ion peak areas of a) m/z 43, b) m/z 86 and m/z -97, and c) m/z 18 and m/z -62 within each particle type.

2.8. Tables

Table 2.1 Averages of PM_{2.5}, relative humidity (RH), temperature (T), wind speed (WS), and gas-phase O₃ concentrations for the sampling periods during 2005-2007. Standard deviations (σ), medians, and measurement ranges are also listed. 'Avg. Daily Maxima' refers to the average time of the daily maximum of each particular factor. Years are listed from lowest to highest values of each type of data.

Year	Data	Unit	Avg.	σ	Median	Range	Avg. Daily Maxima (PST)
2007	PM _{2.5}	$\mu\text{g}/\text{m}^3$	22	± 7	22	5-46	Various
2005	PM _{2.5}		30	± 13	28	4-79	10:00
2006	PM _{2.5}		32	± 14	29	10-74	9:00
2007	RH	%	56	± 22	50	25-100	6:00
2005	RH		71	± 20	71	36-100	4:00
2006	RH		75	± 22	80	25-100	5:00
2006	T	$^{\circ}\text{C}$	23	± 10	21	16-34	13:00
2005	T		26	± 10	24	18-38	13:00
2007	T		28	± 14	28	16-45	13:00
2007	WS	m/s	3.93	± 3.09	3	0-15	14:00
2006	WS		4.37	± 4.28	2	0-25	15:00
2005	WS		4.40	± 2.74	4	1-14	14:00
2006	[O ₃]	ppb	38.8	± 29.8	30	1-106	13:00
2007	[O ₃]		39.5	± 33.7	29	1-131	14:00
2005	[O ₃]		46.4	± 39.6	34	0-155	14:00

Table 2.2 Descriptions of the major ATOFMS submicron particle types from 2005-2007. All particle types showed evidence of aging based on the presence of ammonium ($^{18}\text{NH}_4^+$), sulfate ($^{97}\text{HSO}_4^-$), nitrate ($^{46}\text{NO}_2^-$ and $^{62}\text{NO}_3^-$) and/or organics, including amines ($^{86}\text{C}_5\text{H}_{12}\text{N}^+$) and oxidized OC ($^{43}\text{C}_2\text{H}_3\text{O}^+/\text{CHNO}^+$).

ATO FMS	
Particle Type	Characterization
OC	Carbonaceous ion markers at $^{12}\text{C}^+$, $^{27}\text{C}_2\text{H}_3^+/\text{CHN}^+$, $^{36}\text{C}_3^+$, $^{37}\text{C}_3\text{H}^+$, and $^{43}\text{CH}_3\text{CO}^+/\text{CHNO}^+$
Amine-OC	Contained $^{86}(\text{C}_2\text{H}_5)_2\text{NCH}_2^+$ with less intense amine ion markers at $^{58}\text{C}_2\text{H}_5\text{NHCH}_2^+$, $^{102}(\text{C}_2\text{H}_5)_3\text{NH}^+$, and $^{118}(\text{C}_2\text{H}_5)_3\text{NOH}^+$ and other minor organic carbon ion markers
EC	Characterized by intense carbon cluster positive and negative ion markers from $\text{C}^{+/-}$ to $\text{C}_n^{+/-}$
ECOC	Similar to that of EC with less intense OC ion markers
Biomass	Contained potassium ($^{39/41}\text{K}^+$) with less intense organic carbon ion markers
Sea salt	Intense sodium ($^{23}\text{Na}^+$), $^{39/41}\text{K}^+$, and chlorine ($^{35/37}\text{Cl}^-$) ion markers with smaller ammonium and carbonaceous ion markers
Dust	Inorganic ion markers at $^{23}\text{Na}^+$, magnesium ($^{24}\text{Mg}^+$), calcium ($^{40}\text{Ca}^+$), and/or iron ($^{56}\text{Fe}^+$)
Vanadium	Intense ion markers at $^{51}\text{V}^+$ and $^{67}\text{VO}^+$

2.9. References

- Angelino, S., D.T. Suess, and K.A. Prather, Formation of aerosol particles from reactions of secondary and tertiary alkylamines: Characterization by aerosol time-of-flight mass spectrometry, *Environmental Science & Technology*, 35 (15), 3130-3138, 2001.
- Appel, B.R., E.L. Kothny, E.M. Hoffer, G.M. Hidy, and J.J. Wesolowski, Sulfate and Nitrate Data from California Aerosol Characterization Experiment (Achex), *Environmental Science & Technology*, 12 (4), 418-425, 1978.

- Brook, R.D., S. Rajagopalan, C.A. Pope, J.R. Brook, A. Bhatnagar, A.V. Diez-Roux, F. Holguin, Y.L. Hong, R.V. Luepker, M.A. Mittleman, A. Peters, D. Siscovick, S.C. Smith, L. Whitsel, J.D. Kaufman, A.H.A.C. Epidemiol, C.K.C. Dis, and C.N.P.A. Metab, Particulate Matter Air Pollution and Cardiovascular Disease An Update to the Scientific Statement From the American Heart Association, *Circulation*, 121 (21), 2331-2378, 2010.
- CARB, Area Designation Maps for Ambient Air Quality Standards/State and National, pp. <http://www.arb.ca.gov/desig/adm/adm.htm>, 2010.
- Chow, J.C., J.G. Watson, E.M. Fujita, Z.Q. Lu, D.R. Lawson, and L.L. Ashbaugh, Temporal and Spatial Variations of Pm(2.5) and Pm(10) Aerosol in the Southern California Air-Quality Study, *Atmospheric Environment*, 28 (12), 2061-2080, 1994.
- Creamean, J.M., A.P. Ault, J.E. Ten Hoeve, M.Z. Jacobson, G.C. Roberts, and K.A. Prather, Measurements of Aerosol Chemistry during New Particle Formation Events at a Remote Rural Mountain Site, *Environmental Science & Technology*, 45 (19), 8208-8216, 2011.
- Docherty, K.S., A.C. Aiken, J.A. Huffman, I.M. Ulbrich, P.F. DeCarlo, D. Sueper, D.R. Worsnop, D.C. Snyder, B.D. Grover, D.J. Eatough, A.H. Goldstein, P.J. Ziemann, and J.L. Jimenez, The 2005 Study of Organic Aerosols at Riverside (SOAR-1): instrumental intercomparisons and fine particle composition, *Atmos. Chem. Phys. Discuss.*, 11, 6301–6362, 2011.
- Docherty, K.S., E.A. Stone, I.M. Ulbrich, P.F. DeCarlo, D.C. Snyder, J.J. Schauer, R.E. Peltier, R.J. Weber, S.M. Murphy, J.H. Seinfeld, B.D. Grover, D.J. Eatough, and J.L. Jimenez, Apportionment of Primary and Secondary Organic Aerosols in Southern California during the 2005 Study of Organic Aerosols in Riverside (SOAR-1), *Environmental Science & Technology*, 42 (20), 7655-7662, 2008.
- Draxler, R.R., and G.D. Rolph, HYSPLIT (HYbrid Single-Particle Lagrangian Integrated Trajectory) Model access via NOAA ARL READY Website (<http://ready.arl.noaa.gov/HYSPLIT.php>), NOAA Air Resources Laboratory, Silver Spring, MD, 2011.
- Edinger, J.G., Modification of the Marine Layer over Coastal Southern California, *Journal of Applied Meteorology*, 2 (6), 706-712, 1963.
- Fine, P.M., B. Chakrabarti, M. Krudysz, J.J. Schauer, and C. Sioutas, Diurnal variations of individual organic compound constituents of ultrafine and accumulation mode particulate matter in the Los Angeles basin, *Environmental Science & Technology*, 38 (5), 1296-1304, 2004.
- Finlayson-Pitts, B.J., Pitts, J. N., *Chemistry of the Upper and Lower Atmosphere*, Academic Press, San Diego, 2000.

- Gard, E., J.E. Mayer, B.D. Morrical, T. Dienes, D.P. Fergenson, and K.A. Prather, Real-time analysis of individual atmospheric aerosol particles: Design and performance of a portable ATOFMS, *Analytical Chemistry*, 69 (20), 4083-4091, 1997.
- Gard, E.E., M.J. Kleeman, D.S. Gross, L.S. Hughes, J.O. Allen, B.D. Morrical, D.P. Fergenson, T. Dienes, M.E. Galli, R.J. Johnson, G.R. Cass, and K.A. Prather, Direct observation of heterogeneous chemistry in the atmosphere, *Science*, 279 (5354), 1184-1187, 1998.
- Geller, M.D., P.M. Fine, and C. Sioutas, The relationship between real-time and time-integrated coarse (2.5-10 μ m), intermodal (1-2.5 μ m), and fine (< 2.5 μ m) particulate matter in the Los Angeles Basin, *Journal of the Air & Waste Management Association*, 54 (9), 1029-1039, 2004.
- Harrison, R.M., and J.X. Yin, Particulate matter in the atmosphere: which particle properties are important for its effects on health?, *Science of the Total Environment*, 249 (1-3), 85-101, 2000.
- Hennigan, C.J., A.P. Sullivan, C.I. Fountoukis, A. Nenes, A. Hecobian, O. Vargas, R.E. Peltier, A.T.C. Hanks, L.G. Huey, B.L. Lefer, A.G. Russell, and R.J. Weber, On the volatility and production mechanisms of newly formed nitrate and water soluble organic aerosol in Mexico City, *Atmospheric Chemistry and Physics*, 8 (14), 3761-3768, 2008.
- Hughes, L.S., J.O. Allen, P. Bhave, M.J. Kleeman, G.R. Cass, D.Y. Liu, D.F. Fergenson, B.D. Morrical, and K.A. Prather, Evolution of atmospheric particles along trajectories crossing the Los Angeles basin, *Environmental Science & Technology*, 34 (15), 3058-3068, 2000.
- Hughes, L.S., J.O. Allen, L.G. Salmon, P.R. Mayo, R.J. Johnson, and G.R. Cass, Evolution of nitrogen species air pollutants along trajectories crossing the Los Angeles area, *Environmental Science & Technology*, 36 (18), 3928-3935, 2002.
- Kim, B.M., S. Teffera, and M.D. Zeldin, Characterization of PM_{2.5} and PM₁₀ in the South Coast Air Basin of southern California: Part 1 - Spatial variations, *Journal of the Air & Waste Management Association*, 50 (12), 2034-2044, 2000a.
- Kim, B.M., S. Teffera, and M.D. Zeldin, Characterization of PM_{2.5} and PM₁₀ in the South Coast Air Basin of southern California: Part 2 - Temporal variations, *Journal of the Air & Waste Management Association*, 50 (12), 2045-2059, 2000b.
- Kleeman, M.J., L.S. Hughes, J.O. Allen, and G.R. Cass, Source contributions to the size and composition distribution of atmospheric particles: Southern California in September 1996, *Environmental Science & Technology*, 33 (23), 4331-4341, 1999.

- Latzin, P., M. Roosli, A. Huss, C.E. Kuehni, and U. Frey, Air pollution during pregnancy and lung function in newborns: a birth cohort study, *European Respiratory Journal*, 33 (3), 594-603, 2009.
- Li, C.S., W.H. Lin, and F.T. Jenq, Characterization of Outdoor Submicron Particles and Selected Combustion Sources of Indoor Particles, *Atmospheric Environment Part B-Urban Atmosphere*, 27 (4), 413-424, 1993.
- Liu, D.Y., K.A. Prather, and S.V. Hering, Variations in the size and chemical composition of nitrate-containing particles in Riverside, CA, *Aerosol Science and Technology*, 33 (1-2), 71-86, 2000.
- Mamane, Y., and J. Gottlieb, Nitrate Formation on Sea-Salt and Mineral Particles - a Single-Particle Approach, *Atmospheric Environment Part a-General Topics*, 26 (9), 1763-1769, 1992.
- Mauderly, J.L., and J.C. Chow, Health effects of organic aerosols, *Inhalation Toxicology*, 20 (3), 257-288, 2008.
- Meng, Z., D. Dabdub, and J.H. Seinfeld, Chemical coupling between atmospheric ozone and particulate matter, *Science*, 277 (5322), 116-119, 1997.
- Murphy, S.M., A. Sorooshian, J.H. Kroll, N.L. Ng, P. Chhabra, C. Tong, J.D. Surratt, E. Knipping, R.C. Flagan, and J.H. Seinfeld, Secondary aerosol formation from atmospheric reactions of aliphatic amines, *Atmospheric Chemistry and Physics*, 7 (9), 2313-2337, 2007.
- Mysliwicz, M.J., and M.J. Kleeman, Source apportionment of secondary airborne particulate matter in a polluted atmosphere, *Environmental Science & Technology*, 36 (24), 5376-5384, 2002.
- Nawrot, T.S., L. Perez, N. Kunzli, E. Munters, and B. Nemery, Public health importance of triggers of myocardial infarction: a comparative risk assessment, *Lancet*, 377 (9767), 732-740, 2011.
- Ospital, J., J. Cassmassi, and T. Chico, Multiple Air Toxics Exposure Study in the South Coast Air Basin (MATES III) Final Report, South Coast Air Quality Management District, Diamond Bar, 2008.
- Pastor, S.H., J.O. Allen, L.S. Hughes, P. Bhave, G.R. Cass, and K.A. Prather, Ambient single particle analysis in Riverside, California by aerosol time-of-flight mass spectrometry during the SCOS97-NARSTO, *Atmospheric Environment*, 37, S239-S258, 2003.
- Pey, J., A. Alastuey, X. Querol, N. Perez, and M. Cusack, A simplified approach to the indirect evaluation of the chemical composition of atmospheric aerosols from PM mass concentrations, *Atmospheric Environment*, 44 (39), 5112-5121, 2010.

- Pope, C.A., and D.W. Dockery, Health effects of fine particulate air pollution: Lines that connect, *Journal of the Air & Waste Management Association*, 56 (6), 709-742, 2006.
- Pope, C.A., M.J. Thun, M.M. Namboodiri, D.W. Dockery, J.S. Evans, F.E. Speizer, and C.W. Heath, Particulate Air-Pollution as a Predictor of Mortality in a Prospective-Study of Us Adults, *American Journal of Respiratory and Critical Care Medicine*, 151 (3), 669-674, 1995.
- Poschl, U., Atmospheric aerosols: Composition, transformation, climate and health effects, *Angewandte Chemie-International Edition*, 44 (46), 7520-7540, 2005.
- Pratt, K.A., New Insights into Single-Particle Mixing State using Aircraft Aerosol Time-of-Flight Mass Spectrometry, University of California, San Diego, La Jolla, 2009.
- Pratt, K.A., L.E. Hatch, and K.A. Prather, Seasonal Volatility Dependence of Ambient Particle Phase Amines, *Environmental Science & Technology*, 43, 5276–5281, 2009a.
- Pratt, K.A., J.E. Mayer, J.C. Holecek, R.C. Moffet, R.O. Sanchez, T.P. Rebotier, H. Furutani, M. Gonin, K. Fuhrer, Y.X. Su, S. Guazzotti, and K.A. Prather, Development and Characterization of an Aircraft Aerosol Time-of-Flight Mass Spectrometer, *Analytical Chemistry*, 81 (5), 1792-1800, 2009b.
- Pratt, K.A., and K.A. Prather, Real-Time, Single-Particle Volatility, Size, and Chemical Composition Measurements of Aged Urban Aerosols, *Environmental Science & Technology*, 43 (21), 8276-8282, 2009.
- Pratt, K.A., and K.A. Prather, Mass spectrometry of atmospheric aerosols—Recent developments and applications. Part II: On-line mass spectrometry techniques, *Mass Spectrometry Reviews*, 31 (1), 17-48, 2012.
- Qin, X.Y., L.G. Shields, S.M. Toner, K.A. Pratt, and K.A. Prather, Seasonal comparisons of single-particle chemical mixing state in Riverside, CA, *Atmospheric Environment*, 59, 587-596, 2012.
- Ramsay, T.O., R.T. Burnett, and D. Krewski, The effect of concurvity in generalized additive models linking mortality to ambient particulate matter, *Epidemiology*, 14 (1), 18-23, 2003.
- Rubasinghege, G., R.W. Lentz, M.M. Scherer, and V.H. Grassian, Simulated atmospheric processing of iron oxyhydroxide minerals at low pH: Roles of particle size and acid anion in iron dissolution, *Proceedings of the National Academy of Sciences of the United States of America*, 107 (15), 6628-6633, 2010.
- Russell, A.G., G.R. Cass, and J.H. Seinfeld, On Some Aspects of Nighttime Atmospheric Chemistry, *Environmental Science & Technology*, 20 (11), 1167-1172, 1986.

- Saul, T.D., M.P. Tolocka, and M.V. Johnston, Reactive uptake of nitric acid onto sodium chloride aerosols across a wide range of relative humidities, *Journal of Physical Chemistry A*, 110 (24), 7614-7620, 2006.
- Seaton, A., W. Macnee, K. Donaldson, and D. Godden, *Particulate Air-Pollution and Acute Health-Effects*, *Lancet*, 345 (8943), 176-178, 1995.
- Singh, M., P.A. Jaques, and C. Sioutas, Size distribution and diurnal characteristics of particle-bound metals in source and receptor sites of the Los Angeles Basin, *Atmospheric Environment*, 36 (10), 1675-1689, 2002.
- Song, X.H., P.K. Hopke, D.P. Fergenson, and K.A. Prather, Classification of single particles analyzed by ATOFMS using an artificial neural network, *ART-2A, Analytical Chemistry*, 71 (4), 860-865, 1999.
- Sorooshian, A., S.N. Murphy, S. Hersey, H. Gates, L.T. Padro, A. Nenes, F.J. Brechtel, H. Jonsson, R.C. Flagan, and J.H. Seinfeld, Comprehensive airborne characterization of aerosol from a major bovine source, *Atmospheric Chemistry and Physics*, 8 (17), 5489-5520, 2008.
- Stephens, E.R., *Marine Layer and Its Relation to a Smog Episode in Riverside California*, *Atmospheric Environment*, 2 (4), 393-&, 1968.
- Sullivan, R.C., M.J.K. Moore, M.D. Petters, S.M. Kreidenweis, G.C. Roberts, and K.A. Prather, Timescale for hygroscopic conversion of calcite mineral particles through heterogeneous reaction with nitric acid, *Physical Chemistry Chemical Physics*, 11 (36), 7826-7837, 2009.
- Takekawa, H., H. Minoura, and S. Yamazaki, Temperature dependence of secondary organic aerosol formation by photo-oxidation of hydrocarbons, *Atmospheric Environment*, 37 (24), 3413-3424, 2003.
- Tang, M.J., J. Thieser, G. Schuster, and J.N. Crowley, Uptake of NO₃ and N₂O₅ to Saharan dust, ambient urban aerosol and soot: a relative rate study, *Atmospheric Chemistry and Physics*, 10 (6), 2965-2974, 2010.
- Toner, S.M., L.G. Shields, D.A. Sodeman, and K.A. Prather, Using mass spectral source signatures to apportion exhaust particles from gasoline and diesel powered vehicles in a freeway study., *Abstracts of Papers of the American Chemical Society*, 229, U127-U127, 2005.
- Vedal, S., *Ambient particles and health: Lines that divide*, *Journal of the Air & Waste Management Association*, 47 (5), 551-581, 1997.
- Wenzel, R.J., D.Y. Liu, E.S. Edgerton, and K.A. Prather, Aerosol time-of-flight mass spectrometry during the Atlanta Supersite Experiment: 2. Scaling procedures, *Journal of Geophysical Research-Atmospheres*, 108 (D7), 2003.

Ying, Q., and M.J. Kleeman, Source contributions to the regional distribution of secondary particulate matter in California, *Atmospheric Environment*, 40 (4), 736-752, 2006.

3. Significant Changes in Urban Aerosol Chemistry and CCN Concentrations Induced by Tropical Cyclones

3.1. Introduction

Aerosols from urban pollution cause adverse health effects as well as impact cloud microphysics by serving as cloud condensation nuclei (CCN) [Chubarova *et al.*, 2011; IPCC, 2007; Poschl, 2005]. High concentrations of smaller CCN ($\sim 0.04\text{--}0.2\ \mu\text{m}$) reduce cloud droplet size by slowing down cloud drop coalescence and accretion, thus delaying the conversion of cloud water into precipitation [McFiggans *et al.*, 2006; Rosenfeld, 2000]. Although less numerous than the small CCN, large or giant CCN (typically treated as $>2\ \mu\text{m}$) are thought to result in an early development of large drops at the lower cloud layers [Posselt and Lohmann, 2008; Rosenfeld *et al.*, 2001; Yin *et al.*, 2000]. A combination of giant CCN and high concentrations of small CCN enables clouds to precipitate faster, thus altering the location of precipitation [Johnson, 1982; Yin *et al.*, 2000]. Feingold *et al.* [1999] have shown that the relative impact of giant CCN on precipitation efficiency increases with increasing small CCN concentrations, therefore, the effect of giant CCN on continental clouds is potentially significant [Yin *et al.*, 2000].

Highly-developed continental regions such as Atlanta, GA, are large sources of urban and industrial pollution aerosols which efficiently serve as CCN [Rosenfeld, 2000]. In Atlanta, a significant fraction of fine aerosol ($\leq 2.5\ \mu\text{m}$) is composed of organic compounds and sulfate (up to 56% by mass) due to secondary processing or “aging” of primary emissions with gas phase precursors, such as SO_2 from surrounding coal-fired power plants [Levy *et al.*, 2003]. Further, highly-reactive volatile organic compounds (VOCs) such as isoprene are abundant in the southeastern U.S. and can also contribute to particle aging [Kim *et al.*, 2003; Lee *et al.*, 2002; Millet *et al.*, 2008]. The influence from both anthropogenic and biogenic sources thus demonstrates the complex nature of the Atlanta aerosol chemical composition, which is overall poorly understood [Alston *et al.*, 2011; Liu *et al.*, 2003; Turpin and Lim, 2002]. Further, precipitation distribution in the Atlanta metropolitan area has been shown to vary spatially depending on the CCN

present [Lacke *et al.*, 2009], thus a better understanding of the chemical composition of aerosols that serve as CCN in Atlanta is needed.

Dust can serve as giant CCN in continental regions [Posselt and Lohmann, 2008] and has been shown to be the largest component of coarse aerosol ($\geq 2.5 \mu\text{m}$, 60% by mass) in Atlanta [Kim *et al.*, 2003]. Due to its soluble nature, a more efficient giant CCN is sea salt [Ghan *et al.*, 1998; Pierce and Adams, 2006; Posselt and Lohmann, 2008; Teller and Levin, 2006]. However, sea salt does not constitute a large fraction of the Atlanta aerosol due to its distance from salt water (~ 380 km from the Atlantic Ocean). Previously, Noble and Prather [1997] observed sea salt transported 100 km inland from the Pacific Ocean at an urban location on the west coast of the U.S. in response to winter rainstorms. Based on the fact that smaller rainstorms have the ability to transport marine air masses long distances, more severe meteorological disturbances could potentially have a larger influence on continental air farther inland. Tropical cyclones (TCs) are severe tropical storms associated with high wind speeds, induce heavy precipitation, and have been shown to alter aerosol concentrations [Feng *et al.*, 2007; Greene *et al.*, 2003]. However, few studies have focused on the effects of TCs on aerosol concentrations and composition. Chang *et al.* [2011] observed a decrease in pollutant concentrations of nitrate, sulfate, and ammonium during tropical storm NOCK-TEN in southern Taiwan. In contrast, Feng *et al.* [2007] observed a pollution episode (high PM_{10} , particulate matter $\leq 10 \mu\text{m}$) develop in response to TC Melor in China, however, aerosol chemical composition was not probed. These variable results demonstrate the need to further investigate TC impacts on aerosol pollution in urban regions.

The goal of this study was to investigate the potential of severe storms such as TCs to perturb urban aerosol populations and thereby alter the CCN properties of aerosols found at an inland, urban location. During the 2008 Atlantic hurricane season, TCs Gustav and Hanna impacted the Atlanta area, altering local meteorological conditions such as wind speed and direction. Additionally, the impact of the TCs on ambient aerosol number, size, and composition was examined using aerosol time-of-flight mass spectrometry (ATOFMS), which provides single-particle information that can

be used to differentiate particle source (e.g. the ocean vs. coal combustion) as well as probe atmospheric processing [Guazzotti et al., 2003; Noble and Prather, 1997]. Further, the impact of these findings on cloud microphysics was also investigated by providing a direct link between changes in particle size and chemistry, CCN concentrations, and precipitation. To our knowledge, this is the first time changes in the size-resolved chemistry and cloud formation properties of aerosols have been observed at a highly-polluted, inland city in response to severe storms.

3.2. Experimental

Ambient aerosol and meteorological measurements were made at the Southeastern Aerosol Research and Characterization (SEARCH) Network Jefferson Street site in Atlanta, GA from 8/5-9/10 during the 2008 August Mini-Intensive Gas and Aerosol Study (AMIGAS). $PM_{2.5}$ mass concentrations, SO_2 concentrations, and meteorological measurements including wind speed (WS), wind direction (WD), and precipitation were acquired from Atmospheric Research & Analysis, Inc. (ARA). CCN concentrations were measured at $\sim 0.2\%$ supersaturation using a Droplet Measurement Technologies Continuous-Flow Streamwise Thermal-Gradient Chamber [Roberts and Nenes, 2005b]. Total particle concentrations (condensation nuclei, CN) were obtained using a condensation particle counter (CPC, TSI 3010). An aerodynamic particle sizer (APS) (Model 3321, TSI Inc.) measured particle size distributions from 0.523-20 μm .

ATOFMS was used to characterize the size-resolved chemistry of individual particles between 0.2-3.0 μm [Gard et al., 1997b]. Briefly, single particles enter through a converging nozzle inlet into a differentially-pumped vacuum chamber. The vacuum aerodynamic diameter (D_{va}) of each particle is determined in the light scattering region by measuring the time taken to traverse two continuous wave diode lasers (532 nm) at a fixed distance, providing the terminal velocity of the particle, which can be converted to D_{va} by calibration with polystyrene latex spheres of known sizes. Individual particles are then simultaneously desorbed and ionized by a Q-switched Nd:YAG laser (266 nm), creating positive and negative ions that are detected by a dual polarity time-of-flight mass spectrometer. The Nd:YAG laser was operated at 1.4-1.5 mJ throughout the study at 1.1

mJ from 8/22-8/29. Average relative ion peak areas are presented in order to eliminate any biases that may be caused by the different laser powers.

Single-particle mass spectra were imported into YAADA [Allen, 2004], a software toolkit in Matlab (The Mathworks, Inc.), for detailed analysis of particle size and chemistry. ART-2a, an adaptive resonance theory-based clustering algorithm [Song *et al.*, 1999a], was then used to classify particles into separate groups depending on the presence and intensity of ion peaks within an individual particle's mass spectra. The most populated 75 clusters account for >90% of the total ART-2a classified particles and are considered representative of the overall aerosol composition. Peak identifications within this paper correspond to the most probable ions for a given mass-to-charge ratio. Two nearly identical ATOFMS instruments were used during the study; ATOFMS 1 was operated from 8/5-8/13 whereas ATOFMS 2 was used from 8/22-9/10. Due to instrumental downtime, data were not collected from 8/14-8/22. Data are presented in Eastern Standard Time (EST).

3.3. Results and Discussion

3.3.1. Meteorological changes in Atlanta during TCs

Local meteorological conditions and air mass back trajectories calculated using HYSPLIT [Draxler and Rolph, 2003] provide direct evidence that the TCs transported marine air masses to Atlanta. Figure 3.1 shows the daily 120-hour back trajectories ending 1000 m above the site during Gustav (panel a) and Hanna (panel b), in addition to representative trajectories for days before the TCs (8/5 and 8/11). The central locations of the TCs each day are also shown in Figure 3.1 during time periods where Gustav and Hanna were classified as tropical storms (8/25-9/4 and 8/28-9/7, respectively) [Beven II and Kimberlain, 2009; Brown and Kimberlain, 2008]. For most days during the TCs, air masses originated from over the Atlantic Ocean or Gulf of Mexico. Direct TC influences on Atlanta are supported by the disruption of diurnal patterns in local winds as shown in Figure 3.2. Prevailing diurnal winds in Atlanta were typically slow (peaking at 2-4 m/s) and westerly (180-360°) during three time periods of "normal conditions" as highlighted

by green boxes in Figure 3.2 (i.e., 8/5-8/20, 8/27-9/1, and 9/6-9/10). However, during both TCs, easterly (70-100°) winds rapidly increased to maxima of 4-7 m/s—denoted as time periods with “TC conditions” and highlighted by maroon boxes in Figure 3.2. Table 3.1 provides dates and the maximum wind speed range for each of the periods. The first showers and frontal organization of Gustav occurred in the Atlantic on 8/18 as the front continued to move west, likely explaining increase in wind speed observed in Atlanta prior to when Gustav was classified as a TC [Beven II and Kimberlain, 2009]. Decreased temperature and increased relative humidity also occurred during TCs and are shown in Hatch *et al.* [2011c]. Overall, the TCs served as mechanisms for long-range transport of tropical, marine air masses to Atlanta. Based on the drastic changes in source regions and local meteorology (i.e., winds, temperature, and relative humidity), we would expect a shift in aerosol concentrations and composition, which is discussed herein.

3.3.2. TC effects on aerosol size and chemical composition

Changes in wind speed and direction from the TCs led to advection of the local urban aerosol, as evident by a decrease in PM_{2.5} mass concentrations from an average of 22.5 µg/m³ before the TCs to 12.3 µg/m³ during time periods with TC conditions (Figure 3.3a); this also resulted in differences in particle number, size, and chemical composition. Figure 3.3a also shows the total number concentrations from the APS, along with both submicron (0.2-1.0 µm) and supermicron (1.0-3.0 µm) particle counts per hour measured by ATOFMS. The APS data show higher number concentrations (~120 cm⁻³) during normal conditions before the TCs until a shift to fast, easterly winds during the first time period with TC conditions, then stayed fairly low for the remainder of AMIGAS (~37 cm⁻³). Both submicron and supermicron counts were high before the TCs and decreased during the TCs as well. Supermicron counts remained low for the remainder of AMIGAS; however, submicron particle counts increased as wind speed decreased (starting 9/2), suggesting submicron particles were from local sources and resumed accumulation once advection from TC winds ceased. In addition, the first time period with TC conditions was the only time supermicron particle counts were higher than submicron. These trends suggest that fast TC winds had a large influence on particle

number and size in Atlanta by cleaning out preexisting submicron and supermicron particles and transporting different supermicron particles, as revealed by particle chemical composition.

The ATOFMS particle types measured during AMIGAS were organic carbon (OC), elemental carbon (EC) or soot, EC mixed with OC (ECOC), biomass burning, dust, fly ash, sea salt, and other minor types (<1% of total particles). These types are described by Hatch *et al.* [2011b; 2011c] during AMIGAS and are similar to those previously observed using ATOFMS in Atlanta by Liu *et al.* [2003] during the Atlanta Supersite Experiment. Figure 3.3b and c show the relative number fractions of particle types for both submicron and supermicron particles, respectively. The submicron particles were predominantly organic-containing (OC+ECOC particles) representing ~83% of the particles by number. Supermicron particle chemistry was dominated by fly ash (33%) produced during coal combustion and dust (18%) potentially from local industrial or machining processes, both common in the Atlanta area [Liu *et al.*, 2003; Sodeman, 2004; Spencer *et al.*, 2008], in addition to sea salt (32%) predominantly during the TCs.

As shown in Figure 3.3, the observed submicron and supermicron particle chemistry rapidly changed during the first time period with TC conditions—as Gustav impacted the area. Organic-containing particles, fly ash, and dust decreased while the number fraction of submicron and supermicron sea salt increased to up to 60%, and up to 98% of the total particle counts, respectively, during the largest spike in wind speed from 8/22-8/25. The corresponding shift in particle chemistry during TCs when air masses originated over the ocean confirms the TCs were responsible for the shift to sea salt. During the normal conditions after the first time period with TC conditions, the number fraction of supermicron sea salt decreased then increased once again during the second time period with TC conditions. The submicron ATOFMS counts appeared to follow an anti-correlation with the number fraction of sea salt: when sea salt increased, the submicron counts were low, however, when sea salt particles decreased during the last two normal condition periods, the submicron counts were high similar to before the TCs.

This trend further supports local buildup of organic-containing aerosols during normal conditions and pollution cleanout during marine air mass transport.

As previously mentioned, SO₂ emissions from local coal-fired power plants are significant in the Atlanta area [Levy *et al.*, 2003]. In addition to advecting local aerosol, the TC winds also cleaned out regional SO₂ emissions as shown in Table 3.1. The average SO₂ concentration during normal conditions was 2.94 ppb and decreased to 0.82 ppb during TC conditions. After organic particles enter the atmosphere, secondary species such as sulfate formed through gas- and aqueous-phase oxidation of SO₂, contribute greatly to changes in particle size and chemistry [Finlayson-Pitts, 2000; Poschl, 2005]. Further, particles aged with sulfate are typically more hygroscopic, i.e., better CCN [Baltensperger *et al.*, 2002; Kanakidou *et al.*, 2005]. The relative abundance of sulfate within a particle can be indicative of the age of the particle; the more sulfate, the more aged the particle [Hughes *et al.*, 2000; Ying and Kleeman, 2006], hence, the potential to serve as a more efficient CCN. Based on the fact that TC winds cleaned out preexisting pollutants (i.e., aerosols and SO₂), we would expect less sulfate in organic-containing particles in response to TC conditions, and potentially less-CCN active aerosols.

In order to test this hypothesis, the average relative peak area of sulfate (m/z -97, HSO₄⁻) was used to determine organic-containing particle age, i.e., on OC and ECOC particle types, combined. Relative ion peak areas measured by ATOFMS can indicate the relative abundance of a particular chemical species present in the particles within ~10-20%, provided that the particle matrix is similar (i.e., similar particle types) [Bhave *et al.*, 2002b; Gross *et al.*, 2000]. As shown in Figure 3.3d, the submicron OC+ECOC particles exhibited lower relative ion peak area of m/z -97 during the TCs compared to before, suggesting the organic-containing particles were not highly aged with sulfate, i.e., were “fresher.” One explanation for the relationship between organic-containing aerosols and sulfate is the deficiency in SO₂ during TC conditions. Further, increases in the relative ion peak area of m/z -97 typically corresponded to increases in submicron ATOFMS counts (Figure 3.3a). Preexisting “seed” aerosols are necessary for heterogeneous

reactions and condensation of secondary species, therefore, this relationship was observed because sulfate did not have as many particle surfaces to condense/react upon. The relative ion peak area of m/z -97 started to increase after the TCs when SO_2 increased, but was not as high as before the TCs, indicating the submicron OC and ECOC particles were still fresher than the typical aerosol conditions in Atlanta.

Overall, typical aerosol conditions in Atlanta were characterized by larger relative fractions of submicron organic-containing particles that were highly-aged with sulfate and smaller contributions from supermicron dust and fly ash. Fast winds during severe storms (TCs) cleaned out the highly-aged submicron aerosols and transported supermicron sea salt aerosols. After wind speeds decreased, buildup of fresher submicron organic-containing aerosols occurred. Due to the vast shifts in aerosol composition and size, the CCN-properties of the aerosols changed as well, as discussed below.

3.3.3. Implications of TC influences on CCN activity in Atlanta

Gustav and Hanna introduced atypical meteorological conditions and perturbed the characteristic urban pollution in Atlanta by inducing drastic shifts in aerosol number, size, and chemical composition. The variability in particle chemistry before and during the TCs corresponded to significant changes in CCN concentrations, which potentially influenced the timing of the precipitation. Figure 3.3d and Table 3.1 show $f_{\text{CCN}[0.2]}$, or the ratio of CCN at 0.2% supersaturation to CN, shaded by the CCN number concentration. The hourly precipitation is also shown in Figure 3.3d. Before the TCs when submicron organic-containing particles aged with sulfate were dominant, high $f_{\text{CCN}[0.2]}$ and CCN concentrations were observed (0.56 and 3600 cm^{-3} , respectively). Once the TCs arrived, fast winds advected most organic-containing submicron particles and transported larger sea salt particles; $f_{\text{CCN}[0.2]}$ was similar (0.52) but CCN concentrations decreased substantially to 1300 cm^{-3} , suggesting the sea salt particles were CCN-active, but not high in number due to overall lower supermicron counts. When submicron particle counts increased once again, $f_{\text{CCN}[0.2]}$ decreased substantially and remained low for the remainder of AMIGAS (0.19 on average) while CCN concentrations did not change (1400 cm^{-3} on average), suggesting the presence of fresher organic emissions that were not as CCN-

active as the highly-aged organic-containing particles present before the TCs. Our results are in agreement with previous studies which suggest less-aged organic particles are less hygroscopic, while particles aged with sulfate are better CCN [Baltensperger *et al.*, 2002; Kanakidou *et al.*, 2005].

Interestingly, the heaviest rainfall occurred following the largest increase in CCN-active sea salt on 8/23, with 62 mm accumulating in less than three days (8/24-8/27). Sea salt particles are thought to enhance drizzle particularly in polluted continental clouds [Yin *et al.*, 2000] by adding fewer, larger droplets [Pierce and Adams, 2006; Rosenfeld *et al.*, 2002; Teller and Levin, 2006]. Based on past work and our results, we speculate the sea salt served as large/giant CCN in the polluted clouds over Atlanta and potentially influenced the precipitation timing, particularly during the largest increase in CCN-active sea salt (8/22-8/25). As previously mentioned, relative humidity was high due to the TCs, signifying the availability of water vapor to condense on the sea salt. It is possible the rain scavenged preexisting pollutant and sea salt aerosol, inducing the decrease in particle number and mass. However, decreases in APS, submicron, and supermicron counts occurred roughly three days before the heavy rain started (on 8/21), suggesting: 1) the primary removal mechanism of pollutants was the TC winds, and 2) the sea salt was predominantly removed by serving as large/giant CCN versus by raindrop scavenging. The synergistic relationship between TCs as transport mechanisms of water vapor and sea salt CCN, and rain demonstrate the implications on cloud formation and precipitation over highly-developed urban areas such as Atlanta.

3.4. Conclusions

In summary, intense storm systems such as TCs perturbed the typical background aerosol of Atlanta by cleaning out aged organic aerosols and serving as transport mechanisms for CCN-active sea salt, which have the potential to alter precipitation timing. Our results support those of Chang *et al.* [2011], who also observed a decrease in pollutant aerosol in response to a TC. However, our new findings provide evidence that TCs additionally transported sea salt that served as large/giant CCN and potentially initiated precipitation in the continental clouds above Atlanta. These findings have

important implications for the Atlanta region by affecting cloud formation and shifting precipitation location by driving clouds to rainout sooner, thus altering the regional water cycle. The fact that intense storms such as TCs can perturb characteristic urban aerosol chemistry in Atlanta by introducing CCN-active, sea salt and less CCN-active, fresh urban emissions renders the questions of whether this effect can occur for all tropical storms in the Atlantic and how much this will affect precipitation on a broader regional scale. It is possible all large-scale storms have similar effects on urban aerosol chemistry in regions beyond Atlanta, suggesting a more widespread effect on cloud formation and precipitation over longer periods of time. For instance, the two TCs transported large/giant CCN that likely influenced precipitation initiation for three days. When extrapolating these results to the sixteen total TCs of the 2008 Atlantic hurricane season (assuming they all influence the southeastern U.S.), rainfall location could be altered over longer periods of time and on a larger spatial scale. With the projected rise in sea surface temperature [Xie *et al.*, 2010] and the potential impacts on TC strength [Cione and Uhlhorn, 2003], the magnitude of TC effects on aerosol populations and cloud formation should be considered when predicting the cloud seeding abilities of the urban aerosol and the resulting effects on precipitation.

3.5. Acknowledgements

The authors would like to thank Jerry Brown for site management, Stephanie Shaw and Eladio Knipping from the Electric Power Research Institute (EPRI) for study organization, and Lindsay Hatch and Cassandra Gaston for their insightful discussions. This work was funded by EPRI (EP-P28429/C13491).

3.6. Figures

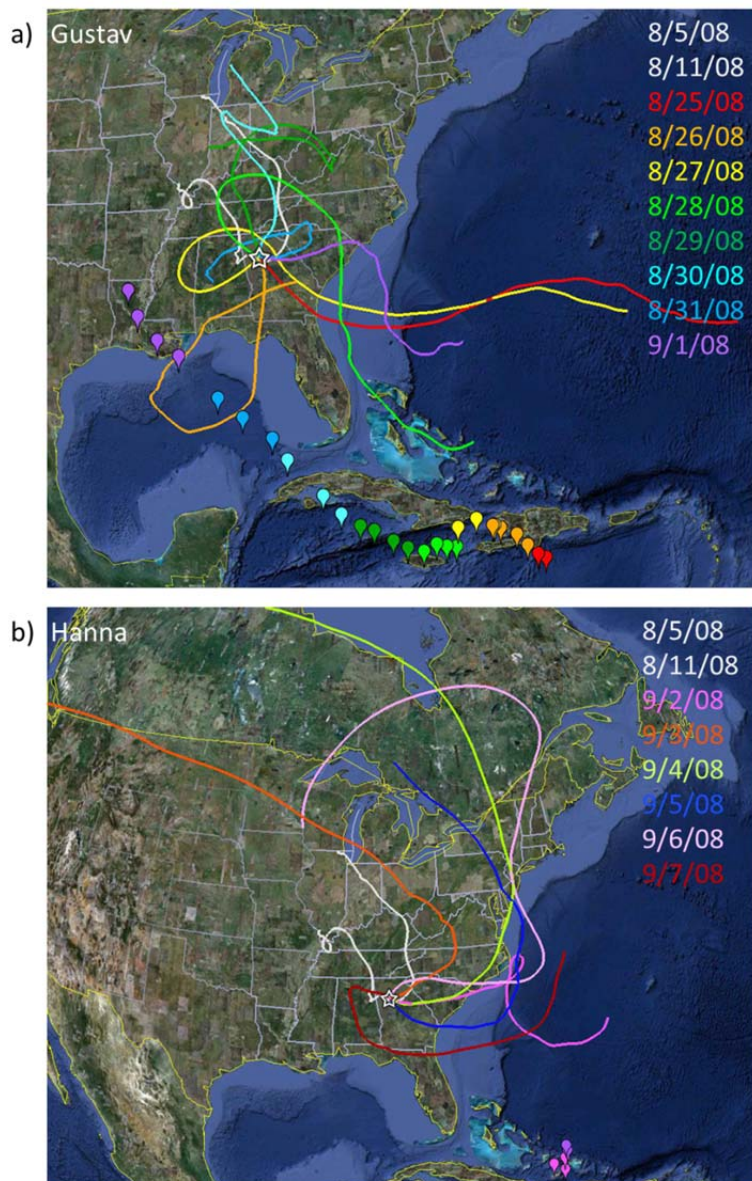


Figure 3.1 Google Earth images including air mass back trajectories calculated with HYSPLIT for TCs a) Gustav and b) Hanna. Markers represent the storm paths in time (<http://www.hurricane-tracking.co.uk/download.php>). Markers and trajectories of same color occurred on the same date.

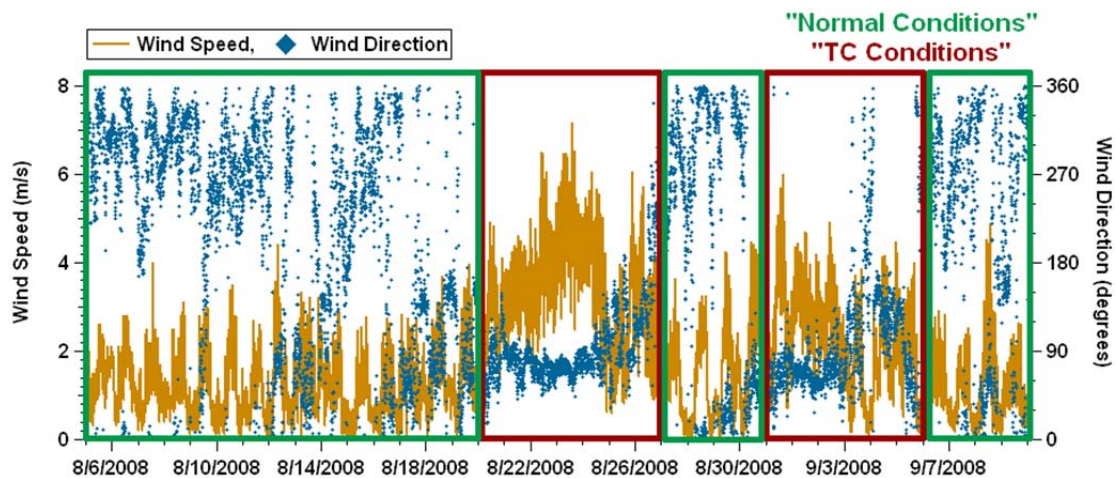


Figure 3.2 Wind speed (m/s) and direction (degrees) during AMIGAS. The green boxes correspond to time periods with “normal conditions,” i.e., time periods uninfluenced by TCs, and maroon boxes correspond to TC time periods or “TC conditions.”

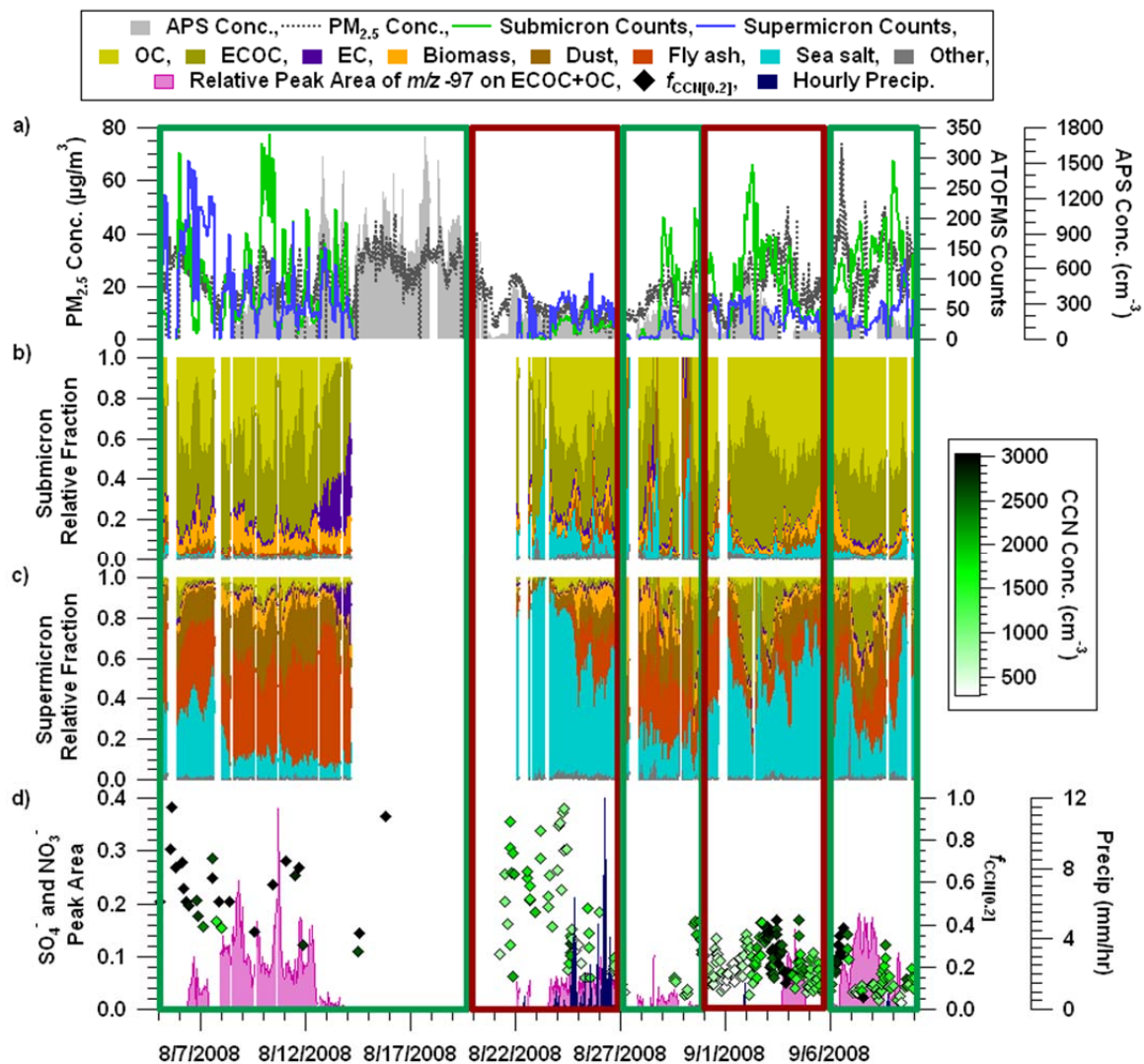


Figure 3.3 Panel a) shows PM_{2.5} mass concentrations ($\mu\text{g}/\text{m}^3$), total number concentrations from the APS (cm^{-3}), and hourly submicron and supermicron particle counts from the ATOFMS. Panels b) and c) show the relative fractions of the submicron and supermicron particle chemistry, respectively. Panel d) shows the average relative ion peak area of m/z -97 on organic-containing particles (OC+ECOC), $f_{\text{CCN}[0.2]}$ shaded by the corresponding CCN concentration (cm^{-3}), and precipitation rate (mm/hr). Time periods with “normal conditions” and “TC conditions” are also shown in boxes similar to Figure 3.2.

3.7. Tables

Table 3.1 Dates and maximum wind speed (WS) corresponding to “normal condition” time periods in green and “TC condition” time periods in maroon. Includes average SO₂ concentrations, $f_{\text{CCN}[0.2]}$, and CCN concentrations during each period.

Dates	Max WS	SO ₂ Conc.	CCN Conc.	
	(m/s)	ppb	$f_{\text{CCN}[0.2]}$	(cm ⁻³)
8/5-8/20	2-4	2.73	0.56	3600
8/20-8/27	5-7	0.58	0.52	1300
8/27-9/1	2-4	2.32	0.20	1000
9/1-9/6	4-6	1.05	0.22	1700
9/6-9/10	2-4	3.78	0.15	1400

3.8. References

- Allen, J.O., Quantitative Analysis of Aerosol Time-of-Flight Mass Spectrometry Data using YAADA, Arizona State University, Tempe, 2004.
- Alston, E.J., I.N. Sokolik, and B.G. Doddridge, Investigation into the Use of Satellite Data in Aiding Characterization of Particulate Air Quality in the Atlanta, Georgia Metropolitan Area, Journal of the Air & Waste Management Association, 61 (2), 211-225, 2011.
- Baltensperger, U., N. Streit, E. Weingartner, S. Nyeki, A.S.H. Prevot, R. Van Dingenen, A. Virkkula, J.P. Putaud, A. Even, H. ten Brink, A. Blatter, A. Neftel, and H.W. Gaggeler, Urban and rural aerosol characterization of summer smog events during the PIPAPO field campaign in Milan, Italy, Journal of Geophysical Research-Atmospheres, 107 (D22), 2002.
- Beven II, J.L., and T.B. Kimberlain, Tropical Cyclone Report Hurricane Gustav, pp. 1-38, NOAA National Hurricane Center, 2009.
- Bhave, P.V., J.O. Allen, B.D. Morrical, D.P. Ferguson, G.R. Cass, and K.A. Prather, A field-based approach for determining ATOFMS instrument sensitivities to ammonium and nitrate, Environmental Science & Technology, 36 (22), 4868-4879, 2002.
- Brown, D.P., and T.B. Kimberlain, Tropical Cyclone Report Hurricane Hanna, pp. 1-36, NOAA National Hurricane Center, 2008.

- Chang, L.T.C., J.H. Tsai, J.M. Lin, Y.S. Huang, and H.L. Chiang, Particulate matter and gaseous pollutants during a tropical storm and air pollution episode in Southern Taiwan, *Atmospheric Research*, 99 (1), 67-79, 2011.
- Chubarova, N.Y., M.A. Sviridenkov, A. Smirnov, and B.N. Holben, Assessments of urban aerosol pollution in Moscow and its radiative effects, *Atmospheric Measurement Techniques*, 4 (2), 367-378, 2011.
- Cione, J.J., and E.W. Uhlhorn, Sea surface temperature variability in hurricanes: Implications with respect to intensity change, *Monthly Weather Review*, 131 (8), 1783-1796, 2003.
- Draxler, R.R., and G.D. Rolph, HYSPLIT (HYbrid Single Particle Lagrangian Integrated Trajectory) v. 4.8 Model access via NOAA ARL READY Website (<http://www.arl.noaa.gov/ready/hysplit4.html>), NOAA Air Resources Laboratory, Silver Spring, MD, 2003.
- Feingold, G., W.R. Cotton, S.M. Kreidenweis, and J.T. Davis, The impact of giant cloud condensation nuclei on drizzle formation in stratocumulus: Implications for cloud radiative properties, *Journal of the Atmospheric Sciences*, 56 (24), 4100-4117, 1999.
- Feng, Y.R., A.Y. Wang, D. Wu, and X.D. Xu, The influence of tropical cyclone Melor on PM10 concentrations during an aerosol episode over the Pearl River Delta region of China: Numerical modeling versus observational analysis, *Atmospheric Environment*, 41 (21), 4349-4365, 2007.
- Finlayson-Pitts, B.J., Pitts, J. N., *Chemistry of the Upper and Lower Atmosphere*, Academic Press, San Diego, 2000.
- Gard, E., J.E. Mayer, B.D. Morrical, T. Dienes, D.P. Fergenson, and K.A. Prather, Real-time analysis of individual atmospheric aerosol particles: Design and performance of a portable ATOFMS, *Analytical Chemistry*, 69 (20), 4083-4091, 1997.
- Ghan, S.J., G. Guzman, and H. Abdul-Razzak, Competition between sea salt and sulfate particles as cloud condensation nuclei, *Journal of the Atmospheric Sciences*, 55 (22), 3340-3347, 1998.
- Greene, N.A., V.R. Morris, A. Aikin, W. Hoegy, and D. Silberman, Use of the electrostatic classification method to investigate the size distribution of aerosols near Hurricane Erika, in *5th Conference on Atmospheric Chemistry: Gases, Aerosols, and Clouds*, Long Beach, CA, 2003.
- Gross, D.S., M.E. Galli, P.J. Silva, and K.A. Prather, Relative sensitivity factors for alkali metal and ammonium cations in single particle aerosol time-of-flight mass spectra, *Analytical Chemistry*, 72 (2), 416-422, 2000.

- Guazzotti, S.A., D.T. Suess, K.R. Coffee, P.K. Quinn, T.S. Bates, A. Wisthaler, A. Hansel, W.P. Ball, R.R. Dickerson, C. Neususs, P.J. Crutzen, and K.A. Prather, Characterization of carbonaceous aerosols outflow from India and Arabia: Biomass/biofuel burning and fossil fuel combustion, *Journal of Geophysical Research-Atmospheres*, 108 (D15), 2003.
- Hatch, L.E., J.M. Creamean, A.P. Ault, J.D. Surratt, M.N. Chan, J.H. Seinfeld, E.S. Edgerton, Y.X. Su, and K.A. Prather, Measurements of Isoprene-Derived Organosulfates in Ambient Aerosols by Aerosol Time-of-Flight Mass Spectrometry - Part 1: Single Particle Atmospheric Observations in Atlanta, *Environmental Science & Technology*, 45 (12), 5105-5111, 2011a.
- Hatch, L.E., J.M. Creamean, A.P. Ault, J.D. Surratt, M.N. Chan, J.H. Seinfeld, E.S. Edgerton, Y.X. Su, and K.A. Prather, Measurements of Isoprene-Derived Organosulfates in Ambient Aerosols by Aerosol Time-of-Flight Mass Spectrometry - Part 2: Temporal Variability & Formation Mechanisms, *Environmental Science & Technology*, Submitted., 2011b.
- Hughes, L.S., J.O. Allen, P. Bhave, M.J. Kleeman, G.R. Cass, D.Y. Liu, D.F. Fergenson, B.D. Morrical, and K.A. Prather, Evolution of atmospheric particles along trajectories crossing the Los Angeles basin, *Environmental Science & Technology*, 34 (15), 3058-3068, 2000.
- IPCC, *Climate Change 2007: The Physical Science Basis. Contribution of Working Group I to the Fourth Assessment Report of the Intergovernmental Panel on Climate Change*, [Solomon, S., D. Qin, M. Manning, Z. Chen, M. Marquis, K.B. Averyt, M. Tignor and H.L. Miller (eds.)] Cambridge University Press, Cambridge, United Kingdom and New York, NY, USA, 2007.
- Johnson, D.B., The Role of Giant and Ultragiant Aerosol Particles in Warm Rain Initiation, *J. Atmos. Sci.*, 39, 448-460, 1982.
- Kanakidou, M., J.H. Seinfeld, S.N. Pandis, I. Barnes, F.J. Dentener, M.C. Facchini, R. Van Dingenen, B. Ervens, A. Nenes, C.J. Nielsen, E. Swietlicki, J.P. Putaud, Y. Balkanski, S. Fuzzi, J. Horth, G.K. Moortgat, R. Winterhalter, C.E.L. Myhre, K. Tsigaridis, E. Vignati, E.G. Stephanou, and J. Wilson, Organic aerosol and global climate modelling: a review, *Atmospheric Chemistry and Physics*, 5, 1053-1123, 2005.
- Kim, E., P.K. Hopke, and E.S. Edgerton, Source identification of Atlanta aerosol by positive matrix factorization, *Journal of the Air & Waste Management Association*, 53 (6), 731-739, 2003.
- Lacke, M.C., T.L. Mote, and J.M. Shepherd, Aerosols and associated precipitation patterns in Atlanta, *Atmospheric Environment*, 43 (28), 4359-4373, 2009.
- Lee, S.H., D.M. Murphy, D.S. Thomson, and A.M. Middlebrook, Chemical components of single particles measured with Particle Analysis by Laser Mass Spectrometry

- (PALMS) during the Atlanta SuperSite Project: Focus on organic/sulfate, lead, soot, and mineral particles, *Journal of Geophysical Research-Atmospheres*, 107 (D1-D2), 2002.
- Levy, J.I., A.M. Wilson, J.S. Evans, and J.D. Spengler, Estimation of primary and secondary particulate matter intake fractions for power plants in Georgia, *Environmental Science & Technology*, 37 (24), 5528-5536, 2003.
- Liu, D.Y., R.J. Wenzel, and K.A. Prather, Aerosol time-of-flight mass spectrometry during the Atlanta Supersite Experiment: 1. Measurements, *Journal of Geophysical Research-Atmospheres*, 108 (D7), -, 2003.
- McFiggans, G., P. Artaxo, U. Baltensperger, H. Coe, M.C. Facchini, G. Feingold, S. Fuzzi, M. Gysel, A. Laaksonen, U. Lohmann, T.F. Mentel, D.M. Murphy, C.D. O'Dowd, J.R. Snider, and E. Weingartner, The effect of physical and chemical aerosol properties on warm cloud droplet activation, *Atmospheric Chemistry and Physics*, 6, 2593-2649, 2006.
- Millet, D.B., D.J. Jacob, K.F. Boersma, T.M. Fu, T.P. Kurosu, K. Chance, C.L. Heald, and A. Guenther, Spatial distribution of isoprene emissions from North America derived from formaldehyde column measurements by the OMI satellite sensor, *Journal of Geophysical Research-Atmospheres*, 113 (D2), 2008.
- Noble, C.A., and K.A. Prather, Real-time single particle monitoring of a relative increase in marine aerosol concentration during winter rainstorms, *Geophysical Research Letters*, 24 (22), 2753-2756, 1997.
- Pierce, J.R., and P.J. Adams, Global evaluation of CCN formation by direct emission of sea salt and growth of ultrafine sea salt, *Journal of Geophysical Research-Atmospheres*, 111 (D6), -, 2006.
- Poschl, U., *Atmospheric aerosols: Composition, transformation, climate and health effects*, *Angewandte Chemie-International Edition*, 44 (46), 7520-7540, 2005.
- Posselt, R., and U. Lohmann, Influence of giant CCN on warm rain processes in the ECHAM5 GCM, *Atmospheric Chemistry and Physics*, 8 (14), 3769-3788, 2008.
- Roberts, G.C., and A. Nenes, A continuous-flow streamwise thermal-gradient CCN chamber for atmospheric measurements, *Aerosol Science and Technology*, 39 (3), 206-221, 2005.
- Rosenfeld, D., Suppression of rain and snow by urban and industrial air pollution, *Science*, 287 (5459), 1793-1796, 2000.
- Rosenfeld, D., R. Lahav, A. Khain, and M. Pinsky, The role of sea spray in cleansing air pollution over ocean via cloud processes, *Science*, 297 (5587), 1667-1670, 2002.

- Rosenfeld, D., Y. Rudich, and R. Lahav, Desert dust suppressing precipitation: A possible desertification feedback loop, *Proceedings of the National Academy of Sciences of the United States of America*, 98 (11), 5975-5980, 2001.
- Sodeman, D.A., Characterization of ambient, automobile, and diesel aerosols utilizing Aerosol Time of Flight Mass Spectrometry, University of California, San Diego, La Jolla, 2004.
- Song, X.H., P.K. Hopke, D.P. Fergenson, and K.A. Prather, Classification of single particles analyzed by ATOFMS using an artificial neural network, ART-2A, *Analytical Chemistry*, 71 (4), 860-865, 1999.
- Spencer, M.T., J.C. Holecek, C.E. Corrigan, V. Ramanathan, and K.A. Prather, Size-resolved chemical composition of aerosol particles during a monsoonal transition period over the Indian Ocean, *Journal of Geophysical Research-Atmospheres*, 113 (D16), 2008.
- Teller, A., and Z. Levin, The effects of aerosols on precipitation and dimensions of subtropical clouds: a sensitivity study using a numerical cloud model, *Atmospheric Chemistry and Physics*, 6, 67-80, 2006.
- Turpin, B.J., and H.J. Lim, Origins of primary and secondary organic aerosol in Atlanta: Results' of time-resolved measurements during the Atlanta supersite experiment, *Environmental Science & Technology*, 36 (21), 4489-4496, 2002.
- Xie, S.P., C. Deser, G.A. Vecchi, J. Ma, H.Y. Teng, and A.T. Wittenberg, Global Warming Pattern Formation: Sea Surface Temperature and Rainfall, *Journal of Climate*, 23 (4), 966-986, 2010.
- Yin, Y., Z. Levin, T.G. Reisin, and S. Tzivion, The effects of giant cloud condensation nuclei on the development of precipitation in convective clouds - a numerical study, *Atmospheric Research*, 53 (1-3), 91-116, 2000.
- Ying, Q., and M.J. Kleeman, Source contributions to the regional distribution of secondary particulate matter in California, *Atmospheric Environment*, 40 (4), 736-752, 2006.

4. Measurements of Aerosol Chemistry during New Particle Formation Events at a Remote Rural Mountain Site

4.1. Introduction

Aerosols are ubiquitous in the troposphere and profoundly impact climate [Solomon *et al.*, 2007]. They scatter and absorb incoming short wave and outgoing long wave radiation, and act as cloud condensation nuclei (CCN) affecting cloud radiative and physical properties. Under supersaturated conditions, CCN compete for available water vapor, creating large populations of small-sized cloud droplets increasing the reflectivity of clouds [Albrecht, 1989; Twomey, 1977]. Smaller, more numerous cloud droplets often cannot grow to large enough sizes to precipitate [Albrecht, 1989].

The impact of aerosols on clouds, referred to as the indirect effect, represents arguably the largest single source of uncertainty out of all contributors to global radiative forcing estimates [Solomon *et al.*, 2007] and therefore a better understanding of the sources of the aerosols that determine the magnitude of this effect is needed. In-situ formation of ultrafine particles (≤ 100 nm) through gas-to-particle conversion of low volatility vapors represents a significant source of tropospheric aerosols, especially in remote environments. The initial critical clusters must grow into larger sizes to activate as CCN, and thus become relevant for cloud formation [Ziemba *et al.*, 2010]. Determining the magnitude and mechanistic drivers of the nucleation and growth processes of newly-formed particles that ultimately become effective CCN will improve regional and global climate models [Ristovski *et al.*, 2010].

New particle formation (NPF) involves two important steps [Seinfeld and Pandis, 2006]. The first step involves homogeneous or ion-induced nucleation of neutral or ion clusters and the second step involves the growth of these clusters into larger particles [Kulmala *et al.*, 2000; Lunden *et al.*, 2006a; Ortega *et al.*, 2008]. In most cases, pristine ambient conditions with lower relative humidity represent favorable conditions for

particle nucleation [Fisher *et al.*, 2010], whereas higher relative humidities [Wang *et al.*, 2010a] and lower temperatures [Lunden *et al.*, 2006a] provide favorable conditions for the subsequent growth of newly-formed particles, depending on the species involved. Formation of new particles is affected by the production of condensable vapor precursors, such as H₂SO₄, formed from oxidation of SO₂ [Kulmala *et al.*, 1995]. Originally, it was hypothesized that the initial step involved cluster formation by H₂SO₄ and water vapor and that H₂SO₄ was also responsible for the subsequent growth of the clusters, however, the involvement of H₂SO₄ alone cannot explain the formation and growth rates of observed particle formation [Wehner *et al.*, 2005]. Therefore, other species in addition to H₂SO₄ must contribute to the growth of new particles via condensation and/or heterogeneous reactions [Smith *et al.*, 2009]. Species that have sufficient low volatility so as to be involved with nucleation are also capable of participating in the subsequent growth, and as particle size increases, so too do the number of possible condensable species and mechanisms. More is known about the species that contribute to particle growth, such as NH₃ [McMurry *et al.*, 2005] or as shown more recently semivolatile organic species [Ristovski *et al.*, 2010; Wang *et al.*, 2010a] than about the species involved with the nucleation process. More specifically, formation of aminium salts has been modeled [Barsanti *et al.*, 2009] and these species have been detected in newly-formed particles [Mäkelä *et al.*, 2001; Wang *et al.*, 2010b]. Amines form salts with organic and inorganic acids during particle growth [Murphy *et al.*, 2007b; Smith *et al.*, 2009], supporting the hypothesis that amines/nitrogen-containing organics and H₂SO₄ play a role in the growth of new particles.

Because of instrumental challenges involved in measuring the chemistry of 1-3 nm particles, the molecular identities of the species involved have eluded scientists for many years. As a result, chemical composition is typically inferred for newly-formed particles by utilizing multiple measurements. Mäkelä *et al.* [2001] detected dimethylammonium ((CH₃)₂NH₄⁺) using 2-stage cascade impactors and ion chromatography during NPF events. Although they were able to identify species down to 5 nm, the time resolution was low and aminium sulfate ((HNR₃)₂SO₄) was inferred from the correlation of bulk particle measurements of (CH₃)NH₂⁺ and sulfate. Smith *et al.*

[2004] measured nitrogen-containing organics and sulfate using a Thermal Desorption Chemical Ionization Mass Spectrometer (TDCIMS). They detected particles from 10-30 nm with 5-10 minute time resolution and found that nitrogen-containing organics played a significant role in the growth of nanoparticles. Chemical measurements at these small sizes represent a significant advancement in the characterization of newly-formed particles. However, the TDCIMS cannot measure amines and sulfate simultaneously in the same particle and therefore questions remain about the associations between amines and sulfate at the single particle level during NPF events.

The challenge with using bulk measurements to determine the primary species involved in particle formation is that the measured mass concentrations represent the average chemical composition of many particles. For instance, when amines and sulfate are detected in particles collected on filters, the detected species can actually occur in separate particles. Single-particle mixing state measurements show whether two species are present within a single particle, a level of detail that is critical for understanding the key species involved in particle formation and growth processes. In the current study, aerosol time-of-flight mass spectrometry (ATOFMS) was used to provide dual polarity, single-particle analysis during NPF events in real-time at a remote rural region in the Sierra Nevada Mountains in Northern California. We report the first observations of nitrogen-containing organic species and sulfate within the same particles after significant particle growth during NPF events. Understanding the sources of the species involved in new particle formation is critical as this could be an important local source of CCN in the Sierra Nevada. Previous studies have suggested that CCN were transported directly from California's Central Valley (CV) [Rosenfeld *et al.*, 2008c], however, in-situ NPF between amines from the CV and long-range transported SO₂ from Asia could also contribute as a CCN source in the Sierra Nevada as described herein.

4.2. Experimental

Ground-based aerosol measurements were made during the CalWater Early Start field campaign during the late winter at the Sugar Pine Reservoir in Foresthill, CA, a remote rural site in the Sierra Nevada Mountains (39° 07' 42.80" N, 120° 48' 04.90" W;

elevation ~1064 m ASL). Particle size distributions were measured between 11-604 nm using a scanning mobility particle sizer (SMPS) (Model 3936L, TSI Inc.). Meteorological measurements including temperature, relative humidity, wind direction, solar radiation, and precipitation were acquired from co-located instruments operated by the National Oceanic and Atmospheric Administration (NOAA). Gas-phase O₃ and SO₂ concentrations were measured using an O₃ analyzer (Model 49C, Thermo Environmental Instruments, Inc.) and a SO₂ analyzer (43C, Thermo Environmental Instruments, Inc.), respectively. Due to calibration problems with the SO₂ analyzer, SO₂ is presented as relative concentrations. Black carbon mass concentrations were measured using a seven wavelength aethalometer (Model AE31, Magee Scientific). CCN concentrations were measured at 0.3% supersaturation using a compact streamwise thermal-gradient diffusion chamber [Roberts and Nenes, 2005a]. Only periods with reliable CCN data are presented. A condensation particle counter (CPC) (Model 3010, TSI Inc.) was used to determine condensation nuclei (CN) concentrations, which were compared to the number concentration of CCN_{0.3} to determine the activated fractions.

An ultrafine (UF)-ATOFMS, a modified version of the standard ATOFMS [Gard *et al.*, 1997a], was utilized for individual aerosol aerodynamic sizing and chemical composition. The UF system is described in detail in Su *et al.* [2004]. The UF-ATOFMS measures the vacuum aerodynamic size ($100 \leq D_{va} \leq 1000$ nm) and chemical composition of particles by laser desorption/ionization which allows us to obtain dual polarity mass spectra [Gard *et al.*, 1997a; Su *et al.*, 2004]. D_{va} is related to the electric mobility diameter (D_{me}) measured by the SMPS through effective density and is discussed in detail elsewhere [Spencer and Prather, 2006]. During the study, 1,146,366 particles were chemically analyzed from 2/21/09-3/10/09 (PST). Single-particle mass spectra were imported into YAADA (www.yaada.org), a software toolkit in Matlab (The Mathworks, Inc.), for detailed analysis of particle size and chemistry. ART-2a, an adaptive resonance theory-based clustering algorithm [Song *et al.*, 1999b], was then used to group single-particle mass spectra with a vigilance factor of 0.80. ART-2a classifies particles into separate clusters depending on the presence and intensity of ion peaks in the respective mass spectra. The most populated 70 clusters account for >90% of the total ART-2a

classified particles. Peak identifications in this paper correspond to the most probable ions for a given m/z ratio based on previous lab and field studies.

4.3. Results and Discussion

4.3.1. Ambient Conditions for NPF

Figure 4.1a shows SMPS, temperature, and relative humidity (RH) data obtained during the study. One polluted period impacted by transport from the CV occurred from 2/21-2/23. NPF events occurred during cleaner periods following precipitation between the dates of 2/24-2/28 (denoted as P1) and 3/6-3/8 (denoted as P2) as shown by high number concentrations in white. Particularly, NPF events had high number concentrations starting at small sizes (~ 11 - 15 nm) followed by subsequent growth to larger sizes (~ 70 - 100 nm). All NPF events started in the late afternoon between $\sim 14:00$ - $16:00$ during low RH, high temperature, and increased solar radiation, followed by particle growth as RH increased and temperature and solar radiation decreased. Mäkelä *et al.* [2001] previously observed NPF events during the afternoons in boreal forest locations. Particle nucleation occurs when there is a reduction in total particle surface area, which often occurs immediately following precipitation events [Covert *et al.*, 1992]. Precipitation removes the atmospheric ‘seed’ particles that low volatility gases would normally condense upon. When elevated gas-phase concentrations are produced by increased solar radiation after precipitation, these species undergo oxidation processes and then homogeneously nucleate to form new particles. This series of events is shown in Figure 4.1a and b, when both NPF periods occurred after periods of precipitation. Clean conditions at the start of the NPF periods are typified by overall low mass concentrations (<185 ng/m^3) of black carbon (BC). BC or soot, formed from combustion sources, serves as an excellent tracer for the presence anthropogenic aerosols [Hansen and Rosen, 1985]. Figure 4.1c shows BC concentrations over the course of the study, which were low (average \pm standard deviation = 142.2 ± 97.8 ng/m^3 during NPF periods) compared to urban environments (on the order of 1 - 5 $\mu\text{g}/\text{m}^3$) [Hitzenberger and Tohno, 2001]. Chapter 9 contains an additional discussion of BC concentrations.

The precipitation periods showed fairly steady decreases in O₃ (ppm) and relative SO₂ concentrations (Figure 4.1c). O₃ concentrations were higher during P1 compared to P2, whereas SO₂ concentrations were higher during P2 compared to P1. This suggests different chemical processes and species were involved during the two NPF periods, as discussed below. During P1, SO₂ varied diurnally, first increasing from ~11:00 the previous day to ~1:00 the day of the NPF events while during P2, SO₂ started increasing at ~20:00 the days previous to both of the NPF events. However, O₃ was consistent during both NPF periods, peaking ~10:00-13:00 on the day of the events. Interestingly, the O₃ maxima occurred 2-5 hours before the NPF events, and then decreased to a minimum, 4-9 hours after the start of the NPF events. Lunden *et al.* [2006a] observed a similar trend with O₃ peaking ~4 hrs before NPF at Blodgett Forest Research Station, a site with similar conditions ~16 miles southeast of Sugar Pine. In the current study, SO₂ decreased from higher, steady concentrations as O₃ and solar radiation increased and before new particles started to form. Observed trends of SO₂ and O₃ in relation to NPF events suggest their involvement in new particle formation and growth processes, as suggested by Berndt *et al.* [2010] who previously observed NPF from reaction of OH (formed from O₃) and SO₂ in a laboratory setting.

4.3.2. Growth of New Particles into CCN

Heavy precipitation periods resulting in clean conditions in conjunction with the presence of necessary gas-phase species that induced NPF produced periods typified by the fast growth of newly-formed particles. Frequent observations of the nucleation of particles only a few nanometers in diameter followed by subsequent growth to ~100 nm have been shown to occur within 1-2 days in the continental boundary layer [Kulmala *et al.*, 2004]. However, during the current study we calculated the upper limit of growth to 100 nm to occur in as rapidly as 15 hours. Having a measure of the time it takes a particle to grow up to 100 nm provides a relevant link between newly-formed particles and those particles that can activate as CCN. Inferred growth rates (GRs) in Figure 4.2 and Table 9.1 were determined using the method discussed by Kulmala *et al.* [2004] and are described in Chapter 9. Briefly, lines were fit to the increasing mean particle sizes during

NPF events. The GRs were calculated from the slopes of these fitted lines. According to Kulmala *et al.* [2004], uncertainties such as distinguishing between new and pre-existing particles and the exact start and end times of these events can lead to uncertainties in the GRs; however, the times and sizes were chosen to limit contributions from these uncertainties as much as possible.

As shown in Figure 4.2, new particles grew faster on average during P2 compared to P1: inferred GRs during P1 and P2 were 4 ± 3 nm/h and 7 ± 1 nm/h, respectively. The difference in inferred GRs between P1 and P2 was most likely due to the involvement of different species as suggested by the air mass trajectories and different concentrations of key gas-phase species, namely O₃ and SO₂, during the two periods. In addition, higher concentrations of organic species due to higher average temperatures [Sharkey and Loreto, 1993] could have contributed to the faster growth rates, on average, observed during P2 (as discussed in Chapter 9). Because amines are basic compounds, they have the potential to undergo rapid acid-base reactions to form salts in/on particles in the presence of sulfuric acid, depending on temperature, the identity of the amine, and the concentrations and identities of acidic species present [Murphy *et al.*, 2007b]. Higher SO₂ concentrations during P2 potentially led to more sulfuric acid in the newly-formed particles making them more acidic, which can induce faster growth through acid-base reactions. Overall, inferred GRs from both periods (2-8 nm/h), particularly during P2, occur on the higher end of previously reported GR ranges for remote rural areas presented by Kulmala *et al.* [2004] and references therein. Notably, GRs during the closely-located Blodgett study (1-7 nm/h) were comparable to these measurements at Sugar Pine [Lunden *et al.*, 2006a].

One of the primary goals of the CalWater field campaign involved developing a better understanding of the sources of CCN that ultimately impact orographic clouds and precipitation in the Sierra Nevada. It has been hypothesized that the majority of CCN are transported from the polluted CV near Fresno and Bakersfield, a region with high agricultural activity [Rosenfeld *et al.*, 2008c]. However, it is possible that local NPF events such as ones described here can produce large numbers of ultrafine particles that

can ultimately grow and become CCN, especially in regions with a low anthropogenic influence at higher elevations [Merikanto *et al.*, 2009]. Figure 4.2 shows the size distribution from Figure 4.1a along with the ratio of CCN_{0.3} to all CN ($f_{CCN[0.3]}$). Importantly, increases in $f_{CCN[0.3]}$ coinciding with the NPF events during particle growth suggest these newly-formed particles can effectively serve as CCN. These findings are consistent with recent studies which have also suggested that newly-formed particles evolve into CCN through modeling [Kerminen *et al.*, 2005; Kuang *et al.*, 2009; Pierce and Adams, 2007] and observations in remote regions with similar conditions during NPF [O'Halloran *et al.*, 2009; Sihto *et al.*, 2010].

4.3.3. Single Particle Chemical Composition during NPF Events

In order to better understand the chemistry of the newly-formed CCN, a more detailed look at particles in the typical CCN size range is merited. Data showing real-time changes in the chemical composition of larger, detectable sizes (>100 nm) have recently been used to provide insight into the chemistry of newly-formed particles [Friedman *et al.*, 2009]. Since the UF-ATOFMS measures particles with $D_{va} \geq 100$ nm, we can only state that the detected species were likely involved in the initial formation and/or growth processes, which is why the term “NPF” is used throughout the paper. However, it is likely that the chemical composition of particles from $100 \leq D_{va} \leq 1000$ nm is a product of condensation, heterogeneous reactions, and coagulation processes occurring during NPF events. To look at the chemistry in detail, P1 was further divided into shorter time periods based on the SMPS data, including before events (non-NPF), growth sub-periods G1 (≤ 20 nm), G2 (20-25 nm), G3 (25-30 nm), G4 (≥ 30 nm at higher number concentrations), and end of events (≥ 30 nm at lower number concentrations). Limited chemical data were obtained during P2 due to instrumental issues; therefore, this period was excluded when looking at chemistry during sub-periods. However, a comparison of chemical species between P1 and species from the limited data collected during P2 is provided in Chapter 9. The initial growth, or the G1 and G2 sub-periods, typically corresponded to the smallest mean sizes and highest number concentrations compared to before and end of the events, which is typical of NPF bursts [Chang *et al.*, 2009]. Figure

4.3 shows the overall particle chemistry from $100 \leq D_{va} \leq 1000$ nm from before the events, growth sub-periods, and the end of events, along with average number concentrations and mean sizes from the SMPS data. The major types observed at Sugar Pine included amine-containing organic carbon (amine-OC), aged organic carbon (aged OC), elemental carbon (EC), EC mixed with OC (ECOC), biomass, salts, and other minor particle types that consisted of <1% of the total number of particles present during NPF. EC, ECOC, biomass, and salts were transported from other regions and clearly not formed during NPF events. Mass spectra and details of these other particle types are included in Chapter 9.

As shown in Figure 4.3, the largest number fractions during NPF belonged to the amine-OC, biomass, and ECOC particle types, which represented 50%, 22%, and 16% of the total particle counts, respectively. Amine-OC types were characterized by markers at m/z 86($(C_2H_5)_2NCH_2^+$), 101($(C_2H_5)_3N^+$), 102($(C_2H_5)_3NH^+$), 118($(C_2H_5)_3NOH^+$), and other carbonaceous ions [Angelino *et al.*, 2001a; Pratt *et al.*, 2009c]. Not only was the amine-OC type the largest fraction, it increased as the newly-formed particles grew into larger sizes, then decreased towards the end of the events. Before the events, amine-OC types comprised on average 44% of the total particle counts then increased to 48% during G1, 59% during G2, 62% during G3, then decreased to 38% during G4 and 37% during the end of events. Amine-OC particles also increased at the smallest sizes observable by the UF-ATOFMS ($D_{va} = 100-300$ nm) during the initial growth sub-periods as shown/discussed in Chapter 9. This trend suggests the presence of background amine-containing particles; the large increase in small-sized amine-OC particles during the initial growth sub-periods suggests semivolatile amine species played a role in the growth of new particles. The amine-OC fraction did not increase as much as one might expect during G1 because the UF-ATOFMS sees larger sizes ($D_{va} \geq 100$ nm) and thus does not directly measure the chemistry of the smallest particles during the initial growth periods of NPF. The decrease toward the end of events when particle number concentrations decreased suggests the amine-OC particles coagulated with other types of particles. Increases of amine species were observed from the beginning to the end of NPF events on aged OC, biomass, and ECOC particle types. By using digital color histograms of

single particles we were able to monitor the evolution of the UF-ATOFMS particles types, which showed increases in the overall number of particles with amine species (m/z 86), and showed the major particle types, aged OC, biomass, and ECOC, coagulated with the small, newly-formed amine-containing particles (see Chapter 9).

The increase in average number fraction as well as the absolute amine peak areas (Chapter 9) suggests amine species were involved in the growth of new particles. As previously mentioned, sulfate is also believed to play a role in NPF. Figure 4.3 shows the number of particles within all particle types containing the sulfate ion marker (m/z -97, HSO_4^-) per 5-minute interval. The average number of particles containing m/z -97 followed a similar trend to the SMPS number concentration: lower numbers before events followed by higher numbers during initial growth sub-periods, ending with lower numbers towards the end.

Both the number of particles containing sulfate and the number and overall fraction of amine-OC particles increased during the initial growth sub-periods compared to before the events and decreased at the end of the events, suggesting that these species played a role in the growth of new particles. Figure 4.4a shows the SMPS data with the fraction of amine-OC particles containing sulfate and total number of particles per 15-minute interval. Panel a) in Figure 9.3 corresponds to the mass spectra for amine-OC particles containing sulfate. Increases in the fraction of amine-OC particles containing sulfate were observed during NPF events, providing clear evidence that amines and sulfate were indeed present in the same, single particles. In addition, the fractions of amine-OC particles containing sulfate were highest mainly during the beginning on NPF events, likely due to the large number concentrations of aminium sulfate particles formed during the NPF bursts. The ability to measure both amine and sulfate species in the same single particles during NPF directly confirms these aminium salts formed, supporting previous inferences of their existence in newly-formed particles.

Figure 4.4b shows a correlation plot of the fraction of particles with m/z 86 versus the fraction with m/z -97 as a function of study date (in color), with the black line representing the 1:1 line. The color matches the respective date and time of markers in

Figure 4.4a. Each marker represents the fraction of particles containing m/z 86 and/or m/z -97 in 15-minute intervals. Three notable groups of points exist with similar colors on the 1:1 line, meaning those points contain roughly equivalent numbers of particles with m/z 86 and m/z -97. The orange group of points (upper right) represents the period of high particle number concentrations, but was not an NPF event. The yellow/green group of points falls within the first NPF period from 2/24-2/28 whereas the blue group of points falls within the second NPF period from 3/6-3/8. Figure 4.4c shows a similar plot with ammonium ($^{18}\text{NH}_4^+$) in place of m/z 86, since ammonium has been shown to contribute to particle nucleation [Finlayson-Pitts, 2000; Ortega et al., 2008]. However, a 1:1 correlation was not observed between ammonium (m/z 18) and sulfate, suggesting ammonium played a different role in nucleation and particle growth. It is possible that ammonium was involved with the initial cluster formation. Previous studies have expressed the significance of ammonium salt formation in ambient aerosol [Pratt et al., 2009c] and ammonium displacement with ammonium species in secondary organic aerosol [Murphy et al., 2007b] and after the initial formation process during NPF in a laboratory setting [Bzdek et al., 2010]. Based on this combination of new results and previous studies, it appears that H_2SO_4 was involved with formation with additional growth from amines at larger particle sizes, forming predominantly ammonium-sulfate salts.

4.3.4. Potential Sources of Gas-Phase Species Involved in New Particle Formation

Although ambient conditions were similar between P1 and P2 (temperature, RH, solar radiation, and pristine air), higher O_3 concentrations were observed during P1 compared to P2 but in contrast, higher SO_2 concentrations occurred during P2 compared to P1. Differences between the two periods can be explained by different air masses impacting the site that transported the species involved in NPF.

Regional airflows were investigated with back trajectories simulated by the Lagrangian model FLEXPART [Stohl et al., 2005; Stohl et al., 1998] to provide insight into the source regions of species potentially playing a role in NPF. O_3 and SO_2 exhibited diurnal behavior during both NPF periods, due to upslope and downslope airflows that

are common in this region; the daytime upslope flow (strongest ~12:00-13:00) transports species from the CV, while the nighttime downslope flow (strongest ~2:00-3:00) carries pollutants toward the Valley floor [Bao *et al.*, 2008; Collett *et al.*, 1990b]. This diurnal behavior also occurred in O₃ measurements at Blodgett and was attributed to the upslope/downslope system, suggesting O₃ came from the CV [Lunden *et al.*, 2006a]. In the current study, O₃ concentrations peaked ~10:00-13:00, which coincided with the strongest upslope flow times. In the CV, O₃ forms in photochemical urban pollution [Finlayson-Pitts, 2000], common in cities including Sacramento and Fresno. In contrast, during P2 SO₂ peaked during the downslope flow, suggesting it was not transported from the CV.

During P2, long-range transport of SO₂ at higher altitudes, which could potentially become entrained from the free troposphere during the day and descend into the stable nighttime boundary layer [Nilsson *et al.*, 2001], appears to be the difference between the two periods and led to higher SO₂ at the site during P2. NASA's Ozone Monitoring Instrument (OMI) sensor onboard the Aura satellite measures backscattered radiation which is used to estimate vertically-integrated SO₂ values. Images acquired for the days before, during, and after NPF events for both periods are shown in Chapter 9. Background levels of SO₂ were observed in Northern California on 2/26. On the same day, an SO₂ plume from the coast of Asia traveled across the Pacific Ocean from 2/26-3/5, arriving off the coast of Washington and ultimately Northern California between 3/6-3/8, corresponding to the peak in SO₂ concentrations. Levels of SO₂ returned to background levels on 3/9, similar to those measured on 2/26. Back trajectories (also shown in Chapter 9) further support trans-Pacific transport during P2, following a high pressure system that provided clear skies and dry conditions known to inhibit in-cloud conversion of SO₂ to sulfate. Together, OMI data and back trajectory analysis suggest the high SO₂ observed during P2 resulted from long-range transport from Asia, which is likely from biomass burning emissions due to slash burn techniques in southeast Asian during this time of year [Streets *et al.*, 2003].

A number of sources exist for the amine precursors. The CV is largely inhabited by significant livestock populations which represent large sources of ammonia as well as amines [Sorooshian *et al.*, 2008]. Local sources of amines from vegetation [Neff *et al.*, 2002] are likely negligible in comparison to bovine sources in the CV, which can be transported by the upslope/downslope system along with O₃. Overall, amines and O₃ likely came from agricultural emissions and photochemical pollution in the CV, respectively. During P1, lower SO₂ concentrations and correspondingly less sulfate (~4 times less in average sulfate peak area and number of particles containing sulfate as described in Chapter 9) were observed compared to P2. In contrast, during P2 Asian-transported SO₂ likely from biomass burning emissions and more sulfate were observed, potentially leading to the faster average particle growth compared to P1.

4.4. Conclusions

NPF periods occurring after heavy precipitation periods began each day during low RH, high temperature, and peak solar radiation, and during pristine, non-precipitating periods, demonstrating the strong dependence of NPF on ambient conditions. Growth of newly-formed particles occurred as RH increased and temperature and solar radiation decreased, and was relatively fast compared to previous observations, which can be attributed to the extremely clean conditions as well as the availability of gas-phase SO₂, O₃, and amines. Using UF-ATOFMS, increases in the overall fraction of amine-containing particles from $100 \leq D_{va} \leq 1000$ nm occurred over the course of the NPF events after substantial particle growth from the smallest sizes. During NPF, amine and sulfate ion markers are observed in the same, single-particle mass spectra, and the number of particles containing sulfate correlated 1:1 to the number of amine-containing particles but not ammonium-containing particles. Although we cannot determine all of the sources of the species involved in these processes, air mass trajectories suggest the amines and O₃ came from animal husbandries and vehicle pollution in the CV, respectively, while SO₂ was likely transported from Asia during P2.

It is important to understand and characterize such small particles that ultimately can activate as CCN and impact cloud formation and potentially precipitation over the

Sierra Nevada. One of the new and more intriguing findings of this study is the key role long-range transported SO₂ from Asia played in CCN formation in the Sierra Nevada. We hypothesize that SO₂ formed sulfate which reacted with amines to form aminium-sulfate salts, particularly during P2 when SO₂ concentrations and particles containing sulfate were highest, ultimately leading to CCN-active particles upon growth to larger sizes. To further quantify the ability of organic salts to activate as CCN, laboratory studies to measure the hygroscopicity parameter kappa (κ) of various aminium-sulfate salts will be performed [Petters and Kreidenweis, 2007]. The range of κ values at Sugar Pine (0.013-0.16) suggest the CCN-active particles contained organic species [Petters and Kreidenweis, 2007]. The presence of aminium salts, which are known to be water soluble [Angelino et al., 2001a; Pratt et al., 2009c], could account for the more hygroscopic and CCN-active particles measured during NPF events. A recently completed field study over Sugar Pine and the CV will allow comparisons between ground and measurements aloft to gain further insight into the regional impact of newly-formed particles on orographic clouds and precipitation in this region.

4.5. Acknowledgments

The Forest Hill Power Utility District is acknowledged for hosting the sampling site. Joseph Mayer, Cassandra Gaston, Dr. Meagan Moore, and Melanie Zauscher are acknowledged for assisting in preparing instrumentation for the study and setting up the site. Also, Professor Joel Norris is acknowledged for assistance with species source determination.

4.6. Figures

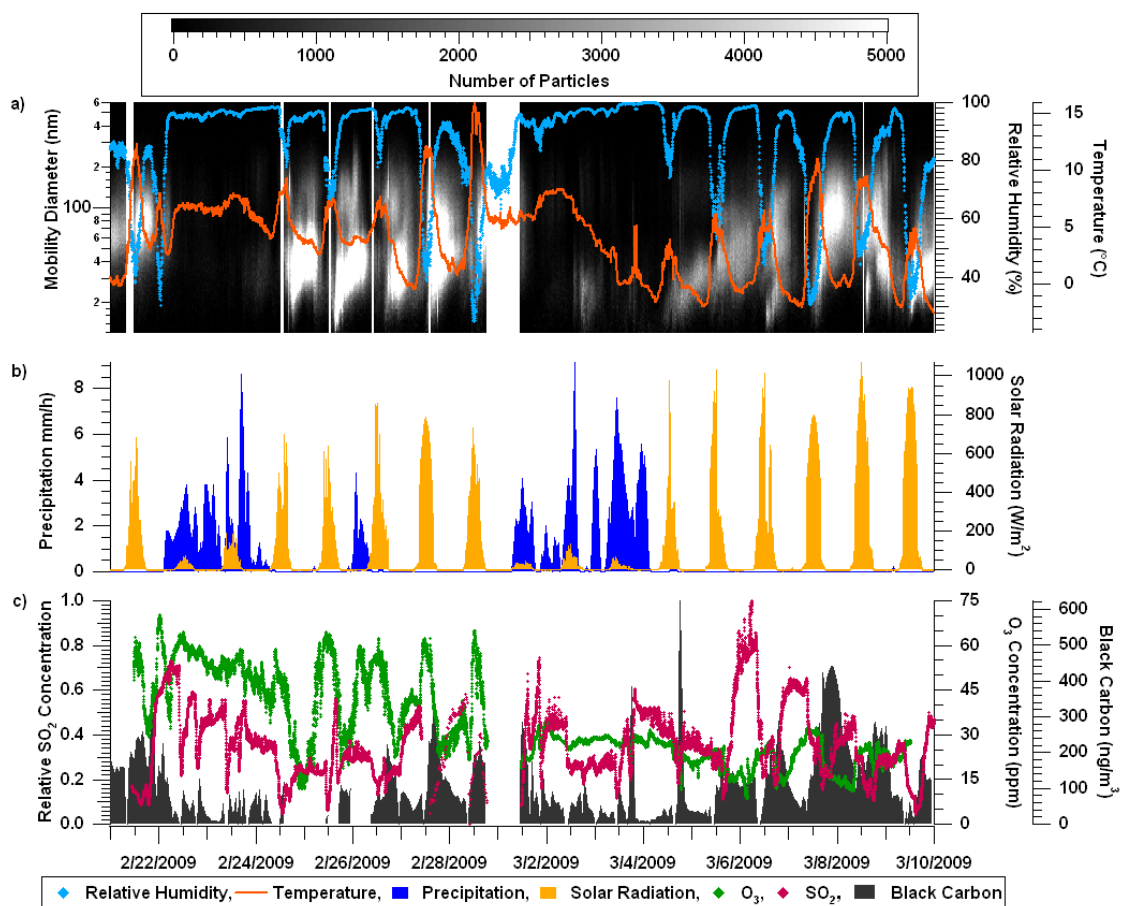


Figure 4.1 a) 5-minute temporally-resolved SMPS size distributions (nm) with superimposed 2-minute relative humidity (%) and temperature (°C), b) hourly precipitation (mm/h) and 2-minute solar radiation (W/m²), and c) hourly gas-phase relative SO₂ and O₃ (ppm) concentrations and black carbon concentrations (ng/m³).

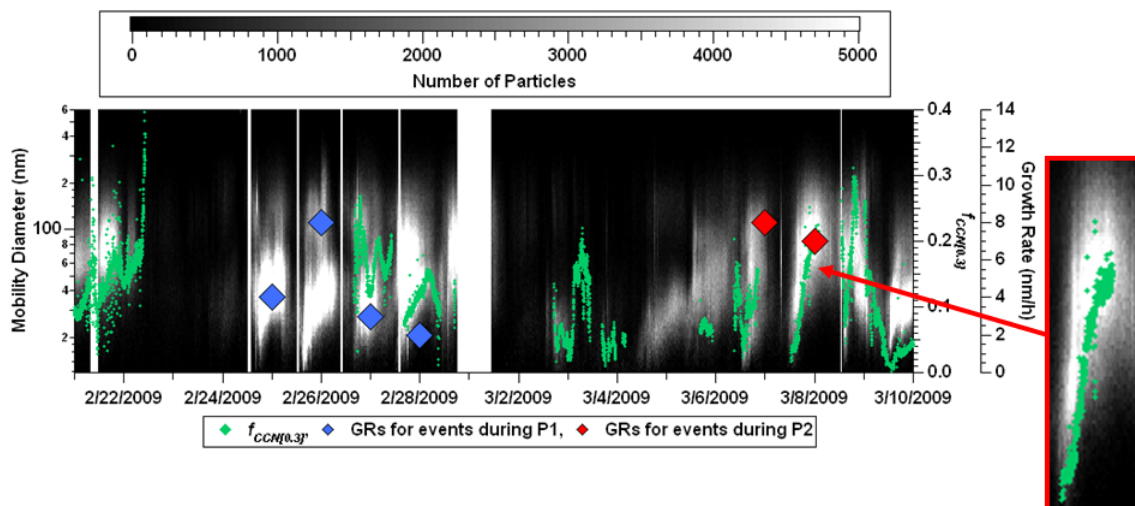


Figure 4.2 SMPS plotted with $f_{CCN(0.3)}$. The inset is the strongest correlation of $f_{CCN(0.3)}$ with an NPF event (3/7-3/8). The markers superimposed over each NPF event are the estimated GRs for the event on that day. Blue and red markers represent GRs during P1 and P2, respectively.

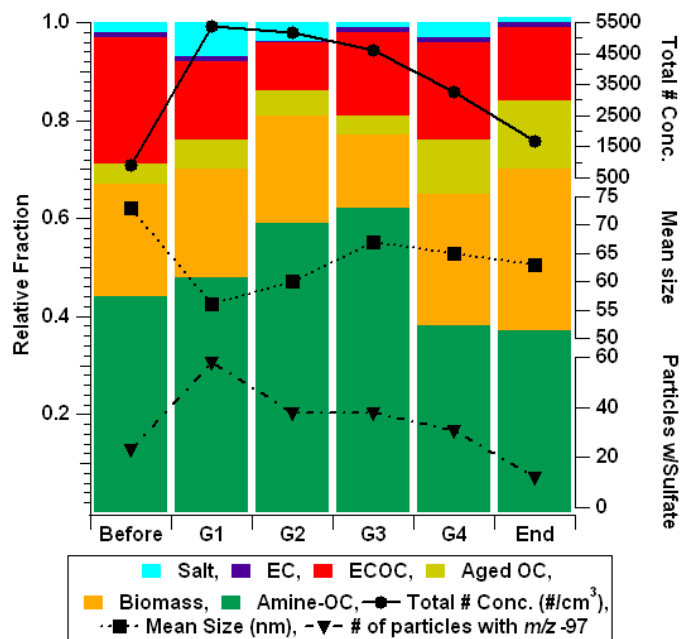


Figure 4.3 ATOFMS particle types in the 100-1000 nm size range measured during P1. Also pictured are the SMPS total particle number concentrations ($\#/cm^3$), SMPS mean sizes (nm), and number of ATOFMS sulfate-containing (m/z -97) particles during each sub-period. All of these values are averaged over the four NPF events in P1.

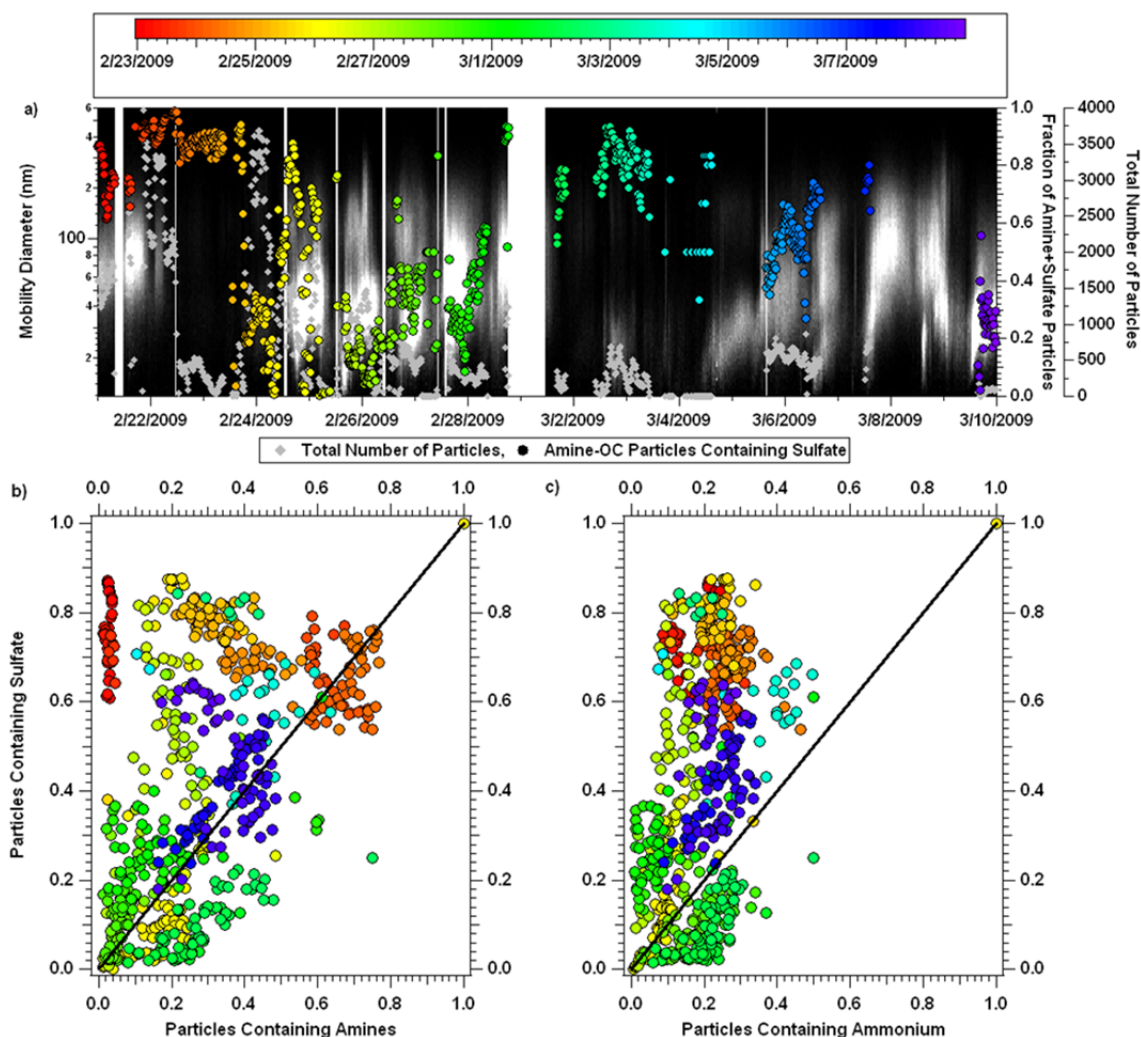


Figure 4.4 a) SMPS plotted with the fraction of amine-OC particles containing sulfate (out of the total number of particles) as a function of study date and time in color and the total number of particles. b) Correlation of the fraction of particles with sulfate (m/z -97) to fraction of particles with amines (m/z 86) also as a function of study date and time. The black line represents the 1:1 line. c) Similar correlation plot to b), but with ammonium (m/z 18) in place of m/z 86. Each marker in all panels represents the fraction of particles per 15-minute interval.

4.7. References

Albrecht, B.A., Aerosols, cloud microphysics, and fractional cloudiness, *Science*, 245 (4923), 1227-1230, 1989.

Angelino, S., D.T. Suess, and K.A. Prather, Formation of aerosol particles from reactions of secondary and tertiary alkylamines: Characterization by aerosol time-of-flight mass spectrometry, *Environ. Sci. Technol.*, 35 (15), 3130-3138, 2001.

- Bao, J.W., S.A. Michelson, P.O.G. Persson, I.V. Djalalova, and J.M. Wilczak, Observed and WRF-simulated low-level winds in a high-ozone episode during the Central California Ozone Study, *J. Appl. Meteorol. Clim.*, 47 (9), 2372-2394, 2008.
- Barsanti, K.C., P.H. McMurry, and J.N. Smith, The potential contribution of organic salts to new particle growth, *Atmos. Chem. Phys. Discuss.*, 9 (9), 2949-2957, 2009.
- Berndt, T., F. Stratmann, M. Sipila, J. Vanhanen, T. Petaja, J. Mikkila, A. Gruner, G. Spindler, R.L. Mauldin III, J. Curtius, M. Kulmala, and J. Heintzenberg, Laboratory study on new particle formation from reaction OH + SO₂: influence of experimental conditions, H₂O vapour, NH₃ and the amine tert-butylamine on the overall process, *Atmos. Chem. Phys.*, 10, 6447-6484, 2010.
- Bzdek, B.R., D.P. Ridge, and M.V. Johnston, Size-dependent reactions of ammonium bisulphate clusters with dimethylamine, *J. Phys. Chem. A*, 114 (43), 11638-11644, 2010.
- Chang, L.S., S.E. Schwartz, R. McGraw, and E.R. Lewis, Sensitivity of aerosol properties to new particle formation mechanism and to primary emissions in a continental-scale chemical transport model, *J. Geophys. Res.*, 114, D07203, doi:10.1029/2008JD011019, 2009.
- Collett, J.L., B.C. Daube, D. Gunz, and M.R. Hoffmann, Intensive studies of Sierra-Nevada cloudwater chemistry and its relationship to precursor aerosol and gas concentrations, *Atmos. Environ. a-Gen.*, 24 (7), 1741-1757, 1990.
- Covert, D.S., V.N. Kapustin, P.K. Quinn, and T.S. Bates, New particle formation in the marine boundary-layer, *J. Geophys. Res.*, 97 (D18), 20581-20589, 1992.
- Finlayson-Pitts, B.J., Pitts, J. N., *Chemistry of the Upper and Lower Atmosphere*, Academic Press, San Diego, 2000.
- Fisher, J.A., D.J. Jacob, M.T. Purdy, M. Kopacz, P. Le Sager, C. Carouge, C.D. Holmes, R.M. Yantosca, R.L. Batchelor, K. Strong, G.S. Diskin, H.E. Fuelberg, J.S. Holloway, E.J. Hyer, W.W. McMillan, J. Warner, D.G. Streets, Q. Zhang, Y. Wang, and S. Wu, Source attribution and interannual variability of Arctic pollution in spring constrained by aircraft (ARCTAS, ARCPAC) and satellite (AIRS) observations of carbon monoxide, *Atmospheric Chemistry and Physics*, 10 (3), 977-996, 2010.
- Friedman, B., H. Herich, L. Kammermann, D.S. Gross, A. Arneth, T. Holst, and D.J. Cziczo, Subarctic atmospheric aerosol composition: 1. Ambient aerosol characterization, *J. Geophys. Res.*, 114, D13203, doi:10.1029/2009JD011772, 2009.
- Gard, E., J.E. Mayer, B.D. Morrical, T. Dienes, D.P. Fergenson, and K.A. Prather, Real-time analysis of individual atmospheric aerosol particles: Design and performance of a portable ATOFMS, *Anal. Chem.*, 69 (20), 4083-4091, 1997.

- Hansen, A.D.A., and H. Rosen, Horizontal Inhomogeneities in the Particulate Carbon Component of the Arctic Haze, *Atmos. Environ.*, 19 (12), 2175-2180, 1985.
- Hitzenberger, R., and S. Tohno, Comparison of black carbon (BC) aerosols in two urban areas - concentrations and size distributions, *Atmos. Environ.*, 35 (12), 2153-2167, 2001.
- Kerminen, V.M., H. Lihavainen, M. Komppula, Y. Viisanen, and M. Kulmala, Direct observational evidence linking atmospheric aerosol formation and cloud droplet activation, *Geophys. Res. Lett.*, 32, L14803, doi:10.1029/2005GL02313, 2005.
- Kuang, C., P.H. McMurry, and A.V. McCormick, Determination of cloud condensation nuclei production from measured new particle formation events, *Geophys. Res. Lett.*, 36, L09822, doi:10.1029/2009GL037584, 2009.
- Kulmala, M., V.M. Kerminen, and A. Laaksonen, Simulations on the effect of sulphuric acid formation on atmospheric aerosol concentrations, *Atmos. Environ.*, 29 (3), 377-382, 1995.
- Kulmala, M., U. Pirjola, and J.M. Makela, Stable sulphate clusters as a source of new atmospheric particles, *Nature*, 404 (6773), 66-69, 2000.
- Kulmala, M., H. Vehkamäki, T. Petaja, M. Dal Maso, A. Lauri, V.M. Kerminen, W. Birmili, and P.H. McMurry, Formation and growth rates of ultrafine atmospheric particles: a review of observations, *J. Aerosol Sci.*, 35 (2), 143-176, 2004.
- Lunden, M.M., D.R. Black, M. McKay, K.L. Revzan, A.H. Goldstein, and N.J. Brown, Characteristics of fine particle growth events observed above a forested ecosystem in the Sierra Nevada Mountains of California, *Aerosol Sci. Tech.*, 40 (5), 373-388, 2006.
- Mäkelä, J.M., S. Yli-Koivisto, V. Hiltunen, W. Seidl, E. Swietlicki, K. Teinila, M. Sillanpää, I.K. Koponen, J. Paatero, K. Rosman, and K. Hameri, Chemical composition of aerosol during particle formation events in boreal forest, *Tellus Series B-Chemical and Physical Meteorology*, 53 (4), 380-393, 2001.
- McMurry, P.H., M. Fink, H. Sakurai, M.R. Stolzenburg, R.L. Mauldin, J. Smith, F. Eisele, K. Moore, S. Sjostedt, D. Tanner, L.G. Huey, J.B. Nowak, E. Edgerton, and D. Voisin, A criterion for new particle formation in the sulfur-rich Atlanta atmosphere, *J. Geophys. Res.*, 110, D22S02, doi:10.1029/2005JD005901, 2005.
- Merikanto, J., D.V. Spracklen, G.W. Mann, S.J. Pickering, and K.S. Carslaw, Impact of nucleation on global CCN, *Atmos. Chem. Phys. Discuss.*, 9, 12999-13037, 2009.
- Murphy, S.M., A. Sorooshian, J.H. Kroll, N.L. Ng, P. Chhabra, C. Tong, J.D. Surratt, E. Knipping, R.C. Flagan, and J.H. Seinfeld, Secondary aerosol formation from atmospheric reactions of aliphatic amines, *Atmos. Chem. Phys.*, 7 (9), 2313-2337, 2007.

- Neff, J.C., E.A. Holland, F.J. Dentener, W.H. McDowell, and K.M. Russell, The origin, composition and rates of organic nitrogen deposition: A missing piece of the nitrogen cycle?, *Biogeochemistry*, 57 (1), 99-136, 2002.
- Nilsson, E.D., U. Rannik, M. Kulmala, G. Buzorius, and C.D. O'Dowd, Effects of continental boundary layer evolution, convection, turbulence and entrainment, on aerosol formation, *Tellus Series B-Chemical and Physical Meteorology*, 53 (4), 441-461, 2001.
- O'Halloran, T.L., J.D. Fuentes, D.R. Collins, M.J. Cleveland, and W.C. Keene, Influence of air mass source region on nanoparticle events and hygroscopicity in central Virginia, US, *Atmos. Environ.*, 43 (22-23), 3586-3595, 2009.
- Ortega, I.K., T. Kurten, H. Vehkamäki, and M. Kulmala, The role of ammonia in sulfuric acid ion induced nucleation, *Atmos. Chem. Phys.*, 8 (11), 2859-2867, 2008.
- Peters, M.D., and S.M. Kreidenweis, A single parameter representation of hygroscopic growth and cloud condensation nucleus activity, *Atmos. Chem. Phys.*, 7 (8), 1961-1971, 2007.
- Pierce, J.R., and P.J. Adams, Efficiency of cloud condensation nuclei formation from ultrafine particles, *Atmos. Chem. Phys.*, 7, 1367-1379, 2007.
- Pratt, K.A., L.E. Hatch, and K.A. Prather, Seasonal volatility dependence of ambient particle phase amines, *Environ. Sci. Technol.*, 43 (14), 5276-5281, 2009.
- Ristovski, Z.D., T. Suni, M. Kulmala, M. Boy, N.K. Meyer, J. Duplissy, A. Turnipseed, L. Morawska, and U. Baltensperger, The role of sulphates and organic vapours in growth of newly formed particles in a eucalyptus forest, *Atmos. Chem. Phys.*, 10, 2919-2926, 2010.
- Roberts, G.C., and A. Nenes, A continuous-flow streamwise thermal-gradient CCN chamber for atmospheric measurements, *Aerosol Sci. Tech.*, 39 (3), 206-221, 2005.
- Rosenfeld, D., W.L. Woodley, D. Axisa, E. Freud, J.G. Hudson, and A. Givati, Aircraft measurements of the impacts of pollution aerosols on clouds and precipitation over the Sierra Nevada, *J. Geophys. Res.*, 113 (), D15203, doi:10.1029/2007JD00954, 2008.
- Seinfeld, J.H., and S.N. Pandis, *Atmospheric Chemistry and Physics*, John Wiley & Sons, Inc., 2006.
- Sharkey, T.D., and F. Loreto, Water-Stress, Temperature, and Light Effects on the Capacity for Isoprene Emission and Photosynthesis of Kudzu Leaves, *Oecologia*, 95 (3), 328-333, 1993.

- Sihto, S.-L., J. Mikkilä, J. Vanhansen, M. Ehn, L. Liao, K. Lehtipalo, P.P. Aalto, J. Duplissy, T. Petaja, V.M. Kerminen, M. Boy, and M. Kulmala, Seasonal variation of CCN concentrations and aerosol activation properties in boreal forest, *Atmos. Chem. Phys. Discuss.*, 10, 28231-28272, 2010.
- Smith, J.N., K.C. Barsanti, H.R. Friedli, M. Ehn, M. Kulmala, D.R. Collins, J.H. Scheckman, B.J. Williams, and P.H. McMurry, Observations of ammonium salts in atmospheric nanoparticles and possible climatic implications, *PNAS*, 107 (15), 6634-6639, 2009.
- Smith, J.N., K.F. Moore, P.H. McMurry, and F.L. Eisele, Atmospheric measurements of sub-20 nm diameter particle chemical composition by thermal desorption chemical ionization mass spectrometry, *Aerosol. Sci. Tech.*, 38 (2), 100-110, 2004.
- Solomon, S., D. Qin, M. Manning, Z. Chen, M. Marquis, K.B. Averyt, and M. Tignor, *Climate Change 2007: The Physical Science Basis, Contribution of Working Group I to the Fourth Assessment Report of the Intergovernmental Panel on Climate Change*, Cambridge Univ. Press, Cambridge, U. K., 2007.
- Song, X.H., P.K. Hopke, D.P. Fergenson, and K.A. Prather, Classification of single particles analyzed by ATOFMS using an artificial neural network, *ART-2A, Anal. Chem.*, 71 (4), 860-865, 1999.
- Sorooshian, A., S.N. Murphy, S. Hersey, H. Gates, L.T. Padro, A. Nenes, F.J. Brechtel, H. Jonsson, R.C. Flagan, and J.H. Seinfeld, Comprehensive airborne characterization of aerosol from a major bovine source, *Atmospheric Chemistry and Physics*, 8 (17), 5489-5520, 2008.
- Spencer, M.T., and K.A. Prather, Using ATOFMS to determine OC/EC mass fractions in particles, *Aerosol Sci. Tech.*, 40 (8), 585-594, 2006.
- Stohl, A., C. Forster, A. Frank, P. Seibert, and G. Wotawa, Technical note: The Lagrangian particle dispersion model FLEXPART version 6.2, *Atmos. Chem. Phys.*, 5, 2461-2474, 2005.
- Stohl, A., M. Hittenberger, and G. Wotawa, Validation of the Lagrangian particle dispersion model FLEXPART against large-scale tracer experiment data, *Atmos. Environ.*, 32 (24), 4245-4264, 1998.
- Streets, D.G., K.F. Yarber, J.H. Woo, and G.R. Carmichael, Biomass burning in Asia: Annual and seasonal estimates and atmospheric emissions, *Global Biogeochemical Cycles*, 17 (4), -, 2003.
- Su, Y.X., M.F. Sipin, H. Furutani, and K.A. Prather, Development and characterization of an aerosol time-of-flight mass spectrometer with increased detection efficiency, *Anal. Chem.*, 76 (3), 712-719, 2004.

- Twomey, S., Influence of Pollution on Shortwave Albedo of Clouds, *J. Atmos. Sci.*, 34 (7), 1149-1152, 1977.
- Wang, L., A.F. Khalizov, J. Zheng, W. Xu, Y. Ma, V. Lal, and R. Zhang, Atmospheric nanoparticles formed from heterogeneous reactions of organics, *Nature Geoscience*, 3, 238-242, 2010a.
- Wang, L., V. Lal, A.F. Khalizov, and R. Zhang, Heterogeneous chemistry of alkylamines with sulfuric acid: Implications for atmospheric formation of alkylammonium sulfates, *Environ. Sci. Technol.*, 44 (7), 2461-2465, 2010b.
- Wehner, B., T. Petaja, M. Boy, C. Engler, W. Birmili, T. Tuch, A. Wiedensohler, and M. Kulmala, The contribution of sulfuric acid and non-volatile compounds on the growth of freshly formed atmospheric aerosols, *Geophys. Res. Lett.*, 32 (17), L17810, doi:10.1029/2005GL023827, 2005.
- Ziemba, L.D., J.E. Dibb, R.J. Griffin, L.G. Huey, and P. Beckman, Observations of particle growth at a remote, Arctic site, *Atmos. Environ.*, 44, 1649-1657, 2010.

5. Dust and Biological Aerosols from the Sahara and Asia Influence Precipitation in the Western U.S.

5.1. Introduction

Aerosols affect cloud microphysical properties including droplet size and phase, and can alter precipitation efficiency [Andreae and Rosenfeld, 2008]. In particular, dust and biological aerosols have been shown to serve as effective ice nuclei (IN) and potentially enhance precipitation in mixed phase clouds [Morris *et al.*, 2004; Rosenfeld *et al.*, 2011]. IN are atmospheric particles that catalyze the freezing of supercooled cloud droplets, producing ice crystals that would not form otherwise at warmer, mixed phase cloud temperatures [Isono *et al.*, 1959]. Dust is omnipresent in the atmosphere and originates from various deserts around the world [Prospero *et al.*, 2002]. Biological residues can be lofted during dust storms and potentially make large contributions to the ice nucleation properties of dust [Conen *et al.*, 2011; Hua *et al.*, 2007]. When lofted to high altitudes (≥ 5000 m), dust and biological aerosols can travel long distances. For example, Uno *et al.* showed dust from the Taklimakan desert in China circled the globe within 13 days [Uno *et al.*, 2009]. Intercontinental transport of dust from Asia is well documented [Ault *et al.*, 2011b; Husar *et al.*, 2001; Sun *et al.*, 2001; Uno *et al.*, 2011], while few have reported trans-Pacific transport from North Africa [Hsu *et al.*, 2012; McKendry *et al.*, 2007]. Dust is lofted into the free troposphere from the Taklimakan as early as February, with a maximum between April and May, while the Gobi has been shown to be a significant Asian dust source in response to strong winter storms in Siberia [Prospero *et al.*, 2002]. However, dust is lofted from the Sahara year round [Prospero *et al.*, 2002].

Even at low concentrations, IN-active aerosols can strongly influence ice crystal concentrations in clouds [DeMott *et al.*, 2010]. These ice crystals grow diffusively at the expense of liquid droplets [Korolev, 2007], and can undergo accretion or aggregation to form graupel or snow [Hosler *et al.*, 1957; Houze, 1993]. Ice crystal formation

produces a mixed phase cloud that initiates precipitation more rapidly than in a supercooled liquid-only cloud due to the faster growth rate of ice particles versus droplets [Pinsky *et al.*, 1998], thus potentially increasing the intensity and altering the location of precipitation. These ice and precipitation processes can have serious ramifications for mountainous regions such as the California Sierra Nevada Mountains, where snowpack supplies copious amounts of water to reservoirs [Guan *et al.*, 2010]. Hence, cloud seeding experiments have been conducted in the region since the 1950s as a possible means of increasing precipitation [Deshler and Reynolds, 1990; Reynolds and Dennis, 1986]. Early discoveries point to glaciation as a key step in precipitation formation, however the source of IN was not identified. It has been suggested that over 50% of precipitation globally is initiated in the ice phase [e.g., Lau and Wu, 2003]. Therefore, it is important to identify natural IN sources as well as determine the overall effects of IN on precipitation processes, which are poorly understood.

Analysis of precipitation samples in combination with storm meteorology provides insights into IN effects on orographic precipitation. For example, Ault *et al.* observed dust as insoluble residues in precipitation over the Sierra Nevada that was suspected to serve as IN during an intense snowstorm in the 2009 winter season [Ault *et al.*, 2011b]. This storm was associated with an atmospheric river (AR, narrow band of enhanced water vapor transport) (e.g., Ralph *et al.* [2004]), as was a preceding storm. Nearby meteorological measurements deployed as part of NOAA's Hydrometeorology Testbed (HMT) [Ralph *et al.*, 2005] showed that during each storm, ARs transported a similar amount of water vapor up the mountain slope, and yet the second storm produced 40% more precipitation. The precipitation samples from the second storm contained dust, but samples from the first storm did not. The dust observed in Ault *et al.* was transported across the Pacific Ocean and based on FLEXPART analysis appeared to originate over East Asia [Ault *et al.*, 2011b]. Herein, we show that dust, which was abundant over California throughout the 2011 winter, unexpectedly originated from arid regions even further east than Asia in North Africa and the Middle East. Dust concentrations became more dilute during transport from distant source regions due to wet and/or dry deposition

processes, yet these lower concentrations still profoundly impacted upper level clouds where precipitation processes were initiated.

5.2. Results and Discussion

The *CalWater* field campaign was designed to directly address aerosol impacts on precipitation in the Sierra Nevada during three consecutive winter seasons (2009-2011). Measurements from a remote ground site at California's Sugar Pine Dam (SPD, 39°07'42.80"N, 120°48'04.90"W; 1064 m, MSL) included aerosol and meteorological instrumentation from 2009-2011. Storms during 2011, the focus of this paper, include additional aircraft observations made onboard the Department of Energy Gulfstream-1 (G-1) and thus provide a more refined picture, spanning from ground-based measurements to the *in situ* vertical profile of the aerosols and cloud microphysics. Aerosol time-of-flight mass spectrometry (ATOFMS) [Gard *et al.*, 1997b] was used to determine the chemical composition of individual re-suspended precipitation residues and *in situ* cloud particle residues. We focused on dust and biological residues, combining them into one classification, because both have been shown to be IN-active and chemical markers for each type were often observed within the same individual residues, as shown by Pratt *et al.* [Pratt *et al.*, 2009a] and discussed in Chapter 10. S-band profiling radar (S-PROF) provided bulk microphysical information using vertical profiles of hydrometeor fall velocity and radar reflectivity, including the presence of a brightband. The brightband is a layer of enhanced radar reflectivity (i.e., melting layer) resulting from the difference in the fall speed and dielectric factor for ice and water and the aggregation of ice particles as they descend and melt [White *et al.*, 2002]. Precipitation processes included non-brightband (warm) rain, brightband (cold) rain, and snow/graupel/hail. Warm rain starts as primarily liquid water and falls in the absence of a brightband, whereas cold rain starts as ice and melts as it falls toward the surface in the presence of a brightband [White *et al.*, 2003]. When surface temperatures were cold enough, snow, graupel, and/or hail reached the surface. Precipitation that starts in the ice phase is termed ice-induced precipitation. Precipitation samples were collected at SPD from Jan 30–Mar

8, 2011. S-PROF time-height cross sections during the times for all 11 of the precipitation sampling periods are shown in Chapter 10.

During all of the storms, dust and biological precipitation residues were frequently present, comprising up to 99% of the total residues per sample. Figure 5.1 shows the percentage of dust plus biological particles (%Dust+Bio), average surface temperature ($^{\circ}\text{C}$), and percentages of different precipitation processes during each sample collection date in 2011. Ice-induced precipitation comprised 74% of the total precipitation that fell at SPD; whereas warm rain only comprised 10% (the remaining 16% was unclassified). The highest %Dust+Bio occurred during storms that contained a higher percentage of ice-induced precipitation (e.g., Jan 30, Feb 16-19, and Feb 24-26). During these storms, surface temperatures were sufficiently low, enabling snow/graupel/hail to reach the surface. During the storms from Feb 14-16, Mar 1-3, and Mar 5-7, surface temperatures were higher resulting in more rain than ice at the surface. Further, more warm rain coincided with lower %Dust+Bio during these time periods. One possible explanation could be that a limited amount of dust and biological residues were available to serve as IN, which could result in less precipitation initiated in the ice phase. Another explanation is the thermal structure of the storm was overall warmer, favoring warm rain processes. For the five samples where >50% of precipitation occurred as snow/graupel/hail, the average %Dust+Bio was 90%, whereas for the four cases where >30% of the precipitation occurred as warm rain, the average %Dust+Bio was 69%. Overall, these results suggest that dust and biological aerosols served as IN and influenced the precipitation phase in the clouds during colder sectors of the storms, reinforcing the observations made by Ault *et al.* in 2009. Synoptic and mesoscale meteorological processes were likely also responsible for the large scale transport of the dust and biological aerosols [Ault *et al.*, 2011b]. However, if dust and biological aerosols were hypothetically absent in these cold air masses, supercooled cloud droplets could remain as liquid instead of forming ice crystals as described herein.

The abundance of dust and biological aerosols observed on days with more ice-induced precipitation leads one to question their origin. Figure 5.2 (A) shows 10-day air

mass backward trajectories calculated using HYSPLIT [Draxler and Rolph, 2011b] ending at SPD during the storms shown in Figure 5.1. Meyers *et al.* suggest that ice nucleation occurs at the tops of orographic clouds [Meyers *et al.*, 1992], and thus trajectories were calculated to end at cloud top heights between 2000-10000 m, MSL using GOES-11 satellite data that was averaged every 3 hours during storms. The boxes highlight major dust regions [Prospero *et al.*, 2002]. Based on previous studies [e.g., Hallar *et al.*, 2011], the biological aerosols were likely co-lofted from arid regions and transported with the dust. Trajectories are colored based on which dust region they traveled over, including North Africa, the Middle East, and East Asia (separated into the Taklimakan desert and Northeast China/Mongolia). Figure 5.2 (B) shows the frequency of trajectories during each storm that traveled over each dust region. Trajectories that originated from over North Africa frequently traveled over the other dust regions on the way to the United States, suggesting these air masses contained a mixture of dust from the various source regions. The frequency of sources shows that the beginning of the study was predominantly affected by Asian influences, whereas towards the end of the study, the frequency of Middle Eastern and North African transport increased. Overall, air masses traveled through North Africa and the Middle East 15% and 21% of the time, respectively, suggesting transport of dust and biological aerosols from source regions other than just Asia.

Determining not only where the air masses traveled but whether they contained dust and possibly biological aerosols is pertinent to defining the sources of IN in the Sierra Nevada. Not only did the air masses travel over the various dust regions, the air intersected dust layers as shown in Figure 5.2 (C). Using time-height cross sections of dust concentrations from the Navy Aerosol Analysis and Prediction System (NAAPS, <http://www.nrlmry.navy.mil/aerosol/>), we estimated the maximum height of dust layers at sites within the boxes on days where the trajectories traveled over each dust region. The height of trajectories that passed through each region typically fell within the height of the dust layers as shown in Figure 5.2 (C). Although transport within the dust layers was infrequent over North Africa, Saharan dust was likely picked up over the Middle East where trajectories, on average, skimmed the top of the layer. Overall, trajectories traveled

through dust layers 6%, 23%, 73%, and 45% of the time in North Africa, the Middle East, the Taklimakan, and Northeast China/Mongolia, respectively, as shown in Chapter 10.

Further evidence that dust was present along the complete trajectory was obtained using Cloud-Aerosol Lidar and Infrared Pathfinder Satellite Observation (CALIPSO) satellite imagery of aerosol subtypes. In combination with NAAPS, CALIPSO provides a method to track dust as it is transported from the source across the Pacific Ocean to SPD, as shown in Chapter 10. Figure 5.3 shows NAAPS modeled aerosol optical depth (AOD) of dust for the trajectories ending on Feb 16th and Feb 25th. These two days represent the storms where the highest %Dust+Bio was present in the precipitation. In addition, Feb 16th was affected by predominantly Asian sources and Feb 25th was influenced by a combination of Saharan and Asian sources as shown in Figure 5.2 (B). The trajectory ending on Feb 16th started 10 days back over the Atlantic Ocean and proceeded to travel north of the Saharan dust layer. Before reaching China, the air mass contained little dust based on CALIPSO imagery (the “N/A” circle). Once the air mass reached Northeast China/Mongolia, it picked up fresh dust and traveled across the Pacific Ocean to SPD. In contrast, the trajectory ending on Feb 25th started 10 days back over Oman where an abundance of fresh dust was present. The air mass continued to travel over Southern China where it likely picked up more dust from the Asian layers. The CALIPSO imagery following the trajectory over the Pacific Ocean shows both fresh and polluted dust. Combined analysis of air mass back trajectories, NAAPS, and CALIPSO imagery provide direct evidence of dust being lofted in the atmosphere and transported across the Pacific Ocean and above SPD.

In the absence of dust and pollution aerosols, low level orographic clouds in the Sierra Nevada can develop in pristine marine air masses [Rosenfeld *et al.*, 2008b]. Measurements herein show that when dust and biological aerosols from various source regions feed into these pristine clouds, they serve as IN and have a profound effect on cloud microphysics. A compact aircraft version of the ATOFMS [Pratt *et al.*, 2009d] measured *in situ* cloud residues. The largest percentages of dust and biological particles

in the cloud residues (69% and 87%) were observed during the flights on Feb 16th and on Feb 25th, respectively. The meteorological conditions were similar during these two days as discussed in Chapter 10. Interestingly, the largest %Dust+Bio in the precipitation samples (93% and 95% on average) was also observed during the corresponding storms (Feb 16-19 and Feb 24-26). Single-particle analysis of both cloud and precipitation residues shows the mineralogy and biological characteristics were quite different during each storm as discussed in Chapter 10, supporting the contribution from different source regions. The dust and biological residues sampled in the precipitation and in-cloud for each storm were chemically similar to each other as discussed in Chapter 10, suggesting that the residues sampled in-cloud precipitated out. In addition, the highest percentages of ice-induced precipitation (75% and 96% on average) were also observed during these storms. These trends suggest that dust and biological aerosols are playing a role in influencing the precipitation phase in the clouds.

Figure 5.4 shows the Feb 16th flight separated into the ascent Figure 5.4 (A) and the descent Figure 5.4 (B). The ascent and descent are shown separately because the cloud layers, including lower level convective clouds (≤ 3500 m) and upper level orographic clouds (~ 4000 - 6000 m, MSL), were decoupled on the ascent while on the descent, the cloud layers became coupled. See Chapter 10 for maps showing the geographical locations of the ascent and descent. Feb 25th data and flight tracks for both flights are presented in Chapter 10. In Figure 5.4, the number of dust and biological residues (“Dust+Bio”) and sea salt are shown in brown and blue bars, respectively, relative to the total number of residues in white. The orange markers show air temperature and the circles indicate IN concentrations measured in the condensation/immersion-freezing regime above water saturation with the Continuous Flow Diffusion Chamber (CFDC), colored by CFDC processing temperature [Rogers *et al.*, 2001]. Error bars represent uncertainties in IN concentrations calculated for 3-10 minute time periods. The grey bars show ice classifications defined by viewing 2D-S imagery. Representative images for each of these classifications are shown in Chapter 10.

During the ascent to high altitudes on Feb 16th, the lower level cloud contained predominately sea salt residues, indicating these were pristine marine clouds. The IN concentrations were very low and highly uncertain (0 to a maximum of $0.15 \pm 0.2 \text{ L}^{-1}$ in a temperature range from -18.4 to -18.9°C). These measurements were consistent with little to no ice in cloud as evidenced by 2D-S cloud particle imagery. The cloud temperatures were as low as -21°C , slightly colder than the CFDC operating temperature. The lack of significant amounts of ice at temperatures colder than the CFDC temperature confirms that there were very few IN active. The IN concentrations in the upper level clouds were higher with more certainty at $0.16 \pm 0.06 \text{ L}^{-1}$ measured at -18.8°C , while 2D-S imagery showed a mixture of ice and liquid droplets. In addition, the upper level cloud residues were predominantly comprised of Dust+Bio residues. The collocation of these residues with IN and ice crystals suggests the dust and biological residues served as IN in these upper level clouds. During the descent back down to lower altitudes, the Dust+Bio residues were detected at a variety of altitudes, but most abundant between 3500-4500 m, MSL. IN concentrations measured at a lower CFDC processing temperature of $-32 \pm 0.5^\circ\text{C}$ trended with the abundance of the Dust+Bio residues, reaching as high as $2.2 \pm 0.3 \text{ L}^{-1}$ in the layer from 4000-4500 m, MSL. These observations suggest that the Dust+Bio were IN-active and formed ice at temperatures present in the 4000-4500 m layer (as low as -36°C). Between 2500 and 3500 m, MSL, the cloud residues were a mixture of sea salt and Dust+Bio, suggesting the cloud layers became mixed as the ice from the upper level clouds fell into the lower level pristine marine clouds. At this point, 2D-S imagery shows the ice became highly rimed. The results are indicative of the seeder-feeder mechanism [Choulaton and Perry, 1986], which has been documented previously in the Sierra Nevada [Meyers et al., 1992] as well as in other mountain regions [Dore et al., 1999; Fowler et al., 1995; Reinking et al., 2000; Saleeby et al., 2009].

Droplets in the lower level pristine marine “feeder” clouds likely accreted to form rime on the ice that fell from the upper level “seeder” clouds. Previous studies have shown that a graupel particle grows much faster than a supercooled raindrop of the same mass in the same convective cloud [Pinsky et al., 1998]. Therefore, seeder-feeder is an efficient precipitation mechanism, especially when the accreted drops are large [Borys et

al., 2000]. Satellite observations have suggested the possibility of dust glaciating high altitude clouds [Choi *et al.*, 2010], however there have not been any *in situ* measurements of dust in clouds over the Sierra Nevada prior to this study. When urban pollution aerosols are incorporated into clouds, precipitation processes are often less efficient and suppression of both warm and mixed phase precipitation has been shown via satellite [Rosenfeld, 2000]. These previous studies were associated with probable suppression of precipitation in low level orographic clouds coupled to the boundary layer pollution [Givati and Rosenfeld, 2004]. The presence of dust feeding deeper and colder orographic cloud levels appears to have the opposite effect i.e., accelerating the efficiency of the precipitation forming processes, especially in situations with decoupled cloud layers.

5.3. Conclusions

Herein we present a direct link between long-range transported dust and biological aerosols affecting cloud ice formation and the resulting precipitation in the Sierra Nevada. Dust and biological aerosols measured as insoluble residues in precipitation samples corresponded to periods with more ice-induced precipitation. *In situ* aircraft measurements confirmed the dust and biological residues were collocated with IN and ice in clouds. Many factors contribute to the type and quantity of precipitation including dynamics, meteorology, and transport conditions; however, our results suggest dust and biological IN are key components in precipitation initiation as they lead to the glaciation of upper level clouds.

Prior to this study, most work has focused on modeling the impacts of regional aerosol pollution sources on precipitation. Our results demonstrate the potentially determinant impact of intercontinental transport of aerosols on precipitation processes. Further, these findings motivate the challenging study of quantifying aerosol effects on not only the phase, but intensity and location of precipitation. Due to the ubiquity of dust in the atmosphere, these findings have global significance. Furthermore, the implications for future water resources become even more substantial when considering the possible increase in Aeolian dust as a result of a warming climate and land use changes.

5.4. Acknowledgments

Funding was provided by the California Energy Commission under contract CEC 500-09-043. J. Mayer, E. Fitzgerald, D. Collins, and J. Cahill provided assistance with UCSD/SIO equipment set-up. The authors gratefully acknowledge the NOAA Air Resources Laboratory (ARL) for the provision of the HYSPLIT transport and dispersion model and/or READY website (<http://www.arl.noaa.gov/ready.php>) used in this publication. P. Minnis (NASA Langley Research Center), and J. Ayers and R. Palikonda (Science Systems and Applications) provided *GOES-11* cloud top heights used for HYSPLIT back trajectory analysis. The deployment of the NOAA and UCSD/SIO equipment at the Sugar Pine site involved many field staff, particularly C. King (NOAA/ESRL/PSD). The deployment of the DOE Gulfstream-1 involved many PNNL/ARM field staff, particularly J. Hubbe and C. Kluzek. J. Tomlinson and J. Comstock provided 2D-S imagery. M. Hubbell and B. Svancara flew the G-1 for the *CalWater* flight campaign. D. Collins and R. Spackman provided insightful discussions during the editing stages of this manuscript. Traci Lersch of R.J. Lee Inc. provided TEM analyses of collected IN. Data available in this paper are available in Chapter 10.

5.5. Figures

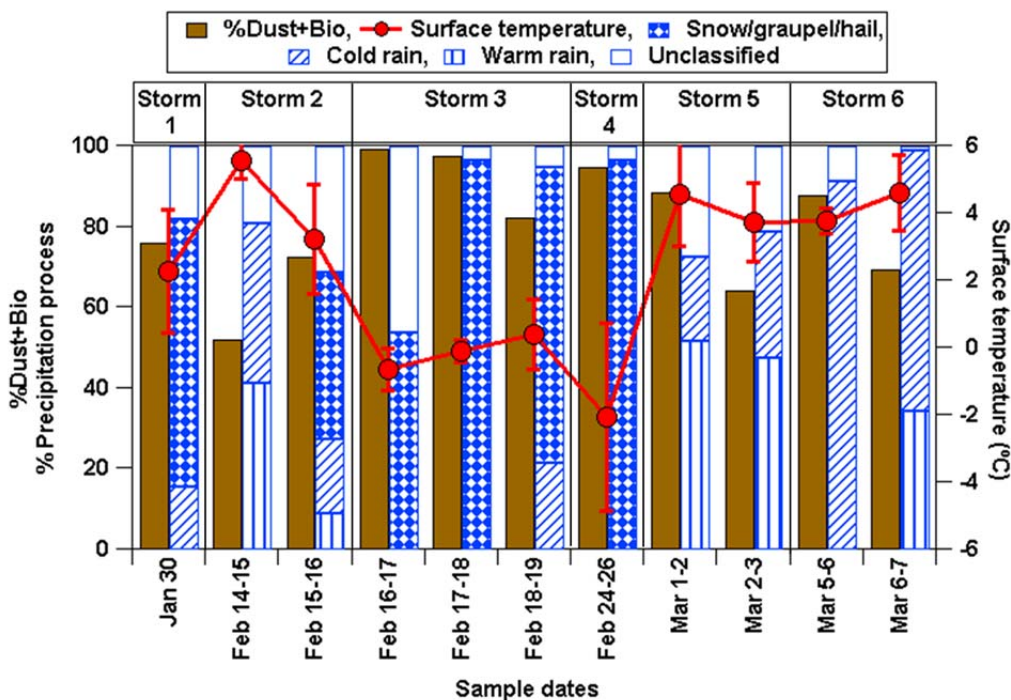


Figure 5.1 Precipitation characteristics during each sample collection dates of the 2011 CalWater study at SPD. Brown bars represent the percentages of dust and biological residues (%Dust+Bio) per sample collection dates at SPD in 2011. Percentages of cold rain, snow, and warm rain per sample are also shown. Red markers represent the average surface temperature (°C) per sample collection dates. Error bars are shown for temperature and represent one standard deviation from the average. The storms in which sample collection dates correspond to during the study are highlighted in order to identify the evolution of precipitation residues, surface temperature, and precipitation processes over the course of the storms.

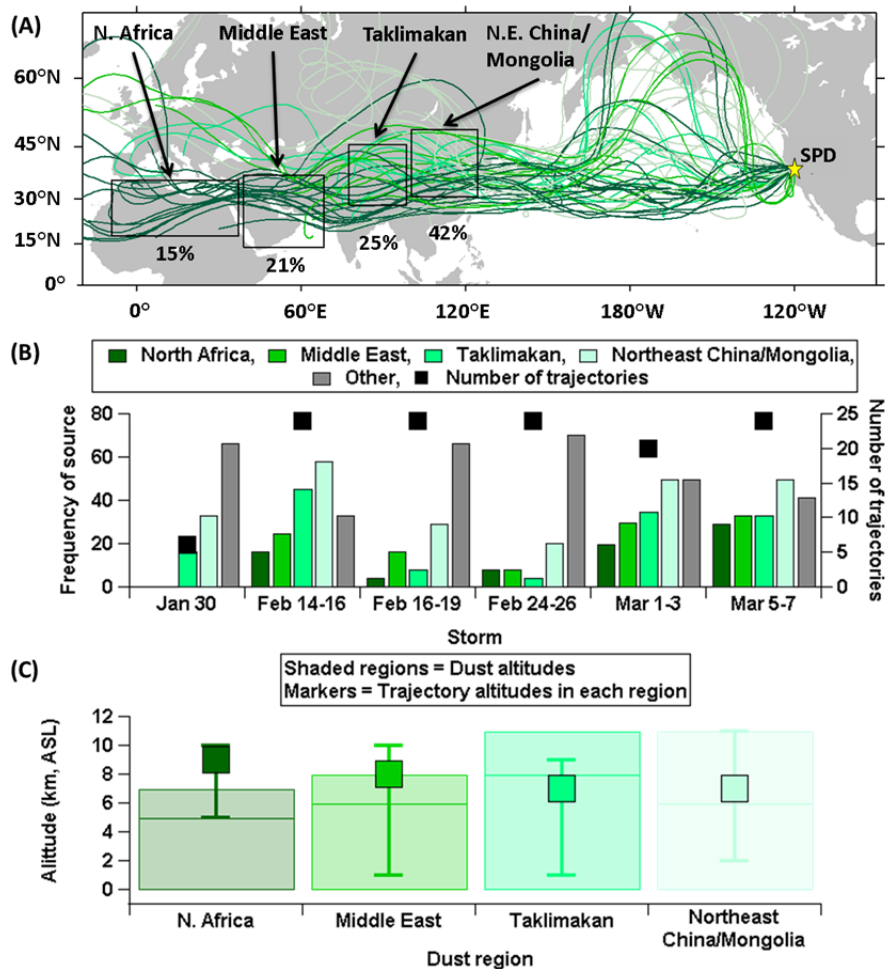


Figure 5.2 Dust source analysis including (A) 10-day back trajectories ending during the storms at SPD in 2011, with the boxes highlighting the four dust regions. Storms were investigated in order to achieve statistical significance. The percentages under each box represent the frequency that the trajectories passed through each arid region. (B) The frequency of back trajectories that originated over North Africa, the Middle East, the Taklimakan, Northeast China/Mongolia, and Other (non-dust origin) ending at cloud top heights over SPD. The four shades of green represent the four different dust regions. The total number of trajectories analyzed per storm is also provided. (C) The average altitudes of trajectories that passed through each region and dust layer heights determined using NAAPS time-height sections at Sedebocker (North Africa), Solar Village (Middle East), Yinchuan (Taklimakan), and Beijing (Northeast China/Mongolia). A map of the sites and examples of the time-height sections are shown in Chapter 10. The middle line of the shaded regions represents the average maximum height of the dust layers in each region. The error bars show the minimum and maximum altitudes for the trajectory endpoints and dust layers.

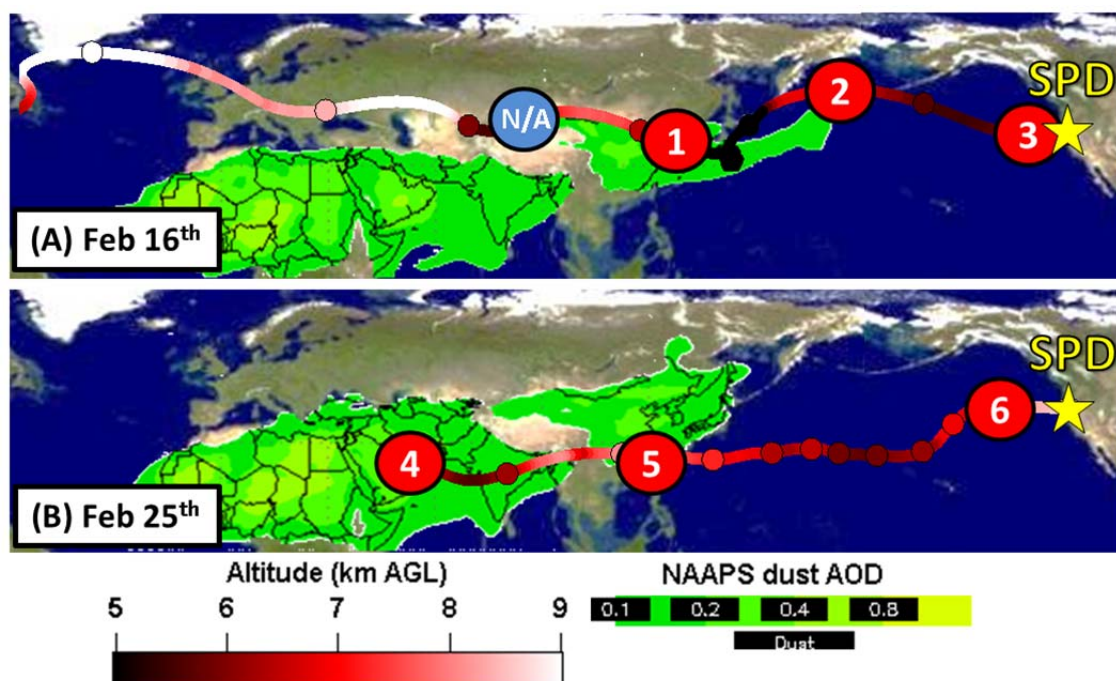


Figure 5.3 Dust tracking for days during the (A) Feb 14-16 and (B) Feb 24-26 storms. The 10-day air mass back trajectories ended at cloud top heights over SPD (shown by the star) on Feb 16th (7390 m, MSL) and Feb 25th (9340 m, MSL). Within each trajectory, the color scale represents the altitude of each hourly endpoint while the circles show each endpoint at 00:00, i.e., each marker represents 1 day back. The last two days from the trajectory ending on Feb 16th are not shown. The circled numbers mark the locations where dust was present along these trajectories determined using CALIPSO imagery (imagery shown in Chapter 10). The green overlays represents dust aerosol optical depth (AOD) from 0.1-0.8 modeled using NAAPS. The dust AOD overlays are composites of the 10 days during each trajectory: (A) Feb 6-16 and (B) Feb 15-25.

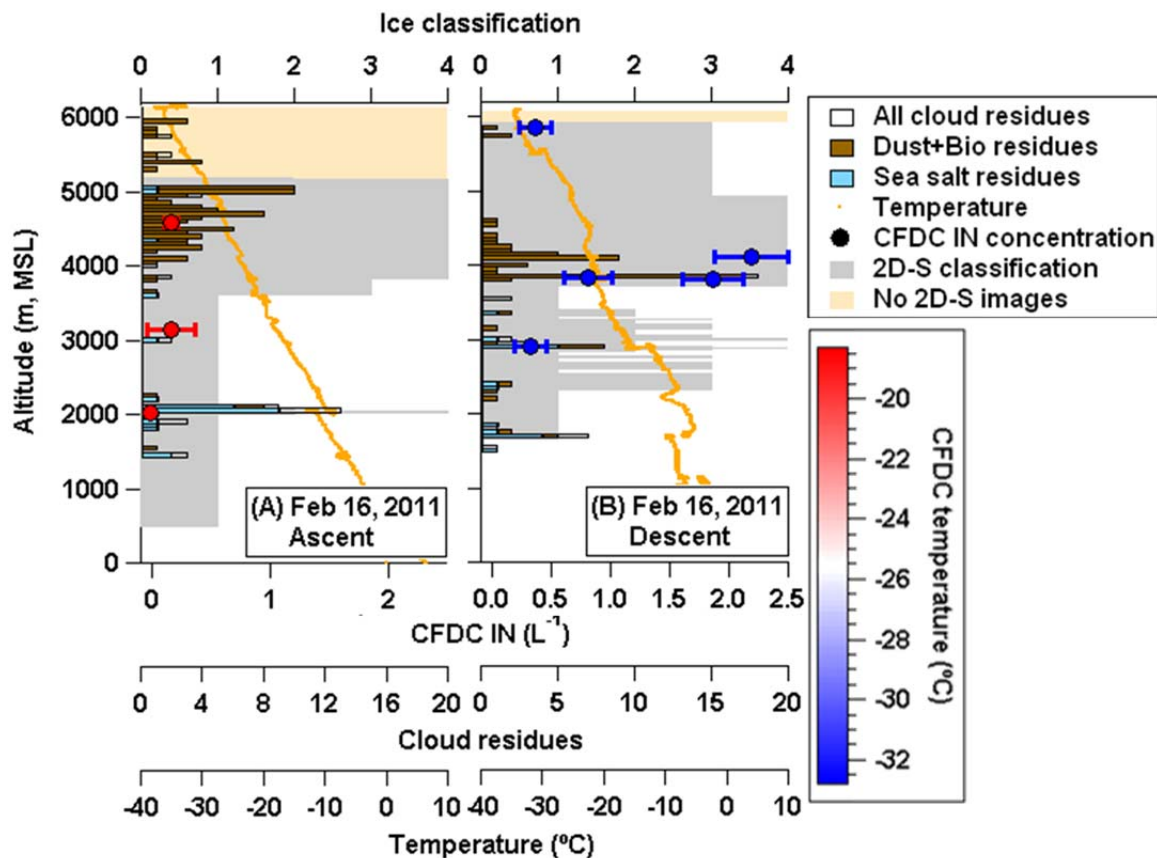


Figure 5.4 Vertical profiles of Dust+bio and sea salt cloud residues, the total number of residues, and temperature for the flight on (A) Feb 16th ascent (17:01-18:29 UTC) and (B) Feb 16th descent (18:29-20:19 UTC). Also shown are cloud particle residual IN concentrations as asterisks with the color representing the temperature at which the measurement was taken and the 2D-S classifications, with 0 = no images/out-of-cloud, 1 = droplets with no ice, 2 = isolated ice crystals, 3 = mixed, and 4 = rimed ice. Cloud residues were not chemically analyzed below 1500 m, MSL because either the 2D-S revealed rain and/or the cloud residues were smaller than the A-ATOFMS size range (<0.1 μm). The peach shading represents time periods where the 2D-S was experiencing instrumental complications.

5.6. References

- Andreae, M.O., and D. Rosenfeld, Aerosol-cloud-precipitation interactions. Part 1. The nature and sources of cloud-active aerosols, *Earth-Science Reviews*, 89 (1-2), 13-41, 2008.
- Ault, A.P., C.R. Williams, A.B. White, P.J. Neiman, J.M. Creamean, C.J. Gaston, F.M. Ralph, and K.A. Prather, Detection of Asian dust in California orographic precipitation, *Journal of Geophysical Research-Atmospheres*, 116, 2011.

- Borys, R.D., D.H. Lowenthal, and D.L. Mitchell, The relationships among cloud microphysics, chemistry, and precipitation rate in cold mountain clouds, *Atmospheric Environment*, 34 (16), 2593-2602, 2000.
- Choi, Y.S., R.S. Lindzen, C.H. Ho, and J. Kim, Space observations of cold-cloud phase change, *Proceedings of the National Academy of Sciences of the United States of America*, 107 (25), 11211-11216, 2010.
- Choullarton, T.W., and S.J. Perry, A Model of the Orographic Enhancement of Snowfall by the Seeder-Feeder Mechanism, *Quarterly Journal of the Royal Meteorological Society*, 112 (472), 335-345, 1986.
- Conen, F., C.E. Morris, J. Leifeld, M.V. Yakutin, and C. Alewell, Biological residues define the ice nucleation properties of soil dust, *Atmospheric Chemistry and Physics*, 11 (18), 9643-9648, 2011.
- DeMott, P.J., A.J. Prenni, X. Liu, S.M. Kreidenweis, M.D. Petters, C.H. Twohy, M.S. Richardson, T. Eidhammer, and D.C. Rogers, Predicting global atmospheric ice nuclei distributions and their impacts on climate, *Proceedings of the National Academy of Sciences of the United States of America*, 107 (25), 11217-11222, 2010.
- Deshler, T., and D.W. Reynolds, Physical Response of Winter Orographic Clouds over the Sierra-Nevada to Airborne Seeding Using Dry Ice or Silver-Iodide, *Journal of Applied Meteorology*, 29 (4), 288-330, 1990.
- Dore, A.J., M. Sobik, and K. Migala, Patterns of precipitation and pollutant deposition in the western Sudete mountains, Poland, *Atmospheric Environment*, 33 (20), 3301-3312, 1999.
- HYSPLIT (HYbrid Single-Particle Lagrangian Integrated Trajectory) Model access via NOAA ARL READY Website (<http://ready.arl.noaa.gov/HYSPLIT.php>), NOAA Air Resources Laboratory, Silver Spring, MD. 2011.
- Fowler, D., I.D. Leith, J. Binnie, A. Crossley, D.W.F. Inglis, T.W. Choullarton, M. Gay, J.W.S. Longhurst, and D.E. Conland, Orographic enhancement of wet deposition in the United Kingdom: Continuous monitoring, *Water Air and Soil Pollution*, 85 (4), 2107-2112, 1995.
- Gard, E., J.E. Mayer, B.D. Morrical, T. Dienes, D.P. Fergenson, and K.A. Prather, Real-time analysis of individual atmospheric aerosol particles: Design and performance of a portable ATOFMS, *Analytical Chemistry*, 69 (20), 4083-4091, 1997.
- Givati, A., and D. Rosenfeld, Quantifying precipitation suppression due to air pollution, *Journal of Applied Meteorology*, 43 (7), 1038-1056, 2004.

- Guan, B., N.P. Molotch, D.E. Waliser, E.J. Fetzer, and P.J. Neiman, Extreme snowfall events linked to atmospheric rivers and surface air temperature via satellite measurements, *Geophysical Research Letters*, 37, 2010.
- Hallar, A.G., G. Chirokova, I. McCubbin, T.H. Painter, C. Wiedinmyer, and C. Dodson, Atmospheric bioaerosols transported via dust storms in the western United States, *Geophysical Research Letters*, 38, 2011.
- Hosler, C.L., D.C. Jensen, and L. Goldshlak, On the Aggregation of Ice Crystals to Form Snow, *Journal of Meteorology*, 14 (5), 415-420, 1957.
- Houze, R.A., *Cloud dynamics*, Academic Press, San Diego, USA, 1993.
- Hsu, S.-C., C.-A. Huh, C.-Y. Lin, W.-N. Chen, N.M. Mahowald, S.-C. Liu, C.C.K. Chou, M.-C. Liang, C.-J. Tsai, F.-J. Lin, J.-P. Chen, and Y.-T. Huang, Dust transport from non-East Asian sources to the North Pacific, *Geophys. Res. Lett.*, 39 (12), L12804, 2012.
- Hua, N.P., F. Kobayashi, Y. Iwasaka, G.Y. Shi, and T. Naganuma, Detailed identification of desert-originated bacteria carried by Asian dust storms to Japan, *Aerobiologia*, 23 (4), 291-298, 2007.
- Husar, R.B., D.M. Tratt, B.A. Schichtel, S.R. Falke, F. Li, D. Jaffe, S. Gasso, T. Gill, N.S. Laulainen, F. Lu, M.C. Reheis, Y. Chun, D. Westphal, B.N. Holben, C. Gueymard, I. McKendry, N. Kuring, G.C. Feldman, C. McClain, R.J. Frouin, J. Merrill, D. DuBois, F. Vignola, T. Murayama, S. Nickovic, W.E. Wilson, K. Sassen, N. Sugimoto, and W.C. Malm, Asian dust events of April 1998, *Journal of Geophysical Research-Atmospheres*, 106 (D16), 18317-18330, 2001.
- Isono, K., M. Komabayasi, and A. Ono, The nature and origin of ice nuclei in the atmosphere, *J. Meteorol. Soc. Japan*, 37, 211-233, 1959.
- Korolev, A., Limitations of the wegener-bergeron-findeisen mechanism in the evolution of mixed-phase clouds, *Journal of the Atmospheric Sciences*, 64 (9), 3372-3375, 2007.
- Lau, K.M., and H.T. Wu, Warm rain processes over tropical oceans and climate implications, *Geophysical Research Letters*, 30 (24), 2003.
- McKendry, I.G., K.B. Strawbridge, N.T. O'Neill, A.M. Macdonald, P.S.K. Liu, W.R. Leaitch, K.G. Anlauf, L. Jaegle, T.D. Fairlie, and D.L. Westphal, Trans-Pacific transport of Saharan dust to western North America: A case study, *Journal of Geophysical Research-Atmospheres*, 112 (D1), 2007.
- Meyers, M.P., P.J. Demott, and W.R. Cotton, New Primary Ice-Nucleation Parameterizations in an Explicit Cloud Model, *Journal of Applied Meteorology*, 31 (7), 708-721, 1992.

- Morris, C.E., D.G. Georgakopoulos, and D.C. Sands, Ice nucleation active bacteria and their potential role in precipitation, *Journal De Physique Iv*, 121, 87-103, 2004.
- Pinsky, M., A. Khain, D. Rosenfeld, and A. Pokrovsky, Comparison of collision velocity differences of drops and graupel particles in a very turbulent cloud, *Atmospheric Research*, 49 (2), 99-113, 1998.
- Pratt, K.A., P.J. DeMott, J.R. French, Z. Wang, D.L. Westphal, A.J. Heymsfield, C.H. Twohy, A.J. Prenni, and K.A. Prather, In situ detection of biological particles in cloud ice-crystals, *Nature Geoscience*, 2 (6), 397-400, 2009a.
- Pratt, K.A., J.E. Mayer, J.C. Holecek, R.C. Moffet, R.O. Sanchez, T.P. Rebotier, H. Furutani, M. Gonin, K. Fuhrer, Y.X. Su, S. Guazzotti, and K.A. Prather, Development and Characterization of an Aircraft Aerosol Time-of-Flight Mass Spectrometer, *Analytical Chemistry*, 81 (5), 1792-1800, 2009b.
- Prospero, J.M., P. Ginoux, O. Torres, S.E. Nicholson, and T.E. Gill, Environmental characterization of global sources of atmospheric soil dust identified with the Nimbus 7 Total Ozone Mapping Spectrometer (TOMS) absorbing aerosol product, *Reviews of Geophysics*, 40 (1), 2002.
- Ralph, F.M., P.J. Neiman, and G.A. Wick, Satellite and CALJET aircraft observations of atmospheric rivers over the eastern north pacific ocean during the winter of 1997/98, *Monthly Weather Review*, 132 (7), 1721-1745, 2004.
- Ralph, F.M., R.M. Rauber, B.F. Jewett, D.E. Kingsmill, P. Pisano, P. Pugnner, R.M. Rasmussen, D.W. Reynolds, T.W. Schlatter, R.E. Stewart, S. Tracton, and J.S. Waldstreicher, Improving short-term (0-48 h) cool-season quantitative precipitation forecasting - Recommendations from a USWRP workshop, *Bulletin of the American Meteorological Society*, 86 (11), 1619+, 2005.
- Reinking, R.F., J.B. Snider, and J.L. Coen, Influences of Storm-Embedded Orographic Gravity Waves on Cloud Liquid Water and Precipitation, *Journal of Applied Meteorology*, 39 (6), 733-759, 2000.
- Reynolds, D.W., and A.S. Dennis, A Review of the Sierra Cooperative Pilot Project, *Bulletin of the American Meteorological Society*, 67 (5), 513-523, 1986.
- Rogers, D.C., P.J. DeMott, S.M. Kreidenweis, and Y.L. Chen, A continuous-flow diffusion chamber for airborne measurements of ice nuclei, *Journal of Atmospheric and Oceanic Technology*, 18 (5), 725-741, 2001.
- Rosenfeld, D., Suppression of rain and snow by urban and industrial air pollution, *Science*, 287 (5459), 1793-1796, 2000.
- Rosenfeld, D., W.L. Woodley, D. Axisa, E. Freud, J.G. Hudson, and A. Givati, Aircraft measurements of the impacts of pollution aerosols on clouds and precipitation

- over the Sierra Nevada, *Journal of Geophysical Research-Atmospheres*, 113 (D15), 2008.
- Rosenfeld, D., X. Yu, G.H. Liu, X.H. Xu, Y.N. Zhu, Z.G. Yue, J. Dai, Z.P. Dong, Y. Dong, and Y. Peng, Glaciation temperatures of convective clouds ingesting desert dust, air pollution and smoke from forest fires, *Geophysical Research Letters*, 38, 2011.
- Saleeby, S.M., W.R. Cotton, D. Lowenthal, R.D. Borys, and M.A. Wetzel, Influence of Cloud Condensation Nuclei on Orographic Snowfall, *Journal of Applied Meteorology and Climatology*, 48 (5), 903-922, 2009.
- Sun, J.M., M.Y. Zhang, and T.S. Liu, Spatial and temporal characteristics of dust storms in China and its surrounding regions, 1960-1999: Relations to source area and climate, *Journal of Geophysical Research-Atmospheres*, 106 (D10), 10325-10333, 2001.
- Uno, I., K. Eguchi, K. Yumimoto, Z. Liu, Y. Hara, N. Sugimoto, A. Shimizu, and T. Takemura, Large Asian dust layers continuously reached North America in April 2010, *Atmospheric Chemistry and Physics*, 11 (14), 7333-7341, 2011.
- Uno, I., K. Eguchi, K. Yumimoto, T. Takemura, A. Shimizu, M. Uematsu, Z.Y. Liu, Z.F. Wang, Y. Hara, and N. Sugimoto, Asian dust transported one full circuit around the globe, *Nature Geoscience*, 2 (8), 557-560, 2009.
- White, A.B., D.J. Gottas, E.T. Strem, F.M. Ralph, and P.J. Neiman, An automated brightband height detection algorithm for use with Doppler radar spectral moments, *Journal of Atmospheric and Oceanic Technology*, 19 (5), 687-697, 2002.
- White, A.B., P.J. Neiman, F.M. Ralph, D.E. Kingsmill, and P.O.G. Persson, Coastal orographic rainfall processes observed by radar during the California land-falling jets experiment, *Journal of Hydrometeorology*, 4 (2), 264-282, 2003.

6. Inter-annual Evidence of Aerosols Affecting Orographic Precipitation in the Sierra Nevada

6.1. Introduction

Aerosols that serve as nuclei for cloud particle formation have a profound impact on climate. In particular, aerosols that act as cloud condensation nuclei (CCN) in high number concentrations slow down cloud drop coalescence and accretion by creating large populations of small-sized cloud droplets, thus delaying the conversion of cloud water into precipitation [Borys *et al.*, 2000; Guan *et al.*, 2010]. In contrast, aerosols which serve as ice nuclei (IN) form cloud ice crystals and have been shown to enhance precipitation via secondary ice formation processes and aggregation [Bergeron, 1935; Hosler *et al.*, 1957; Morris *et al.*, 2004; Ryoo *et al.*, 2011]. Once formed, the crystals can develop rime when encountering supercooled cloud droplets ($\geq 10 \mu\text{m}$) [Yuter and Houze, 2003], particularly in more turbulent clouds [Pinsky *et al.*, 1998]. In regions with orographically-enhanced cloud formation such as the Sierra Nevada Mountains [Pandey *et al.*, 1999], IN are theorized to become incorporated into the top of high-altitude clouds to form ice crystals [Meyers *et al.*, 1992], whereas CCN are thought to seed the bottom of the orographic clouds [Rosenfeld *et al.*, 2008a]. In subfreezing conditions, a precipitating ice cloud overlaying a pristine marine liquid water cloud enables growth of precipitation particles via the seeder-feeder process [Choulaton and Perry, 1986], in which nucleated ice crystals fall through the supercooled liquid water cloud and collect droplets (i.e., riming) [Saleeby *et al.*, 2009]. However, if the lower cloud contains high concentrations of CCN, such as those from pollution aerosols [Rosenfeld, 2000], ice crystal riming efficiency is reduced, and snow growth rates and deposition location are altered [Saleeby *et al.*, 2009]. Although the effects of CCN on precipitation suppression in the Sierra Nevada are well-documented [Borys *et al.*, 2000; Colle and Zeng, 2004; Givati and Rosenfeld, 2004; Guan *et al.*, 2010; Rosenfeld and Givati, 2006], the combined effects of CCN and IN on precipitation in mixed-phase clouds are not well established [Muhlbauer *et al.*, 2010].

The Sierra Nevada is influenced by numerous sources of CCN, including regional transport of organic-containing species from biomass burning, urban, agricultural, and industrial emissions from the Central Valley (CV) [Collett *et al.*, 1990a; Guan *et al.*, 2010] in addition to *in situ* formation of CCN from transported gas phase species [Hatch *et al.*, 2011a; Lunden *et al.*, 2006b]. On the other hand, IN such as dust have been shown to be long-range transported to the Sierra Nevada from arid regions in Africa and Asia [Ault *et al.*, 2011a; Creamean *et al.*, 2012; Husar *et al.*, 2001; McKendry *et al.*, 2007; Uno *et al.*, 2011]. Furthermore, biological species (e.g., bacteria, spores, and detritus) have been shown to be more effective IN [Despres *et al.*, 2012] since they activate at temperatures as warm as -1°C [Morris *et al.*, 2004] compared to dust (~ -38 to -17°C) [Field *et al.*, 2006; Marcolli *et al.*, 2007]. Conen *et al.* [2011] have shown even biological fragments such as proteins can largely define ice nucleation properties of soil dust.

Aircraft and ground-based cloud seeding experiments in the Sierra Nevada suggest aerosols that have the ability to serve as IN are more frequently removed by forming ice crystals versus scavenging during snowfall, and increased precipitation rates by 0.1-1.0 mm/h [Deshler and Reynolds, 1990; Warburton *et al.*, 1995]. Frozen winter precipitation in the Sierra Nevada produces a deep snowpack which gradually feeds reservoirs in the spring [Dettinger *et al.*, 2011]. However, the presence of CCN may also influence the snowpack, potentially resulting in reduction of snowfall and significant implications for water resource distribution [Saleeby *et al.*, 2009]. An understanding of the interplay between CCN and IN activity of aerosols in this region could therefore have a major impact on depth of the Sierra Nevada snowpack and thus, the water resources available to California.

The *CalWater Phase I* field campaign was designed to study aerosol-cloud-precipitation interactions in California during winter storms. A unique combination of radar and satellite technology, ground-based aerosol measurements, and hydrometeorological sensors were stationed in the Sierra Nevada for 2-6 weeks of the winter seasons from 2009-2011. Results presented herein describe an inter-annual and

multisite analysis of the potential contribution of CCN and IN in the Sierra Nevada. In particular, examining aerosols as insoluble residues in precipitation samples has provided valuable insight into their potential involvement as CCN or IN [Ault *et al.*, 2011a; Creamean *et al.*, 2012; Holecek *et al.*, 2007]. By using a combination of precipitation, radar, and satellite measurements, we have generated inter-annual and spatial relationships between aerosols, cloud microphysical properties, and precipitation to better understand aerosol-cloud-precipitation interactions in the Sierra Nevada and their broader implications on the California water cycle.

6.2. Measurements

6.2.1. The CalWater Phase I Field Campaign

The *CalWater Phase I* field campaign conducted during three consecutive winter seasons (2009-2011) involved a unique combination of meteorological and aerosol measurements to better characterize factors that influence precipitation quantity and type during storms in California. Simultaneous aerosol and meteorological measurements for *CalWater Phase I* were made from Feb 22 – Mar 11, Jan 27 – Mar 15, and Jan 28 – Mar 8 in 2009, 2010, and 2011, respectively, at Sugar Pine Dam (SPD, elevation 1064 msl) in the Sierra Nevada. Precipitation samples were collected at SPD during all three winter seasons and at three additional sites in Yosemite National Park in 2011: Crane Flat (CF, 1900 msl), Badger Pass (BP, 2200 msl), and Tuolumne Meadows (TM, 2600 msl). Each sampling site is shown in Figure 6.1. Multi-year measurements at SPD and measurements at multiple, remote locations in 2011 provide an extensive dataset to determine the impact aerosols have during winter storms in California.

6.2.2. Meteorological Measurements at SPD and Offshore of California

Surface air temperature (°C) and accumulated precipitation (mm) measurements at SPD were acquired from the National Oceanic and Atmospheric Administration's Hydrometeorological Testbed Network (NOAA HMT-West) (http://hmt.noaa.gov/field_programs/hmt-west/2011/). The S-band profiling radar (S-PROF), a fixed dish antenna, was operated at 2875 MHz and directed vertically to study

the backscatter of energy from hydrometeors and cloud droplets via Rayleigh scattering and to monitor the radar brightband melting layer (an approximation of the freezing level) [White *et al.*, 2003]. The total accumulation and percentage of precipitation type including snow/graupel/hail, brightband rain (BB rain), non-brightband rain (NBB rain), mixed precipitation, and convective (Conv) precipitation was estimated using the rainfall process-partitioning algorithm developed by White *et al.* [2010; 2003], which was applied to the S-PROF profiles. Analysis was performed on all half-hour periods when the precipitation rate exceeded ~ 1 mm/h. Composites of Special Sensor Microwave Imager (SSM/I) data from polar orbiting satellites were used to determine column measurements of maximum integrated water vapor (IWV, cm) 500 km offshore of California [Ralph *et al.*, 2004; Schluessel and Emery, 1990].

6.2.3. Satellite-Retrieved Cloud Properties

Hourly averaged percentages of cloud ice (%Ice), effective cloud temperatures (T_{eff} , °C), and average cloud optical depth (τ_{cloud}) were derived using *GOES-11* satellite data and retrieval methods. These included the Visible Infrared Solar-infrared Split-Window Technique (VISST) used over snow-free surfaces, the Shortwave-infrared Infrared Near-infrared Technique (SINT) used for snow or ice covered surfaces during the daytime, and the Shortwave-infrared Infrared Split-window Technique (SIST) used for all surface conditions at night [Minnis *et al.*, 2011]. The 10-km resolution *GOES-11* data were analyzed over SPD (2009-2011), CF, BP, and TM using the methods described by Minnis *et al.* [2011; 2008]. The five channels on the *GOES-11* imager include a visible channel (0.65 μm), which was calibrated to the Aqua MODIS 0.64- μm channel following the methods of Minnis *et al.* [2002], as well as four infrared channels, including a central wavelength at 3.9 μm used to discriminate water from ice clouds. T_{eff} was determined from the top-of-atmosphere (TOA) radiance corresponding to the 10.8- μm brightness temperature of a cloudy pixel after removing the attenuation by the atmosphere above the cloud and, when the cloud emissivity is less than unity, the contribution of the surface and atmosphere below the cloud to the radiance [Minnis *et al.*,

2011]. Effective cloud drop radius (R_{eff}) was inferred based on cloud optical depth [Minnis *et al.*, 2011].

6.2.4. Chemical Characterization of Insoluble Precipitation Residues

Dates, times, and analysis statistics for each of the precipitation samples collected during the storms from 2009-2011 and at SPD, CF, BP, and TM are shown in Table 6.1. Methods for collection and chemical analysis of insoluble precipitation residues are described elsewhere [Ault *et al.*, 2011a; Holecek *et al.*, 2007]. Briefly, insoluble residues in the precipitation samples were resuspended using a Collison nebulizer, dried using two silica gel diffusion driers, and sampled by an aerosol time-of-flight mass spectrometer (ATOFMS) [Gard *et al.*, 1997b]. ATOFMS provided the size-resolved chemical composition of individual particles in dust samples and residues in precipitation samples from 0.2-3.0 μm (vacuum aerodynamic diameter, D_{va}). Single particles enter a differentially pumped vacuum chamber through a converging nozzle inlet, reaching a size-dependent terminal velocity. Particles then traverse and scatter the light of two continuous wave lasers (532 nm) at a set distance apart from which particle size is calculated based on particle speed from calibration using polystyrene latex spheres of known sizes. A third pulsed laser (266 nm) is then triggered and simultaneously desorbs and ionizes the particle, generating positive and negative ions which are introduced into a dual polarity reflectron time-of-flight mass spectrometer chamber.

Positive and negative mass spectra generated for each individual re-suspended insoluble residue were characterized into different types based on combinations of ion signals. Note that classification labels do not reflect all of the species present within a specific residue classification but reflect a distinct source common among single-particle spectra. Peak identifications correspond to the most probable ions for a given mass-to-charge (m/z) ratio based on previous lab and field studies. Initially, single-particle mass spectra were imported into YAADA [Allen, 2004], a software toolkit for Matlab (The Mathworks, Inc.), for detailed analysis of particle size and chemistry. An adaptive resonance theory-based clustering algorithm (ART-2a) [Song *et al.*, 1999b], was then used to group single-particle mass spectra into clusters. Clusters were formed based upon

similarities in the presence and intensity of ion peaks between single-particle mass spectra. The ART-2a identified clusters accounted for >90% of the total residues analyzed by the ATOFMS. ART-2a classified residues from SPD in 2011 were compared to manual chemical classifications. The average errors associated with comparing manual to ART-2a classifications were $\pm 3\text{-}4\%$ for each of the classified residue types. Due to the relatively low error when comparing the two classification methods, precipitation residues from the three Yosemite sites were classified using ART-2a. Precipitation sample sets each winter at SPD (2009, 2010, and 2011) and each site in 2011 (CF, BP, and TM) were analyzed using ART-2a separately.

6.2.5. Ice Nuclei Measurements

Ice nuclei concentrations were estimated for a select set of precipitation samples and a dry soil sample by counting the number of 50 or 80 μl aliquots ($n = 32\text{-}96$) frozen in 96-well polypropylene polymerase chain reaction (PCR) trays. Trays were cooled to -9.0°C in a thermal cycler (PTC-200, MJ Research, Waltham, MA) descending in 1°C increments, and then in 96-well aluminum incubation blocks to -20°C . Cumulative numbers of ice nuclei (IN) per ml re-suspension water were estimated using formula $\frac{-\ln(f)}{V}$ where f is the proportion of droplets not frozen and V the volume of each aliquot [Vali, 1971], and using the total water volume and volume of air sampled converted to IN per liter air. After initial testing, samples were heated to $95\text{-}105^\circ\text{C}$ to eradicate IN-active bacteria and most IN activity from other organic sources [Christner *et al.*, 2008]. Heat treating samples can indicate the relative contribution of IN activity from living biological sources. Precipitation samples were filtered and resuspended to determine the presence of high-temperature IN. Filtering the samples concentrates the insoluble material and enables developing the full IN spectrum at the higher temperatures.

6.3. Results and Discussion

6.3.1. Overall Chemical Composition of Insoluble Precipitation Residues

The precipitation residue chemical composition during the three winter sampling seasons (2009-2011) and at the Yosemite sites in 2011 was mainly composed of mineral dust, biological material, and organic carbon (OC). Other types contributed to $\leq 8\%$ of the total residues each year and at each site. The chemical compositions of the aforementioned residue types have been previously measured in precipitation samples using ATOFMS [Ault *et al.*, 2011a; Holecek *et al.*, 2007].

Overall, dust represented some of the highest percentages of all residue types (20-94% for each precipitation sample collected). Dust residues varied in mineralogy, but typically contained a combination of lithium (${}^6\text{Li}^+$), sodium (${}^{23}\text{Na}^+$), magnesium (${}^{24}\text{Mg}^+$), aluminum (${}^{27}\text{Al}^+$), potassium (${}^{39,41}\text{K}^+$), calcium (${}^{40}\text{Ca}^+$, ${}^{56}\text{CaO}^+$ / ${}^{57}\text{CaOH}^+$), titanium (${}^{48}\text{Ti}^+$, ${}^{64}\text{TiO}^+$), iron (${}^{54,56}\text{Fe}^+$), and/or aluminosilicates (${}^{70}\text{Al}_2\text{O}^+$) in the positive ion mass spectra. The negative ion mass spectra for the dust residues varied, but commonly contained ion peaks for aluminosilicates (${}^{43}\text{AlO}^-$, ${}^{59}\text{AlO}_2^-$, ${}^{60}\text{SiO}_2^-$, ${}^{76}\text{SiO}_3^-$, ${}^{77}\text{HSiO}_3^-$) and/or biological markers (${}^{26}\text{CN}^-$, ${}^{42}\text{CNO}^-$, ${}^{79}\text{PO}_3^-$). Residues containing combinations of these peaks are representative of mineral dust and have been previously observed in precipitation and cloud ice crystals using ATOFMS [Ault *et al.*, 2011a; Pratt *et al.*, 2009a]. A unique type of calcium-rich dust particularly present in samples at SPD in 2011 was classified by ion peaks at ${}^{23}\text{Na}^+$, ${}^{24}\text{Mg}^+$, ${}^{39,41}\text{K}^+$, ${}^{40}\text{Ca}^+$, ${}^{56}\text{CaO}^+$, ${}^{57}\text{CaOH}^+$, ${}^{84}\text{Ca}_2^+$, ${}^{96}\text{Ca}_2\text{O}^+$, ${}^{113}(\text{CaO})_2\text{H}^+$, ${}^{26}\text{CN}^-$, ${}^{42}\text{CNO}^-$, ${}^{64}\text{SO}_2^-$, and ${}^{80}\text{SO}_3^-$. Chemical signatures of the calcium-rich dust are similar to the calcite samples and Asian dust shown by Sullivan *et al.* [2007; 2009b]. Figure 6.2 shows representative positive and negative ion mass spectra of dust containing the different ion peak combinations in (a) and (b), and calcium-rich dust (c). Not all ion peaks discussed are labeled in Figure 6.2. Overall, the chemical heterogeneity observed in dust particles is a result of the large number of mineral species that are present in soil and sand, and thus one particle can be enriched with an element that is not observed in another particle [Silva *et al.*, 2000].

Ion mass spectra of the two main types of biological residues detected in the precipitation samples are shown in Figure 6.2. Positive ion mass spectra from biological residues containing peak combinations similar to these were previously observed in

precipitation residues [Ault et al., 2011a; Holecek et al., 2007] and cloud ice crystals [Pratt et al., 2009a]. The first biological type contained markers at $^{39,41}\text{K}^+$, $^{26}\text{CN}^-$, $^{42}\text{CNO}^-$, $^{63}\text{PO}_2^-$, $^{79}\text{PO}_3^-$, and $^{97}\text{H}_2\text{PO}_4^-$ shown in (d). The second type shown in (e) contained ion peaks of weaker intensity at $^{12}\text{C}^+$, $^{23}\text{Na}^+$, $^{27}\text{Al}^+/\text{C}_2\text{H}_3^+/\text{NCH}^+$, $^{29}\text{C}_2\text{H}_4^+/\text{N}_2\text{H}^+$, $^{37}\text{C}_3\text{H}^+$, $^{38}\text{C}_3\text{H}_2^+$, $^{39}\text{C}_3\text{H}_3^+/\text{K}^+$, $^{40}\text{C}_3\text{H}_4^+/\text{Ca}^+$, $^{41}\text{C}_3\text{H}_5^+/\text{K}^+$, $^{43}\text{AlO}^+$, $^{55}\text{C}_2\text{HNO}^+$, $^{56}\text{Fe}^+/\text{CaO}^+$, and $^{57}\text{CaOH}^+$ in the positive ion mass spectra. The negative ion markers were similar to those of the first biological type mentioned with additional contribution from chloride ($^{35,37}\text{Cl}^-$) and organic fragments ($^{45}\text{CHOO}^-$, $^{59}\text{CH}_3\text{COO}^-$, $^{71}\text{C}_3\text{H}_3\text{OO}^-$, and $^{73}\text{CH}_3\text{CH}_2\text{CHOO}^-$) [Sullivan and Prather, 2007]. While chloride and $^{71}\text{C}_3\text{H}_3\text{OO}^-$ have been observed in biological mass spectra from previous studies [e.g., Fergenson et al., 2004; Silva, 2000], chloride and all of the organic fragments on this biological particle type have been observed in biomass burning aerosols [Silva et al., 1999], suggesting this biological particle type could be from vegetation burning. Biological aerosols are typically composed of insoluble organics previously shown by empirical and modeling studies [Phillips et al., 2009; Phillips et al., 2008], however, can contain soluble materials (e.g. organic acids, mycotoxins, antigens, endotoxins) which could be lost/redistributed during the re-suspension process [Burge and Solomon, 1987; Kumar et al., 2003]. The possible sources of biological residues are discussed herein.

OC consisted of three main types as shown in Figure 6.2: OC-aromatic (OC with peaks indicative of aromatic fragment ions) at $^{51}\text{C}_4\text{H}_3^+$, $^{63}\text{C}_5\text{H}_3^+$, $^{77}\text{C}_6\text{H}_5^+$, and $^{91}\text{C}_7\text{H}_7^+$ (f), OC enriched with Na and K (weaker ion intensities at $^{23}\text{Na}^+$ and $^{39}\text{K}^+$, $^{27}\text{C}_2\text{H}_3^+/\text{NCH}^+$ and $^{43}\text{C}_2\text{H}_3\text{O}^+/\text{CHNO}^+$ (g), and polycyclic aromatic hydrocarbons (PAHs, high mass OC peaks between m/z 180-250 (h)). These water soluble species most likely originated from CCN-active biomass burning aerosols that were dissolved/transformed and resuspended during the atomization process, therefore, it is likely the OC residues served as CCN as previously suggested [Ault et al., 2011a; Holecek et al., 2007; Petters et al., 2009; Qin and Prather, 2006b]. Negative ion mass spectra for the OC types typically contained $^{26}\text{CN}^-$, $^{42}\text{CNO}^-$, and organic fragment ion markers. The negative ion mass spectra also contained soluble species including nitrate ($^{46}\text{NO}_2^-$ and $^{62}\text{NO}_3^-$) and sulfate ($^{80}\text{SO}_3^-$ and $^{97}\text{HSO}_4^-$). Nitrate and sulfate may be incorporated into the insoluble residues through

encasement in an insoluble organic shell, which has been observed in biomass burning aerosols [Posfai *et al.*, 2004], and/or dissolution in the precipitation solution followed by coating of the insoluble residues upon re-suspension [Holecek *et al.*, 2007].

6.3.2. Inter-annual Precipitation Trends during *CalWater Phase I*

6.3.2.1. Links between Residue Composition and Precipitation Properties

The chemical composition of the residues varied greatly between the three winter seasons. In addition to surface temperature, these residues likely induced changes in precipitation type including snow, BB rain, mixed precipitation, NBB rain, convective rain (Conv), and precipitation where the type was not determined (Insuf). The S-PROF radar can distinguish between different precipitation types by detecting a “brightband” or melting layer, where the phase of falling precipitation changes from solid to liquid. The enhanced reflectivity is caused by aggregation of wetted snow crystals near this layer, or by relatively large single ice crystals developing a wet surface during melting [White *et al.*, 2002]. Mixed precipitation (i.e., a mixture of snow, rain, and/or graupel) corresponded to time periods where the melting layer was either non-existent or too low to be detected by the S-PROF radar [White *et al.*, 2010], whereas NBB rain is precipitation that did not pass through a melting layer, therefore the precipitation originated as liquid droplets [White *et al.*, 2003]. For convective rain, the brightband melting layer structure was often not visible because of enhanced turbulence or the presence of graupel or hail, even though convective rain clouds may have extended well above the melting layer [White *et al.*, 2003].

Figure 6.3-6.5 show: (a) the total accumulated precipitation per storm in addition to the maximum offshore vertically integrated water vapor (IWV, cm—the amount of atmospheric water vapor within a column measurement from the surface to space), (b) the percentage of each type of precipitation and average surface air temperature, and (c) the percentage of each type of precipitation residue averaged during each storm from 2009, 2010, and 2011. Percentages of dust and biological residue are stacked to simulate the

total percentage of aerosols that potentially served as IN and their combined percentages are herein denoted as “%Dust+Bio.”

The results from 2009 were presented in detail by Ault *et al.* [2011a], therefore will only be briefly discussed. At the beginning of the study during storms 1 and 2, the residues were mainly composed of OC from biomass burning (Figure 6.3c). However, during storm 3, the residue composition shifted to predominantly dust. Concurrently, we observed a change in precipitation type from mainly NBB rain to BB rain, and snow as surface temperatures decreased (b). In addition, storm 3 produced more total precipitation compared to the first two storms (a).

As seen in Figure 6.4, the trends in 2010 are not as obvious as in 2009; however, the results suggests the involvement of aerosols as CCN and IN in the precipitation. In 2010, high percentages of OC (%OC) were present throughout the entire study (34-66% per storm), particularly during storms 2-4 (average $60\pm 6\%$) where the %Dust+Bio was lowest (average $38\pm 7\%$). Further, the highest percentages of NBB rain occurred during these time periods (average $44\pm 18\%$), i.e., precipitation was not initiated in the ice phase, and the total amounts of precipitation were lower. These results suggest the OC served as CCN hence suppressing precipitation [Rosenfeld and Givati, 2006]. Unlike in 2009, the storms with the most snow that had the highest %Dust+Bio did not correspond to the most precipitation (storms 6 and 7). This could be because almost half of the residues were OC (45% and 46%, respectively), which potentially led to inefficient riming of any existing cloud ice crystals by serving as CCN, therefore suppressing precipitation [Rosenfeld and Givati, 2006; Saleeby *et al.*, 2009; Weaver *et al.*, 2002]. In contrast, the highest %Dust+Bio (particularly the biological residues) and lowest %OC occurred during storm 1 (66% and 34%, respectively), concurrent with the highest combined percentages of snow, BB rain, and mixed precipitation (95%) and the lowest percentage of NBB rain (0%). A likely explanation for the relationship between snow/BB rain/mixed precipitation and %Dust+Bio is that more precipitation is initiated as ice during time periods with more dust and biological residues because IN were present, as shown in previous work during *CalWater* sampling [Ault *et al.*, 2011a; Creamean *et al.*, 2012].

In 2011, dust and biological residues were dominant during each of the storms; the %Dust+Bio ranged from 66% to 94% (average $79\pm 14\%$) as seen in Figure 6.5c. Storms 1-3 exhibited the largest percentages of dust (average $64\pm 16\%$) compared to any other sample in 2011. Interestingly, copious amounts of snow, BB rain, and mixed precipitation combined (average $87\pm 8\%$) fell at the surface during these three storms, predominantly in the form of snow. During storm 4, the residue composition shifted to predominantly biological (83%) which also coincided with a high percentage of snow (96%). Also evident are the low %OC (average $8\pm 8\%$) and large total quantities of precipitation during storms 2-4, further supporting evidence that OC served as CCN but since they were in low abundance compared to dust and biological material, more extensive riming thrived in-cloud, leading to more precipitation initiated as ice and more total precipitation. Storms 5 and 6 contained high %Dust+Bio (66% and 81%, respectively), but the bulk of the precipitation fell as BB rain (26% and 78%, respectively) due to the higher surface air temperatures ($\sim 4^\circ\text{C}$). Trends with precipitation type and %Dust+Bio for 2011 are discussed in more detail in Creamean *et al.* [2012].

The total amount of precipitation per storm shown in Figure 6.3-6.5 (a) typically increased and decreased with the amount of atmospheric water vapor available offshore (IWV), which would be expected. However, %Dust+Bio also followed trends with total precipitation, suggesting the combined need for the presence of both IN and water vapor. Within each winter, several cases existed where IWV was fairly constant between two storms but one of the storms produced more total precipitation such as storm 3 in 2009 [Ault *et al.*, 2011a]. In 2010, storms 4 and 5 had the same IWV (3.33 cm), but more precipitation and higher %Dust+Bio during storm 5 (60 mm and 50% compared to storm 4 with 56 mm and 30%). Further, storms from all three winters with less precipitation typically corresponded to lower %Dust+Bio and higher %OC. Two possible explanations for this observation are: 1) the absence of dust and biological IN reduced ice crystal formation, and 2) OC aerosols served as CCN, decreasing size and increasing number concentrations of cloud droplets, and inhibiting riming on the ice crystals that were formed [Saleeby *et al.*, 2009].

For all cases, temperature controlled the precipitation type at the surface, regardless of whether dust and biological IN influenced ice formation. The highest snowfall totals were observed during the lowest surface air temperatures as shown in Figure 6.3-6.5 and coincided with high %Dust+Bio. During periods with higher surface air temperatures and high %Dust+Bio, BB rain was observed, rather than frozen precipitation. Temperature was variable during time periods with mixed precipitation, however, was typically near freezing (roughly 0-4°C), suggesting this precipitation was initially formed in the ice phase. During time periods with NBB rain and high %OC, surface air temperature was high, however, these time periods also corresponded to low %Dust+Bio. These results suggest the absence of dust and biological IN and presence of OC as CCN initiated the formation of liquid cloud droplets which grew and fell as rain. Comparing temperatures in-cloud where the ice crystals or liquid droplets were initially formed can confirm these results, which are discussed below.

6.3.2.2. Links between Residue Composition and Cloud Properties

We provide convincing evidence that dust and biological aerosols served as IN while OC aerosols served as CCN, influencing precipitation quantity and type depending on surface temperature. However, examining physical characteristics of clouds above SPD elucidates the link between insoluble residues in precipitation samples and which aerosols served as CCN or IN in clouds. Figure 6.6-6.8 (a) show the precipitation rate (mm/h) and percentages of residues per sample (S1, S2, etc.), while (b) shows hourly liquid water path (LWP, g/m²), ice water path (IWP, g/m²), and the height/depth of the clouds (km) over SPD for the 2009-2011 winter seasons, respectively, estimated from *GOES-11* satellite retrievals. The top and bottom of the shaded region is the cloud top and bottom, respectively, and the color of the shading represents the hourly effective cloud temperature (T_{eff}). In general, %OC corresponded to time periods with larger LWP and shallower, warmer clouds (e.g., S4-S7 in Figure 6.7, storm 3 in 2010), whereas samples with higher %Dust+Bio corresponded to time periods with larger IWP and deeper, colder clouds (e.g., S4-S6 in Figure 6.8, storm 3 in 2011). The cloud temperature was typically within the range for dust and biological aerosols to form ice

heterogeneously (roughly between -38 and -1°C), therefore, we observed these residues in all of the samples, along with the ubiquity of cloud ice and precipitation initiated in the ice phase (snow, BB rain, and/or mixed precipitation) during all of the sample collection time periods for each winter season. Even in the warmer clouds, dust and biological aerosols and ice were still present; however temperatures may have been too warm for sufficient IN-activation. For the case of storm 3 in 2010, warm shallow clouds likely enabled OC aerosols to activate as CCN (and prevented dust and biological aerosols to all activate as IN), leading to mostly NBB rain and mixed precipitation (32% and 38%, respectively) as shown in Figure 6.4. For the case of storm 3 in 2011, the cold, high-altitude clouds enabled dust and biological aerosols to serve as IN and initiate ice precipitation, which remained as snow at the surface as shown in Figure 6.5. Overall, these results suggest that when clouds were higher and deeper, temperatures were colder and enabled the dust and biological aerosols to efficiently nucleate ice, likely at the top of these clouds [Meyers *et al.*, 1992], and led to more precipitation initiated in the ice phase. When clouds were shallower and warmer, OC aerosols activated as CCN as previously shown and led to inefficient riming of the IN present, hence less precipitation, although what did fall at the surface was either mostly NBB or BB rain [Rosenfeld *et al.*, 2008a].

Although the trends discussed above occurred frequently each winter season, there were some discrepancies, such as storm 3 from 2009 (Figure 6.6). At the beginning of the storm, the samples contained high %OC, but deeper and colder clouds containing large IWP (i.e., S4-S6). Although the clouds reached high altitudes (up to 13 km), the bottoms of the clouds were quite low (down to 3 km), therefore it is possible the OC aerosols could have still become incorporated into the lower layers of the clouds. The clouds during this time period could also be mature or dissipating clouds seeded by CCN as discussed by Rosenfeld *et al.* [2008a]. Mature or dissipating clouds can reach high altitudes and cold temperatures, where ice production can also be influenced by strong vertical updrafts [Churchill and Houze, 1984; Pinsky *et al.*, 1998] and instability within the deep cloud system [Rosenfeld *et al.*, 2008a], as observed during the beginning of storm 3 in 2009 (cloud temperatures reached below -40°C for the majority of the sample time periods). Towards the end of storm 3 in 2009 (S7-S10), the %Dust+Bio increases

rapidly even though the clouds were shallow (2-6 km) but still fairly cold (down to -40°C). Ault *et al.* [2011a] showed that dust was indeed transported to the tops of these lower altitude clouds. Although storm 3 in 2009 is a unique case, conditions were still suitable for ice to form in the clouds towards the end of the storm and lead to snow at the surface.

6.3.3. Elevation Dependent Trends: Further Insight into Relationships between Residue Composition and Cloud Properties

In 2011, additional precipitation samples collected at three sites in Yosemite National Park showed striking trends in precipitation residue chemistry and cloud properties with increasing elevation. Figure 6.9 shows the total precipitation residue composition for each site, including SPD, CF, BP, and TM. Precipitation samples from Yosemite are available only for storms in February and early March 2011, so the analysis here will be restricted to those particular storms (see Table 6.1). Also shown in Figure 6.9 are the T_{eff} and percentage of cloud ice (%Ice) and liquid (%Liq) averaged from *GOES-11* satellite retrievals during all sample collection time periods for each site. The inset shows the correlation between the %Ice and %Dust+Bio, and the %Liq and %OC. Overall, the average %Ice increased with elevation (from 56% at SPD to 75% at TM) and correlates with the average %Dust+Bio ($r^2 = 0.69$). A decrease in the average T_{eff} with elevation would be expected based on the relative amount of ice in the clouds, however, this is not the case: average T_{eff} increased from SPD to CF (-28 ± 3 to $-23 \pm 4^\circ\text{C}$), then proceeded to decrease at BP ($-24 \pm 4^\circ\text{C}$) and TM ($-29 \pm 3^\circ\text{C}$). Further, we would expect higher average T_{eff} at SPD than any of the other sites, however, the average T_{eff} was actually higher at CF and BP even though they had higher average %Ice. The average T_{eff} at SPD was roughly equivalent to TM, even though clouds above TM had 1.5 times more ice on average. Interestingly, precipitation samples at TM had 1.3 times more dust and biological residues combined compared to SPD. These results suggest that low temperature, alone, is not a sufficient metric to determine the presence of ice and that IN, specifically dust and biological IN, are necessary for ice formation, i.e., the largest %Ice did not require the lowest T_{eff} for a high percentage of dust and biological residues to be

observed in precipitation. *In situ* aircraft measurements of cloud residues and ice presented in Creamean *et al.* [2012] confirm the relationship between dust and biological residues and ice at SPD in 2011.

In contrast, the %Liq decreased with elevation (from 44% at SPD to 25% at TM) and strongly correlates with %OC ($r^2 = 0.92$, decreased from 16% at SPD to 4% at TM), even though the T_{eff} did not consistently decrease. This result suggests that the presence of OC influenced the portion of the clouds that were liquid droplets, hence serving as CCN. In the graph inset, the correlation between the %Liq and %OC are colored by average effective cloud drop radius (R_{eff} , μm), with white being the smallest and black being the largest R_{eff} . A strong correlation between %OC and R_{eff} was observed ($r^2 = 0.85$). Large number concentrations of CCN increase cloud lifetime and suppress precipitation by reducing cloud droplet size [Rosenfeld, 2000], thus the smaller R_{eff} is likely a result of the additional CCN at lower elevation sites. These results provide further evidence that the OC residues served as CCN and influenced cloud microphysical properties.

6.3.4. Ice Forming Potential of Dust and Biological Precipitation Residues

The *GOES-11* cloud properties in combination with S-PROF radar and ATOFMS measurements provided valuable insight into the sources of aerosols that serve as CCN and IN, and their resulting effects on cloud microphysics and precipitation formation. These results were additionally supported by determining the freezing temperatures of re-suspended residues in precipitation samples. Because dust and biological residues were omnipresent in all of the samples from all winter seasons and sites, the focus was placed on IN measurements.

Figure 6.10 shows results from the IN measurements of selected samples. The goal was to acquire IN measurements of samples that contained the highest percentages of residues that could serve as IN, including S4 from 2011 with a high percentage of dust (94%, denoted as the “dust precip sample”) and S7 from 2011 with a high percentage of biological residues (83%, denoted as the “bio 1 precip sample”). To discriminate between

dust and the different biological IN, the sample with the highest biological to dust residue ratio (5:1) was also analyzed (S4 from 2010, denoted as “bio 2 precip sample”). The dust precip sample was predominantly the Ca-dust type residue (Figure 6.2c), the bio 1 precip sample was particularly high in the residue type shown in Figure 6.2d, and the bio 2 precip sample contained the most residues shown in Figure 6.2e. For comparison, a dry soil sample from Dunhuang, Gansu in Western China was analyzed as well and shown in Figure 6.10. Arizona test dust, the standard dust used for experimentation, has been shown to activate as high as -17°C [Marcolli *et al.*, 2007]. The Dunhuang dry dust sample activated as high as -5.6°C , however activation decreased after heat treatment, suggesting the sample contained biological material [Conen *et al.*, 2011]. In contrast, the precipitation sample with the high percentage of dust did not show a large change after heat treatment and did not activate as readily as the dry soil sample. Therefore, the dust in S4 did not contain biological material, suggesting solely dust was responsible for nucleating ice in cloud during the sample collection time period. This also suggests aerosols containing dust and biological signatures activate more efficiently than dust alone as previously shown [Conen *et al.*, 2011].

As seen in Figure 6.10, the bio 2 precip sample activated at very high temperatures (up to -5°C), which is expected based on past measurements [e.g., Schnell, 1974]. However, the bio 2 precip sample did not show as high of IN concentrations at the same temperature as the dry soil sample. One possible explanation is that the combination of dust and biological material within one sample could be more efficient at nucleating ice compared to samples containing predominantly dust or biological residues. The highest temperature at which the bio 1 sample activated at was -8.7°C . Further, there was not a significant decrease in activation after heat treatment: residues in the bio 1 sample activated from -18.3 to -8.7°C before and from -20.5 to -12.6°C after heat treatment. Although this suggests there was not a large amount of biological material in the original sample that could efficiently serve as IN, nuclei can potentially remain after heat treatment if they required colder temperatures to activate, depending on the biological material present [Maki *et al.*, 1974]. We speculate the biological material present in the bio 1 precip sample could be spores or fragments of spores which are known to activate

between -28.5 and -10°C —temperatures lower than most biological material require [Despres *et al.*, 2012, and references therein]. The main ion peaks in the biological sample, in addition to weak, unidentified peaks at m/z +70, +84, +86, -59, -66, -71, -159 (not labeled in Figure 6.2d), have all previously been observed in spore samples [Czerwieniec *et al.*, 2005; Fergenson *et al.*, 2004; Steele *et al.*, 2005]. Spores are known to contain potassium and DNA, which is possibly the source of phosphate [Elbert *et al.*, 2007]. One explanation for the IN activity remaining roughly the same after heat treatment is because the dominant species in these residues are inorganic, i.e., potassium and phosphate.

Overall, the precipitation samples containing dust and biological residues contained IN-active material and activated at temperatures within the range of the cloud temperatures observed during each of the samples (Figure 6.6-6.8) and at times even warmer temperatures (i.e., the bio 2 precip sample). These results provide insight into the remaining precipitation samples and how the residues affected cloud microphysical properties during collection time periods; more ice could form in clouds with mixed dust and biological aerosols compared to dust or biological aerosols alone.

6.3.5. Insight into Precipitation Residue Sources

Based on the results presented herein, we are able to provide insight into the sources of aerosols that serve as seeds for cloud formation and affect precipitation in the Sierra Nevada. These results support those of Ault *et al.* [2011a], who suggested the source of the dust during the 2009 winter season was from high-altitude, long-range transport versus from a local or regional source, i.e., the CV. Further, Creamean *et al.* [2012] demonstrated that dust and biological aerosols during the 2011 measurements were long-range transported and incorporated into the tops of high-altitude clouds. Ault *et al.* [2011a] also illustrated the ubiquitous presence of OC from biomass burning in precipitation at SPD and highlighted the potential importance of these aerosols in cloud formation and precipitation processes, i.e., serving as CCN [Holecek *et al.*, 2007]. Aerosols from regional biomass burning in the CV can be orographically lifted alongside the Sierra Nevada via the upslope airflows and incorporated into regions of cloud

formation [Carroll and Dixon, 2002; Parish, 1982]. The biological residues could be from regional sources or long-range transported. Biological species are commonly lofted and transported with dust [Hallar et al., 2011; Hua et al., 2007], which could explain why dust and biological residues are observed within the sample samples. Further, aerial transport of biological material from agricultural crops has been documented to occur up to 500 km [Aylor, 1986] and found in fairly high concentrations in cloudwater and snow samples [Bauer et al., 2002]. In the CV, biological aerosols containing organic nitrogen have been shown to originate from biomass burning [Zhang and Anastasio, 2001], which could explain the presence of the organic fragments in the negative spectra of the biological residue type shown in Figure 6.2e. Therefore, we speculate that dust and the bio 1 residues (Figure 6.2d) were long-range transported, whereas the OC and bio 2 residues (Figure 6.2e) were from regional biomass burning.

6.4. Conclusions

The sources of CCN and IN in the Sierra Nevada and their resulting impacts on orographic precipitation were investigated during the 2009-2011 winter seasons of *CalWater Phase I*. Insoluble residues in precipitation samples were chemically determined and linked with trends in precipitation and cloud microphysical properties. An inter-annual and multisite aerosol and meteorological comparison enabled the development of the main conclusions listed below:

- Dust and biological residues likely served as IN, leading to more ice in-cloud in deeper, colder clouds systems, subsequently influencing the relative amount of snow at lower surface temperatures and BB rain at higher surface temperatures. Larger quantities of precipitation were dependent not only on the amount of atmospheric water vapor, but also on the relative abundance of dust and biological aerosols.
- We also deduce that the OC residues may have served as CCN in shallower, warmer clouds, which decreased the riming efficiency of the ice crystals formed from dust and biological aerosols, subsequently leading to time periods with lower precipitation totals.

- Our results support previous work during *CalWater* measurements which determined dust and biological aerosols were long-range transported and incorporated into high-altitude clouds. We speculate that OC and biological aerosols containing organic fragments likely originated from regional sources such local biomass burning and agricultural sources in the CV.
- Dust and biological residues in select precipitation samples were IN-active, supporting our results deduced from radar and satellite measurements.

In general, our results suggest dust and biological aerosols efficiently serve as IN and contribute to precipitation enhancement, whereas OC aerosols serve as CCN and delay the growth of cloud ice crystals, leading to precipitation suppression. A future publication will discuss the sources of the residues in detail for all three winter seasons, particularly those which are thought to be long-range transported. Nevertheless, results presented herein provide a noteworthy advancement in understanding the effects of aerosols on the type and amount of precipitation in the Sierra Nevada. Long-term and multisite observations presented herein could help improve modeling aerosol-cloud-precipitation effects on orographic precipitation and will enable the modeling community to better assess how weather patterns and/or regional climate may change due to the effects from aerosols, particularly for long-range transport which has been shown to be very important. Improving our ability to model the interaction between aerosols, clouds, and precipitation will lead to better winter storm preparedness, water resource management, and flood mitigation.

6.5. Acknowledgements

Funding was provided by the California Energy Commission under contract UCOP/CIEE C-09-07 and CEC 500-09-043. J. Mayer, M. Zauscher, E. Fitzgerald, C. Gaston, and M. Moore from UCSD provided assistance with equipment preparation and set-up at SPD. The deployment of the NOAA and UCSD/SIO equipment at SPD involved many field staff, particularly C. King (NOAA/ESRL). The Forest Hill Power Utility District is acknowledged for hosting the sampling site at SPD. Also, Rebecca Rising,

Chuck Carter, Dick Ewart, Virgia Bryan, George O'Hare, and Jim Roche are acknowledged for precipitation sample collection at the Yosemite National Park sites.

6.6. Figures



Figure 6.1 Google Earth image of CalWater Phase I sites where meteorological measurements and/or precipitation samples were acquired, including Sugar Pine Dam (39.129°N, 120.801°W), Crane Flat (38.106°N, 119.844°W), Badger Pass (37.666°N, 119.654°W), and Tuolumne Meadows (37.870°N, 119.361°W).

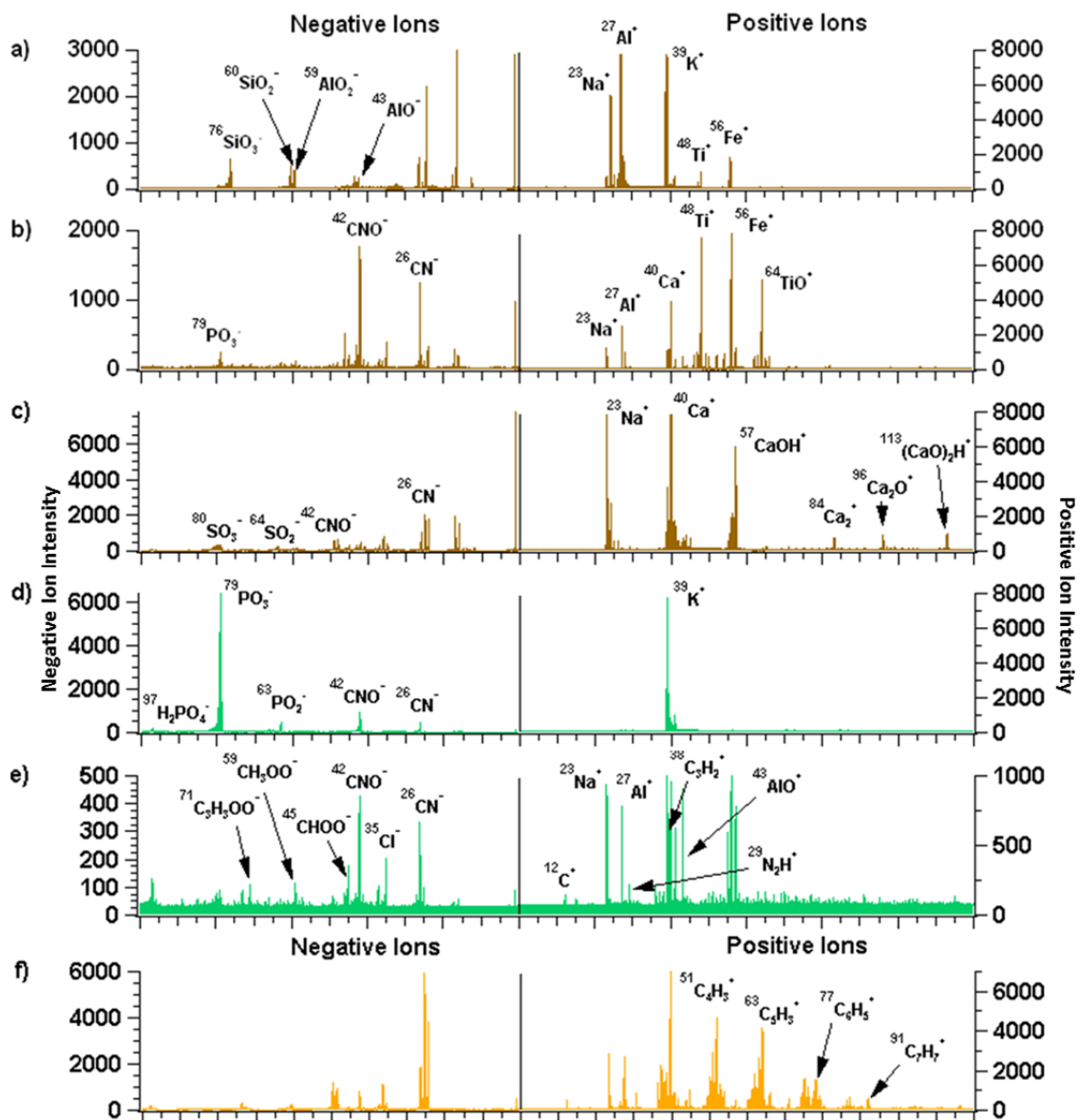


Figure 6.2 Representative mass spectra for ATOFMS precipitation residues. Examples include dust (panels a-c), biological (panels d and e), and OC residues (panels f-h). Positive and negative ion intensities vary by type.

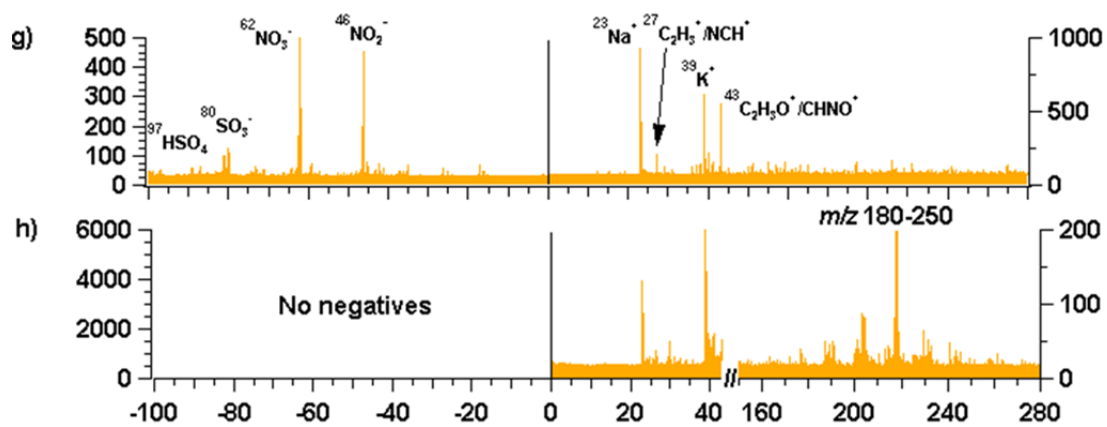


Figure 6.2 continued.

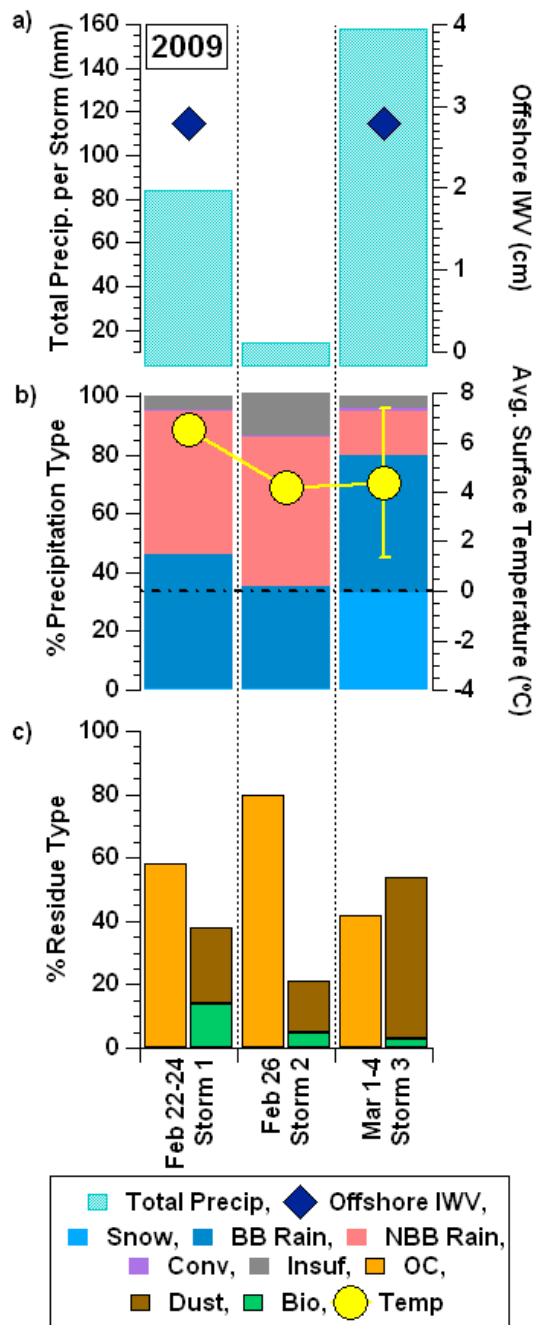


Figure 6.3 Panel (a) shows the total accumulated precipitation per storm (mm) and the maximum offshore IWV (cm) during each storm in 2009. Panel (b) shows the percentage of snow, BB rain, NBB rain, Conv, and Insuf estimated by S-PROF and the average surface air temperature (T_{surf} , °C) during each storm. The dashed line represents freezing temperature. Panel (c) shows the relative percentage of ATOFMS residues averaged during each storm.

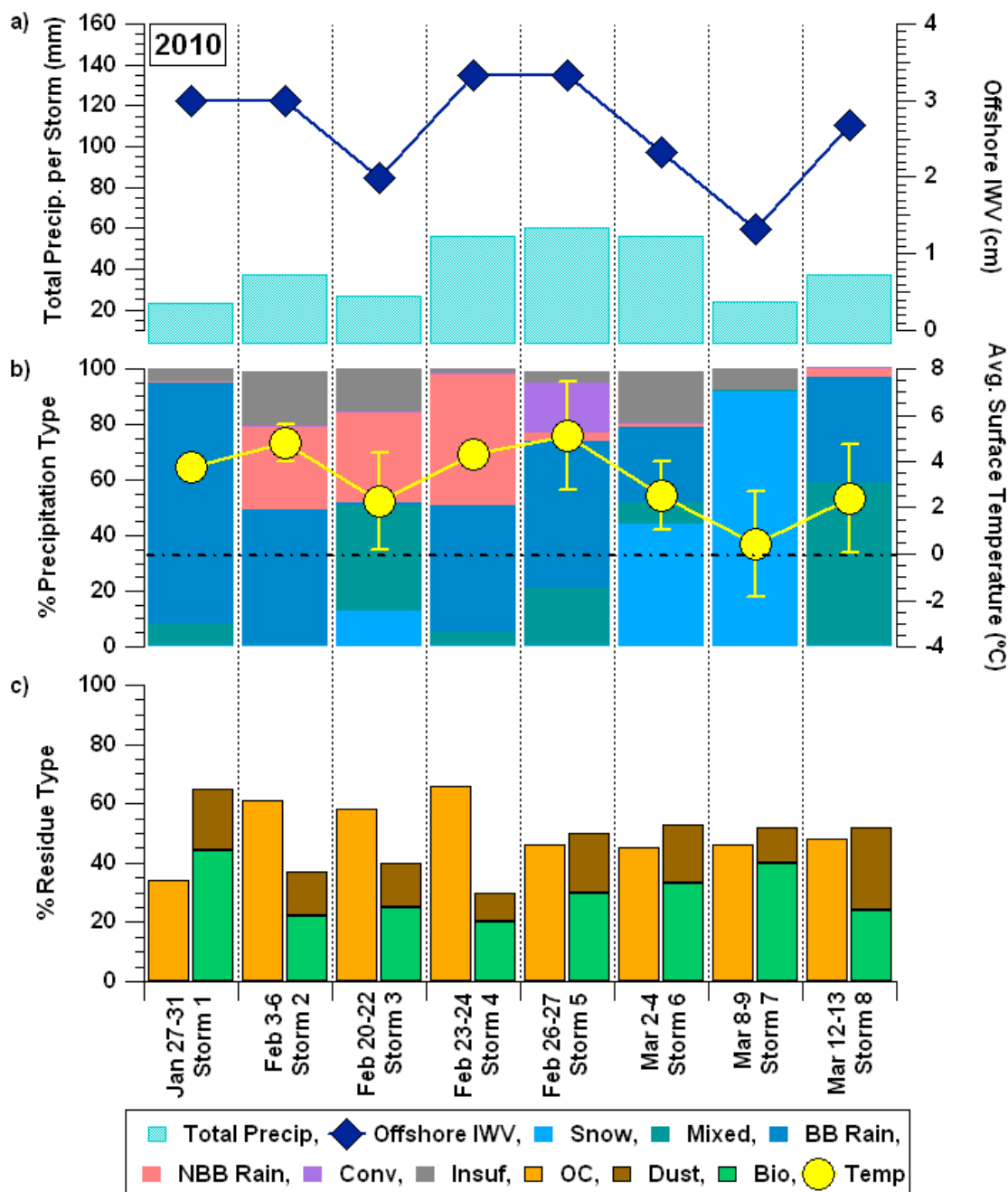


Figure 6.4 Panel (a) shows the total accumulated precipitation per storm (mm) and the maximum offshore IWV (cm) during each storm in 2010. Panel (b) shows the percentage of snow, BB rain, mixed precipitation, NBB rain, Conv, and Insuf estimated by S-PROF and the average surface air temperature (T_{surf} , $^{\circ}\text{C}$) during each storm. The dashed line represents freezing temperature. Panel (c) shows the relative percentage of ATOFMS residues averaged during each storm.

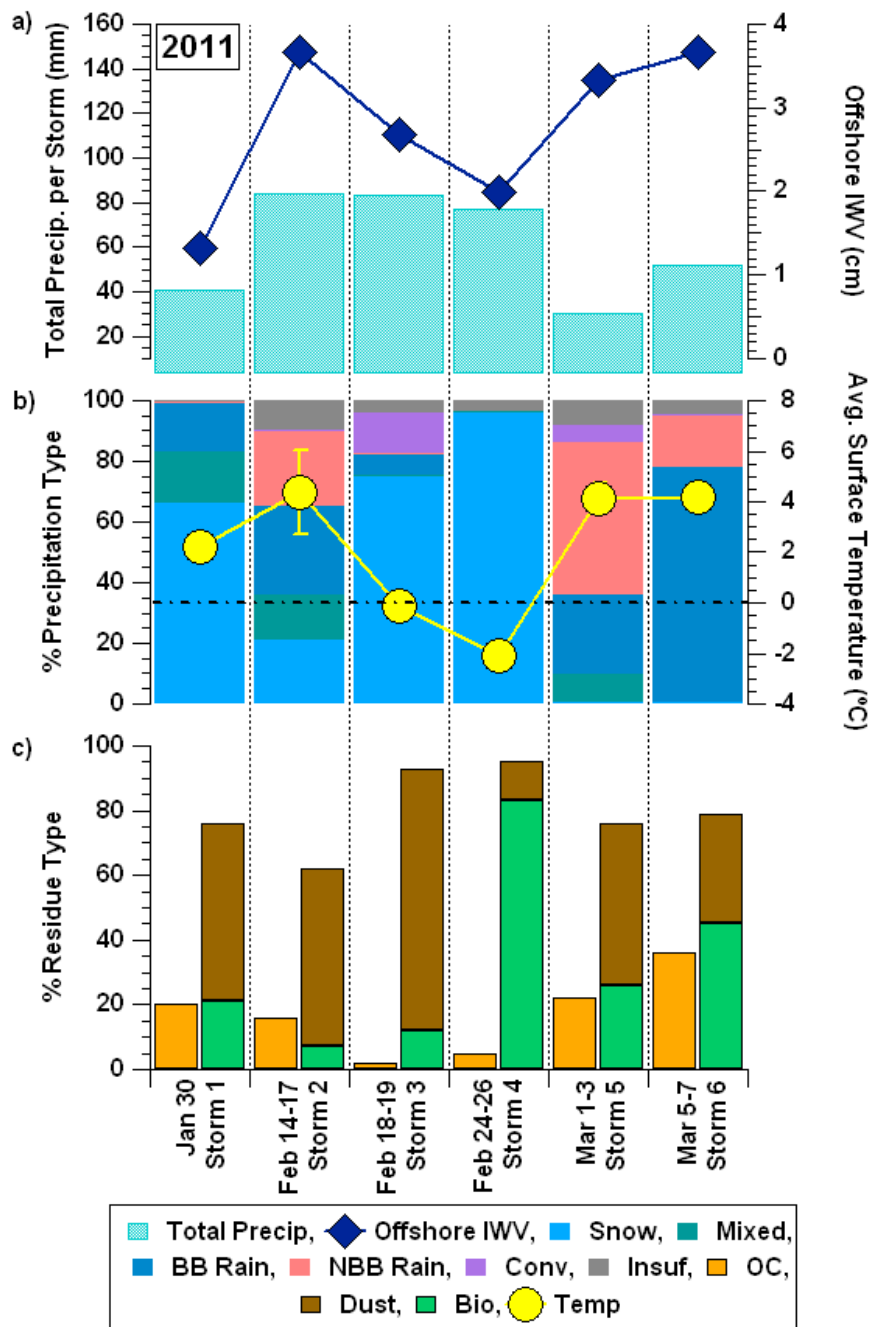


Figure 6.5 Panel (a) shows the total accumulated precipitation per storm (mm) and the maximum offshore IWV (cm) during each storm in 2011. Panel (b) shows the percentage of snow, BB rain, mixed precipitation, NBB rain, Conv, and Insuf estimated by S-PROF and the average surface air temperature (T_{surf} , $^{\circ}\text{C}$) during each storm. The dashed line represents freezing temperature. Panel (c) shows the relative percentage of ATOFMS residues averaged during each storm.

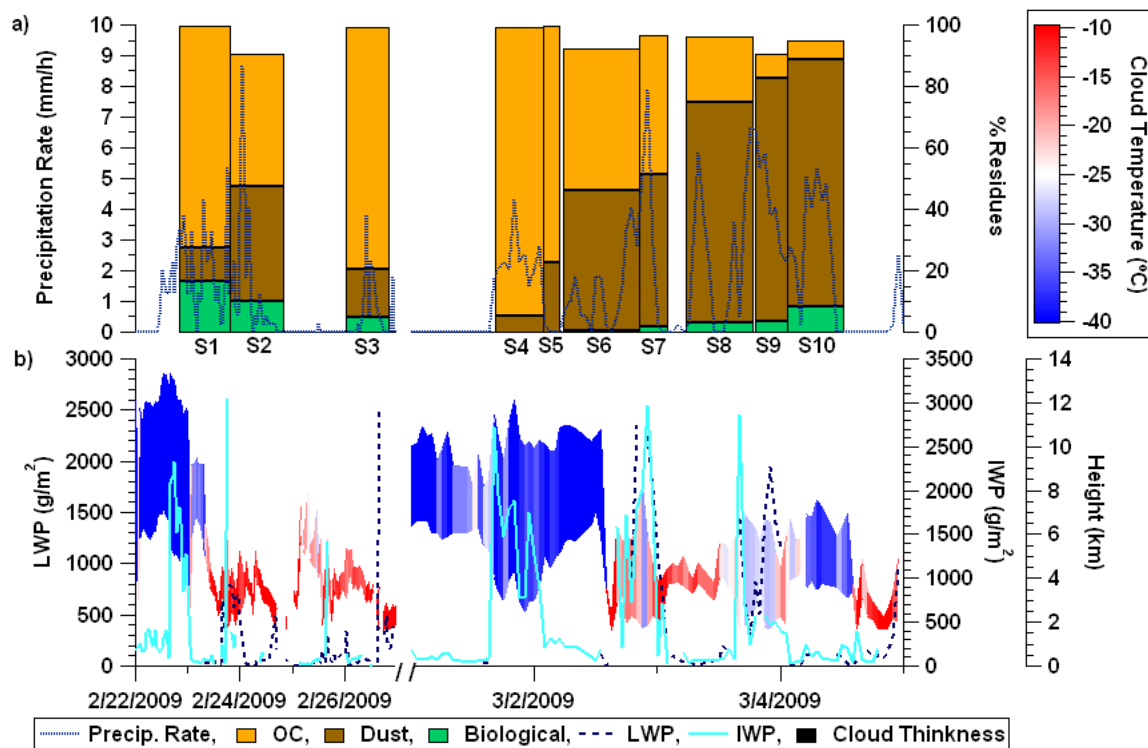


Figure 6.6 Panel (a) shows precipitation rate (mm/h) at the surface at SPD and the percentage of dust, biological, and OC residues in each sample in 2009. The width of the bars reflect the duration of the sample collection. Panel (b) shows hourly liquid water path (LWP), ice water path (IWP), and the location of the cloud for each year over SPD. The shaded region represents the hourly effective cloud temperature (T_{eff} , °C) within a 10-km pixel over SPD.

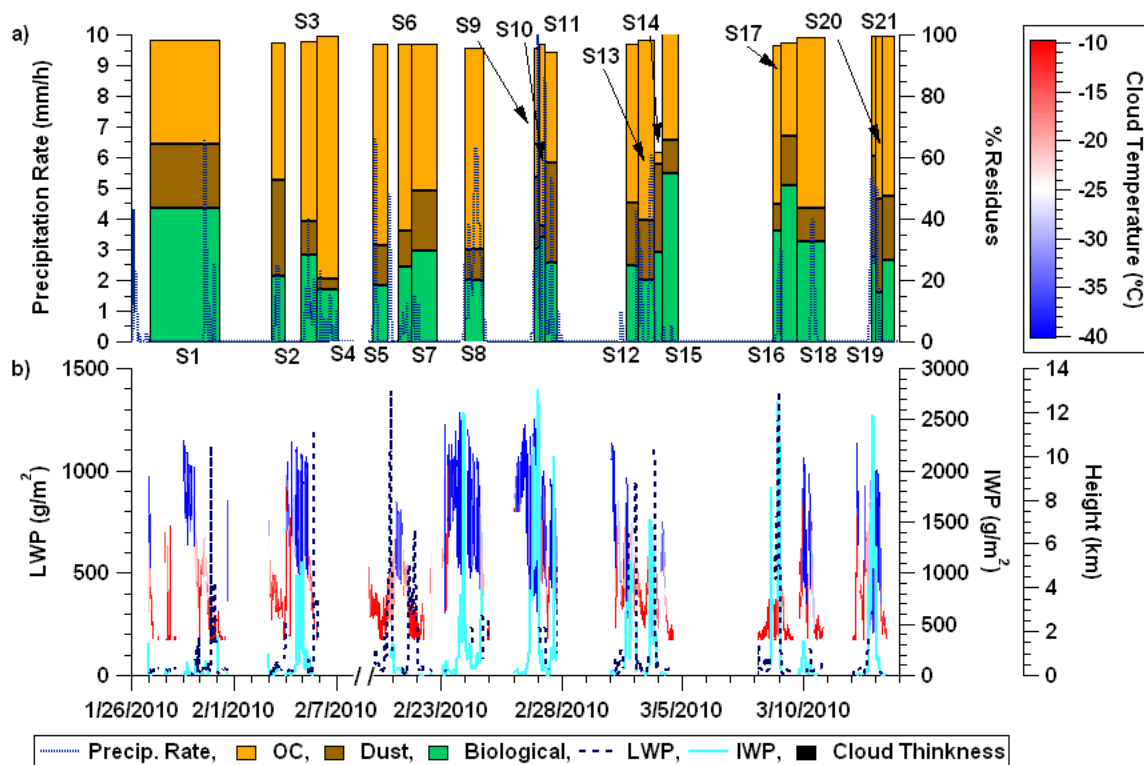


Figure 6.7 Panel (a) shows precipitation rate (mm/h) at the surface at SPD and the percentage of dust, biological, and OC residues in each sample in 2010. The width of the bars reflect the duration of the sample collection. Panel (b) shows hourly liquid water path (LWP), ice water path (IWP), and the location of the cloud for each year over SPD. The shaded region represents the hourly effective cloud temperature (T_{eff} , °C) within a 10-km pixel over SPD.

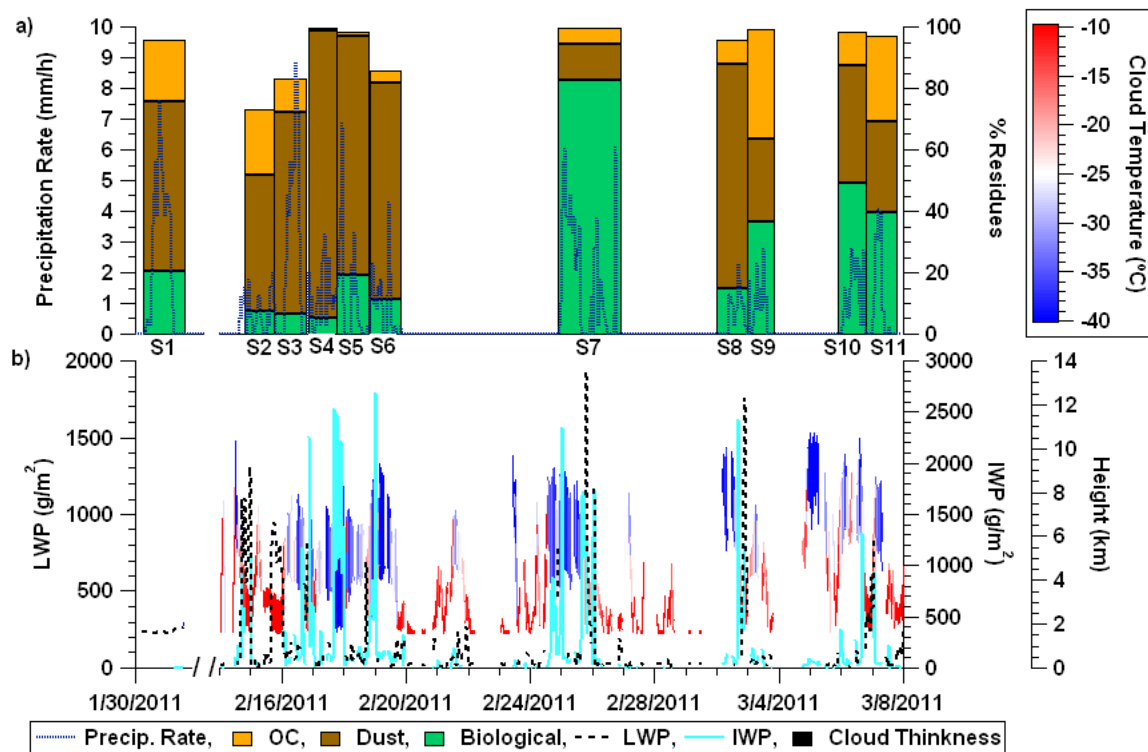


Figure 6.8 Panel (a) shows precipitation rate (mm/h) at the surface at SPD and the percentage of dust, biological, and OC residues in each sample in 2011. The width of the bars reflect the duration of the sample collection. Panel (b) shows hourly liquid water path (LWP), ice water path (IWP), and the location of the cloud for each year over SPD. The shaded region represents the hourly effective cloud temperature (T_{eff} , °C) within a 10-km pixel over SPD.

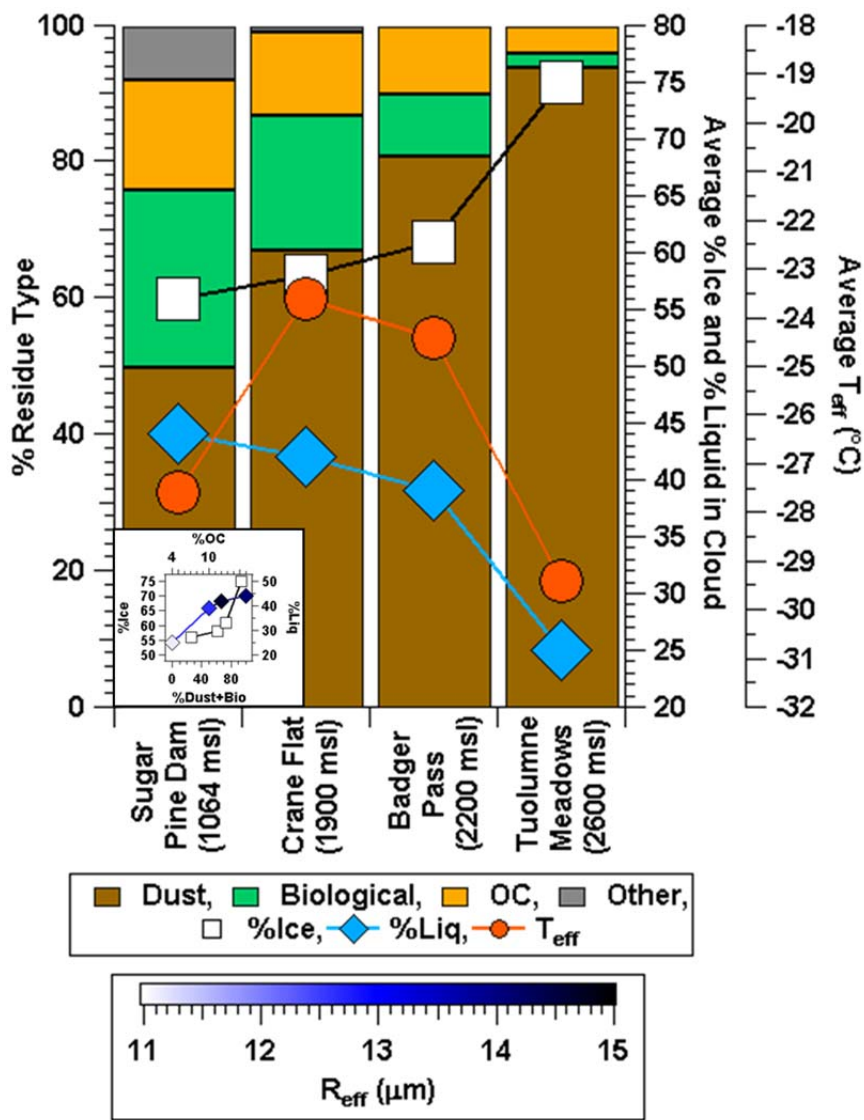


Figure 6.9 Bar graph showing the percentage of each residue type at SPD and each of the Yosemite sites in 2011. Also shown are the percentage of ice in cloud (%Ice), percentage of liquid in cloud (%Liq), and effective cloud temperatures (T_{eff} , $^{\circ}C$) averaged during sample collection time periods combined. The inset shows a correlation plot between %Ice and %Dust, and between %Liq and %OC. The color of the %Liq versus %OC represents the average effective cloud drop radius (R_{eff} , μm).

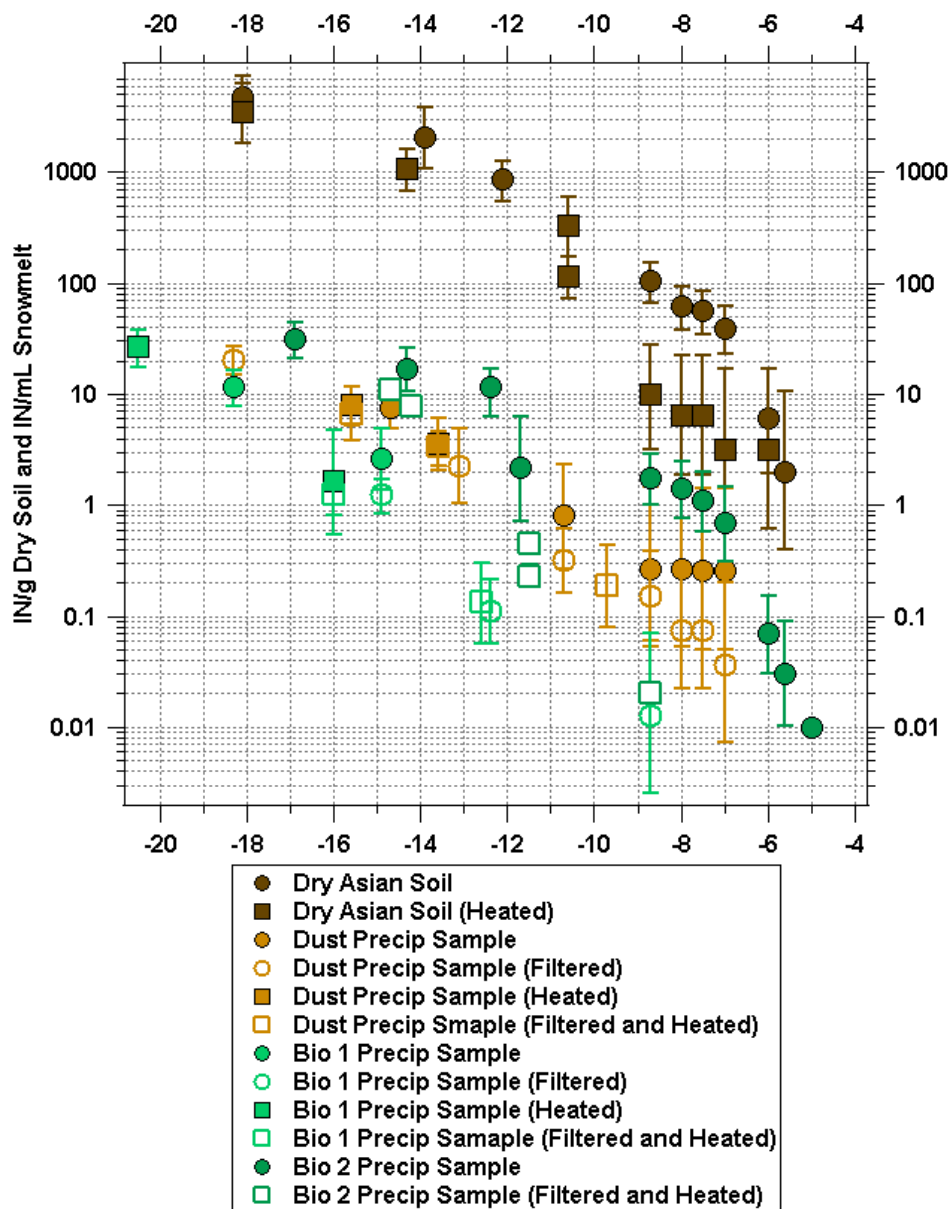


Figure 6.10 IN measurements for the dry Asian soil samples, S4 from 2011 (“dust precip sample”), S7 from 2011 (“bio 1 precip sample”), and S4 from 2010 (“bio 2 precip sample”). “Heated” represents samples that were heat treated for biological material and “Filtered” represents samples that were filtered to enable development of the full IN spectrum.

6.7. Tables

Table 6.1 Statistics for precipitation sample collection from 2009-2011 at SPD, CF, BP, and TM. Includes start and end dates and times for sample collection and number of residues that were chemically analyzed. Storms are also labeled for corresponding samples.

Year	Site	Storm	Sample	Start Date (UTC)	End Date (UTC)	Number of Residues Analyzed
2009	SPD	1	S1	2/22/09 19:30	2/23/09 18:45	399
		1	S2	2/23/09 18:45	2/24/09 19:20	70
		2	S3	2/26/09 00:00	2/26/09 19:45	236
		3	S4	3/1/09 16:00	3/2/09 01:30	6252
		3	S5	3/2/09 01:30	3/2/09 04:30	505
		3	S6	3/2/09 05:20	3/2/09 20:20	749
		3	S7	3/2/09 20:20	3/3/09 01:45	251
		3	S8	3/3/09 05:20	3/3/09 18:20	547
		3	S9	3/3/09 18:45	3/4/09 01:00	253
		3	S10	3/4/09 01:00	3/4/09 12:00	82
2010	SPD	1	S1	1/27/10 01:00	1/31/10 01:00	153
		2	S2	2/3/10 03:00	2/3/10 21:00	134
		2	S3	2/4/10 19:15	2/5/10 17:45	119
		2	S4	2/5/10 17:45	2/6/10 23:00	29
		3	S5	2/20/10 02:45	2/20/10 17:45	460
		3	S6	2/21/10 03:25	2/21/10 17:15	643
		3	S7	2/21/10 17:15	2/22/10 18:06	405
		4	S8	2/23/10 22:30	2/24/10 17:15	79
		5	S9	2/26/10 18:45	2/27/10 00:00	225
		5	S10	2/27/10 00:00	2/27/10 06:15	351
		5	S11	2/27/10 06:15	2/27/10 17:20	46
		6	S12	3/2/10 14:45	3/3/10 03:00	190
		6	S13	3/3/10 03:00	3/3/10 19:00	444
		6	S14	3/3/10 19:00	3/4/10 02:00	245
		6	S15	3/4/10 02:00	3/4/10 19:00	487
		7	S16	3/8/10 16:00	3/9/10 00:40	497
		7	S17	3/9/10 00:40	3/9/10 16:00	253
		7	S18	3/9/10 16:00	3/10/10 20:30	461
		8	S19	3/12/10 18:15	3/12/10 23:15	239
		8	S20	3/12/10 23:15	3/13/10 05:00	376
		8	S21	3/13/10 05:00	3/13/10 17:30	299
2011	SPD	1	S1	1/30/11 02:53	1/30/11 20:00	130
		2	S2	2/14/11 18:40	2/15/11 17:00	360
		2	S3	2/15/11 17:05	2/16/11 18:00	266
		3	S4	2/16/11 19:45	2/17/11 17:30	233
		3	S5	2/17/11 17:30	2/18/11 18:40	208
		3	S6	2/18/11 19:15	2/19/11 18:40	163
		4	S7	2/24/11 20:30	2/26/11 21:00	94
		5	S8	3/1/11 23:00	3/2/11 23:00	26
		5	S9	3/2/11 23:00	3/3/11 19:00	398
		6	S10	3/5/11 21:00	3/6/11 18:15	351
		6	S11	3/6/11 18:15	3/7/11 18:00	204

Table 6.1 continued.

Year	Site	Storm	Sample	Start Date (UTC)	End Date (UTC)	Number of Residues Analyzed
2011	CF	2,3	S1	2/15/11 00:15	2/17/11 21:55	468
		3	S2	2/18/11 00:15	2/22/11 22:40	1109
		4	S3	2/25/11 00:10	2/28/11 15:45	850
		5	S4	3/2/11 15:00	3/4/11 20:30	905
2011	BP	2,3	S1	2/14/11 21:45	2/17/11 19:45	467
		3	S2	2/17/11 19:50	2/22/11 21:10	664
		4	S3	2/24/11 08:00	2/26/11 19:15	452
		6	S4	3/6/11 19:00	3/7/11 18:40	469
2011	TM	2	S1	2/16/11 08:00	2/16/11 10:00	3058
		3	S2	2/16/11 10:00	2/17/11 16:00	6468
		3	S3	2/17/11 16:00	2/18/11 16:30	964
		3	S4	2/18/11 16:00	2/19/11 16:00	1900
		4	S5	2/24/11 16:00	2/25/11 16:05	6468
		4	S6	2/25/11 16:05	2/26/11 00:00	2212
		6	S7	3/6/11 16:00	3/7/11 16:05	3472

6.8. References

- Allen, J.O., Quantitative Analysis of Aerosol Time-of-Flight Mass Spectrometry Data using YAADA, Arizona State University, Tempe, 2004.
- Ault, A.P., C.R. Williams, A.B. White, P.J. Neiman, J.M. Creamean, C.J. Gaston, F.M. Ralph, and K.A. Prather, Detection of Asian dust in California orographic precipitation *Journal of Geophysical Research-Atmospheres*, 116 (D16205), doi:10.1029/2010JD015351, 2011.
- Aylor, D.E., A Framework for Examining Interregional Aerial Transport of Fungal Spores, *Agricultural and Forest Meteorology*, 38 (4), 263-288, 1986.
- Bauer, H., A. Kasper-Giebl, M. Loflund, H. Giebl, R. Hitzemberger, F. Zibuschka, and H. Puxbaum, The contribution of bacteria and fungal spores to the organic carbon content of cloud water, precipitation and aerosols, *Atmospheric Research*, 64 (1-4), 109-119, 2002.
- Bergeron, T., On the physics of cloud and precipitation, in 5th Assembly of the U.G.G.I., pp. 156–178, Paul Dupont, Paris, 1935.
- Borys, R.D., D.H. Lowenthal, and D.L. Mitchell, The relationships among cloud microphysics, chemistry, and precipitation rate in cold mountain clouds, *Atmospheric Environment*, 34 (16), 2593-2602, 2000.
- Burge, H.A., and W.R. Solomon, Sampling and Analysis of Biological Aerosols, *Atmospheric Environment*, 21 (2), 451-456, 1987.

- Carroll, J.J., and A.J. Dixon, Regional scale transport over complex terrain, a case study: tracing the Sacramento plume in the Sierra Nevada of California, *Atmospheric Environment*, 36 (23), 3745-3758, 2002.
- Choullarton, T.W., and S.J. Perry, A Model of the Orographic Enhancement of Snowfall by the Seeder-Feeder Mechanism, *Quarterly Journal of the Royal Meteorological Society*, 112 (472), 335-345, 1986.
- Christner, B.C., C.E. Morris, C.M. Foreman, R.M. Cai, and D.C. Sands, Ubiquity of biological ice nucleators in snowfall, *Science*, 319 (5867), 1214-1214, 2008.
- Churchill, D.D., and R.A. Houze, Mesoscale Updraft Magnitude and Cloud-Ice Content Deduced from the Ice Budget of the Stratiform Region of a Tropical Cloud Cluster, *Journal of the Atmospheric Sciences*, 41 (10), 1717-1725, 1984.
- Colle, B.A., and Y.G. Zeng, Bulk microphysical sensitivities within the MM5 for orographic precipitation. Part I: The Sierra 1986 event, *Monthly Weather Review*, 132 (12), 2780-2801, 2004.
- Collett, J.L., B.C. Daube, D. Gunz, and M.R. Hoffmann, Intensive Studies of Sierra-Nevada Cloudwater Chemistry and Its Relationship to Precursor Aerosol and Gas Concentrations, *Atmospheric Environment Part a-General Topics*, 24 (7), 1741-1757, 1990.
- Conen, F., C.E. Morris, J. Leifeld, M.V. Yakutin, and C. Alewell, Biological residues define the ice nucleation properties of soil dust, *Atmospheric Chemistry and Physics*, 11 (18), 9643-9648, 2011.
- Creamean, J.M., A.P. Ault, J.E. Ten Hoeve, M.Z. Jacobson, G.C. Roberts, and K.A. Prather, Measurements of Aerosol Chemistry during New Particle Formation Events at a Remote Rural Mountain Site, *Environmental Science & Technology*, 45 (19), 8208-8216, 2011.
- Creamean, J.M., K.J. Suski, A. Carzola, D.B. Collins, A.B. White, F.M. Ralph, P. Minnis, J.K. Ayers, R. Palikonda, D. Rosenfeld, and K.A. Prather, Long Range Transported Dust and Biological Aerosols Impact Precipitation during Multiple Winters in the Sierra Nevada, *Science*, submitted, 2012.
- Czerwieniec, G.A., S.C. Russell, H.J. Tobias, M.E. Pitesky, D.P. Fergenson, P. Steele, A. Srivastava, J.M. Horn, M. Frank, E.E. Gard, and C.B. Lebrilla, Stable isotope labeling of entire *Bacillus atrophaeus* spores and vegetative cells using bioaerosol mass spectrometry, *Analytical Chemistry*, 77 (4), 1081-1087, 2005.
- Deshler, T., and D.W. Reynolds, Physical Response of Winter Orographic Clouds over the Sierra-Nevada to Airborne Seeding Using Dry Ice or Silver-Iodide, *Journal of Applied Meteorology*, 29 (4), 288-330, 1990.

- Despres, V.R., J.A. Huffman, S.M. Burrows, C. Hoose, A.S. Safatov, G. Buryak, J. Frohlich-Nowoisky, W. Elbert, M.O. Andreae, U. Poschl, and R. Jaenicke, Primary biological aerosol particles in the atmosphere: a review, *Tellus Series B-Chemical and Physical Meteorology*, 64 (015598), DOI: 10.3402/tellusb.v64i0.15598, 2012.
- Dettinger, M., F.M. Ralph, T. Das, P.J. Neiman, and D.R. Cayan, Atmospheric Rivers, Floods and the Water Resources of California, *Water*, 3, 445-478; doi:10.3390/w3020445, 2011.
- Elbert, W., P.E. Taylor, M.O. Andreae, and U. Poschl, Contribution of fungi to primary biogenic aerosols in the atmosphere: wet and dry discharged spores, carbohydrates, and inorganic ions, *Atmospheric Chemistry and Physics*, 7 (17), 4569-4588, 2007.
- Ferguson, D.P., M.E. Pitesky, H.J. Tobias, P.T. Steele, G.A. Czerwieniec, S.C. Russell, C.B. Lebrilla, J.M. Horn, K.R. Coffee, A. Srivastava, S.P. Pillai, M.T.P. Shih, H.L. Hall, A.J. Ramponi, J.T. Chang, R.G. Langlois, P.L. Estacio, R.T. Hadley, M. Frank, and E.E. Gard, Reagentless detection and classification of individual bioaerosol particles in seconds, *Analytical Chemistry*, 76 (2), 373-378, 2004.
- Field, P.R., O. Mohler, P. Connolly, M. Kramer, R. Cotton, A.J. Heymsfield, H. Saathoff, and M. Schnaiter, Some ice nucleation characteristics of Asian and Saharan desert dust, *Atmospheric Chemistry and Physics*, 6, 2991-3006, 2006.
- Gard, E., J.E. Mayer, B.D. Morrical, T. Dienes, D.P. Ferguson, and K.A. Prather, Real-time analysis of individual atmospheric aerosol particles: Design and performance of a portable ATOFMS, *Analytical Chemistry*, 69 (20), 4083-4091, 1997.
- Givati, A., and D. Rosenfeld, Quantifying precipitation suppression due to air pollution, *Journal of Applied Meteorology*, 43 (7), 1038-1056, 2004.
- Guan, B., N.P. Molotch, D.E. Waliser, E.J. Fetzer, and P.J. Neiman, Extreme snowfall events linked to atmospheric rivers and surface air temperature via satellite measurements, *Geophysical Research Letters*, 37, 2010.
- Hallar, A.G., G. Chirokova, I. McCubbin, T.H. Painter, C. Wiedinmyer, and C. Dodson, Atmospheric bioaerosols transported via dust storms in the western United States, *Geophysical Research Letters*, 38, 2011.
- Holecek, J.C., M.T. Spencer, and K.A. Prather, Analysis of rainwater samples: Comparison of single particle residues with ambient particle chemistry from the northeast Pacific and Indian oceans, *Journal of Geophysical Research-Atmospheres*, 112 (D22), 2007.
- Hosler, C.L., D.C. Jensen, and L. Goldshlak, On the Aggregation of Ice Crystals to Form Snow, *Journal of Meteorology*, 14 (5), 415-420, 1957.

- Hua, N.P., F. Kobayashi, Y. Iwasaka, G.Y. Shi, and T. Naganuma, Detailed identification of desert-originated bacteria carried by Asian dust storms to Japan, *Aerobiologia*, 23 (4), 291-298, 2007.
- Husar, R.B., D.M. Tratt, B.A. Schichtel, S.R. Falke, F. Li, D. Jaffe, S. Gasso, T. Gill, N.S. Laulainen, F. Lu, M.C. Reheis, Y. Chun, D. Westphal, B.N. Holben, C. Gueymard, I. McKendry, N. Kuring, G.C. Feldman, C. McClain, R.J. Frouin, J. Merrill, D. DuBois, F. Vignola, T. Murayama, S. Nickovic, W.E. Wilson, K. Sassen, N. Sugimoto, and W.C. Malm, Asian dust events of April 1998, *Journal of Geophysical Research-Atmospheres*, 106 (D16), 18317-18330, 2001.
- Kumar, P.P., K. Broekhuizen, and J.P.D. Abbatt, Organic acids as cloud condensation nuclei: Laboratory studies of highly soluble and insoluble species, *Atmospheric Chemistry and Physics*, 3, 509-520, 2003.
- Lunden, M.M., D.R. Black, M. McKay, K.L. Revzan, A.H. Goldstein, and N.J. Brown, Characteristics of fine particle growth events observed above a forested ecosystem in the Sierra Nevada Mountains of California, *Aerosol Science and Technology*, 40 (5), 373-388, 2006.
- Maki, L.R., E.L. Galyan, Changchi.Mm, and D.R. Caldwell, Ice Nucleation Induced by *Pseudomonas-Syringae*, *Applied Microbiology*, 28 (3), 456-459, 1974.
- Marculli, C., S. Gedamke, T. Peter, and B. Zobrist, Efficiency of immersion mode ice nucleation on surrogates of mineral dust, *Atmospheric Chemistry and Physics*, 7 (19), 5081-5091, 2007.
- McKendry, I.G., K.B. Strawbridge, N.T. O'Neill, A.M. Macdonald, P.S.K. Liu, W.R. Leitch, K.G. Anlauf, L. Jaegle, T.D. Fairlie, and D.L. Westphal, Trans-Pacific transport of Saharan dust to western North America: A case study, *Journal of Geophysical Research-Atmospheres*, 112 (D1), 2007.
- Meyers, M.P., P.J. Demott, and W.R. Cotton, New Primary Ice-Nucleation Parameterizations in an Explicit Cloud Model, *Journal of Applied Meteorology*, 31 (7), 708-721, 1992.
- Minnis, P., L. Nguyen, D.R. Doelling, D.F. Young, W.F. Miller, and D.P. Kratz, Rapid calibration of operational and research meteorological satellite imagers. Part I: Evaluation of research satellite visible channels as references, *Journal of Atmospheric and Oceanic Technology*, 19 (9), 1233-1249, 2002.
- Minnis, P., S. Sun-Mack, D.F. Young, P.W. Heck, D.P. Garber, Y. Chen, D.A. Spangenberg, R.F. Arduini, Q.Z. Trepte, W.L.S. Jr., J.K. Ayers, S.C. Gibson, W.F. Miller, V. Chakrapani, Y. Takano, K.-N. Liou, Y. Xie, and P. Yang, CERES Edition-2 cloud property retrievals using TRMM VIRS and Terra and Aqua MODIS data, Part I: Algorithms, *Ieee Transactions on Geoscience and Remote Sensing*, 49 (11), doi: 10.1109/TGRS.2011.2144601, 2011.

- Minnis, P., Q.Z. Trepte, S. Sun-Mack, Y. Chen, D.R. Doelling, D.F. Young, D.A. Spangenberg, W.F. Miller, B.A. Wielicki, R.R. Brown, S.C. Gibson, and E.B. Geier, Cloud Detection in Nonpolar Regions for CERES Using TRMM VIRS and Terra and Aqua MODIS Data, *Ieee Transactions on Geoscience and Remote Sensing*, 46 (11), 3857-3884, 2008.
- Morris, C.E., D.G. Georgakopoulos, and D.C. Sands, Ice nucleation active bacteria and their potential role in precipitation, *Journal De Physique Iv*, 121, 87-103, 2004.
- Muhlbauer, A., T. Hashino, L. Xue, A. Teller, U. Lohmann, R.M. Rasmussen, I. Geresdi, and Z. Pan, Intercomparison of aerosol-cloud-precipitation interactions in stratiform orographic mixed-phase clouds, *Atmospheric Chemistry and Physics*, 10 (17), 8173-8196, 2010.
- Pandey, G.R., D.R. Cayan, and K.P. Georgakakos, Precipitation structure in the Sierra Nevada of California during winter, *Journal of Geophysical Research-Atmospheres*, 104 (D10), 12019-12030, 1999.
- Parish, T.R., Barrier Winds Along the Sierra-Nevada Mountains, *Journal of Applied Meteorology*, 21 (7), 925-930, 1982.
- Petters, M.D., C.M. Carrico, S.M. Kreidenweis, A.J. Prenni, P.J. DeMott, J.L. Collett, and H. Moosmuller, Cloud condensation nucleation activity of biomass burning aerosol, *Journal of Geophysical Research-Atmospheres*, 114, 2009.
- Phillips, V.T.J., C. Andronache, B. Christner, C.E. Morris, D.C. Sands, A. Bansemer, A. Lauer, C. McNaughton, and C. Seman, Potential impacts from biological aerosols on ensembles of continental clouds simulated numerically, *Biogeosciences*, 6 (6), 987-1014, 2009.
- Phillips, V.T.J., P.J. DeMott, and C. Andronache, An empirical parameterization of heterogeneous ice nucleation for multiple chemical species of aerosol, *Journal of the Atmospheric Sciences*, 65 (9), 2757-2783, 2008.
- Pinsky, M., A. Khain, D. Rosenfeld, and A. Pokrovsky, Comparison of collision velocity differences of drops and graupel particles in a very turbulent cloud, *Atmospheric Research*, 49 (2), 99-113, 1998.
- Posfai, M., A. Gelencser, R. Simonics, K. Arato, J. Li, P.V. Hobbs, and P.R. Buseck, Atmospheric tar balls: Particles from biomass and biofuel burning, *Journal of Geophysical Research-Atmospheres*, 109 (D6), 2004.
- Pratt, K.A., P.J. DeMott, J.R. French, Z. Wang, D.L. Westphal, A.J. Heymsfield, C.H. Twohy, A.J. Prenni, and K.A. Prather, In situ detection of biological particles in cloud ice-crystals, *Nature Geoscience*, 2 (6), 397-400, 2009.

- Qin, X.Y., and K.A. Prather, Impact of biomass emissions on particle chemistry during the California Regional Particulate Air Quality Study, *International Journal of Mass Spectrometry*, 258 (1-3), 142-150, 2006.
- Ralph, F.M., P.J. Neiman, and G.A. Wick, Satellite and CALJET aircraft observations of atmospheric rivers over the eastern north pacific ocean during the winter of 1997/98, *Monthly Weather Review*, 132 (7), 1721-1745, 2004.
- Rosenfeld, D., Suppression of rain and snow by urban and industrial air pollution, *Science*, 287 (5459), 1793-1796, 2000.
- Rosenfeld, D., and A. Givati, Evidence of orographic precipitation suppression by air pollution-induced aerosols in the western United States, *Journal of Applied Meteorology and Climatology*, 45 (7), 893-911, 2006.
- Rosenfeld, D., U. Lohmann, G.B. Raga, C.D. O'Dowd, M. Kulmala, S. Fuzzi, A. Reissell, and M.O. Andreae, Flood or drought: How do aerosols affect precipitation?, *Science*, 321 (5894), 1309-1313, 2008.
- Ryoo, J.-M., D.E. Waliser, and E.J. Fetzer, Trajectory analysis on the origin of air mass and moisture associated with Atmospheric Rivers over the west coast of the United States, *Atmos. Chem. Phys. Discuss.*, 11, 11109-11142, 2011.
- Saleeby, S.M., W.R. Cotton, D. Lowenthal, R.D. Borys, and M.A. Wetzel, Influence of Cloud Condensation Nuclei on Orographic Snowfall, *Journal of Applied Meteorology and Climatology*, 48 (5), 903-922, 2009.
- Schluessel, P., and W.J. Emery, Atmospheric Water-Vapor Over Oceans From SSM/I Measurements, *International Journal of Remote Sensing*, 11 (5), 753-766, 1990.
- Schnell, R.C., Biogenic Sources of Atmospheric Ice Nuclei, *Bulletin of the American Meteorological Society*, 55 (6), 670-670, 1974.
- Silva, P.J., Source Profiling and Apportionment of Airborne Particles: A New Approach Using Aerosol Time-of-Flight Mass Spectrometry, University of California, Riverside, Riverside, 2000.
- Silva, P.J., R.A. Carlin, and K.A. Prather, Single particle analysis of suspended soil dust from Southern California, *Atmospheric Environment*, 34 (11), 1811-1820, 2000.
- Silva, P.J., D.Y. Liu, C.A. Noble, and K.A. Prather, Size and chemical characterization of individual particles resulting from biomass burning of local Southern California species, *Environmental Science & Technology*, 33 (18), 3068-3076, 1999.
- Song, X.H., P.K. Hopke, D.P. Fergenson, and K.A. Prather, Classification of single particles analyzed by ATOFMS using an artificial neural network, *ART-2A, Anal. Chem.*, 71 (4), 860-865, 1999.

- Steele, P.T., A. Srivastava, M.E. Pitesky, D.P. Fergenson, H.J. Tobias, E.E. Gard, and M. Frank, Desorption/ionization fluence thresholds and improved mass spectral consistency measured using a flattop laser profile in the bioaerosol mass spectrometry of single *Bacillus endospores*, *Analytical Chemistry*, 77 (22), 7448-7454, 2005.S
- Sullivan, R.C., S.A. Guazzotti, D.A. Sodeman, and K.A. Prather, Direct observations of the atmospheric processing of Asian mineral dust, *Atmospheric Chemistry and Physics*, 7, 1213-1236, 2007.
- Sullivan, R.C., M.J.K. Moore, M.D. Petters, S.M. Kreidenweis, G.C. Roberts, and K.A. Prather, Timescale for hygroscopic conversion of calcite mineral particles through heterogeneous reaction with nitric acid, *Physical Chemistry Chemical Physics*, 11 (36), 7826-7837, 2009.
- Sullivan, R.C., and K.A. Prather, Investigations of the diurnal cycle and mixing state of oxalic acid in individual particles in Asian aerosol outflow, *Environmental Science & Technology*, 41 (23), 8062-8069, 2007.
- Uno, I., K. Eguchi, K. Yumimoto, Z. Liu, Y. Hara, N. Sugimoto, A. Shimizu, and T. Takemura, Large Asian dust layers continuously reached North America in April 2010, *Atmospheric Chemistry and Physics*, 11 (14), 7333-7341, 2011.
- Warburton, J.A., L.G. Young, and R.H. Stone, Assessment of Seeding Effects in Snowpack Augmentation Programs - Ice Nucleation and Scavenging of Seeding Aerosols, *Journal of Applied Meteorology*, 34 (1), 121-130, 1995.
- Weaver, J.F., J.A. Knaff, D. Bikos, G.S. Wade, and J.M. Daniels, Satellite observations of a severe supercell thunderstorm on 24 July 2000 made during the GOES-11 science test, *Weather and Forecasting*, 17 (1), 124-138, 2002.
- White, A.B., D.J. Gottas, A.F. Henkel, P.J. Neiman, F.M. Ralph, and S.I. Gutman, Developing a Performance Measure for Snow-Level Forecasts, *Journal of Hydrometeorology*, 11 (3), 739-753, 2010.
- White, A.B., D.J. Gottas, E.T. Strem, F.M. Ralph, and P.J. Neiman, An automated brightband height detection algorithm for use with Doppler radar spectral moments, *Journal of Atmospheric and Oceanic Technology*, 19 (5), 687-697, 2002.
- White, A.B., P.J. Neiman, F.M. Ralph, D.E. Kingsmill, and P.O.G. Persson, Coastal orographic rainfall processes observed by radar during the California land-falling jets experiment, *Journal of Hydrometeorology*, 4 (2), 264-282, 2003.
- Yuter, S.E., and R.A. Houze, Microphysical modes of precipitation growth determined by S-band vertically pointing radar in orographic precipitation during MAP, *Quarterly Journal of the Royal Meteorological Society*, 129 (588), 455-476, 2003.

Zhang, Q., and C. Anastasio, Chemistry of fog waters in California's Central Valley - Part 3: concentrations and speciation of organic and inorganic nitrogen, *Atmospheric Environment*, 35 (32), 5629-5643, 2001.

7. Conclusions and Future Work

7.1. Synopsis

The focus of this dissertation aimed to investigate the chemical composition of aerosols that have the potential to impact cloud formation and potentially precipitation at various locations, and in most cases, for long time periods. This research demonstrates the variability associated with cloud seeds over time and in different regions. The Riverside study afforded information on the inter-annual variability of urban aerosol due to changes in aerosol transport and meteorological conditions. Tropical cyclones (TCs) shifted the representative aged urban aerosol to a less-aged, less-cloud condensation nuclei (CCN) active aerosol population, having implications on regional cloud formation after extreme weather events in Atlanta. In the remote Sierra Nevada Mountains of California, observations of newly-formed aerosols containing amines and sulfate presented a new source of CCN, while inter-annual trends in precipitation provided insight into how transported ice nuclei (IN) potentially influenced precipitation quantity and phase. Section 7.2 provides a general summary, while Section 7.3 introduces some ongoing and future work of the research presented throughout this dissertation.

7.2. Conclusions

7.2.1. Sources and Chemical Composition of Aerosols as CCN at different Urban Locations

A large part of the research presented in this dissertation involved investigating sources and composition of aerosols that potentially serve as CCN in two different urban regions: Riverside and Atlanta. In both regions, a significant number fraction of the aerosol was often organic in nature, supporting previous observations of a high organic fraction from primary sources such as motor vehicles and railroads as well as secondary formation from gas-phase species [Blanchard *et al.*, 2011; Hatch *et al.*, 2011b; Kim *et al.*, 2004; Liu *et al.*, 2003]. The composition of the urban aerosol is highly complex and

poorly understood due to the number of different sources, as well as the heterogeneous reactions that occur between gases and aerosol surfaces [Alston *et al.*, 2011; Liu *et al.*, 2003; Turpin and Lim, 2002].

Chapter 2 presented *in situ* single-particle mass spectrometry data collected during three consecutive summers (2005-2007) in the heavily polluted region of Riverside to probe the major sources and processes affecting aerosol chemistry on a long-term basis. Submicron particle chemistry was vastly different during all three summers namely due to differences in meteorological conditions, which impacted the dominant sources and chemical mixing states. Although aerosols were frequently transported from the Los Angeles area and local agricultural areas, such as Chino, CA, during the summers of 2005 and 2006, highly aged organic aerosols were present in the summer of 2005 due to enhanced photochemistry, while during the summer of 2006, ammonium sulfate and nitrate condensed onto preexisting particles due to highly humid conditions. In contrast, the summer of 2007 was characterized by hot and dry conditions leading to a reduced influence from secondary species condensing onto dust and sea salt particles transported from less populated regions. The relationship between single-particle chemistry, sources, and meteorology developed from this long-term study can be used to predict the effects of human exposure to particles of different chemical compositions in not only Riverside, but other areas impacted by similar sources. Further, because urban and industrial aerosols serve as CCN and are emitted in high number concentrations, studying long-term urban aerosols is also important for regional cloud formation [Rosenfeld, 2000]. An improvement in our understanding of aerosol composition trends is necessary for thoroughly evaluating the impacts of aerosols on human health and cloud microphysics [Andreae and Rosenfeld, 2008; Vedral, 1997].

Aerosol composition in Atlanta was presented in Chapter 3, which provides interesting comparisons to Riverside. Severe weather systems such as TCs can perturb the size and chemical composition of urban aerosol populations; however, the overall effects of these perturbations are currently unknown. During the 2008 summer in Atlanta, aerosol time-of-flight mass spectrometry (ATOFMS) was used to probe changes in the

size-resolved chemistry of individual particles before, during, and after TCs Gustav and Hanna. When Gustav approached the southeastern United States, fast winds (6-7 m/s) originating from the Atlantic Ocean rapidly removed aged organic aerosols (0.2-1.0 μm) present before TCs and transported sea-spray aerosols (0.2-3.0 μm). Sea-spray enriched in salts has been shown to act as giant CCN, with high concentrations leading to the development of large cloud drops and early onset of precipitation. Although the sea-spray aerosols were CCN-active, the CCN concentrations were lower (1300 cm^{-3}) compared to the typical urban conditions before the TCs (3600 cm^{-3}). Following aerosol scavenging by precipitation, CCN concentrations remained low (1000-1700 cm^{-3}) while fresh urban emissions increased, evident by the presence of less-aged organic aerosols, which were not as CCN-active as the aged organic particles or sea-spray. The overall decrease in CCN concentrations caused by the TCs can impact regional cloud formation by removing the seeds that cloud droplets form upon. Thus, the ability of TCs to drastically alter the aerosol composition and CCN properties to those typically found in an inland, urban location has significant implications for the microphysical properties of clouds.

Typical urban conditions in both Riverside and Atlanta were evident by large relative fractions of aged organic carbon aerosols. Figure 7.1 shows the overall composition of the aerosols in Riverside from 2005-2007 (panels a-c, respectively) and Atlanta (panel d). The major types of aerosols that were similar between the different sites included organic carbon (OC), amine-OC, elemental carbon (EC or soot), ECOC (aged soot), dust, and salt (includes sea salt and sea-spray). 'Other' includes types that were not similar between the sites. Overall, submicron particle chemistry was similar at Riverside and Atlanta, but not for the entire duration of measurements. In fact, only the summer of 2005 in Riverside and prior to TCs in Atlanta were representative of urban pollution, i.e., highly organic in nature. Extreme weather events in Atlanta led to a shift in aerosol source and altered the extent of aging on urban emissions whereas the Riverside aerosol aging changed each year due to variable sources and meteorological conditions. However, the summers of 2006 and 2007 in Riverside and during TCs in Atlanta represent unique time periods that do not follow the aerosol aged organic carbon signatures. The aerosol composition at both sites was strongly dependent on

meteorological conditions, which determined the sources. These results demonstrate the dependence of aerosol composition on changes in sources and weather, even in highly populated urban regions where aerosol composition is thought to be predominantly highly aged organic carbon species.

7.2.2. Sources of CCN at a Remote Region

Chapter 4 investigated the sources of CCN in a more remote region compared to Riverside and Atlanta during the 2009 winter season. The *CalWater* field campaign (2009-2011) was designed to study aerosol-cloud-precipitation effects in the remote Sierra Nevada at Sugar Pine Dam (SPD). Measurements were conducted in the winter season because the Sierra Nevada receives large quantities of water during intense winter storms; therefore, studying aerosols that act as CCN during these storms can improve upon existing knowledge of the California water cycle. Previous studies have suggested that CCN are transported directly from the Central Valley (CV) west of mountains [Rosenfeld *et al.*, 2008b]; however, *in situ* formation of new aerosols was found to be a major source of CCN in the Sierra Nevada [Hatch *et al.*, 2011a]. During the 2009 *CalWater* field campaign, nucleation events occurred during two pristine periods following precipitation, with higher gas-phase SO₂ concentrations during the second period, when faster particle growth occurred (7-8 nm/h). Amines, as opposed to ammonia [Bzdek *et al.*, 2010; Ortega *et al.*, 2008], and sulfate were detected in the particle phase throughout new particle formation (NPF) events, increasing in number as the particles grew to larger sizes. Interestingly, long-range transport of SO₂ from Asia appeared to potentially play a role in NPF during faster particle growth. Understanding the propensity of newly-formed particles to act as CCN is critical for predicting the effects of NPF on orographic cloud formation during winter storms along the Sierra Nevada. The potential impact of newly-formed particles in remote regions needs to be compared to that of transported urban aerosols when evaluating the impact of aerosols on clouds and climate. Although formed through different mechanisms (i.e., condensation versus nucleation), the aerosol composition during the summer of 2006 in Riverside was similar to the overall composition during the NPF events at SPD as shown in Figure 7.1b and e. Both

shared a fairly similar source of amine species—the Chino dairies and CV agricultural regions—although other sources also affected each location, such as residential biomass burning at SPD and aged organics from urban pollution at Riverside. NPF events were not frequently observed during 2010 and 2011; however inter-annual trends of the sources of IN and precipitation patterns were observed and discussed herein.

7.2.3. Sources and Precipitation Effects of IN at a Remote Region

The measurements during the 2009 winter also afforded valuable information regarding the types of aerosols that are involved in ice crystal formation in clouds as discussed in Chapters 5 and 6. Precipitation from winter storms increases snowpack in the Sierra Nevada and provides critical water resources for all of California. Thus, the mechanisms influencing precipitation in this region have been the subject of research for decades. Some studies suggest aerosol pollution suppresses orographic precipitation [Rosenfeld *et al.*, 2008c], whereas more recent studies show precipitation enhancement during periods of dust transport from over Asia [Ault *et al.*, 2011a]. Precipitation samples were collected during two intense storms and aerosols as insoluble residues in precipitation were chemically analyzed using ATOFMS to provide insight into their potential involvement as IN during the 2009 winter study [Ault *et al.*, 2011a]. These two storms had similar meteorological conditions including atmospheric water content and water vapor transport; however, the second storm produced 1.4 times as much precipitation and increased snowpack by 1.6 times relative to the first storm likely due to transported Asian dust serving as IN [Ault *et al.*, 2011a]. Measurements continued in the winters of 2010 and 2011 to investigate the sources of cloud seeds in the region over time. To gain a more complete understanding of aerosol-cloud-precipitation interactions in California, the 2011 *CalWater* field campaign utilized aircraft measurements to characterize the sources of aerosols seeding clouds and the resulting impact on microphysics and precipitation. Dust and biological aerosols transported from as far as the Sahara were present in high altitude clouds, coincident with elevated IN concentrations and ice-induced precipitation.

When comparing the precipitation residues from all three winter seasons, the chemical composition of insoluble precipitation residues was linked with trends in precipitation type and quantity, and cloud microphysical properties at SPD and three sites in Yosemite National Park (2011 only). Similar to Riverside, the inter-annual observations were quite different in terms of precipitation residue composition and meteorological conditions. Figure 7.2 illustrates the variation in precipitation residue composition during the three winter seasons and at the three sites in Yosemite. From the results presented, it is likely that organic residues from local biomass burning and agricultural sources in the CV may have served as CCN, which decreased the riming efficiency of ice crystals during time periods with lower precipitation totals. In contrast, biological residues and long-range transported dust influenced the amount of cloud ice content and relative amount of precipitation initiated in the ice phase by serving as IN. The total amount of precipitation per storm depended not only on the amount of available atmospheric water vapor during the onset of storms, but also likely on the relative abundance of dust and biological aerosols. Long-term and multi-site observations such as these could enable the modeling community to better assess how regional weather and climate may change due to the effects from aerosols. Improving our ability to model aerosol-cloud-precipitation interactions will lead to better winter storm preparedness, water resource management, and flood mitigation.

7.2.4. Overall Conclusions

The aerosols that served as either CCN or IN were highly variable at the various locations presented throughout this dissertation. Not only does the aerosol composition vary between similar urban locations as demonstrated by the Riverside and Atlanta studies, but also at the same location over three-year time periods (shown by both the inter-annual studies at Riverside and SPD). Understanding the variability in aerosol composition in a particular region over time or between similar regions has implications for modeling the effects aerosols have on clouds and precipitation. For instance, one cannot assume urban aerosol composition is consistently highly aged organics. Different aerosols have diverse effects with regards to CCN and IN properties; thus changing

aerosol composition could result in broader effects on regional cloud formation. The aim of this dissertation was to provide information to enable the modeling community to better assess changes in aerosol composition due to changes in sources and meteorology, and hence improve predictions of cloud and precipitation formation in multiple regions over long time scales.

The questions presented in Chapter 1 were addressed throughout this dissertation. The types of aerosols that affect air quality and serve as CCN or IN were investigated and proved to be quite different in terms of chemical composition at Riverside and Atlanta. Further, the size and chemical composition can indeed change abruptly on give spatial and temporal scales, as demonstrated by the multiple field studies discussed in this dissertation. Microscale (<1 km horizontal resolution), mesoscale (5 to several hundred km), and even synoptic scale (thousands of km) weather patterns can affect aerosol composition and number as well by introducing different sources of aerosols to one location. For instance, the mesoscale TCs introduced sea salt to Atlanta while synoptic scale transport of SO₂ from Asia over the Pacific Ocean appeared to contribute to NPF at the remote SPD. In addition, these dynamics over the Pacific Ocean also create ideal conditions for trans-Pacific transport of dust into clouds over the Sierra Nevada.

Finally, the results presented at the different locations, and in most cases, over long periods of time could contribute to develop a larger scale distribution or even a global picture of aerosols that serve as cloud seeds, and hence resulting precipitation effects. Currently, modeling of global CCN is limited to certain types of aerosols, such global distributes of CCN predictions based solely on nucleation aerosols [*Spracklen et al., 2008*], carbonaceous aerosols [*Spracklen et al., 2011*], or sea salt [*Pierce and Adams, 2006*], while global IN models have improved but still have errors associated with aerosol chemical composition [*DeMott et al., 2010*]. Models need to incorporate the variable and often competing effects of both IN and CCN, by understanding the sources and chemical composition of aerosols. Although the results presented in this dissertation represent a significant contribution to understand the spatial and temporal variability in CCN and IN, considerable future work is needed as discussed herein.

7.3. Ongoing and Future Work

7.3.1. Continuous Precipitation Measurements at SPD

Future work should concentrate on aerosol and meteorological measurements over longer periods of time and in additional regions. Investigating changes in cloud seeds represents a longer-term goal to reduce uncertainty associated with modeling and predicting aerosol-cloud-precipitation interactions. In particular, I plan to continue measurements at SPD during my postdoctoral research at the National Oceanic and Atmospheric Administration's Earth System Research Laboratory in Boulder, CO (NOAA/ESRL). NOAA/ESRL is currently planning for *CalWater Phase II* (2015-2017) to continue to study aerosol effects in a changing climate. Measurements for a *CalWater* bridging study during the 2013-2014 winter seasons are currently being planned to provide continuous data. Therefore, a total of eight years of aerosol, precipitation, and meteorological measurements will be conducted at SPD to develop an even longer-term picture of aerosol effects on clouds and precipitation in comparison to the three years presented in Chapter 6. The overall goal is to further probe how aerosols interact with clouds and hence affect precipitation on the west coast of the United States. To expand on previous *CalWater* measurements, the combined effects of larger-scale dynamics and cloud microphysics from aerosols on orographic precipitation will be examined during intense atmospheric river (AR) conditions. Implementing continuous and more detailed examination of aerosols to a meteorological-based area for future *CalWater* measurements will allow us to provide a better link between aerosols, clouds, and precipitation. Further, samples will be collected at a coastal mountain site, Cazadero, to investigate transitions in precipitation chemistry from the point where storms hit the coastal mountains of California to the Sierra Nevada further inland. Collecting precipitation samples is a simple process, which can be extended to more sites, provided that personnel are available to position collection containers outside during the onset of a storm. Coordinating future *CalWater* precipitation collection with several of NOAA's Hydrometeorological Testbed (HMT)-West sites shown in Figure 7.3 will be an efficient way to increase the spatial scale of measurements. Wide spatial coverage of precipitation

residue composition and meteorological measurements are needed to better understand trends in cloud formation and precipitation and to provide more detail for regional and global model parameterizations. Plans to incorporate *CalWater* aerosol data into Weather Research and Forecasting (WRF) model simulations to investigate extreme precipitation in California are underway as well [Leung and Qian, 2009a].

7.3.2. Source Determination of IN during *CalWater*

In addition to investigating the chemical composition of the aerosols potentially acting as cloud seeds, information about how aerosols are emitted into the atmosphere and interact with weather systems is needed. As an extension of Chapters 5 and 6, I have been investigating the sources of the dust and biological aerosols that served as IN at SPD using HYSPLIT, modeling/observational data from the *Navy Aerosol Analysis and Prediction System (NAAPS)*, imagery from the Cloud-Aerosol Lidar and Infrared Pathfinder Satellite Observation (CALIPSO) satellite, and reanalysis from the National Centers for Environmental Prediction/National Center for Atmospheric Research (NCEP/NCAR) to characterize dust storm locations and transport of the resulting airborne dust for all three years of *CalWater*. Although NAAPS and CALIPSO cannot distinguish biological aerosols, biological species are lofted during dust storms in regions such as Asia [Hua *et al.*, 2007] and can thereafter be transported with the dust [Griffin *et al.*, 2002]. Chapter 6 shows results from NAAPS, CALIPSO, and HYSPLIT analysis for only the 2011 winter study, but this analysis will be extended to all three winter seasons in the future. NCEP/NCAR reanalysis provides a global picture of meteorological parameters, such as geopotential height, precipitation, temperature, etc. to develop a timeline for aerosol transport to California from as far back as the Sahara.

Trajectories, calculated every 3 hours, that ended at cloud top heights over SPD during storm time periods are shown in Figure 7.4. Figure 7.5 shows an overall picture from the three year analysis, looking at the relative contribution from the different dust source regions introduced in Chapter 5. The pies show the overall ATOFMS chemical composition of the precipitation residues, while the bars show the frequency of transport from each dust region. The shaded portion of the bar represents if trajectories passed

through a dust layer determined using NAAPS time-height sections of dust at sites within each region. For example, if the dust layer was 8000 m high and a point in the trajectory was 7000 m during the same time period, this would be considered as passing through the dust layer. Thus the air mass likely contained dust. The relative contribution from dust sources does not directly follow the amount of dust observed in the precipitation at SPD, due to external factors such as transport conditions. For instance, Figure 7.6, Figure 7.7, and Figure 7.8 show geopotential height anomalies (calculated with reference to a 1981-2010 average value), mean wind speed, and mean precipitation rate, respectively, at 500 mb (~5500 m) from Jan 1-Mar 31 during each winter season. This height was chosen based on the typical transport heights of dust over the Pacific Ocean from the HYSPLIT analysis. Thus far, it is possible the least amount of dust was present during 2010 due to the highest mean precipitation over the Pacific Ocean, potentially leading to more wet deposition of the dust in addition to the low pressure area off the coast of the United States (shown in blue for geopotential height in Figure 7.6b). In 2011, the winds were fastest off the coast of Asia where the trajectories traveled (Figure 7.7c) and transport occurred south of the precipitation (Figure 7.8c), potentially leading to less trans-Pacific transport time and hence less time for wet or dry removal of the dust. This could be why the most dust was observed in the precipitation samples during 2011. The high pressure zone off the coast of the United States in 2009 (Figure 7.6a) led to transport over the high pressure region and through Alaska, meaning that the aerosol experienced longer transport times, which is possibly why less dust was observed in the precipitation compared to 2011. These general conclusions are preliminary and more detailed work on the meteorological conditions in relation to precipitation chemistry is needed and will be conducted during my postdoctoral research at NOAA/ESRL.

This information is a key factor to understanding the sources and types of aerosols that may affect winter storms in California for the *CalWater* studies. A combination of images to determine NAAPS and CALIPSO data can be used with special sensor microwave imager (SSM/I) if, when, and where dust layers possibly interact with the winter storms to form ice in-cloud: NAAPS/CALIPSO can determine the source, location, and vertical and spatial extent of the dust layers, the SSM/I can determine the

spatial extent and water vapor content of winter storms approaching the west coast of California, and CALIPSO can thereafter determine if the combined dust-laden air and concentrated water vapor formed ice in clouds. Meteorological conditions influencing the relative amount of dust transported to California can be determined using NCEP/NCAR reanalysis. Further, the combination of these measurements will be used to corroborate when the ATOFMS measures dust in precipitation samples during storms. Overall, using a combination of NAAPS, CALIPSO, HYSPLIT, SSM/I, and NCEP/NCAR reanalysis will help to improve characterization of the sources and transport mechanisms of aerosols, as well as improve upon the current understanding of water vapor, atmospheric dynamics, and cloud formation during winter storms in California.

To conclude, the results and future work discussed throughout this dissertation provide insight into the variability of aerosols that serve as cloud seeds on a large spatial and temporal scale. In order to fully characterize CCN and IN, these results need to be expanded upon at other locations on longer time scales. The ultimate goal is to develop an improved global picture of aerosol-cloud-precipitation effects to better predict the effects associated with a changing climate.

7.4. Acknowledgements

John F. Cahill is acknowledged for helping edit this chapter.

7.5. Figures

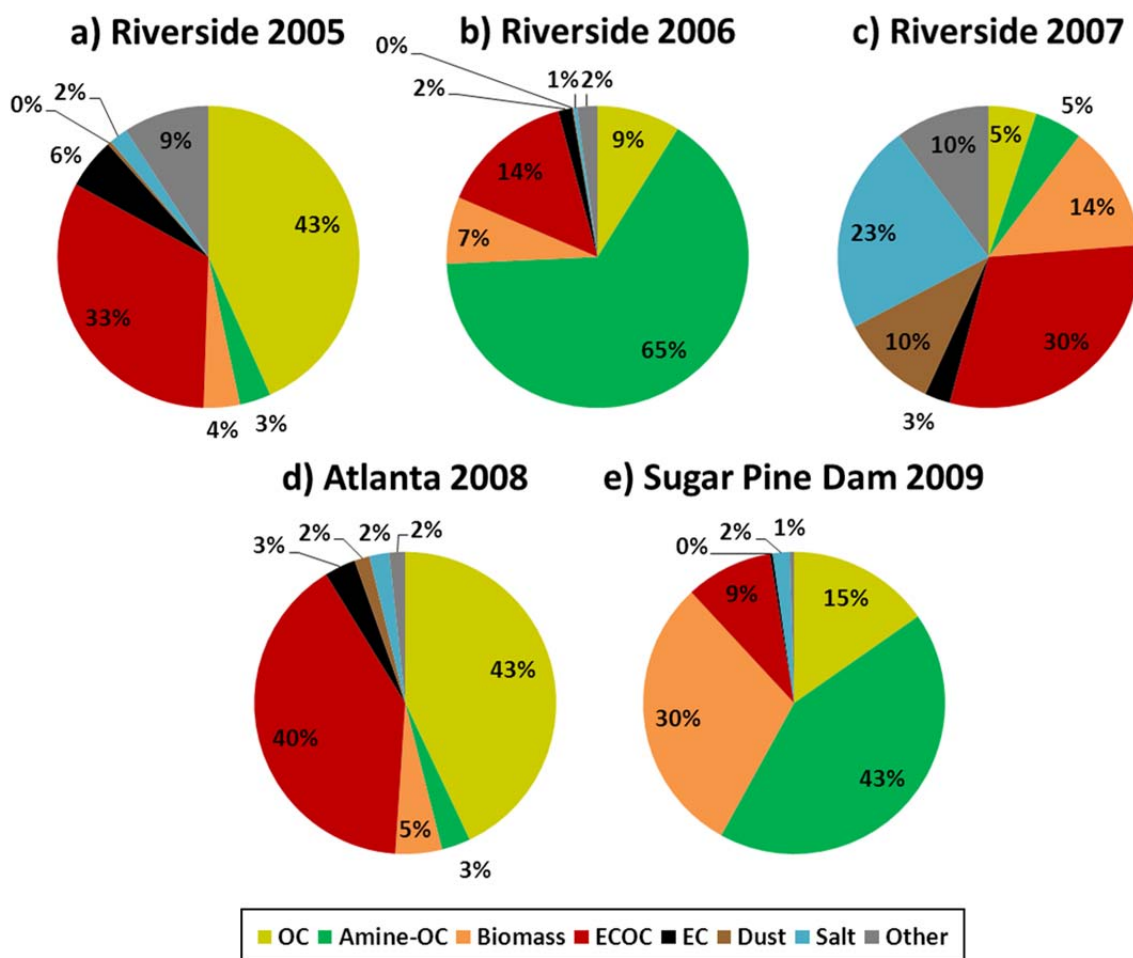


Figure 7.1 Overall ambient aerosol chemical composition at Riverside during the summers of a) 2005, b) 2006, and c) 2007, at Atlanta during the summer of 2008, and at Sugar Pine Dam during the winter of 2009.

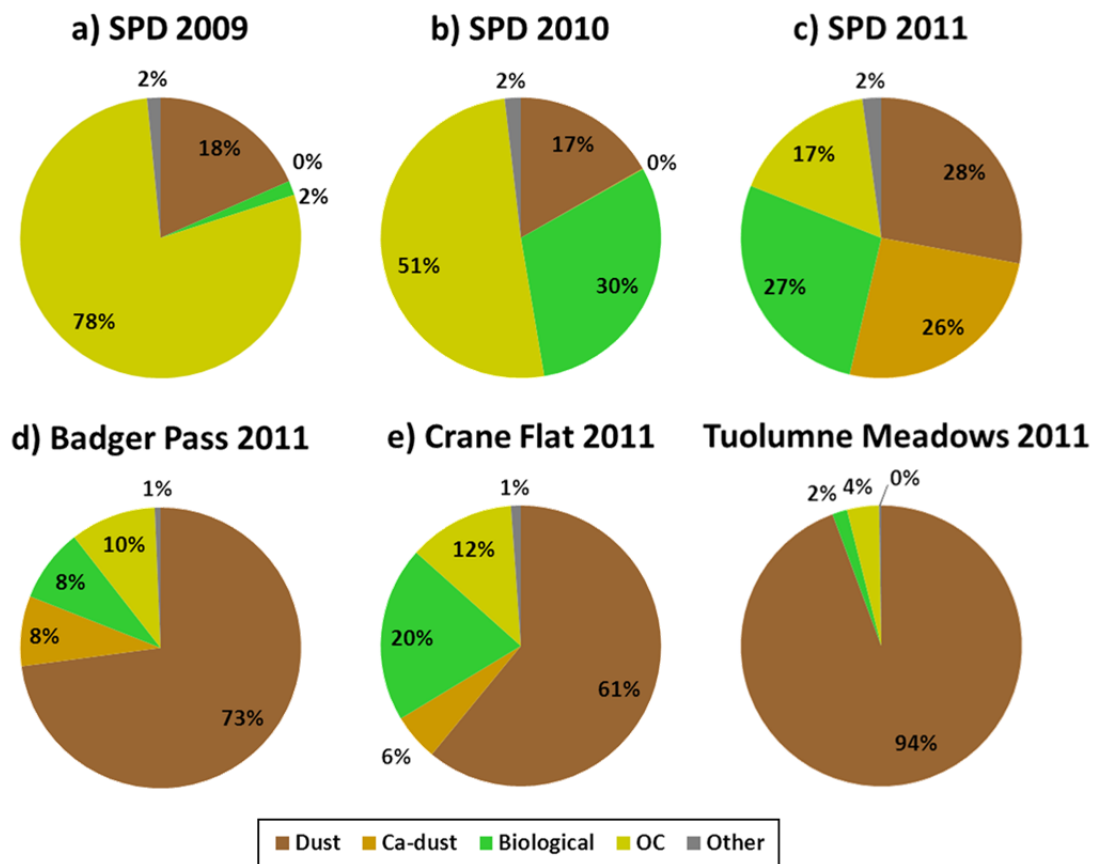


Figure 7.2 Pie graphs representing the overall chemical composition of the aerosols as insoluble residues in precipitation samples collected from SPD in a) 2009, b) 2010, and c) 2011 and at sites of variable elevation in Yosemite National Park in 2011 only, including d) Badger Pass, e) Crane Flat, and f) Tuolumne Meadows. Fractions of each type of residue represent the number of that type relative to the total number of residues analyzed.

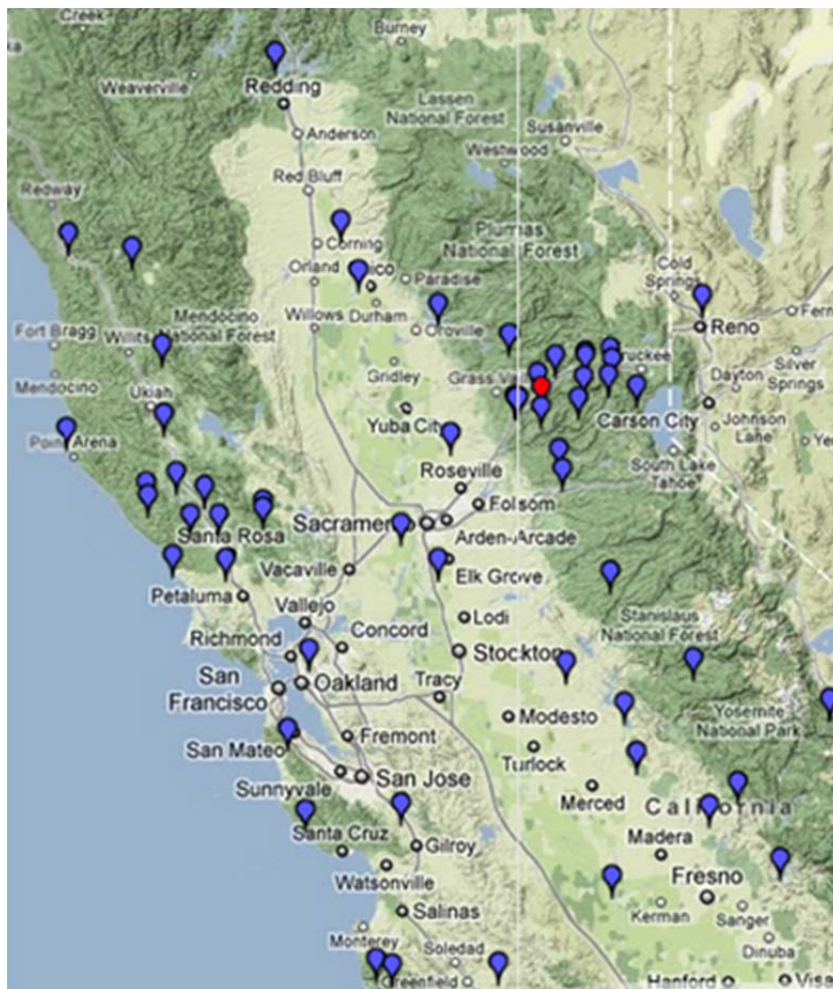


Figure 7.3 NOAA HMT-West sites in California. Site inventory list is provided at <http://www.esrl.noaa.gov/psd/data/obs/sites/>. The red marker shows the location of Sugar Pine Dam (SPD).

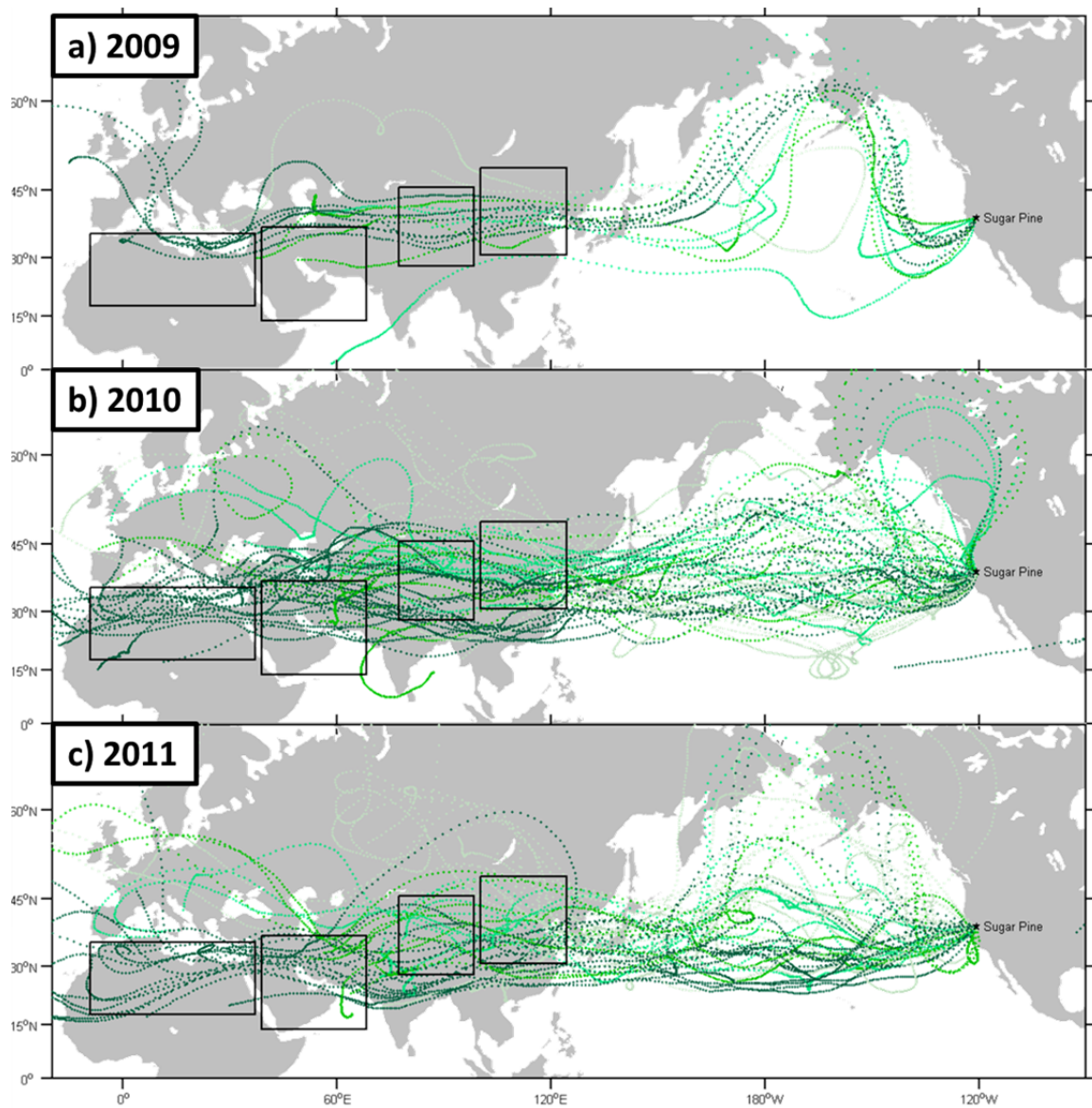


Figure 7.4 Air mass back trajectories calculated using HYSPLIT for every 3 hours during storm time periods within the a) 2009, b) 2010, and c) 2011 winter seasons of *CalWater*. The boxes highlight the major arid regions, including North Africa, the Middle East, the Taklimakan, and East Asia (includes Mongolia and Northeast China), shown in order from left to right.

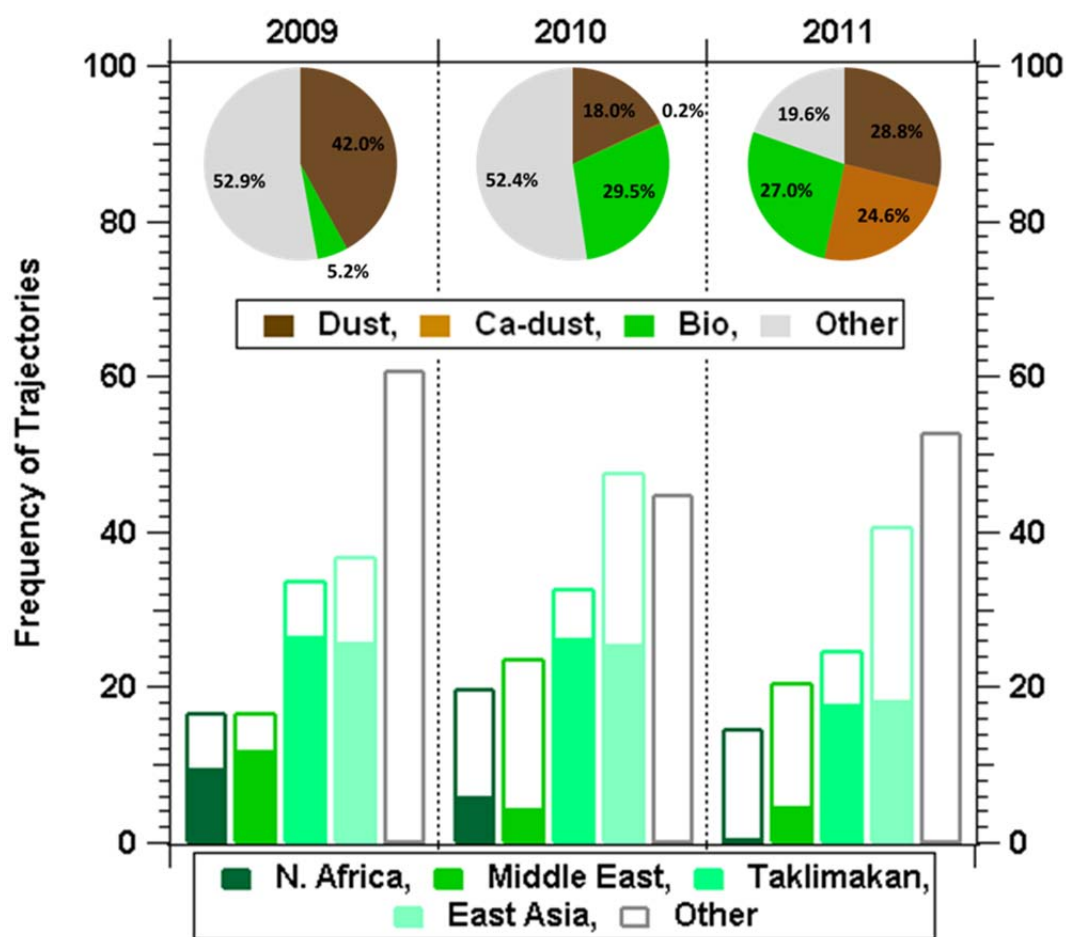


Figure 7.5 Simplified pie graphs of insoluble precipitation residues from the *CalWater* winter seasons. The bars represent the frequency of trajectories that traveled over each dust region presented in Chapter 5. The shaded portion of the bars represents the relative frequency of times a trajectory passed through a dust plume in each of the dust regions.

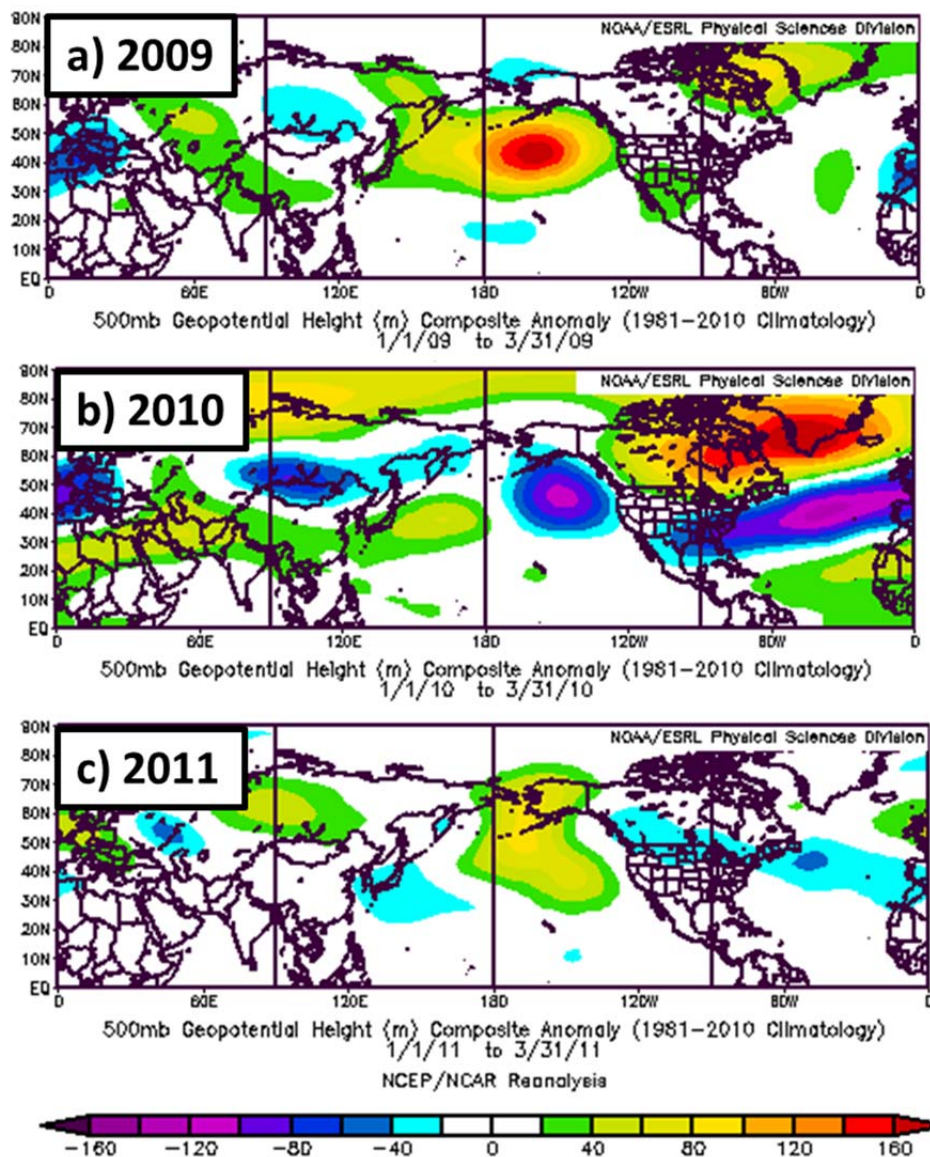


Figure 7.6 Geopotential height anomalies from Jan 1-Mar 31 during a) 2009, b) 2010, and c) 2011.

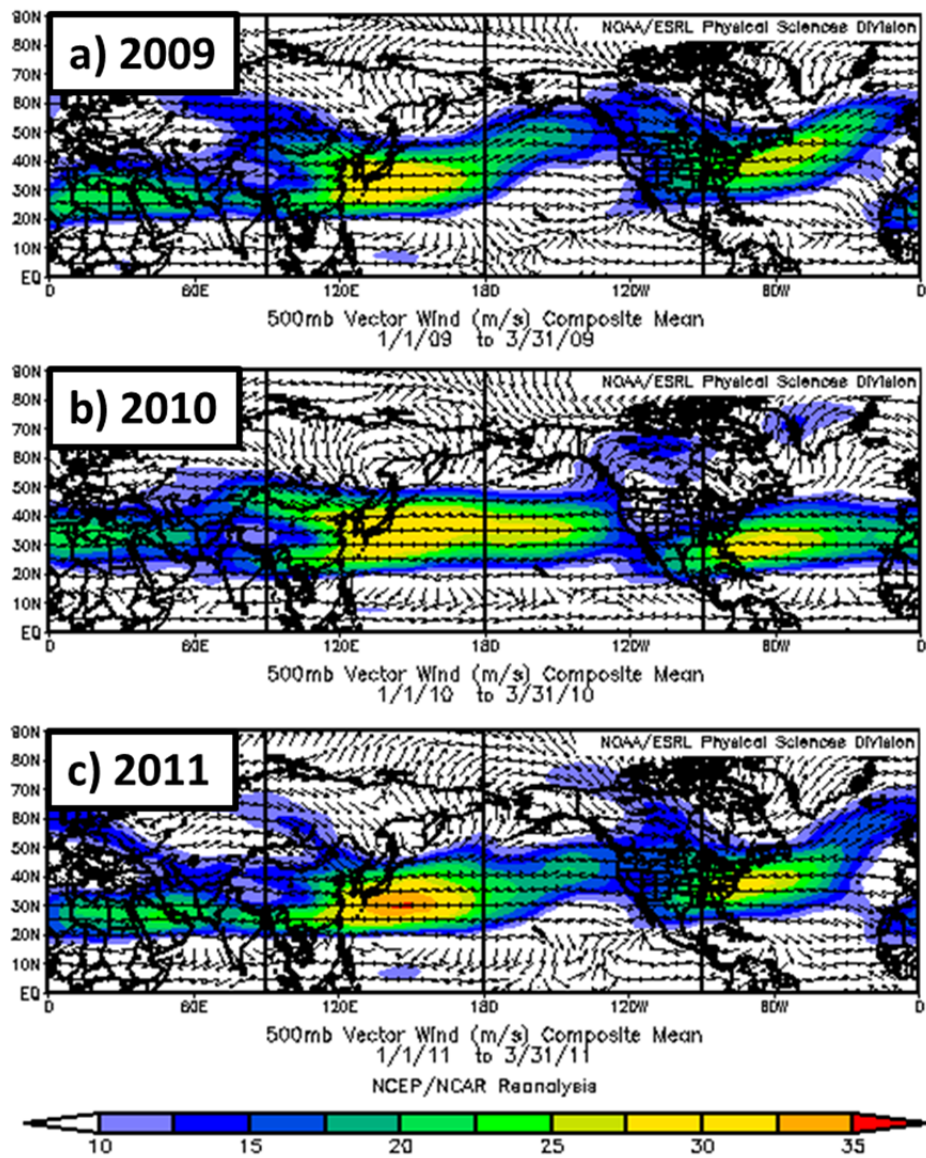


Figure 7.7 Mean wind speeds from Jan 1-Mar 31 during a) 2009, b) 2010, and c) 2011.

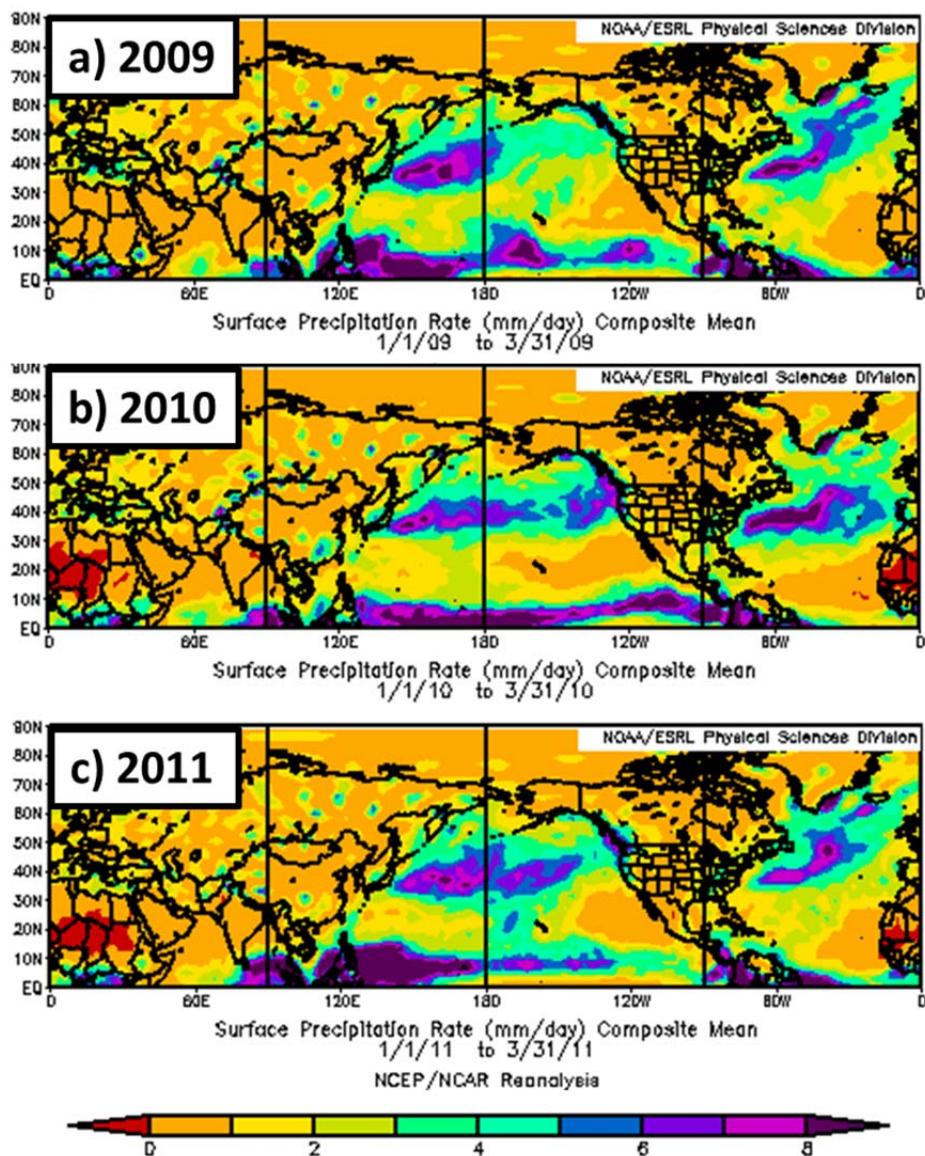


Figure 7.8 Mean precipitation rates from Jan 1-Mar 31 during a) 2009, b) 2010, and c) 2011.

7.6. References

Alston, E.J., I.N. Sokolik, and B.G. Doddridge, Investigation into the Use of Satellite Data in Aiding Characterization of Particulate Air Quality in the Atlanta, Georgia Metropolitan Area, *Journal of the Air & Waste Management Association*, 61 (2), 211-225, 2011.

- Andreae, M.O., and D. Rosenfeld, Aerosol-cloud-precipitation interactions. Part 1. The nature and sources of cloud-active aerosols, *Earth-Science Reviews*, 89 (1-2), 13-41, 2008.
- Ault, A.P., C.R. Williams, A.B. White, P.J. Neiman, J.M. Creamean, C.J. Gaston, F.M. Ralph, and K.A. Prather, Detection of Asian dust in California orographic precipitation *Journal of Geophysical Research-Atmospheres*, 116 (D16205), doi:10.1029/2010JD015351, 2011.
- Blanchard, C.L., G.M. Hidy, S. Tanenbaum, and E.S. Edgerton, NMOC, ozone, and organic aerosol in the southeastern United States, 1999-2007: 3. Origins of organic aerosol in Atlanta, Georgia, and surrounding areas, *Atmospheric Environment*, 45 (6), 1291-1302, 2011.
- Bzdek, B.R., D.P. Ridge, and M.V. Johnston, Size-dependent reactions of ammonium bisulphate clusters with dimethylamine, *J. Phys. Chem. A*, 114 (43), 11638-11644, 2010.
- Creamean, J.M., A.P. Ault, J.E. Ten Hoeve, M.Z. Jacobson, G.C. Roberts, and K.A. Prather, Measurements of Aerosol Chemistry during New Particle Formation Events at a Remote Rural Mountain Site, *Environmental Science & Technology*, 45 (19), 8208-8216, 2011.
- DeMott, P.J., A.J. Prenni, X. Liu, S.M. Kreidenweis, M.D. Petters, C.H. Twohy, M.S. Richardson, T. Eidhammer, and D.C. Rogers, Predicting global atmospheric ice nuclei distributions and their impacts on climate, *Proceedings of the National Academy of Sciences of the United States of America*, 107 (25), 11217-11222, 2010.
- Griffin, D.W., C.A. Kellogg, V.H. Garrison, and E.A. Shinn, The global transport of dust - An intercontinental river of dust, microorganisms and toxic chemicals flows through the Earth's atmosphere, *American Scientist*, 90 (3), 228-235, 2002.
- Hatch, L.E., J.M. Creamean, A.P. Ault, J.D. Surratt, M.N. Chan, J.H. Seinfeld, E.S. Edgerton, Y.X. Su, and K.A. Prather, Measurements of Isoprene-Derived Organosulfates in Ambient Aerosols by Aerosol Time-of-Flight Mass Spectrometry - Part 1: Single Particle Atmospheric Observations in Atlanta, *Environmental Science & Technology*, 45 (12), 5105-5111, 2011.
- Hua, N.P., F. Kobayashi, Y. Iwasaka, G.Y. Shi, and T. Naganuma, Detailed identification of desert-originated bacteria carried by Asian dust storms to Japan, *Aerobiologia*, 23 (4), 291-298, 2007.
- Kim, E., P.K. Hopke, and E.S. Edgerton, Improving source identification of Atlanta aerosol using temperature resolved carbon fractions in positive matrix factorization, *Atmospheric Environment*, 38 (20), 3349-3362, 2004.

- Leung, L.R., and Y. Qian, Atmospheric rivers induced heavy precipitation and flooding in the western US simulated by the WRF regional climate model, *Geophysical Research Letters*, 36, doi 10.1029/2008gl036445, 2009.
- Liu, D.Y., R.J. Wenzel, and K.A. Prather, Aerosol time-of-flight mass spectrometry during the Atlanta Supersite Experiment: 1. Measurements, *Journal of Geophysical Research-Atmospheres*, 108 (D7), -, 2003.
- Ortega, I.K., T. Kurten, H. Vehkamäki, and M. Kulmala, The role of ammonia in sulfuric acid ion induced nucleation, *Atmos. Chem. Phys.*, 8 (11), 2859-2867, 2008.
- Pierce, J.R., and P.J. Adams, Global evaluation of CCN formation by direct emission of sea salt and growth of ultrafine sea salt, *Journal of Geophysical Research-Atmospheres*, 111 (D6), -, 2006.
- Rosenfeld, D., Suppression of rain and snow by urban and industrial air pollution, *Science*, 287 (5459), 1793-1796, 2000.
- Rosenfeld, D., W.L. Woodley, D. Axisa, E. Freud, J.G. Hudson, and A. Givati, Aircraft measurements of the impacts of pollution aerosols on clouds and precipitation over the Sierra Nevada, *Journal of Geophysical Research-Atmospheres*, 113 (D15), 2008a.
- Rosenfeld, D., W.L. Woodley, D. Axisa, E. Freud, J.G. Hudson, and A. Givati, Aircraft measurements of the impacts of pollution aerosols on clouds and precipitation over the Sierra Nevada, *J. Geophys. Res.*, 113 (), D15203, doi:10.1029/2007JD00954, 2008b.
- Spracklen, D.V., K.S. Carslaw, M. Kulmala, V.M. Kerminen, S.L. Sihto, I. Riipinen, J. Merikanto, G.W. Mann, M.P. Chipperfield, A. Wiedensohler, W. Birmili, and H. Lihavainen, Contribution of particle formation to global cloud condensation nuclei concentrations, *Geophysical Research Letters*, 35 (6), 2008.
- Spracklen, D.V., K.S. Carslaw, U. Poschl, A. Rap, and P.M. Forster, Global cloud condensation nuclei influenced by carbonaceous combustion aerosol, *Atmospheric Chemistry and Physics*, 11 (17), 9067-9087, 2011.
- Turpin, B.J., and H.J. Lim, Origins of primary and secondary organic aerosol in Atlanta: Results' of time-resolved measurements during the Atlanta supersite experiment, *Environmental Science & Technology*, 36 (21), 4489-4496, 2002.
- Vedal, S., Ambient particles and health: Lines that divide, *Journal of the Air & Waste Management Association*, 47 (5), 551-581, 1997.

8. Appendix for Chapter 2

8.1. Figures

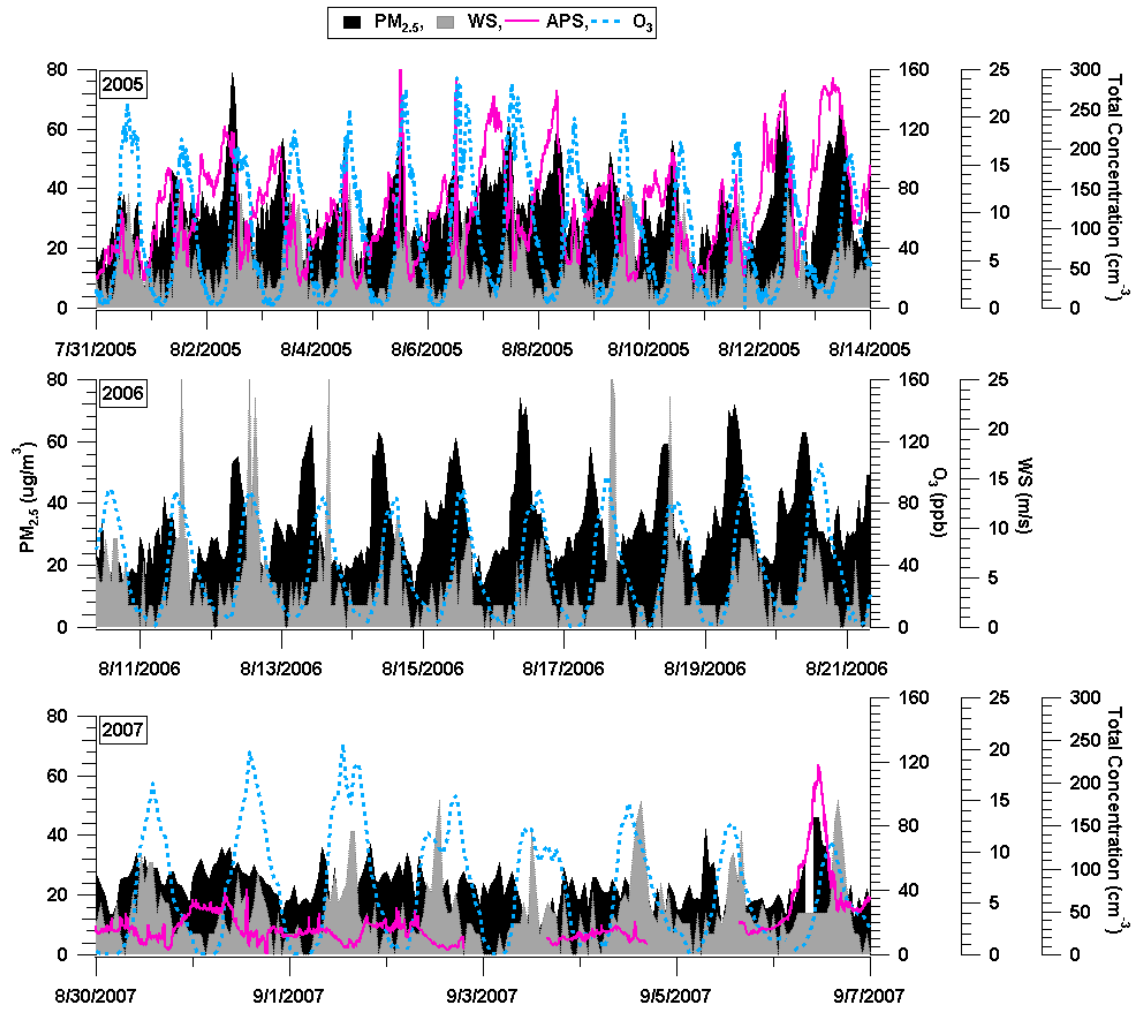


Figure 8.1 Hourly PM_{2.5} mass concentrations (μg/m³), gas-phase O₃ concentrations (ppb), wind speed (WS, m/s), and particle number concentrations (#/cm³) from 0.523-10 μm, as measured by an aerodynamic particle sizer (APS), for the summers of 2005-2007 in Riverside, CA. Particle number concentrations in this size range were not measured during 2006.

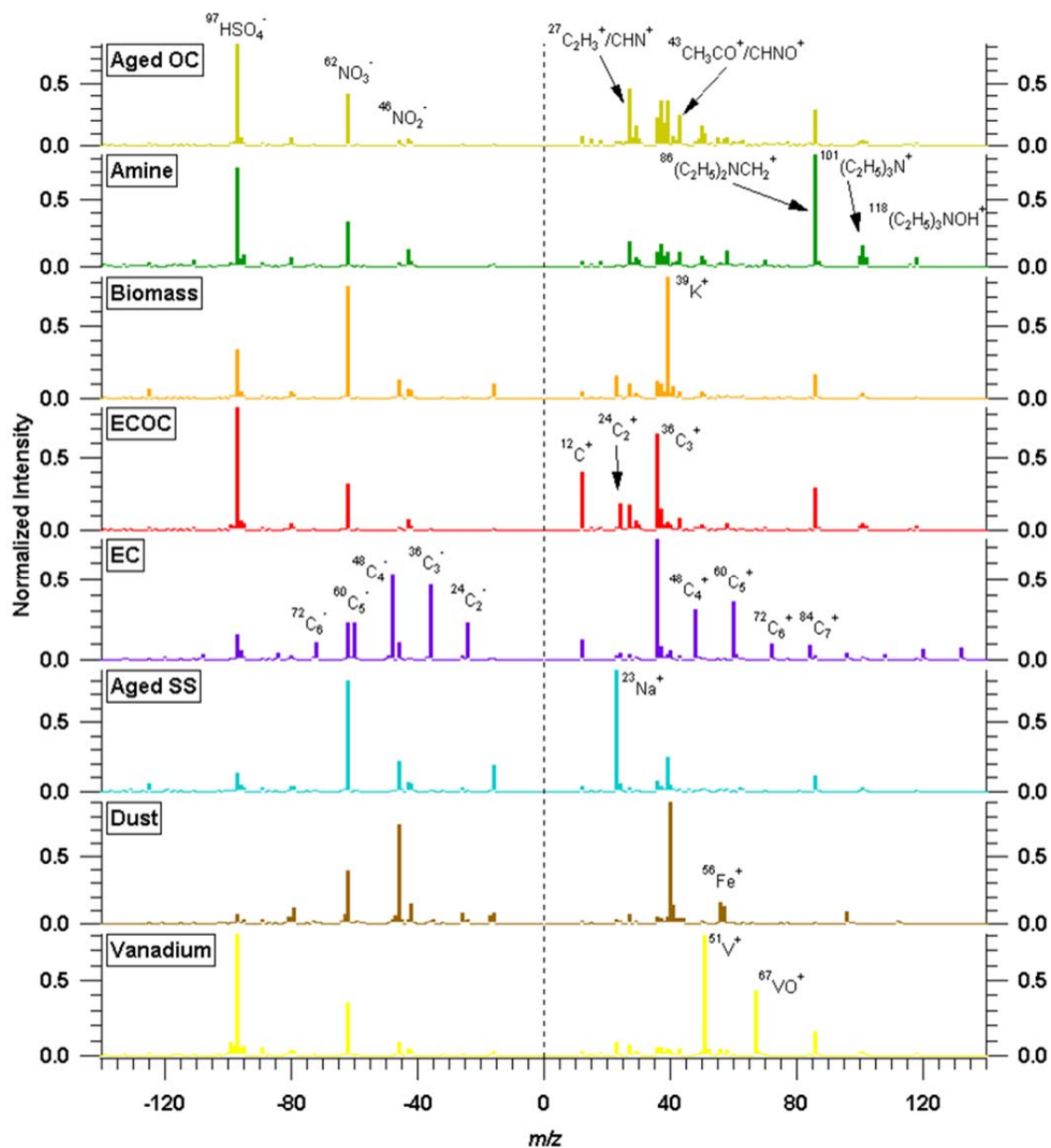


Figure 8.2 Representative mass spectra of the ATOFMS particle types in Riverside during the summers of 2005-2007 from the average of a cluster of each particle type. The particle types shown are not always mixed with the same negative ion species; the negative spectra shown are for reference of negative ion markers only.

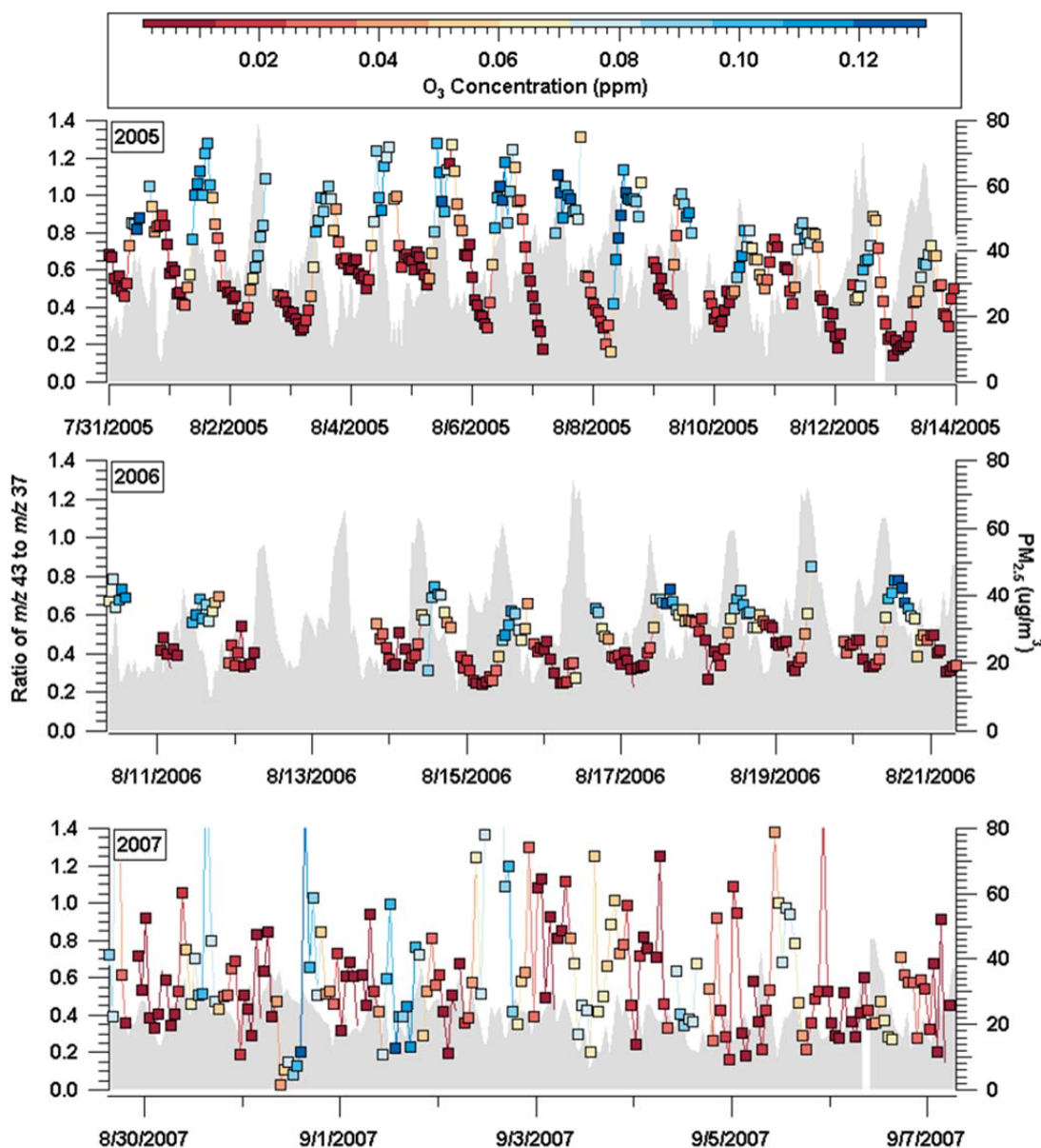


Figure 8.3 The ratio of the sum of peak areas m/z 43 ($C_2H_3O^+/CHNO^+$) to m/z 37 (C_3H^+) plotted as a function of O_3 concentration (ppm) from 2005-2007. Also pictured is the temporal profile of $PM_{2.5}$ mass concentrations ($\mu g/m^3$). The fact that this ratio is highest during the highest O_3 concentration (13:00-14:00) suggests that particles during this time are more aged with oxidized organics, potentially from oxidized organic gases that condense onto particles or heterogeneous reactions, versus being primary.

9. Appendix for Chapter 4

9.1. Supplemental Methods

9.1.1. Growth Rate Calculations

Growth rates (GRs) were calculated based on Kulmala *et al.* [2004], the most widely used method for estimating new particle GRs. GRs are calculated using Equation S1, where the mean diameter of the nucleation mode, D_m , increases over a time interval Δt and where D_m is defined by the size range $[D, D_{\max}]$ [Kulmala *et al.*, 2004].

$$GR = \frac{\Delta D_m}{\Delta t} \quad (9.1)$$

Figure 9.1 shows the increase in the mean diameters over time during the NPF event on 2/24. Linear regression lines were fit to these data for each NPF event. The slopes of the equations for these fitted lines represent the GRs per 5-minute interval (time per one SMPS scan). These GRs are then multiplied by twelve to obtain the calculated GR in nm/h. Table 9.1 shows the start and end mean sizes, the calculated GRs from the linear regression equations, and the time it would take using the regression equation to reach 100 nm.

As shown in Figure 9.1, the larger mean sizes did not reach 100 nm, therefore, growth to 100 nm was inferred based on the fitted linear regression equations. The calculated GRs are therefore upper limits of potential GRs because growth from the end sizes to 100 nm may not have been linear. In fact, GRs are only expected to be linear with particle diameter only during growth in the kinetic regime, which would be for particles smaller than approximately 76 nm at the elevation of Sugar Pine. However, this does not mean newly-formed particles did not reach 100 nm. The reason mean diameters did not reach 100 nm is potentially because the GR is calculated from one 5-minute SMPS scan, which includes measurement of the smallest sizes of particles currently being formed along with particles that were already formed and have continued to grow into larger

sizes. Qian [2003] also observed a small maximum mean diameter (~40 nm) during a regional nucleation event.

At the beginning of the events, growth for the smallest mean sizes (49-53 nm) was faster than the subsequent growth of the larger mean sizes (54-68 nm). The faster growth at the smallest sizes is potentially due to higher concentrations of precursors, while growth slows over time as the precursors are depleted [Clement *et al.*, 2002; Ehn *et al.*, 2010]. The discontinuity between the smallest and largest mean sizes (circled in Figure 9.1) is due to the bimodal size distribution during the NPF events. Before and after the events, the distribution contained one mode or was bimodal with lower number concentrations. Inferred GRs for each period, along with mean sizes and number concentrations for each sub-period (before, G1-G4, and end), are given in Table 9.2. It is important to note that the calculated GRs are estimates and there are uncertainties associated with calculating GRs using Equation 9.1 as explained in the manuscript. Because of these uncertainties and the extrapolation of the GRs from a linear regression, which may not be true for particle diameters greater than 76 nm as mentioned above, we emphasize our GRs are inferred upper limits for actual GRs.

9.2. Supplemental Results and Discussion

9.2.1. Size and Number Distributions of NPF

Two types of high particle concentrations were observed during the study at Sugar Pine and are differentiated in the SMPS data. The white areas in the SMPS data correspond to high particle concentrations related to either aged particle pollution or NPF events. The shape of the particle number concentrations, showing an increase over time, provides a distinction between these two cases: for the polluted period, high particle concentrations occurred over a larger size range (spot-like shape) with a consistent size distribution mode, while NPF events are characterized by a high concentrations at the smallest sizes (~11-15 nm, SMPS mode 16-40 nm) followed by an immediate increase in number concentrations of larger sizes (~25-50 nm) and then an increase in number concentration at even larger sizes (~70-100 nm) towards the end of the events. Higher

concentrations at larger sizes (~25-50 nm) are present immediately after the start of the event likely from the newly-formed particles rapidly growing to these sizes. This results in the smooth growth of smaller, newly-formed particles to larger sizes by condensation, heterogeneous reactions, and coagulation (less efficient when particles are the same size) processes during NPF events [Dal Maso et al., 2002; Modini et al., 2009; Seinfeld and Pandis, 2006], as depicted in Figure 9.2 from the NPF event on 2/25 during P1.

9.2.2. Black Carbon Measurements

BC peaked daily (16:00-19:00) during both NPF periods, with P1 averaging ($101.4 \pm 7.4 \text{ ng/m}^3$) and P2 averaging ($185.4 \pm 13.0 \text{ ng/m}^3$). The late afternoon increase in BC during both NPF periods can be attributed to the transport and advection of emissions from the CV [Lunden et al., 2006a] during the upslope/downslope conditions. A transport time of ~7 hours was previously calculated for an air parcel to arrive from Sacramento in the CV to Blodgett [Lunden et al., 2006a]. On this timescale, any ultrafine particles emitted from combustion sources [Bukowiecki et al., 2002] would be atmospherically processed into larger sizes during transport and would not contribute to high particle concentrations at the smallest sizes observed during the beginning of NPF at Sugar Pine. BC concentrations for P2 were almost twice those during P1, suggesting a stronger anthropogenic influence for P2.

9.2.3. Classifications of Major Ambient Particle Types

In addition to the amine-OC particle types, there were other major ambient particle types observed at Sugar Pine, including biomass, aged OC, EC, ECOC, and salts. Biomass particles contained potassium (m/z 39) with less intense carbonaceous positive ions [Qin and Prather, 2006a]. The aged OC type contained major carbonaceous ion markers at $^{12}\text{C}^+$, $^{27}\text{C}_2\text{H}_3^+/\text{CHN}^+$, $^{29}\text{C}_2\text{H}_5^+$, $^{36}\text{C}_3^+$, $^{37}\text{C}_3\text{H}^+$, $^{39}\text{C}_3\text{H}_3^+$, $^{43}\text{CH}_3\text{CO}^+/\text{CHNO}^+$, and other minor organic fragments [Spencer and Prather, 2006]. EC particles contained carbon cluster positive ions ($^{12}\text{C}_1^+$, $^{24}\text{C}_2^+$, ..., C_n^+) and negative ions ($^{12}\text{C}_1^-$, $^{24}\text{C}_2^-$, ..., C_n^-), while ECOC particles contained carbon cluster positive ions ($^{12}\text{C}_1^+$, $^{24}\text{C}_2^+$, ..., C_n^+), in addition to low intensity OC and amine ions [Moffet et al., 2008]. Salt types had intense

$^{39}\text{K}^+$, sodium ($^{23}\text{Na}^+$), sodium chlorine clusters ($^{81/83}\text{Na}_2\text{Cl}^+$) and minor organic fragments. Representative mass spectra for each of the major particles types are pictured in Figure 9.3. The main mass spectral signatures used to classify each type are labeled in the spectra. Other species may be present in the particles (not pictured); for instance, less intense amine markers may be present on aged OC, ECOC, or the biomass particle types. Also, each particle type may contain different negative ion species than pictured; however, common negative ion markers are shown for reference. The major particle types were mainly mixed with nitrate ($^{46}\text{NO}_2^-$ and $^{62}\text{NO}_3^-$), sulfate ($^{97}\text{HSO}_4^-$), and/or other smaller negative carbonaceous ion markers suggesting the particles containing these species were aged.

9.2.4. Size Distributions of Amine-OC Particle Types during NPF Events

Not only did the fraction of amine-OC particles increase during NPF growth sub-periods, the number size distributions of amine-OC-type particles shifted throughout the events. Figure 9.4 shows the size distributions of the amine-OC-type particles from before events, G1-G4, and end of events from 100-600 nm averaged over the first NPF period. The particle transmission efficiency for the UF-ATOFMS is highest at ~290 nm (~47%) and only ~0.5% at 95 nm [*Su et al., 2004*], which can explain why particles close to 100 nm are not observed during NPF. However, differences still exist in the size distribution modes during the NPF sub-periods and suggest amines played a role in particle growth. Before the events (red), the number of amine-OC particles was low and the distribution was widely spread out over the size range, which is attributed to background amine-containing particles. During G1 (orange), the number of amine-OC particles increased, particularly at smaller sizes as seen by the narrower size distribution mode around 280 nm. G2 (yellow) is similar to G1, but with a higher number of amine-OC particles at 280 nm. The size distribution mode shifts to 310 nm during G3 (green); suggesting particles grew to larger sizes. A wider distribution was observed during G4 (blue) and at the end of NPF events (purple). Although background amine-OC particles may be present during NPF sub-periods, these distributions suggest a larger number of amine-OC particles at smaller sizes were present during the initial growth sub-periods

compared to before NPF events, and the shift in size mode suggests particles were smaller during the initial growth sub-periods and grew throughout the duration of the NPF events.

9.2.5. Increases in Amine Species on Ambient Particles

Decreases in particle number towards the end of NPF events suggest particle coagulation occurred [Dal Maso et al., 2002]. To verify this, we examined the evolution of single-particle mass spectra to see if a change in the fraction of particles mixed with amine species occurred over time. We were able to determine what types of particles within the UF-ATOFMS size range were coagulating with newly-formed amine-containing particles based on increases in the area of the amine species marker (m/z 86) on different particle types. Digital color histograms of major particle types: Aged OC, biomass, ECOC, EC, and salts were compiled from before, the beginning, and the end of each NPF event. Digital color histograms have been previously used and provide valuable information on the mass spectral characteristics and the chemical associations for different particle types over various periods of time [Qin and Prather, 2006a]. An example of the evolution of the histograms for aged OC during the event on 2/24 is given in

Figure 9.5, with a) larger particles before the event, b) smaller, fresher particles before the event, c) all sizes during the beginning of the event, and d) all sizes during the end of the event. The y-axis of each histogram represents the fraction of particles for a given particle type that contain an ion with a peak area within a particular range at each m/z given in the legend. Before the events, larger particles (300-1000 nm) contained more m/z 86 than the “fresh” smaller particles (100-300 nm), suggesting these particles were highly aged and were from the previous day (i.e. 2/23). Altogether, the evolution of the aged OC particles show increases in m/z 86, suggesting these particles coagulated with the small, newly-formed amine-containing particles.

9.2.6. Analysis of Absolute Peak Areas of Key Spectral Markers

It is important not only to study the number of amine-containing particles present during NPF events, but also to investigate the amount of amine species present on particles during these events. By knowing the amount of certain species in particles during NPF events, we can determine whether these species increased due to particle growth. Absolute area can provide insight into the amount of species present throughout the NPF events [Bhave *et al.*, 2002a]. The average area for a given collection of particles of like composition (herein known as just the average area) during a particular time resolution reduces errors and can be used to study trends [Pratt *et al.*, 2009c]. Figure 9.6 shows the average areas for m/z 86 and m/z -97. Both markers generally increased over the course of the NPF events, suggesting these species were involved in the growth of the newly-formed particles.

Amine and sulfate ion markers also exhibited differences between the two NPF periods: both the average area of particles containing m/z 86 and m/z -97 were much higher during P2. Interestingly, higher relative concentrations of SO_2 occurred during P2 compared to P1. The average area and number of particles containing m/z -97 were both ~ 4 times higher during P2 compared to P1, which can be attributed to the higher SO_2 concentrations potentially leading to more sulfate. The m/z 86 also increased in average area during P2 to 4 times that of P1. Amines are strong bases, and thus it is likely more amine-containing particles were observed with higher average areas of m/z 86 to neutralize the acidic aerosol during P2 [Pratt *et al.*, 2009c]. The average area of the non-neutralized sulfate ion marker (m/z -195, $\text{H}_2\text{SO}_4\text{HSO}_4^-$) [Pratt *et al.*, 2009c] increased by a factor of ~ 2 between P1 and P2; therefore, most of the H_2SO_4 was indeed neutralized by amine species to form amine-sulfate salts, as cited in the manuscript. Recall that the upper limit for GRs during P2 were higher on average. We speculate this is due to potentially more gas-phase amines and H_2SO_4 present during P2 and the tendency of low-volatility amines to partition to the particle phase and form aminium sulfate salts with H_2SO_4 [Pratt *et al.*, 2009c].

9.2.7. SO_2 Source Determination

The Lagrangian particle dispersion model FLEXPART [Stohl *et al.*, 1998] version 8.1 was run with NOAA Global Forecast System $0.5^\circ \times 0.5^\circ$ global data at 26 levels using Sugar Pine as the point source for 7-day backward air mass trajectory calculations using the cluster analysis feature. Analyses at 0000, 0600, 1200, and 1800 UTC and forecasts at 0300, 0900, 1500, and 2100 UTC were used. Calculations with releases of 400-500 particles were conducted at times corresponding to increases in SO_2 each day from 500, 1000, 2000, and 4000 m. Tu *et al.* [2004] previously observed SO_2 -enhanced layers between 2000-4000 m over the Central Pacific during transport to the Western United States, therefore, we focused on the 2000 and 4000 m trajectories. Figure 9.7 shows the 7-day FLEXPART back trajectories for each day corresponding to an NPF event. On most of the NPF days, air masses typically traveled from over the ocean directly west of the site. However, during P2, air masses were transported from over Asia to the site, particularly at the higher altitudes (2000 and 4000 m). Throughout the study period, a large high-pressure system was located approximately between 170°E and 130°W , influencing the trajectory pattern during 3/6 and 3/7 where air masses traveled up near Alaska into Canada, ultimately arriving from north of the site. Back trajectories followed this transport pattern only during this time period (P2) and suggest the high SO_2 concentrations are potentially transported long-range from Asia. These simulations are supported by satellite observations of SO_2 discussed below.

Figure 9.8 shows vertically-integrated SO_2 values estimated from backscattered radiances detected by the Ozone Monitoring Instrument (OMI) onboard the Aura satellite for the days of and leading up to P2 during the highest observed SO_2 concentrations. The OMI sensor can only detect SO_2 column concentrations, and so a comparison to SO_2 surface concentrations measured at the site is not possible. However, Figure 9.8 suggests that a plume of SO_2 did transport across the Pacific Ocean and may have contributed to the higher SO_2 concentrations during NPF P2. The data presented are from the Level 2 Version 3 OMSO2G product [Krotkov *et al.*, 2008; Krotkov *et al.*, 2006], specifically for the lower troposphere (0-5 km). Values are reported in units of Dobson Units (DU). Missing data are the result of coverage gaps in the orbital path, pixels with optically thick clouds, “poor” quality data, as well as row anomalies resulting from an instrument error

with the onboard charged coupled device. We also averaged the $0.125^\circ \times 0.125^\circ$ data to a resolution of $0.5^\circ \times 0.5^\circ$ for better visualization.

The SO₂ plume is traced from East Asia, across the Pacific Ocean, and eventually over the Western United States. Long-range transport of SO₂ is possible in clear skies absent of clouds. The e-folding lifetime of gas-phase oxidation of SO₂ to HSO₃ by the hydroxyl radical at a concentration of 5×10^5 molecules/cm³ is about 26 days, which is sufficiently enough time for the long-range transport of SO₂ [Jacobson, 2005]. In the presence of clouds, however, the e-folding lifetime reduces to tens of minutes. The large high-pressure system between 170°E and 130°W moved eastward with the SO₂ plume, providing the clear skies and dry conditions needed to inhibit aqueous conversion of SO₂. The SO₂ plume followed the high pressure streamlines, moving northward near the Aleutian Islands, and then dipping southward over the California coast. Long-range transport of SO₂ over the Pacific has also been observed by aircraft, and has been linked to volcanic and anthropogenic sources in East Asia [Tu *et al.*, 2004]. The fact that Tu *et al.* [2004] observed a dense SO₂ layer between 2000 and 4000 m justifies our choice of using the lower-troposphere OMI SO₂ model. In fact, when the mid-troposphere OMI SO₂ model was used (5000-10000 m), lower vertically-integrated SO₂ values were found, suggesting that SO₂ was primarily in the mid to lower troposphere between 2/26 and 3/09.

9.3. Figures

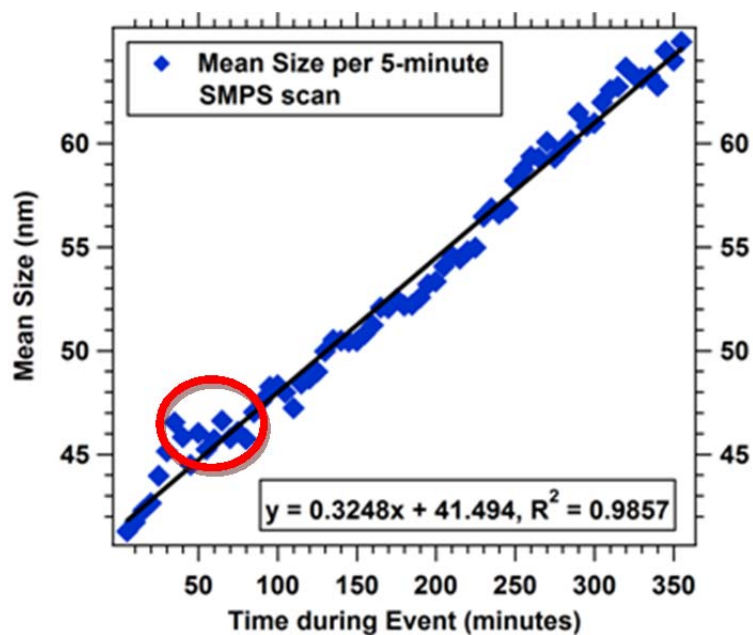


Figure 9.1 Particle mean diameters plotted from the event on 2/24. The fitted line is pictured and the slope of the equation for this line represents the estimated GR. The red circle highlights the discontinuity between the smallest and largest mean sizes.

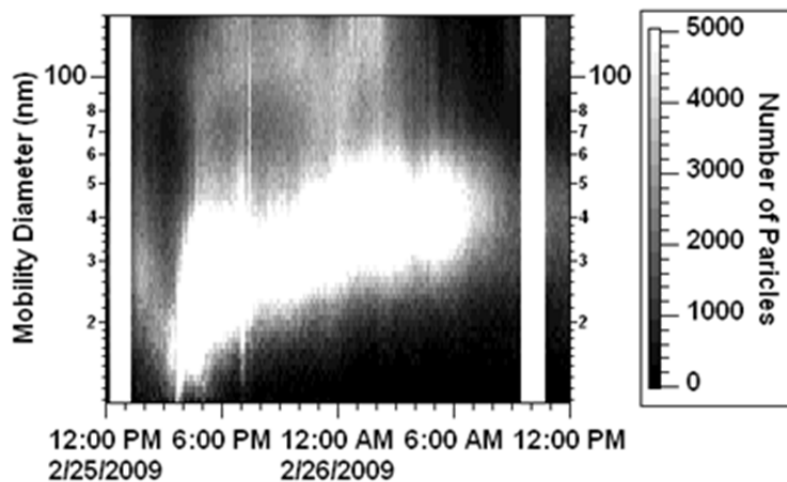


Figure 9.2 SMPS size distribution of an NPF event (2/25 of the current study). The shading represents the number concentrations of particles for each size bin.

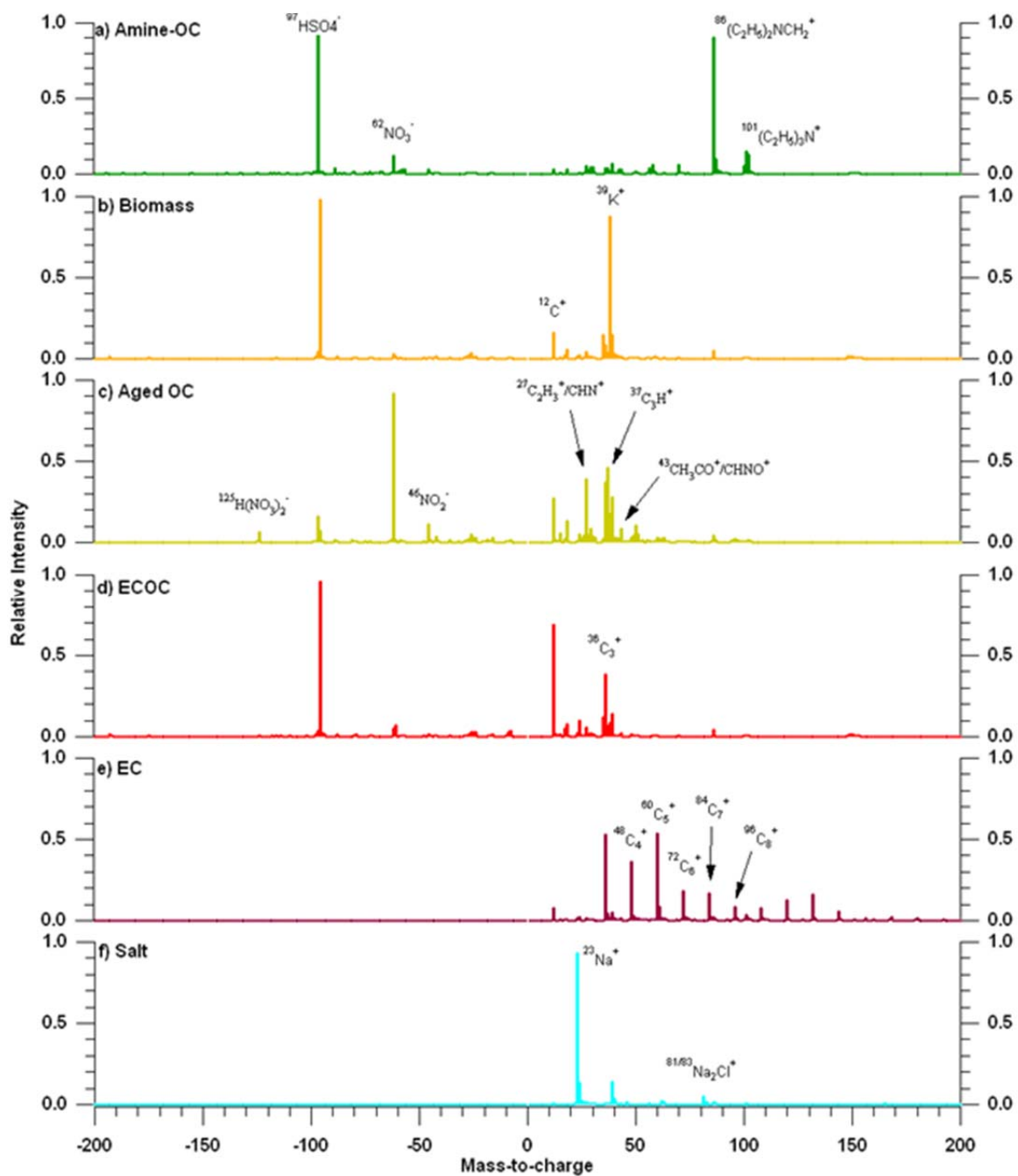


Figure 9.3 Representative mass spectra of the major UF-ATOFMS particle types present at Sugar Pine, which included: a) amine-OC, b) biomass, c) aged OC, d) ECOC, e) EC, and f) salt particle types.

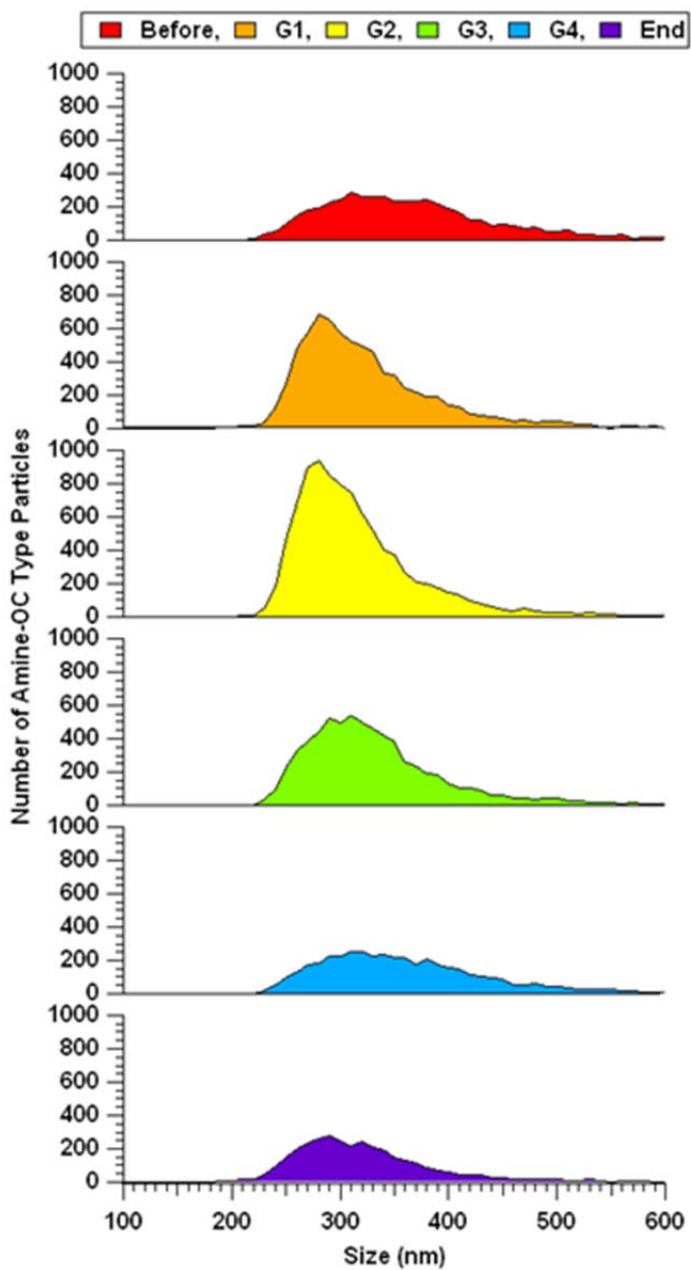


Figure 9.4 UF-ATOFMS size distributions of amine-OC particle types from 100-600 nm during the NPF sub-periods. Values are given in number of amine-OC particle types per 10-nm size bin.

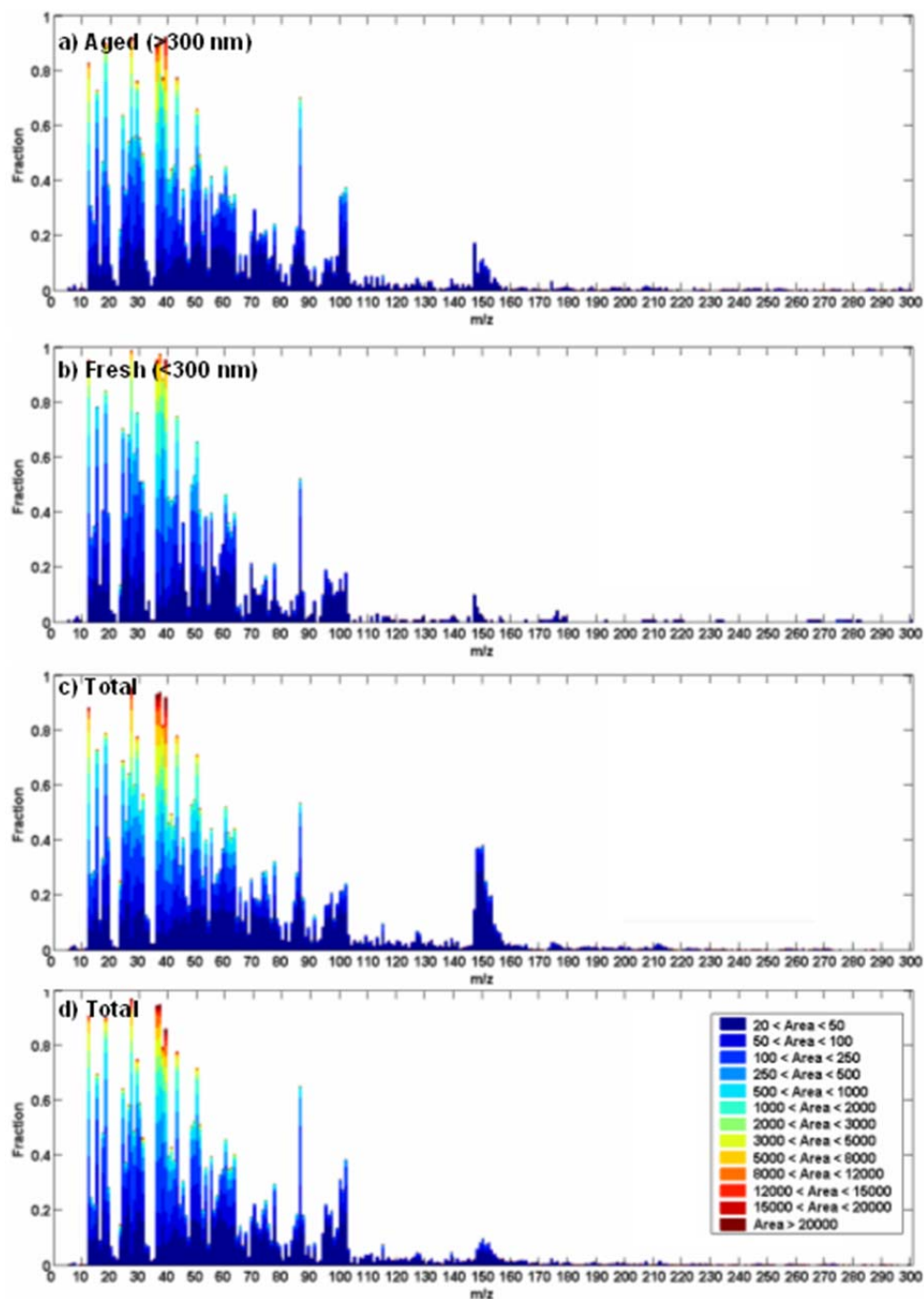


Figure 9.5 Digital color histograms from the NPF event on 2/24 from a) before the event at larger sizes (300-1000 nm), b) before the event at smaller sizes (100-300 nm), c) during the beginning of the event at all sizes (100 -1000 nm), and d) during the end of the event at all sizes.

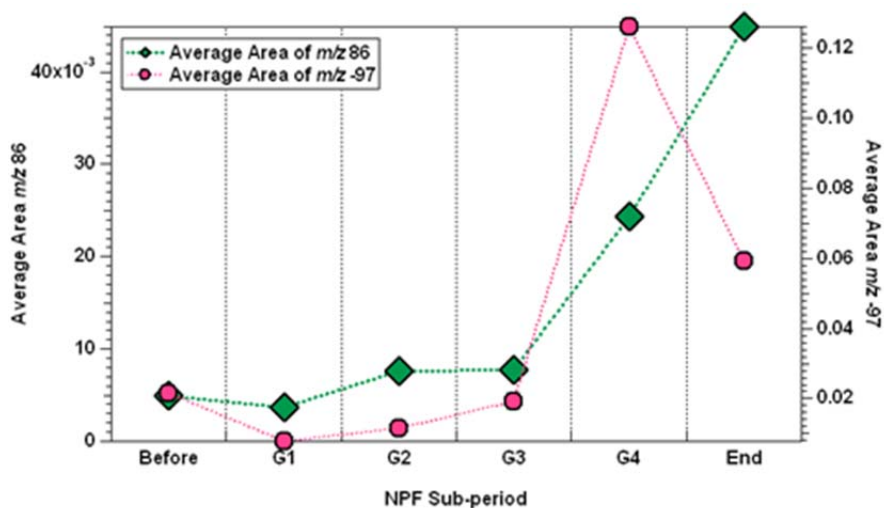


Figure 9.6 The areas of m/z 86 and m/z -97 during each sub-period, which were averaged over the first NPF period.

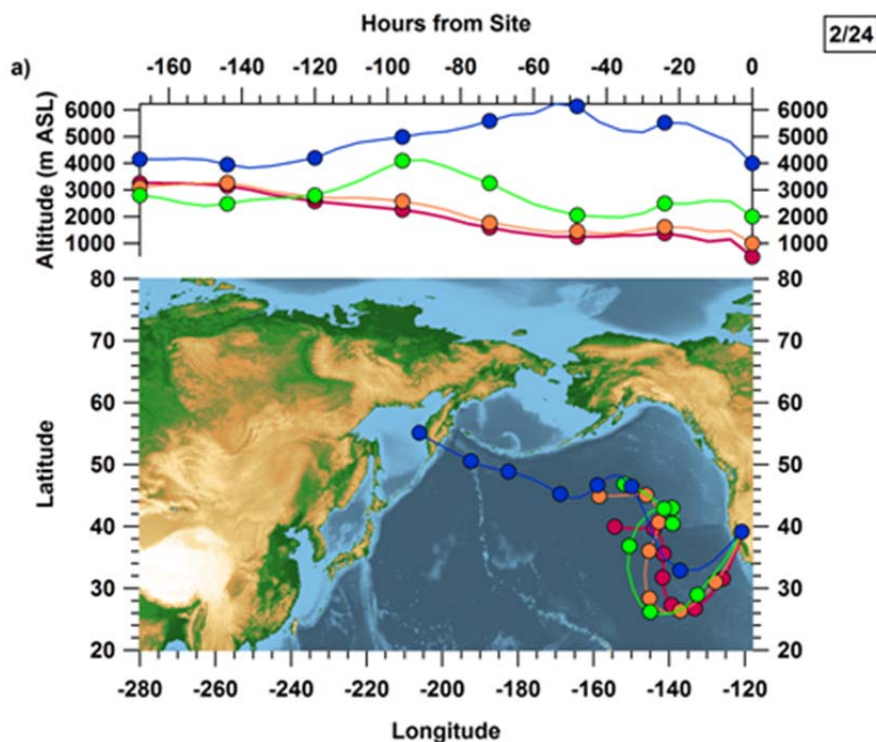


Figure 9.7 Back trajectories calculated using FLEXPART for each day corresponding to an NPF event. Trajectories plotted by release height for 500, 1000, 2000, and 4000 m plotted by altitude and latitude and longitude over time are shown in a), b), c), d), e), and f) for 2/24, 2/25, 2/26, 2/27, 3/6, and 3/7, respectively. Simulation start times corresponded to when SO_2 started to increase before each NPF event: 10:00 (2/23), 19:00 (2/24), 19:00 (2/25), 1:00 (2/27), 19:00 (3/5), and 19:00 (3/6) in PST.

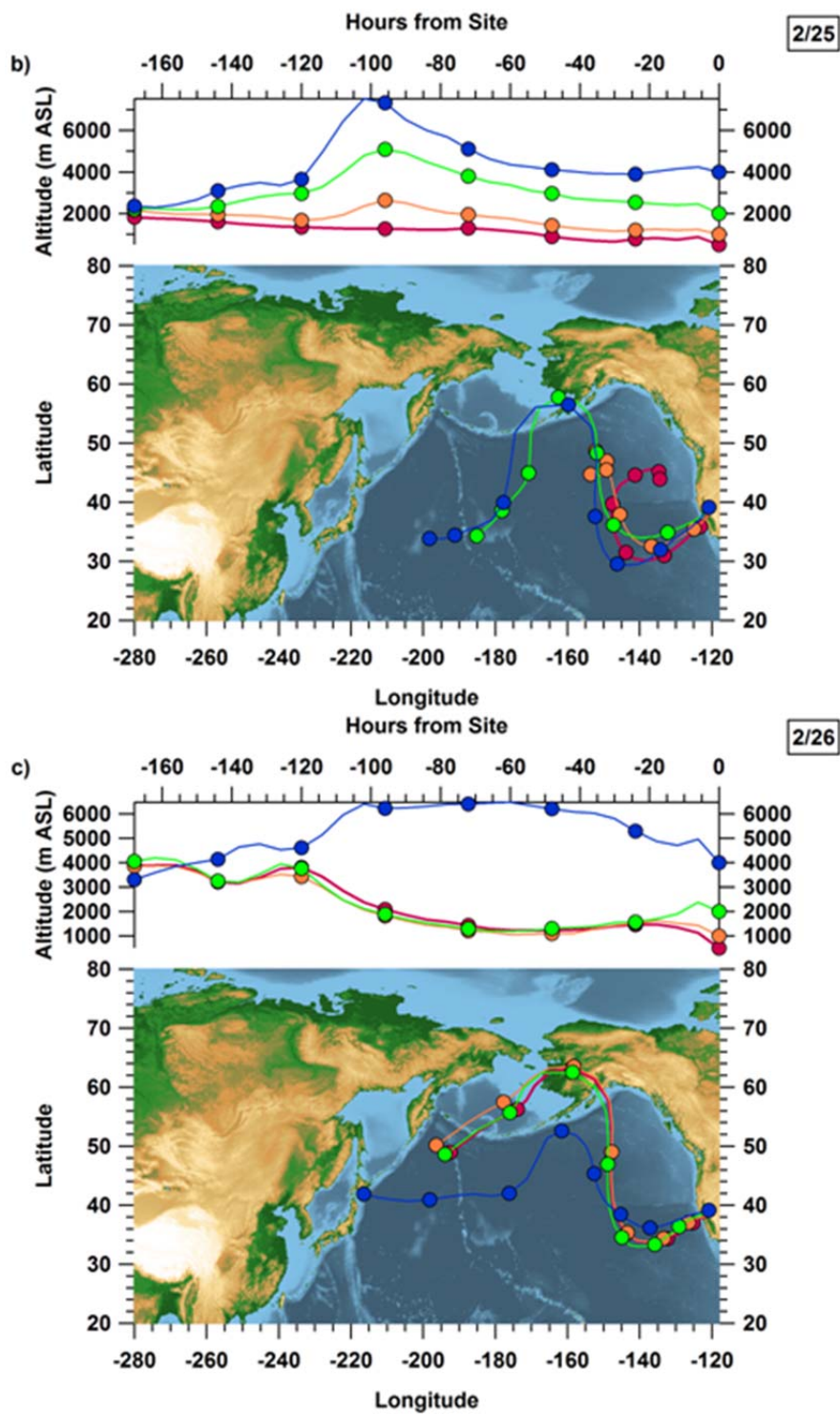


Figure 9.7 continued.

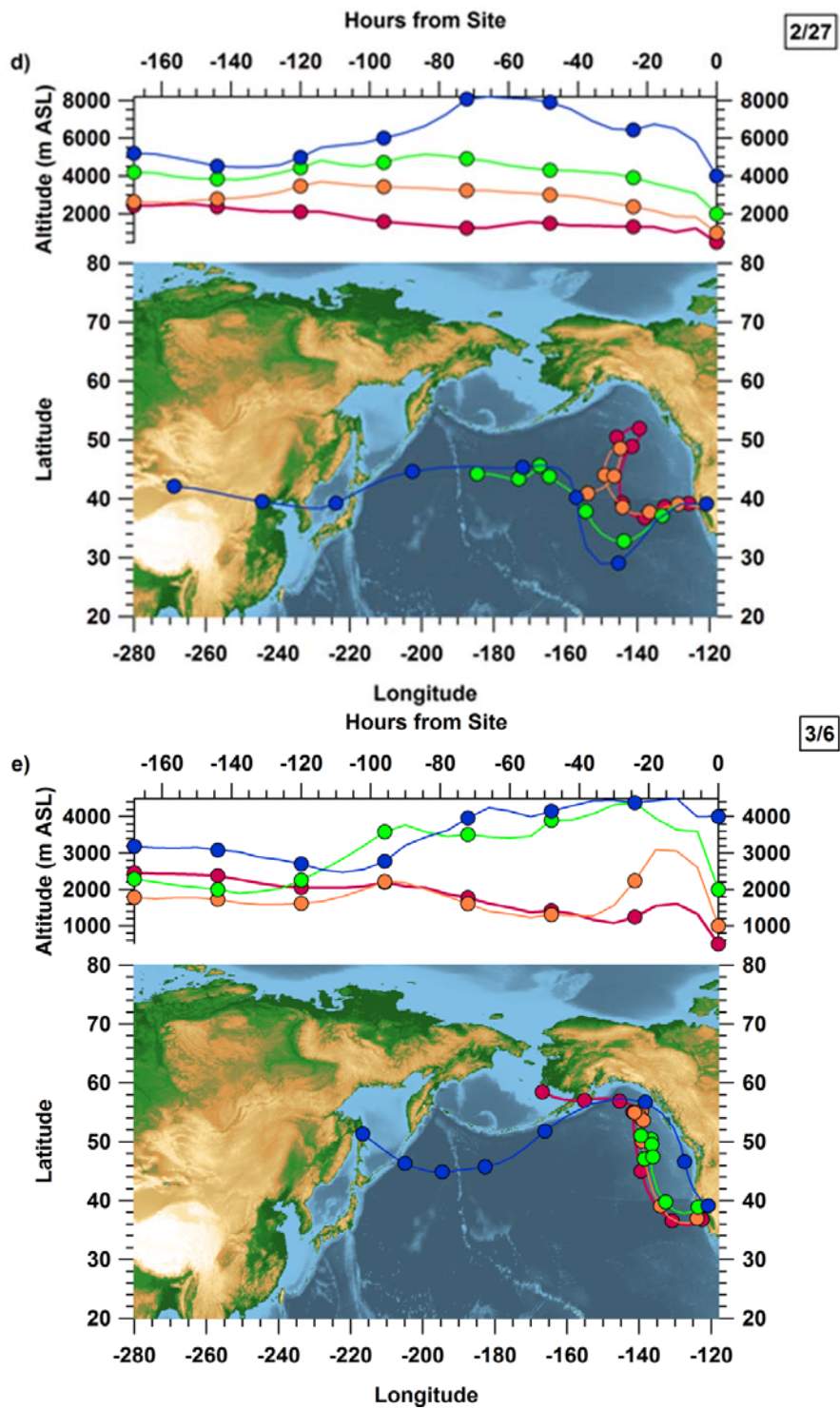


Figure 9.7 continued.

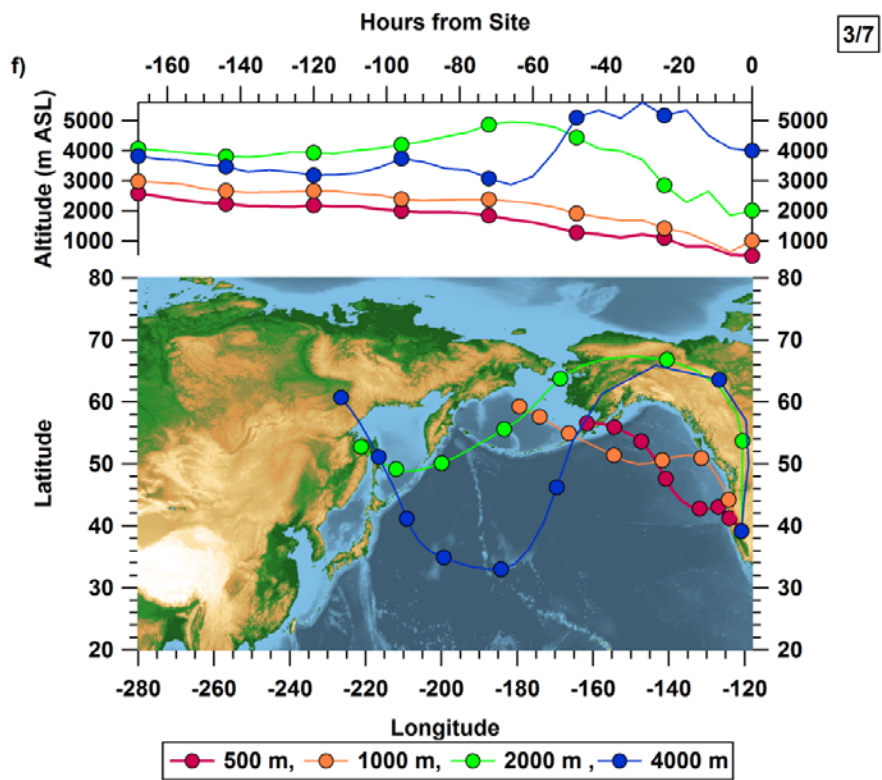


Figure 9.7 continued.

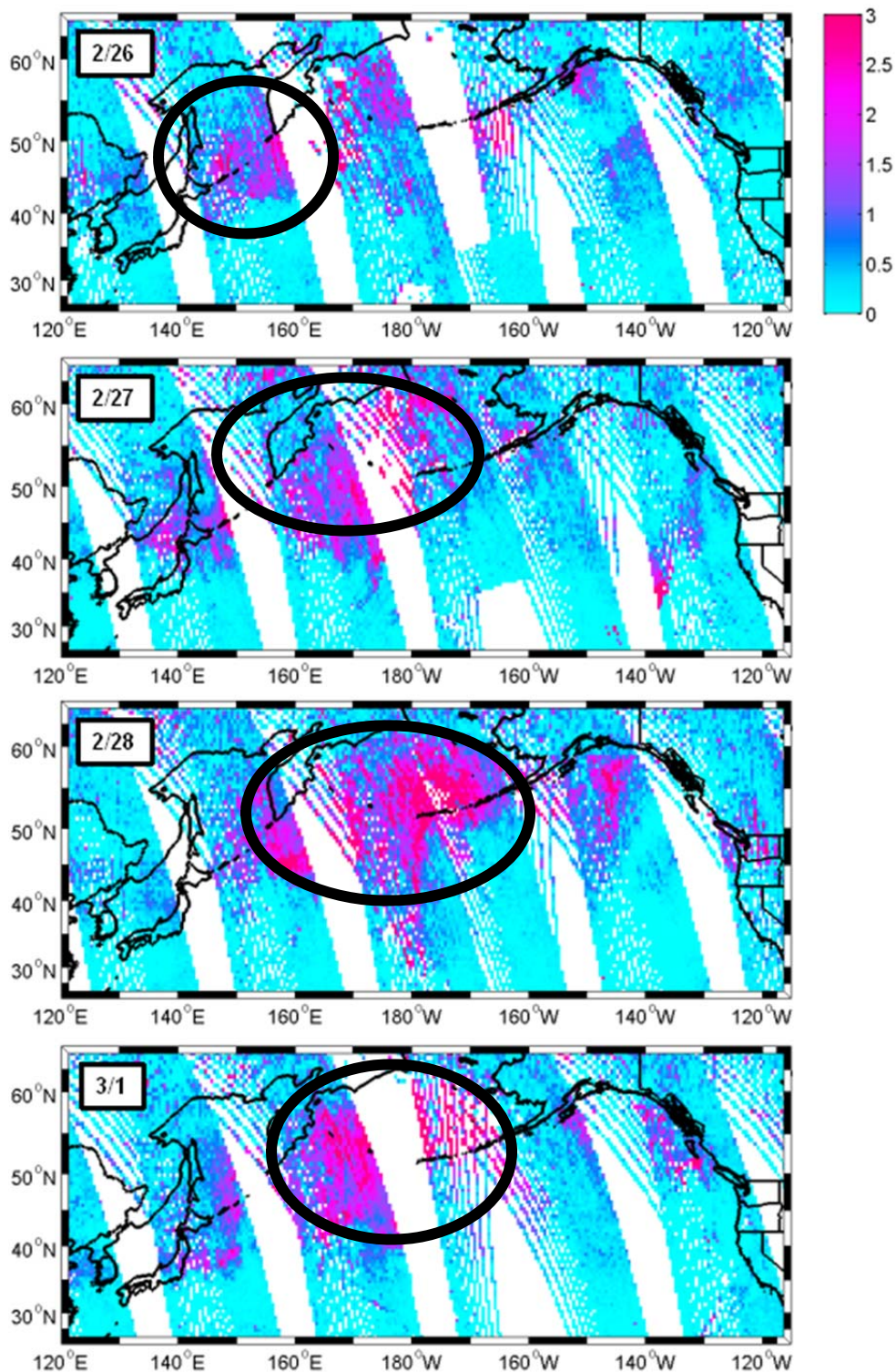


Figure 9.8 OMI images during the days of SO₂ transport including the day following P2, when SO₂ returned to background levels. The black circles illustrate the evolution of the long-range trans-Pacific SO₂ plume.

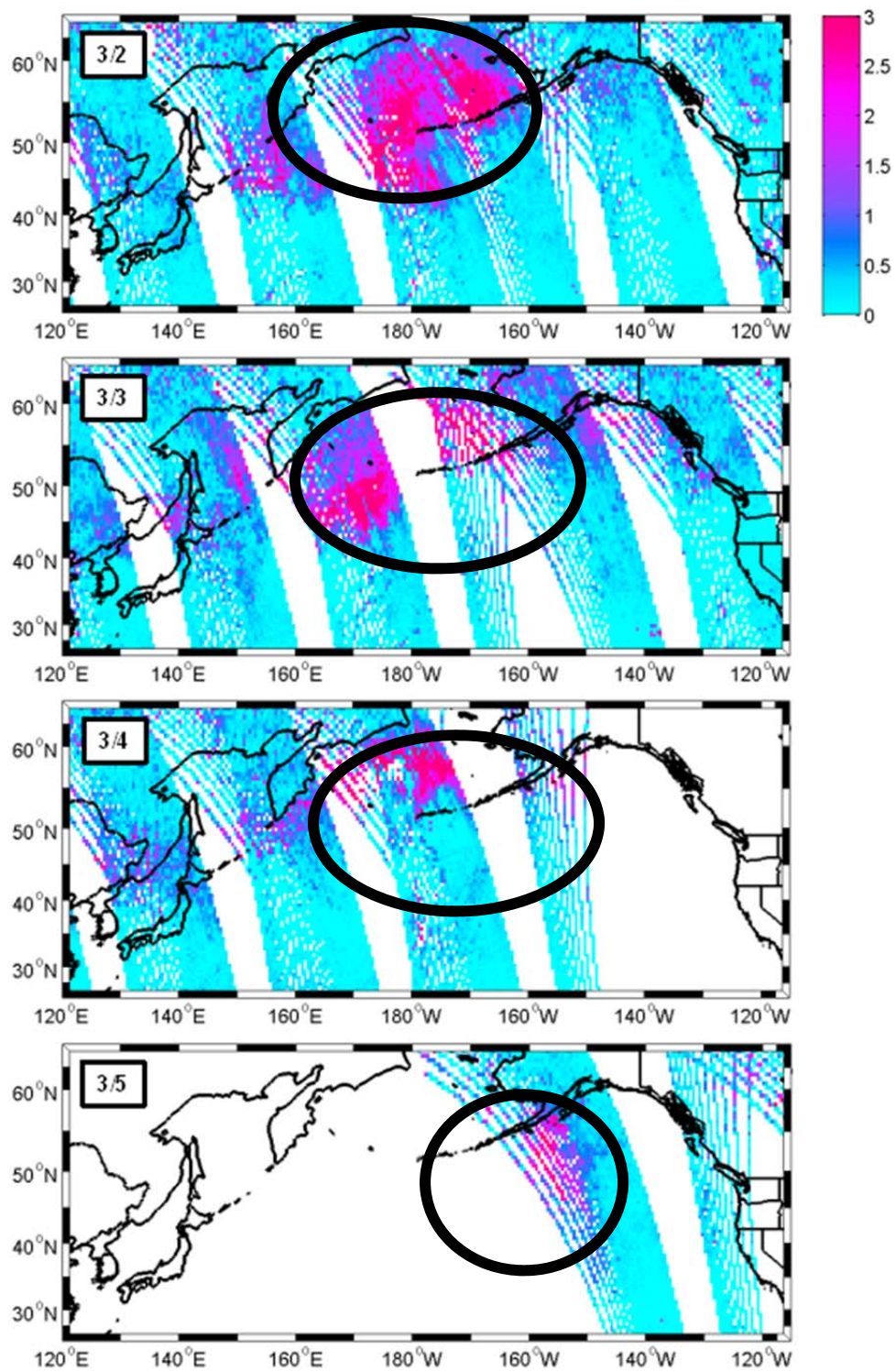


Figure 9.8 continued.

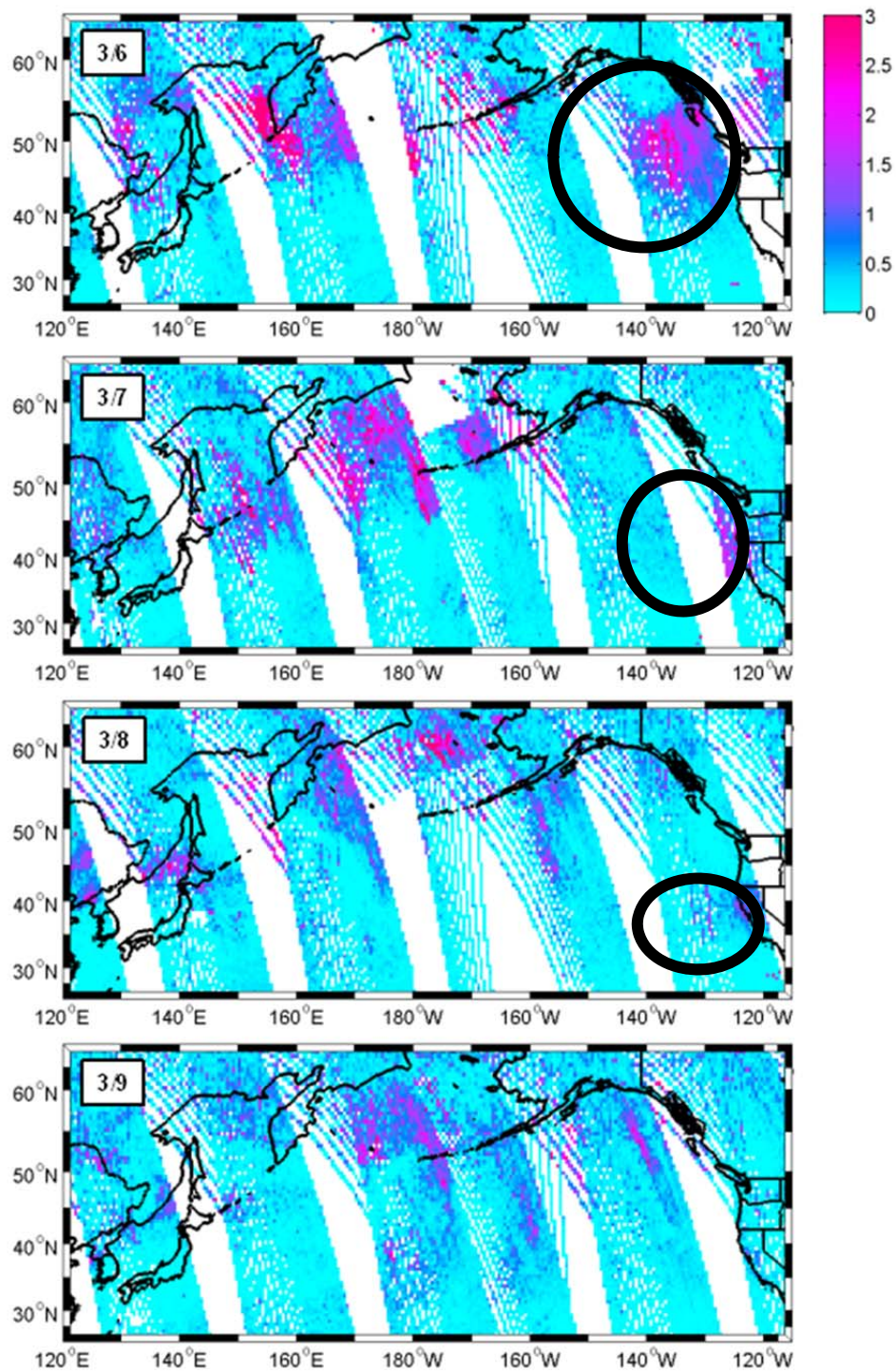


Figure 9.8 continued.

9.4. Tables

Table 9.1 Mean sizes used to estimate GRs. Variables in the linear regression equation are mean size (y) in nm and time (x) per 5-minute SMPS scan. Time to 100 nm (h) is calculated from the linear regression equation and multiplied by 12 to give time in hours.

Period	Event	Date	Start Size (nm)	End Size (nm)	GR (nm/h)	Linear Regression Equation	Time to 100 nm (h)
P1	1	2/24	41	65	4	$y = 0.3248x + 41.494$	36
	2	2/25	29	46	8	$y = 0.6829x + 29.522$	21
	3	2/26	55	70	3	$y = 0.2578x + 54.825$	35
	4	2/27	65	71	2	$y = 0.1434x + 64.226$	50
P2	5	3/6	50	66	8	$y = 0.6467x + 52.285$	15
	6	3/7	54	89	7	$y = 0.5861x + 50.255$	17

Table 9.2 Dates of P1 and P2 separated into before events, G1 (≤ 20 nm), G2 (20-25 nm), G3 (25-30 nm), G4 (≥ 30 nm at higher number concentrations), and end events (≥ 30 nm at lower number concentrations). The SMPS size distribution mean sizes (nm) and number concentrations ($\#/cm^3$) are averaged over the course of these periods, shown with standard deviations. GRs are also given for each NPF period.

Period	Dates	GR (nm/h)	Sub-period	Size Range (nm)	Mean (nm)	# Conc. ($\#/cm^3$)
P1	2/24-2/28	2-8	Before	All (11-600 nm)	73 \pm 14	897 \pm 480
			G1	≤ 20 nm	56 \pm 12	5359 \pm 735
			G2	20-25 nm	60 \pm 8	5179 \pm 831
			G3	25-30 nm	67 \pm 9	4607 \pm 723
			G4	≥ 30 nm (High)	65 \pm 9	3251 \pm 671
			End	≥ 30 nm (Low)	63 \pm 6	1668 \pm 343
P2	3/6-3/8	7-8	Before	All (11-600 nm)	75 \pm 2	846 \pm 301
			G1	≤ 20 nm	62 \pm 0	3189 \pm 573
			G2	20-25 nm	69 \pm 4	3737 \pm 442
			G3	25-30 nm	77 \pm 9	3191 \pm 474
			G4	≥ 30 nm (High)	88 \pm 19	2735 \pm 524
			End	≥ 30 nm (Low)	89 \pm 15	1716 \pm 261

9.5. References

- Bhave, P.V., J.O. Allen, B.D. Morrical, D.P. Fergenson, G.R. Cass, and K.A. Prather, A field-based approach for determining ATOFMS instrument sensitivities to ammonium and nitrate, *Environ. Sci. Technol.*, 36 (22), 4868-4879, 2002.
- Bukowiecki, N., D.B. Kittelson, W.F. Watts, H. Burtscher, E. Weingartner, and U. Baltensperger, Real-time characterization of ultrafine and accumulation mode particles in ambient combustion aerosols, *J. Aerosol Sci.*, 33 (8), 1139-1154, 2002.
- Clement, C.F., I.J. Ford, C.H. Twohy, A. Weinheimer, and T. Campos, Particle production in the outflow of a midlatitude storm, *J. Geophys. Res.*, 107 (D21), 4559, doi:10.1029/2001JD001352, 2002.
- Dal Maso, M., M. Kulmala, K.E.J. Lehtinen, J.M. Mäkelä, P. Aalto, and C.D. O'Dowd, Condensation and coagulation sinks and formation of nucleation mode particles in coastal and boreal forest boundary layers, *J. Geophys. Res.*, 107 (D15), 8097, doi:10.1029/2001JD001053, 2002.
- Ehn, M., H. Vuollekoski, T. Petäjä, V.M. Kerminen, M. Vana, P. Aalto, G. de Leeuw, D. Ceburnis, R. Dupuy, C.D. O'Dowd, and M. Kulmala, Growth rates during coastal

- and marine new particle formation in western Ireland, *J. Geophys. Res.*, 115, D18218, doi:10.1029/2010JD014292, 2010.
- Jacobson, M.Z., *Fundamentals of Atmospheric Modeling*, Cambridge University Press, New York, 2005.
- Krotkov, M.A., B. McClure, R.R. Dickerson, S.A. Carn, C. Li, P.K. Bhartia, K. Yang, A.J. Krueger, Z. Li, P. Levelt, H. Chen, P. Wang, and D.R. Lu, Validation of SO₂ retrievals from the Ozone Monitoring Instrument (OMI) over NE China, *J. Geophys. Res.*, 113, D16S40, doi:10.1029/2007JD008818, 2008.
- Krotkov, N.A., S.A. Carn, A.J. Krueger, P.K. Bhartia, and K. Yang, Band residual difference algorithm for retrieval of SO₂ from the Aura Ozone Monitoring Instrument (OMI), *IEEE Trans. Geosci. Remote Sensing*, AURA Special Issue, 44 (5), 1259-1266, 2006.
- Kulmala, M., H. Vehkamäki, T. Petaja, M. Dal Maso, A. Lauri, V.M. Kerminen, W. Birmili, and P.H. McMurry, Formation and growth rates of ultrafine atmospheric particles: a review of observations, *J. Aerosol Sci.*, 35 (2), 143-176, 2004.
- Lunden, M.M., D.R. Black, M. McKay, K.L. Revzan, A.H. Goldstein, and N.J. Brown, Characteristics of fine particle growth events observed above a forested ecosystem in the Sierra Nevada Mountains of California, *Aerosol Sci. Tech.*, 40 (5), 373-388, 2006.
- Modini, R.L., Z.D. Ristovski, G.R. Johnson, C. He, N. Surawski, L. Morawska, T. Suni, and M. Kulmala, New particle formation and growth at a remote, sub-tropical coastal location, *Atmos. Chem. Phys.*, 9 (19), 7607-7621, 2009.
- Moffet, R.C., B. de Foy, L.T. Molina, M.J. Molina, and K.A. Prather, Measurement of ambient aerosols in northern Mexico City by single particle mass spectrometry, *Atmos. Chem. Phys.*, 8 (16), 4499-4516, 2008.
- Pratt, K.A., L.E. Hatch, and K.A. Prather, Seasonal volatility dependence of ambient particle phase amines, *Environ. Sci. Technol.*, 43 (14), 5276-5281, 2009.
- Qian, S., Continuous measurements of 3 nm to 10 μm aerosol size distributions, University of Minnesota, St. Louis, MN, 2003.
- Qin, X.Y., and K.A. Prather, Impact of biomass emissions on particle chemistry during the California Regional Particulate Air Quality Study, *Int. J. Mass Spectrom.*, 258 (1-3), 142-150, 2006.
- Seinfeld, J.H., and S.N. Pandis, *Atmospheric Chemistry and Physics*, John Wiley & Sons, Inc., 2006.
- Spencer, M.T., and K.A. Prather, Using ATOFMS to determine OC/EC mass fractions in particles, *Aerosol Sci. Tech.*, 40 (8), 585-594, 2006.

- Stohl, A., M. Hittenberger, and G. Wotawa, Validation of the Lagrangian particle dispersion model FLEXPART against large-scale tracer experiment data, *Atmos. Environ.*, 32 (24), 4245-4264, 1998.
- Su, Y.X., M.F. Sipin, H. Furutani, and K.A. Prather, Development and characterization of an aerosol time-of-flight mass spectrometer with increased detection efficiency, *Anal. Chem.*, 76 (3), 712-719, 2004.
- Tu, F.H., D.C. Thornton, A.R. Bandy, G.R. Carmichael, Y.H. Tang, K.L. Thornhill, G.W. Sachse, and D.R. Blake, Long-range transport of sulfur dioxide in the central Pacific, *J. Geophys. Res.*, 109, D15S08, doi:10.1029/2003JD004309, 2004.

10. Appendix for Chapter 5

10.1. Supplemental Materials and Methods

Surface temperature measurements (2-minute resolution) at Sugar Pine Dam (SPD) were acquired from the NOAA Hydrometeorological Testbed Network (HMT-West) (http://hmt.noaa.gov/field_programs/hmt-west/2011/). The S-band profiling radar (S-PROF) provided vertical profiles of radar reflectivity and Doppler vertical velocity, with 60-m vertical resolution and 40 s temporal resolution, that were used to monitor the radar brightband melting level [White *et al.*, 2000; White *et al.*, 2003]. The total accumulation and percentage of snow/graupel/hail, brightband (BB) or cold rain, and non-brightband (NBB) or warm rain were estimated using the rainfall process-partitioning algorithm developed by White *et al.* [2003], which was applied to the S-PROF profiles. Analysis was performed on all half-hour periods when the rain rate exceeded ~1 mm/h. This is illustrated in Figure 10.1, which shows time-height cross sections of signal-to-noise-ratio (SNR) measured by the S-PROF radar at SPD. These sections include the times for all 11 of the aerosol sampling periods (Table 10.1). The results of White *et al.* [2003] precipitation process partitioning algorithm are also shown in Figure 10.1.

Eleven precipitation samples were collected during six storms from Jan 30–Mar 8, 2011. Collection times are provided in Table 10.1. Insoluble residues in the precipitation samples were resuspended and dried using a Collison nebulizer and two silica gel diffusion driers, then sampled using aerosol time-of-flight mass spectrometry (ATOFMS), which is described elsewhere [Gard *et al.*, 1997b]. Particles between 0.2–3.0 μm were individually sized and chemically analyzed by the ATOFMS, providing dual polarity mass spectra for each particle. Particles were classified into different types based on combinations of characteristic ion peaks in both negative and positive spectra, however, only dust and biological particle types are presented. Representative mass spectra of dust and biological types are provided in Figure 10.2. Dust residues varied in mineralogy as shown in (A)–(D), but typically contained a combination of lithium (${}^6\text{Li}^+$),

sodium ($^{23}\text{Na}^+$), magnesium ($^{24}\text{Mg}^+$), aluminum ($^{27}\text{Al}^+$), potassium ($^{39,41}\text{K}^+$), calcium ($^{40}\text{Ca}^+$, $^{56}\text{CaO}^+ / ^{57}\text{CaOH}^+$), titanium ($^{48}\text{Ti}^+$, $^{64}\text{TiO}^+$), iron ($^{54,56}\text{Fe}^+$), and/or aluminosilicates ($^{70}\text{Al}_2\text{O}^+$) in the positive ion mass spectra. The negative ion mass spectra for the dust residues varied, but commonly contained ion peaks for aluminosilicates ($^{43}\text{AlO}^-$, $^{59}\text{AlO}_2^-$, $^{60}\text{SiO}_2^-$, $^{76}\text{SiO}_3^-$, $^{77}\text{HSiO}_3^-$) and biological markers ($^{26}\text{CN}^-$, $^{42}\text{CNO}^-$, $^{79}\text{PO}_3^-$). Residues containing combinations of these peaks are representative of soil dust and have been previously observed in ambient conditions using ATOFMS [Silva *et al.*, 2000]. A unique type of calcium-rich dust particularly present in samples at SPD in 2011 was classified by ion peaks at $^{23}\text{Na}^+$, $^{24}\text{Mg}^+$, $^{39,41}\text{K}^+$, $^{40}\text{Ca}^+$, $^{56}\text{CaO}^+$, $^{57}\text{CaOH}^+$, $^{84}\text{Ca}_2^+$, $^{96}\text{Ca}_2\text{O}^+$, and $^{113}(\text{CaO})_2\text{H}^+$. Dust similar to the calcium-rich dust observed in the current study has previously been observed in sand samples by Silva *et al.* [2000]. Not all ion peaks discussed are labeled in Figure 10.2. The first biological residue type contained markers at $^{39,41}\text{K}^+$, $^{26}\text{CN}^-$, $^{42}\text{CNO}^-$, $^{63}\text{PO}_2^-$, $^{79}\text{PO}_3^-$, and $^{97}\text{H}_2\text{PO}_4^-$ shown in (E). The second type shown in (F) contained ion peaks of weaker intensity at $^{12}\text{C}^+$, $^{23}\text{Na}^+$, $^{27}\text{Al}^+ / \text{C}_2\text{H}_3^+ / \text{NCH}^+$, $^{29}\text{C}_2\text{H}_4^+ / \text{N}_2\text{H}^+$, $^{37}\text{C}_3\text{H}^+$, $^{38}\text{C}_3\text{H}_2^+$, $^{39}\text{C}_3\text{H}_3^+ / \text{K}^+$, $^{40}\text{C}_3\text{H}_4^+ / \text{Ca}^+$, $^{41}\text{C}_3\text{H}_5^+ / \text{K}^+$, $^{43}\text{AlO}^+$, $^{55}\text{C}_2\text{HNO}^+$, $^{56}\text{Fe}^+ / \text{CaO}^+$, and $^{57}\text{CaOH}^+$ in the positive ion mass spectra. Positive ion mass spectra from biological particles containing peak combinations similar to these were previously observed in cloud ice crystals [Pratt *et al.*, 2009a]. The negative ion markers were similar to those of the first bio type mentioned with additional contribution from chloride ($^{35,37}\text{Cl}^-$) and carbohydrates ($^{45}\text{CHOO}^-$, $^{59}\text{CH}_3\text{COO}^-$, $^{71}\text{C}_3\text{H}_3\text{OO}^-$, $^{73}\text{CH}_3\text{CH}_2\text{CHOO}^-$).

In situ aircraft measurements included chemical composition of aerosols as cloud residues, temperature, ice nuclei (IN) concentrations, and cloud droplet and ice crystal images. During the CalWater 2011 flight campaign, 25 flights (68.5 flight hours) were flown on the Department of Energy Gulfstream-1 aircraft based out of the McClellan Airfield in Sacramento, CA. Multiple flight tracks provided a large sampling area that spanned from the eastern Pacific Ocean into the Sierra Nevada. See Figure 10.3 for flight tracks of all 25 flights. The flight tracks for the Feb 16 and Feb 25 flights are shown in Figure 10.4 and Figure 10.5, respectively. The color of the flight tracks is time, with the size of the marker representing the altitude. On the right panel of Figure 10.4, the flight track shows the ascent in black and the descent in white. The ascent and descent were

made in similar geographical areas by backtracking over the initial flight track. Therefore, comparing the ascent and descent is valid because they are sampling the same cloud system in the same geographical area over time.

The aircraft data used in Chapter 5 were limited to times when particles were sampling using the Counterflow Virtual Impactor inlet (CVI Inlet Model 1204, BMI) to include only cloud particles with a variable cut-off size of 6–18 μm . The CVI works by using a counterflow of air to allow the passage of only cloud droplets and ice crystals that are of sufficient size to have enough inertia to overcome this counterflow and pass into a minor flow beyond the inlet plane [Ogren *et al.*, 1985]. The cloud particles thus captured melt/evaporate, leaving residual particles that are sampled by the ATOFMS and the continuous flow diffusion chamber (CFDC). The Feb 16th flight was 3 hours 17 minutes and 30 seconds long with 1 hour 57 minutes and 36 seconds of the flight on the CVI inlet. The Feb 25th flight was 3 hours 34 minutes and 52 seconds long with 1 hour 56 minutes and 54 seconds on the CVI inlet. Sampling on the CVI comprised roughly 2/3 of the sampling time for each flight.

The aircraft (A)-ATOFMS is a compact version of the ATOFMS, packaged to fit on a double wide aircraft rack [Pratt *et al.*, 2009d]. It uses a compact Z-shaped dual polarity mass spectrometer and optically decoupled detectors. An aerodynamic lens inlet focuses particles from 0.1-2.5 μm . These particles are then sized, chemically analyzed and the spectra are grouped, as described above. Representative spectra from the A-ATOFMS are shown in Figure 10.6. There were several dust types observed. One dust type had silicon ($^{28}\text{Si}^+$) in the positive spectra and silicates ($^{60}\text{SiO}_2^-$, $^{88}\text{Si}_2\text{O}_2^-$) in the negative spectra. Other dust types had sodium ($^{23}\text{Na}^+$), aluminum ($^{27}\text{Al}^+$), potassium ($^{39,41}\text{K}^+$), and iron ($^{54,56}\text{Fe}^+$) in the positive spectra with chlorine ($^{35}\text{Cl}^-$), silicates ($^{60}\text{SiO}_2^-$, $^{76}\text{SiO}_3^-$), nitrate ($^{62}\text{NO}_3^-$), nitrite ($^{46}\text{NO}_2^-$) and sometimes phosphate ($^{79}\text{PO}_3^-$) in the negative spectra, consistent with previous observations [Silva *et al.*, 2000]. Biological particles generally had sodium ($^{23}\text{Na}^+$) and potassium ($^{39,41}\text{K}^+$) and were sometimes enriched in metals ($^{24}\text{Mg}^+$, $^{27}\text{Al}^+$, $^{40}\text{Ca}^+$, $^{56}\text{Fe}^+$ or $^{52}\text{Cr}^+$) or organic carbon and organic nitrogen ($^{12}\text{C}^+$, $^{27}\text{Al}^+/\text{C}_2\text{H}_3^+/\text{NCH}^+$, $^{29}\text{N}_2\text{H}^+$, $^{77}\text{C}_6\text{H}_5^+$, $^{91}\text{C}_7\text{H}_7^+$) in the positive spectra with

biological markers ($^{26}\text{CN}^-$, $^{42}\text{CNO}^-$, $^{63}\text{PO}_2^-$, $^{79}\text{PO}_3^-$, and $^{97}\text{H}_2\text{PO}_4^-$) and sometimes nitrate ($^{62}\text{NO}_3^-$) and nitrite ($^{46}\text{NO}_2^-$) in the negative spectra [Ferguson et al., 2003; Pratt et al., 2009a; Russell, 2009]. Sea salt residues contained sodium ($^{23}\text{Na}^+$), sodium clusters ($^{81/83}\text{Na}_2\text{Cl}^+$, $^{93/95}\text{NaCl}_2^-$), chloride ($^{-35/-37}\text{Cl}$), nitrite ($^{46}\text{NO}_2^-$), and nitrate ($^{62}\text{NO}_3^-$) [Gard et al., 1998; Gaston et al., 2011].

The static air temperature was measured onboard the Gulfstream-1 using a Rosemount 102E. Cloud droplet and ice crystal images were collected with a 2D-S (2D-S Stereo Probe, SPEC, Inc.). 2D-S images were classified into 4 categories based on the amount and type of ice present. Representative images for each type are shown in Figure 10.7. Ice nuclei measurements were made from separate isokinetic and CVI inlets on the G-1 using the Colorado State University CFDC [DeMott et al., 2010; Rogers et al., 2001]. The sample aerosol (1.5 vlpm) is focused by particle-free sheath air (8.5 vlpm) in the annular space between two cylindrical, ice-coated walls in the processing section of the CFDC. Processing temperature and humidity at the aerosol lamina are defined by the inner and outer wall temperature difference. Processing temperature was set to be representative of conditions in sampled clouds. Processing relative humidity was typically set to 104-105% with respect to water to favor the contributions of ice nucleation mechanisms as occur in mixed phase cloud conditions (condensation and immersion freezing) [DeMott et al., 2010]. After ~ 5 s in the growth section, the aerosols enter ice saturated conditions for ~ 3 s to evaporate activated cloud droplets and allow detection of ice nuclei as particles larger than ~ 3 μm exiting the CFDC into an optical particle counter (OPC). An inertial impactor was used upstream of the CFDC to restrict assessment of ice nuclei to aerosols smaller than ~ 2.5 μm (aerodynamic diameter), and to ensure that large aerosol particles are not falsely counted as ice crystals. To improve sampling statistics for the low sample flow rates used, ice nuclei concentrations were calculated for integrated time periods for which uncertainties could be well defined based on Poisson sampling errors. The typical sample period was 3 to 10 minutes long. Sample periods were alternated with periods sampling particle free air in order to correct for any background frost production [DeMott et al., 2010].

An inertial impactor with a 50% cut-point aerodynamic diameter of 2.9 μm located immediately downstream of the CFDC OPC was used to capture ice crystals on Transmission Electron Microscope (TEM) grids, allowing for subsequent identification of the elemental composition of activated ice nuclei. IN were collected onto carbon-coated Formvar films supported by 200 mesh Cu TEM grids (Ted Pella Inc.). TEM analyses was performed by the RJLee Group, Inc. (Monroeville, PA) using a Hitachi HD-2300 dedicated 200 kV scanning transmission electron microscope (STEM). The analysis was conducted primarily in the bright field transmission electron mode at magnifications up to 450,000x. Compositional information was obtained through collection of characteristic X-rays using a Thermo Scientific Si(Li) energy dispersive X-ray spectroscopy (EDS) system. On the order of 50 particles were examined per sample and micrographs of each particle were recorded to illustrate morphological characteristics. An energy dispersive spectrum was also acquired for each particle and in some cases for separate features within particles. Background spectra acquired from particle-free areas indicate the presence of carbon and oxygen (from the support film), copper (from the TEM grid), and silicon (from an unknown source within the TEM). Therefore identification of these elements in particles can be less certain in some cases; however, Si (e.g., from minerals) and C were distinguished on the basis of significantly higher EDS counts compared to background spectra. Particle categories were defined from the elemental spectra. For this study, categories were selected for alignment with those defined for single particle mass spectral categorization and include mineral dusts, dust/salt/biological, biological, and carbonaceous particles with likely sources from biomass burning and other organic materials. Dusts were defined as particles of irregular morphology containing oxidized Ca-Mg-Fe-Al silicates, sometimes with S and Cl. No attempt was made to distinguish industrial from natural dusts, so metal oxides also went into this category. Nevertheless, desert dust-like particles predominated in the sample. The dust/salt/biological particles contained more carbonaceous material and salts than the pure minerals. Biological particles were typed based on a smooth morphology, excess of C, the presence of non-oxidized Si, and a relative deficiency of Al or other metals, when present, compared to dust particles. Carbonaceous particles showed few spectral

signatures aside from C, but appeared as solid carbon components within an apparent organic C matrix.

Air mass back trajectories (10-day) were calculated using HYSPLIT 4 [Draxler and Rolph, 2011b] ending at the average cloud top heights (Z_{tops}) from the geostationary *GOES-11* during precipitation sample collection time periods above SPD. To attain the most accuracy in estimating the transport paths during each sample, Z_{tops} ranging from 1-10 km ASL were averaged every 3 hours and used as the ending altitudes for the back trajectory analysis, resulting in 122 total trajectories for the six storms. Back trajectories were calculated ending at 0000, 0300, 0600, 0900, 1200, 1500, 1800, and 2100 each day a precipitation sample was collected and ended at the averaged Z_{top} . The averaged Z_{tops} also typically corresponded to precipitation time periods during the storms. The *GOES-11* satellite is centered over the Pacific Ocean and the Americas. Data from Jan 30–Mar 8, 2011 were retrieved for the CalWater field campaign. The five channels on the *GOES-11* imager include a visible channel (0.65 μm), which was calibrated to the Aqua MODIS 0.64- μm channel following the methods of Minnis *et al.* [Minnis *et al.*, 2011], as well as four infrared channels, including a central wavelength at 3.9 μm used to discriminate water from ice clouds. The 10-km pixel *GOES-11* data were analyzed over SPD using the methods described by Minnis *et al.* [Minnis *et al.*, 2011].

Data from the Navy Aerosol Analysis and Prediction System (NAAPS) provided by the Naval Research Laboratory (NRL) were acquired from the NRL website (<http://www.nrlmry.navy.mil/aerosol/>). NAAPS is a transport model driven by wind fields and described in detail on the NRL website. The NAAPS global aerosol model uses meteorological fields from the Navy Operational Global Atmospheric Prediction System (NOGAPS) [Hogan and Brody, 1993; Hogan and Rosmond, 1991] and land use types from the United States Geological Survey (USGS) Land Cover Characteristics Database to predict the spatial distribution and relative amount of dust in the atmosphere. Dust emission occurs whenever the friction velocity exceeds a threshold value, snow depth is less than a critical value, and the surface moisture is less than a critical value. The model is validated daily with satellite data from MODIS and the National Environmental

Satellite, Data, and Information Service (NESDIS) of NOAA. Archived global data were used in Figure 5.3 of Chapter 5 from the global NAAPS plot generator and included simulations from Feb 6-16 (A) and Feb 15-25 (B). Time-height sections used to calculate dust plume altitudes were also acquired from the NRL website using NAAPS. These plots provide unitless dust concentrations at specific AERONET (Aerosol Robotic Network) sites. Site used for this study are location within the dust regions shown in Figure 5.2 (C) of Chapter 5 and include Sedebocker (30°N, 34°E), Solar Village (24°N, 46°E), Yinchuan (38°N, 106°E), and Beijing (39°N, 116°E) (see Figure 10.8). There were no sites directly in the Taklimakan dust region; therefore the closest site to the east was chosen (Yinchuan). Figure 10.9 shows examples of images used to determine the dust plume heights. These data were used during each time a trajectory passed through each of the dust regions. Figure 10.10 shows each point in time when a trajectory passed through a dust region in addition to mean altitude of that trajectory point and maximum heights of the dust plumes acquired from the NAAPS time-height sections. Each data point in Figure 10.10 was used for the average, minimum, and maximum values in Figure 5.2 (C) of Chapter 5.

The Cloud-Aerosol Lidar and Infrared Pathfinder Satellite Observation (CALIPSO) satellite was used to determine the presence of dust and ice clouds over arid regions where air mass back trajectories travelled, including North Africa, the Middle East (specifically Saudi Arabia, Oman, Iran, Iraq, and Afghanistan), the Taklimakan (West China), and East Asia (specifically Northeast China and Mongolia). CALIPSO flies at 705 km in the A-train satellite constellation and measures total attenuated backscatter at 532 nm and 1064 nm, and the depolarization at 532 nm through its Lidar, CALIOP (Cloud-Aerosol Lidar with Orthogonal Polarization), with a 60-m vertical resolution [Winker *et al.*, 2010]. CALIPSO determined the coverage, water/ice content, and altitude of clouds in addition to the type of aerosol, including clean marine, dust, polluted continental, clean continental, polluted dust, and smoke. The CALIPSO images that correspond to the markers in Figure 5.3 are shown in Figure 10.11.

10.2. Supplemental Results and Discussion

The flights on Feb 16th and 25th both corresponded to conditions a few hours after the passage of a cold front. Just 4-8 hours prior to each of these flights, the experimental meteorological observations showed that a Sierra Barrier Jet (SBJ, terrain parallel blocked flow) was present in the lowest 2000 m, MSL, and a weak AR was present above that. In both cases the AR and SBJ had ended several hours prior to the flight, and winds were westerly. In short, conditions were postfrontal with weak upslope forcing.

The chemical markers of the dust and biological cloud residues on Feb 16th and Feb 25th were distinct. On Feb 16th, a high fraction of the residues contained ion markers at $^{23}\text{Na}^+$, $^{27}\text{Al}^+$, $^{28}\text{Si}^+$, and/or $^{60}\text{SiO}_2^-$ and were strongly absorbing of the UV laser (e.g., Figure 10.6 (A) and (B)). However, on Feb 25th, a high fraction of the dust residues contained intense ion markers for phosphate ($^{79}\text{PO}_3^-$) (e.g., Figure 10.6 (D) and (F)) and no ion markers for aluminosilicates. These results suggest the Feb 16th residues were more “dust-like” whereas Feb 25th was influenced more by biological residues. In addition, precipitation residues during these days support observations from the flights. On Feb 16th precipitation residues were similar to those shown in Figure 10.2 (A)-(D), while on Feb 25th precipitation residues resembled those shown in Figure 10.2 (E) and (F). Thus, this supports the trajectory analysis that shows the clouds were affected by different source regions.

Aircraft data, including cloud residues, IN concentrations, 2D-S classifications, and temperature, for the flight on Feb 16th are presented in Chapter 5. The dominance of dust and biological cloud residues during this flight was confirmed using TEM analysis of IN activated in the CFDC. Figure 10.12 shows images and spectra from TEM analysis for a dust IN residue ((A) and (B)) and a biological residue ((C) and (D)). Overall, 43 residues were analyzed from the IN TEM grids during the flight on Feb 16th. Dust residues represented 53% of the total, while a mix of dust, biological, and salt represented 26%. What were thought to be purely biological residues represented 9% and the remaining 12% was carbonaceous, likely from biomass burning or other organic sources. Thus, the residues that served as IN were predominantly dust and/or biological as observed by the A-ATOFMS.

Measurements from Feb 25th are also discussed in the Chapter 5, but Figure 10.13 provides more details on cloud residues and the presence of ice. Similar to Feb 16th (Figure 5.4), Figure 10.13 shows the number of dust and biological residues (“Dust+Bio”) in brown bars, relative to the total number of residues in white. Sea salt was not present during the flight on Feb 25th unlike Feb 16th. The orange markers show air temperature and the black markers indicate IN concentrations measured in the immersion-freezing regime above water saturation from cloud residues with the CFDC, colored by CDFC temperature [Rogers *et al.*, 2001]. The grey bars show ice classifications defined by viewing 2D-S imagery. The afternoon flight on Feb 25th shows an ample amount of Dust+Bio was present. Lower level clouds were not pristine on this day, as they were on Feb 16th, because dust and biological cloud residues introduced into the seeder clouds had already fallen down into the feeder clouds. As a result, dust was present at all levels during this afternoon flight and ice was present throughout both the ascent and descent.

10.3. Figures

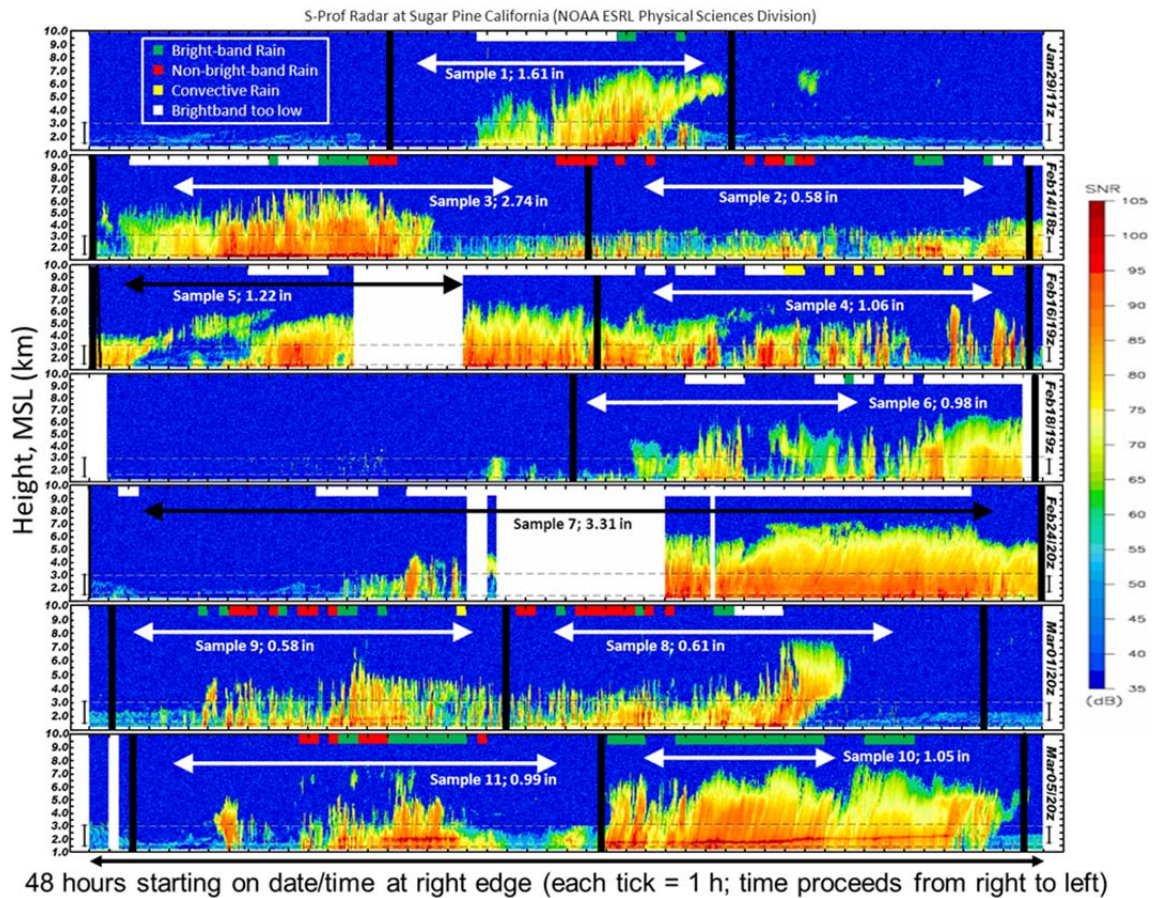


Figure 10.1 Time-height cross sections (with time reversed per meteorological convention) of S-PROF radar-observed vertical profiles of precipitation above Sugar Pine Dam (SPD). The parameter shown is the signal-to-noise ratio (SNR), essentially the strength of the radar pulse scattered back to the radar as it propagated up through the atmosphere. Most of these radar “echoes” come from precipitation particles, but some are from cloud particles. Blue represents background noise where no echo was detected. The time period for each of the co-located precipitation samples used to diagnose aerosol residues using ATOFMS is shown, along with the raingage-observed precipitation accumulation during each sample period. Color-filled squares are shown when the precipitation process partitioning algorithm identified a type of precipitation. A key feature that distinguishes the precipitation type is the presence of a radar bright band, which occurs at an altitude range where snow falls and melts. It is evidenced by a band of bright (strong) echo that is nearly horizontal in the type of plot shown in this figure. Horizontal dashed lines mark the upper and lower edges of the lowest radar beams from the two nearest NEXRAD scanning radars.

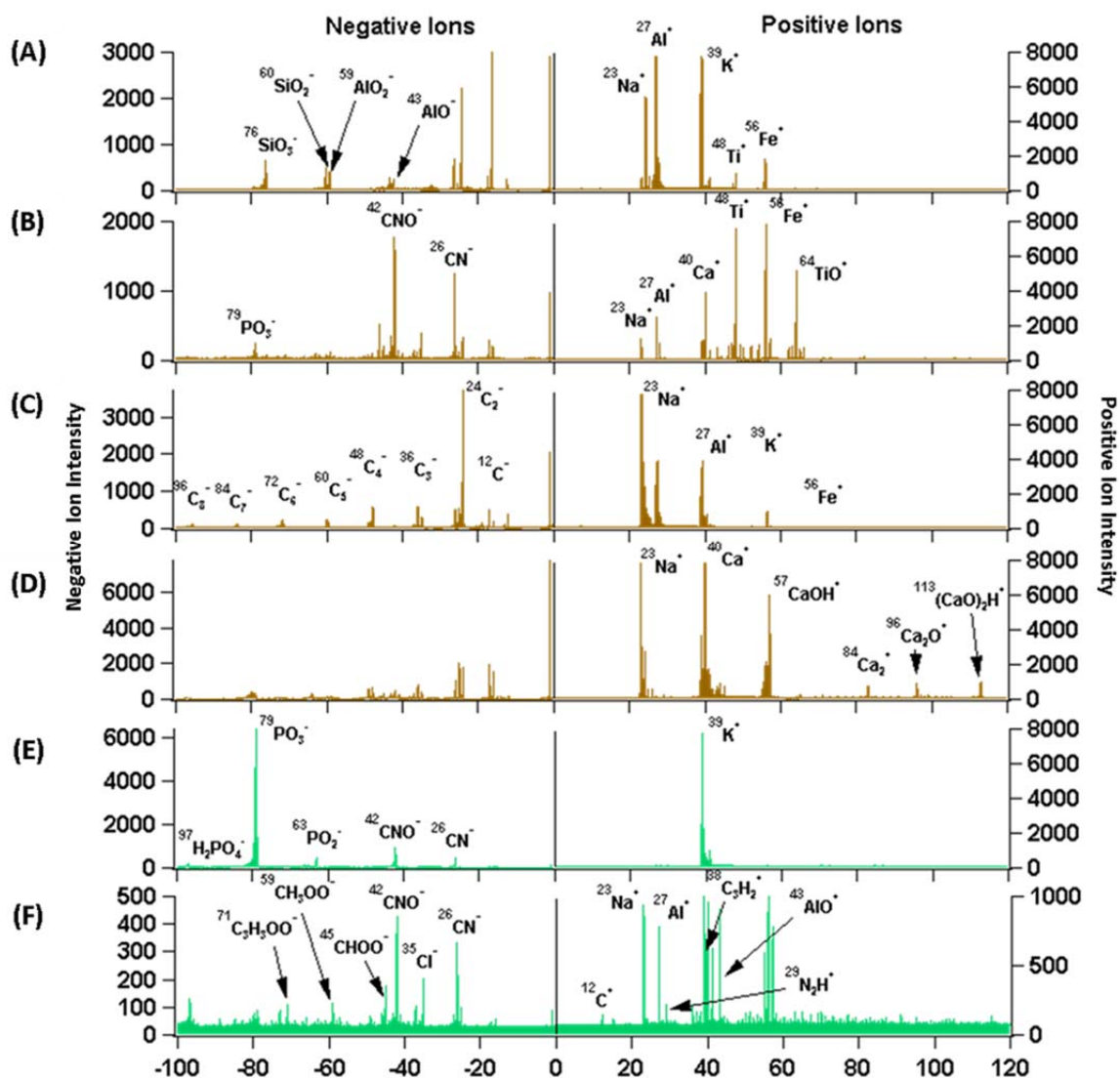


Figure 10.2 Representative mass spectra for ATOFMS precipitation residues. Examples include dust (A)-(D) and biological residues (E) and (F). Positive and negative ion intensities vary by type.

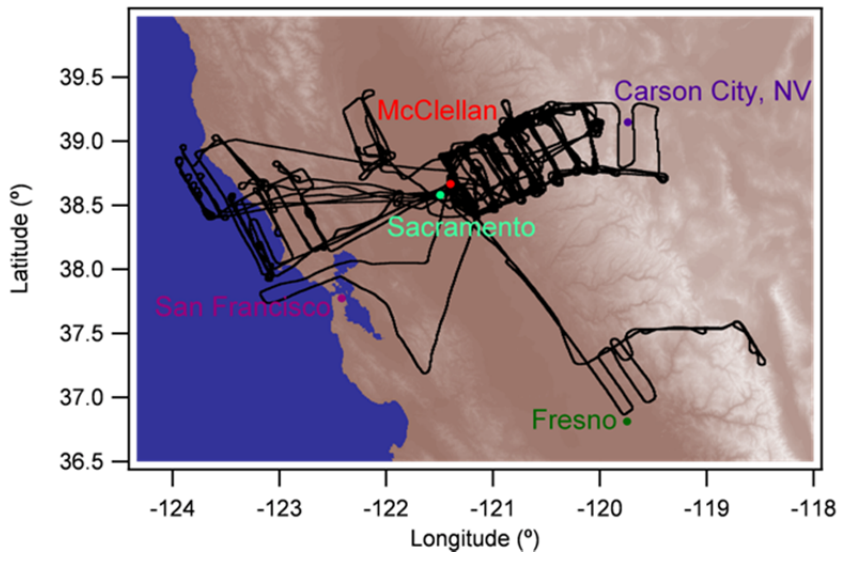


Figure 10.3 Map showing the flight tracks for all 25 *CalWater* flights. McClellan Airfield is labeled in red.

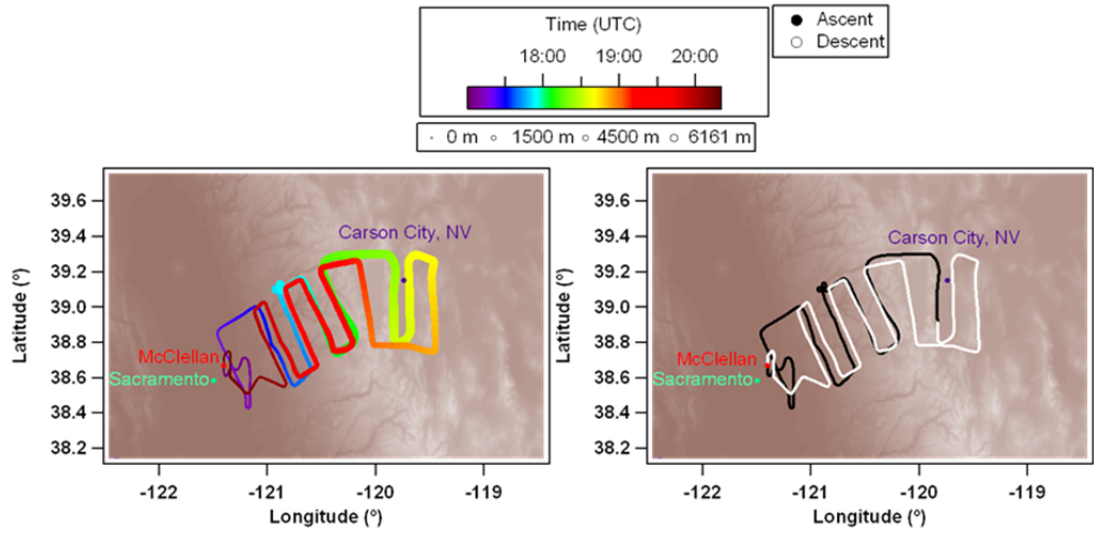


Figure 10.4 Feb 16th flight track colored by time on the left and by ascent or descent on the right. The size of the markers in the left panel represents altitude (m, MSL).

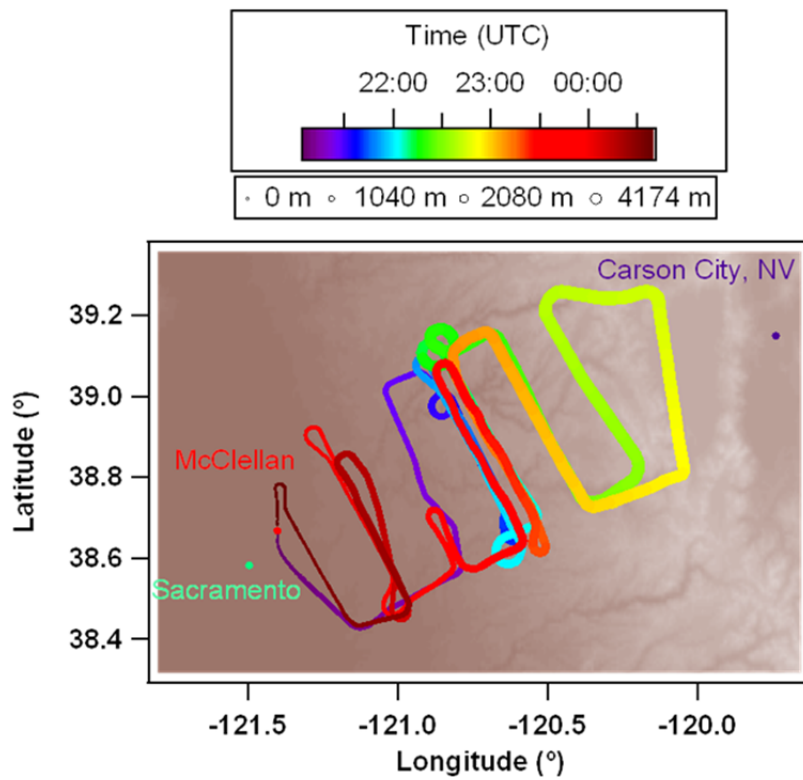


Figure 10.5 The Feb 25th flight track colored by time with altitude (m, MSL) shown by the size of the markers.

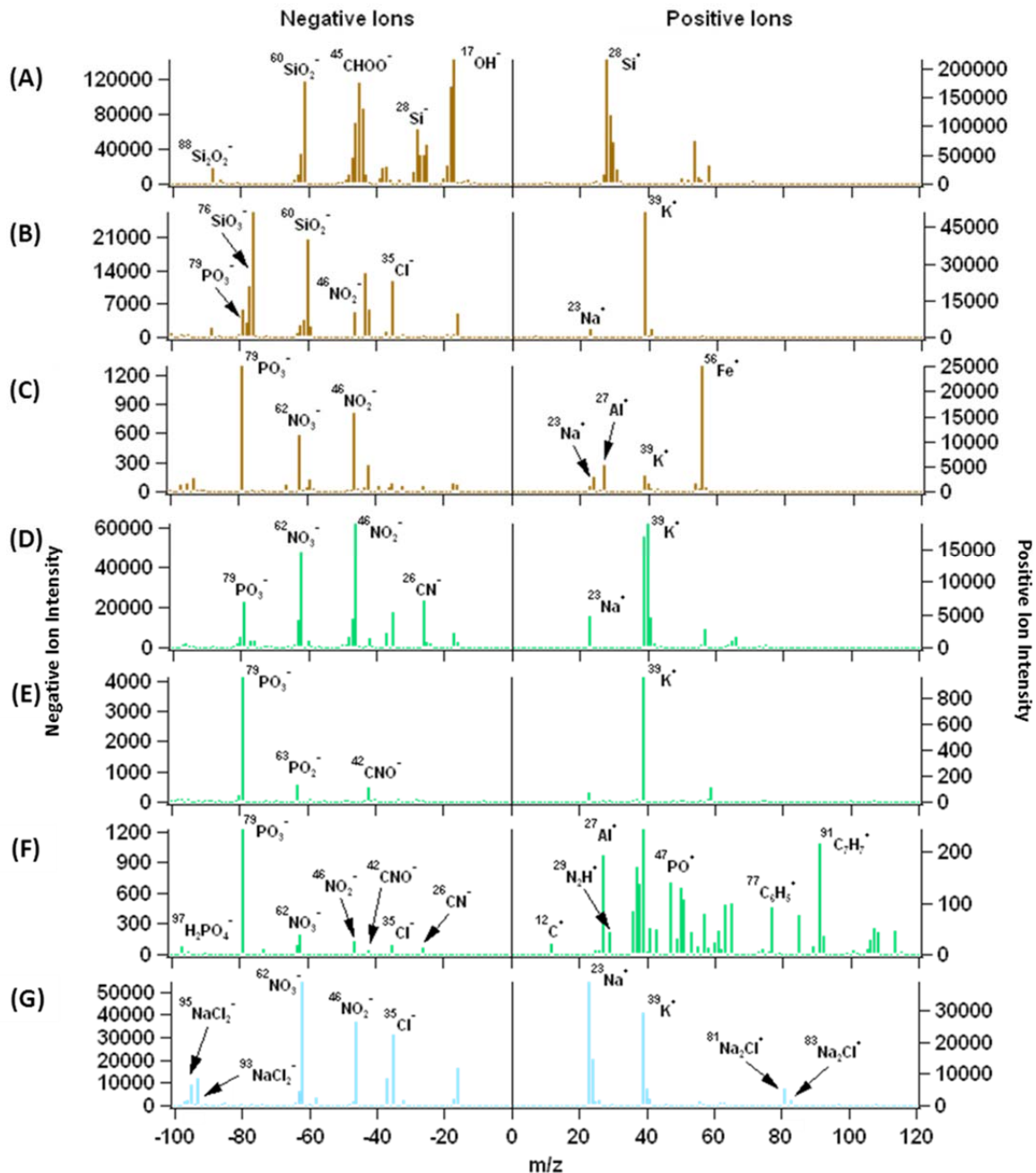


Figure 10.6 Representative mass spectra for A-ATOFMS cloud residues. Examples include dust (A)-(C), biological residues (D)-(F), and sea salt (G). Positive and negative ion intensities vary by type.

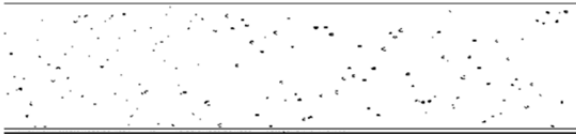



2D-S Classification	Representative Image
0 no images	no images
1 droplets, no ice	
2 isolated ice crystals	
3 mixed	
4 rimed ice	

Figure 10.7 Representative 2D-S images including the classifications for 0-4.



Figure 10.8 Example NAAPS time-height cross sections for (A) Sedeboker, (B) Solar Village, (C) Yinchuan, and (D) Beijing.

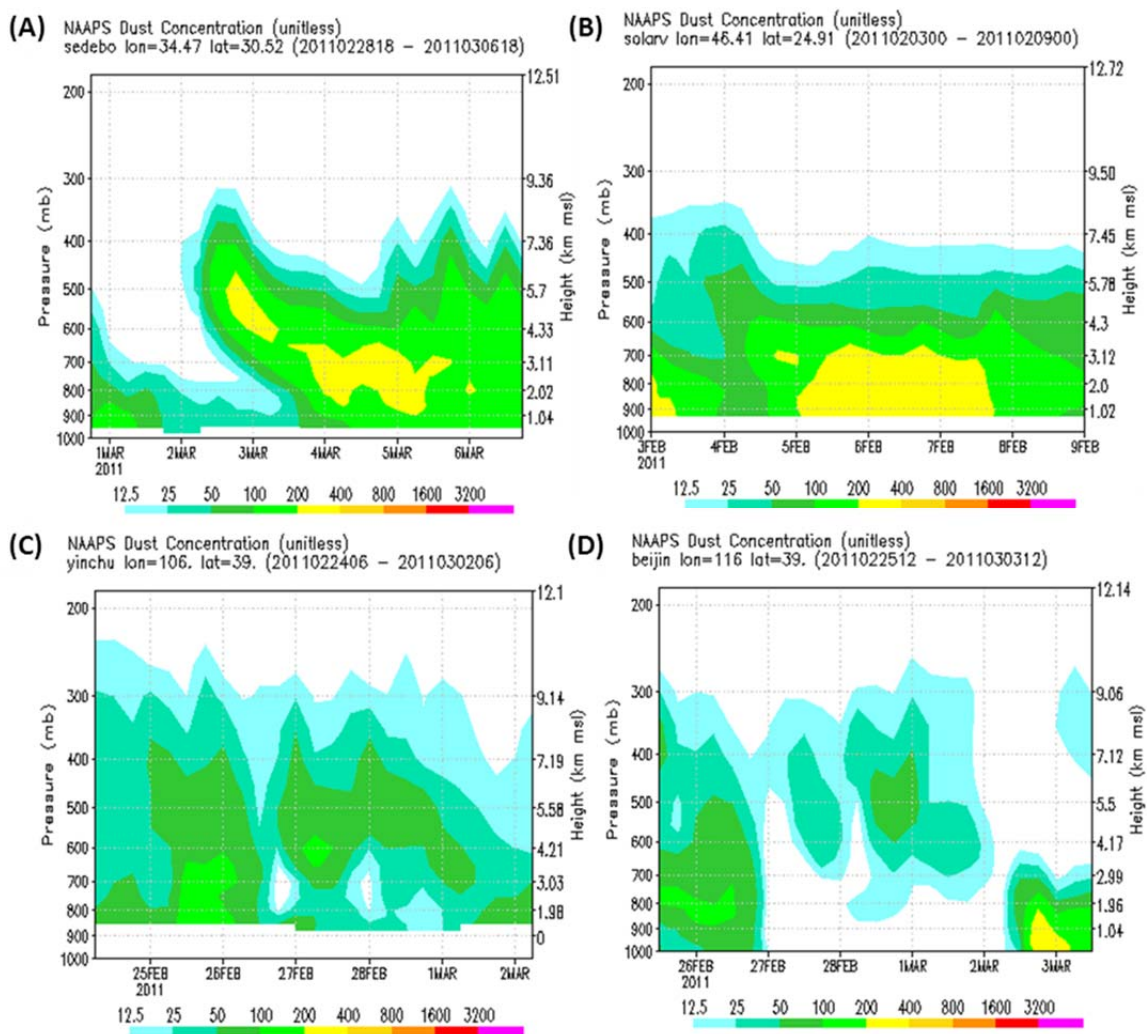


Figure 10.9 Example NAAPS time-height cross sections for (A) Sedebo, (B) Solar Village, (C) Yinchuan, and (D) Beijing.

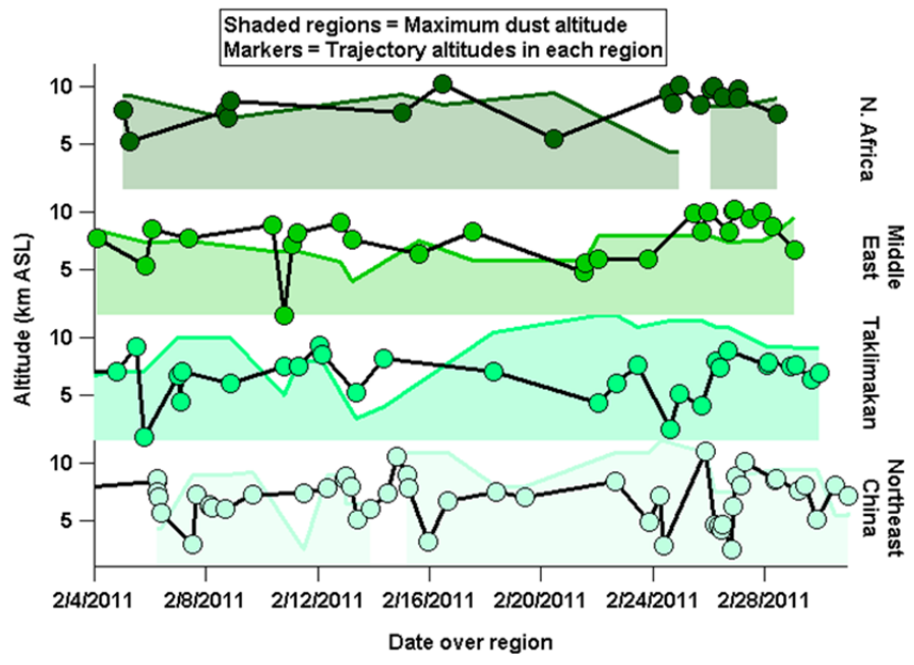


Figure 10.10 NAAPS time-height cross section data used to determine the maximum height of dust plumes at sites in each of the dust regions. The times of the dust plume heights correspond to times when trajectories passed through the dust regions. Also shown are the altitudes of these trajectories endpoints.

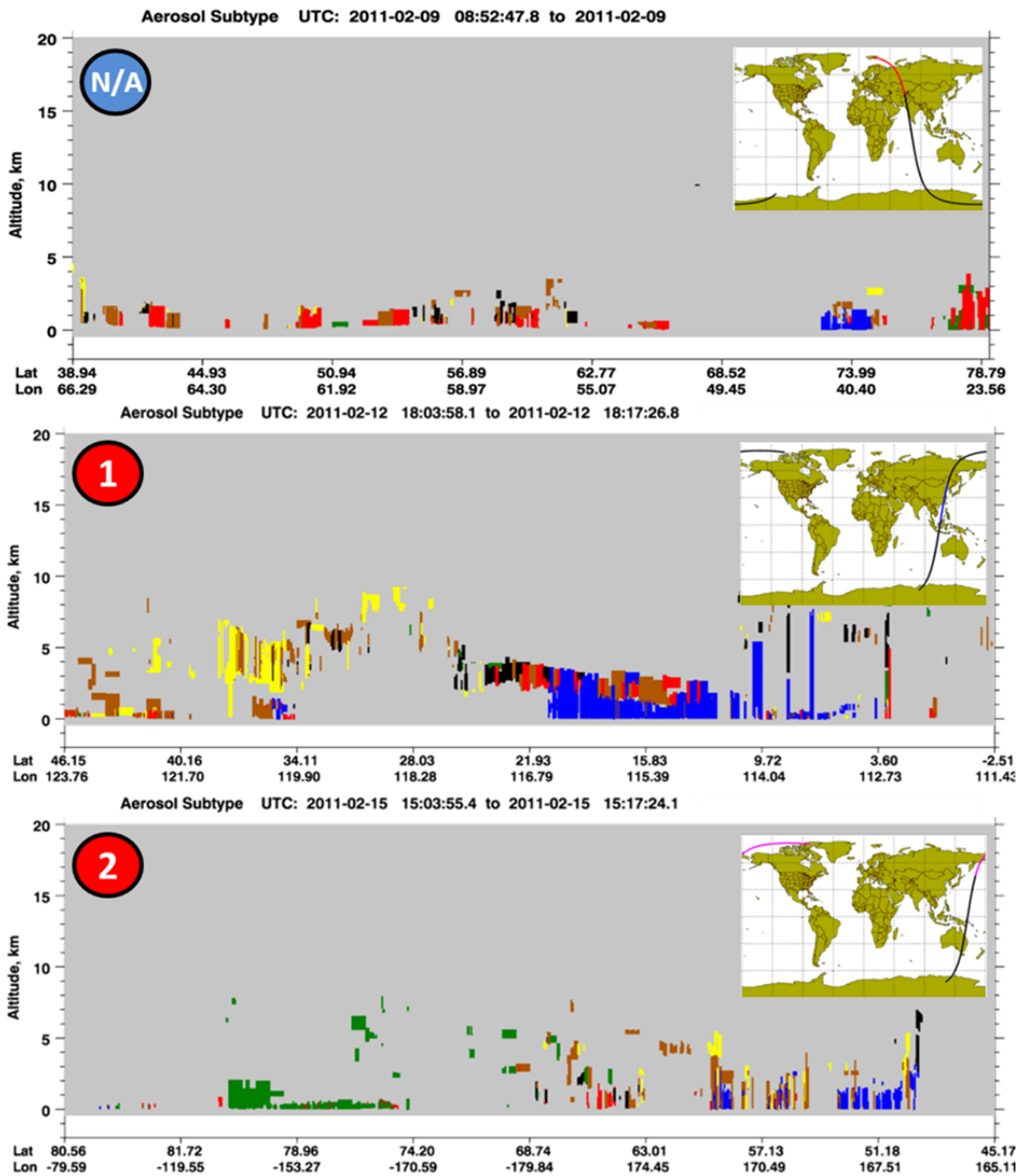


Figure 10.11 CALIPSO images that correspond to the numbered markers in Figure 5.3 of Chapter 5. Latitude and longitude correspond to highlighted portion of satellite path in the map insets. N/A and panels 1-3 correspond to the trajectory ending on Feb 16th while panels 4-6 correspond to the trajectory ending on Feb 25th above SPD.

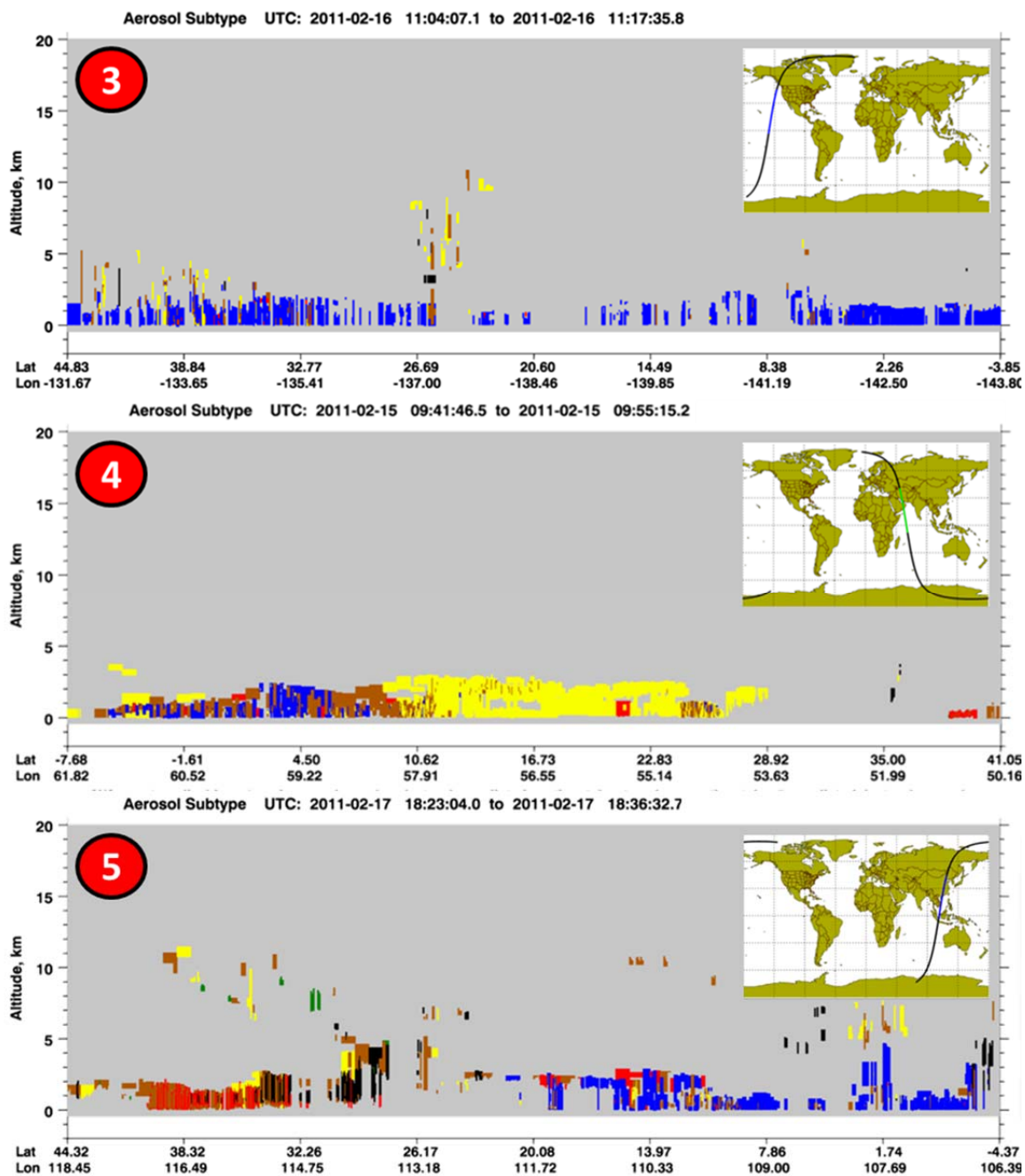


Figure 10.11 continued.

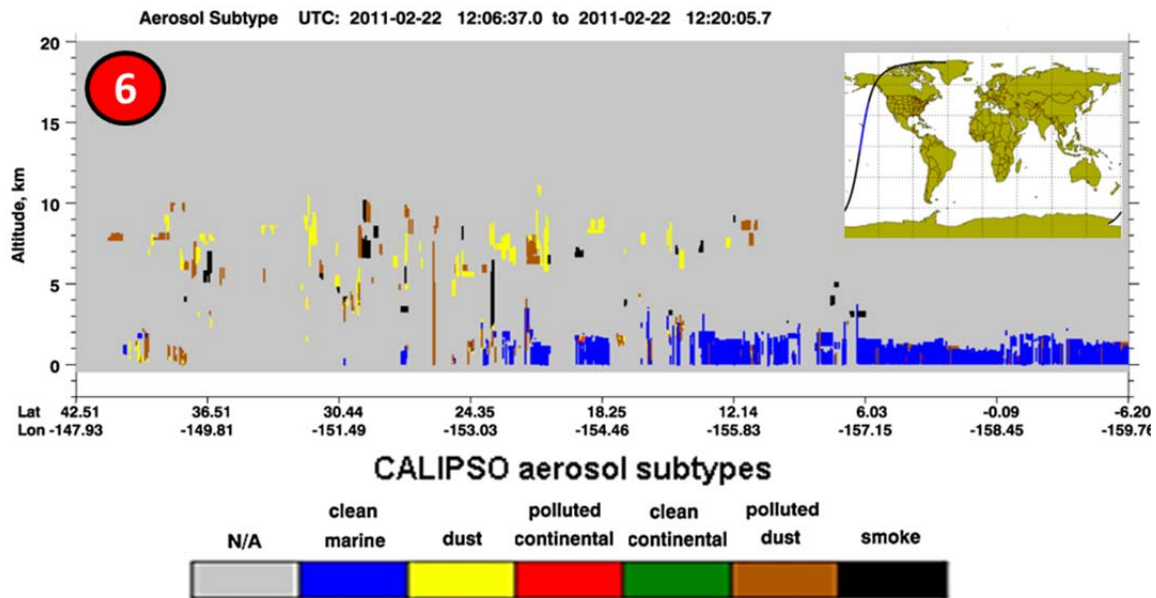


Figure 10.11 continued.

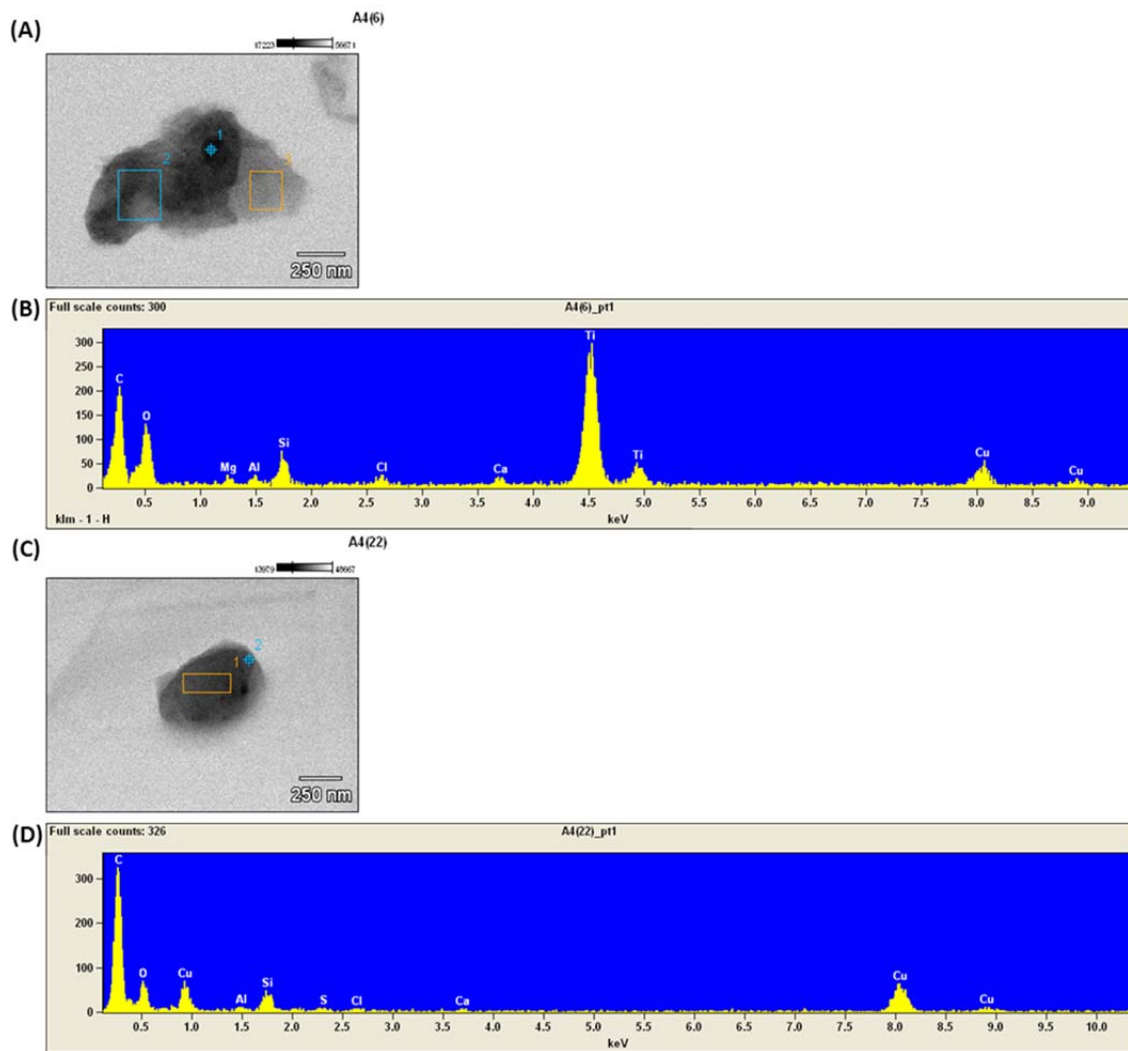


Figure 10.12 TEM analysis of collected ice nuclei categorized as dust and biological. Includes: (A) image of dust IN, (B) spectrum for the dust IN shown in (A), (C) image of a biological IN, and (D) spectrum for the biological IN shown in (C).

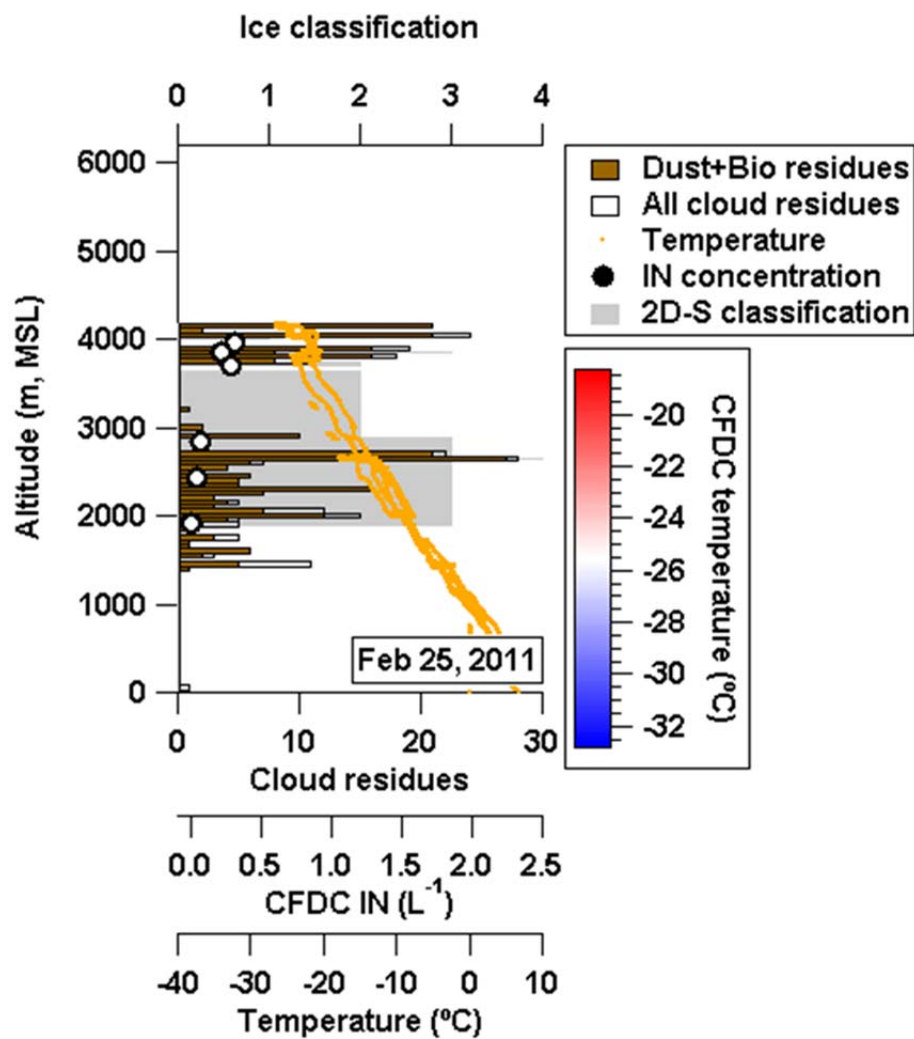


Figure 10.13 Vertical profiles of Dust+bio cloud residues, the total number of residues, and temperature for the flight on Feb 25th, 2011 (20:57 – 00:36 UTC). Also shown are cloud particle residual IN concentrations as asterisks with the color representing the temperature at which the measurement was taken and the 2D-S classifications, with 0 = no images/out-of-cloud, 1 = droplets with no ice, 2 = isolated ice crystals, 3 = mixed, and 4 = rimed ice.

10.4. Tables

Table 10.1 Statistics for precipitation sample collection during winter storms in 2011 at SPD. Includes start and end dates and times for sample collection and number of residues that were chemically analyzed. Storms are also labeled for corresponding samples.

Storm	Sample	Start Date (UTC)	End Date (UTC)	Number of Residues Analyzed
1	S1	1/30/11 02:53	1/30/11 20:00	130
2	S2	2/14/11 18:40	2/15/11 17:00	360
2	S3	2/15/11 17:05	2/16/11 18:00	266
3	S4	2/16/11 19:45	2/17/11 17:30	233
3	S5	2/17/11 17:30	2/18/11 18:40	208
3	S6	2/18/11 19:15	2/19/11 18:40	163
4	S7	2/24/11 20:30	2/26/11 21:00	94
5	S8	3/1/11 23:00	3/2/11 23:00	26
5	S9	3/2/11 23:00	3/3/11 19:00	398
6	S10	3/5/11 21:00	3/6/11 18:15	351
6	S11	3/6/11 18:15	3/7/11 18:00	204

10.5. Author Contributions

J.M.C. made ground-based ATOFMS precipitation measurements in the field and in the laboratory, analyzed aerosol data, analyzed *GOES-11* data, and wrote the manuscript. K.J.S. made aircraft-based A-ATOFMS measurements in the field, analyzed aerosol data, analyzed cloud probe data, and wrote the manuscript. D.R. provided intellectual contribution and contributed to the writing of manuscript. A.C. assisted with aircraft-based A-ATOFMS measurements in the field and source analysis using HYSPLIT. P.J.D. and R.C.S. provided ice nuclei concentration and composition measurements and intellectual contribution. A.B.W. and F.M.R. analyzed the surface meteorological and S-PROF data and description of meteorological data. K.A.P. is the principal investigator for this work and contributed to the writing of the manuscript. All authors reviewed and commented on the paper.

10.6. References

DeMott, P.J., A.J. Prenni, X. Liu, S.M. Kreidenweis, M.D. Petters, C.H. Twohy, M.S. Richardson, T. Eidhammer, and D.C. Rogers, Predicting global atmospheric ice

nuclei distributions and their impacts on climate, *Proceedings of the National Academy of Sciences of the United States of America*, 107 (25), 11217-11222, 2010.

HYSPLIT (HYbrid Single-Particle Lagrangian Integrated Trajectory) Model access via NOAA ARL READY Website (<http://ready.arl.noaa.gov/HYSPLIT.php>), NOAA Air Resources Laboratory, Silver Spring, MD. 2011.

Fergenson, D.P., M.E. Pitesky, H.J. Tobias, P.T. Steele, G.A. Czerwieniec, S.C. Russell, C.B. Lebrilla, J.M. Horn, K.R. Coffee, A. Srivastava, S.P. Pillai, M.-T.P. Shih, H.L. Hall, A.J. Ramponi, J.T. Chang, R.G. Langlois, P.L. Estacio, R.T. Hadley, M. Frank, and E.E. Gard, Reagentless Detection and Classification of Individual Bioaerosol Particles in Seconds, *Analytical Chemistry*, 76 (2), 373-378, 2003.

Gard, E., J.E. Mayer, B.D. Morrical, T. Dienes, D.P. Fergenson, and K.A. Prather, Real-time analysis of individual atmospheric aerosol particles: Design and performance of a portable ATOFMS, *Analytical Chemistry*, 69 (20), 4083-4091, 1997.

Gard, E.E., M.J. Kleeman, D.S. Gross, L.S. Hughes, J.O. Allen, B.D. Morrical, D.P. Fergenson, T. Dienes, M.E. Galli, R.J. Johnson, G.R. Cass, and K.A. Prather, Direct observation of heterogeneous chemistry in the atmosphere, *Science*, 279 (5354), 1184-1187, 1998.

Gaston, C.J., H. Furutani, S.A. Guazzotti, K.R. Coffee, T.S. Bates, P.K. Quinn, L.I. Aluwihare, B.G. Mitchell, and K.A. Prather, Unique ocean-derived particles serve as a proxy for changes in ocean chemistry, *Journal of Geophysical Research-Atmospheres*, 116, 2011.

Hogan, T.F., and L.R. Brody, Sensitivity Studies of the Navy Global Forecast Model Parameterizations and Evaluation of Improvements to Nogaps, *Monthly Weather Review*, 121 (8), 2373-2395, 1993.

Hogan, T.F., and T.E. Rosmond, The Description of the Navy Operational Global Atmospheric Prediction Systems Spectral Forecast Model, *Monthly Weather Review*, 119 (8), 1786-1815, 1991.

Minnis, P., S. Sun-Mack, D.F. Young, P.W. Heck, D.P. Garber, Y. Chen, D.A. Spangenberg, R.F. Arduini, Q.Z. Trepte, W.L.S. Jr., J.K. Ayers, S.C. Gibson, W.F. Miller, V. Chakrapani, Y. Takano, K.-N. Liou, Y. Xie, and P. Yang, CERES Edition-2 cloud property retrievals using TRMM VIRS and Terra and Aqua MODIS data, Part I: Algorithms, *Ieee Transactions on Geoscience and Remote Sensing*, 49 (11), doi: 10.1109/TGRS.2011.2144601, 2011.

Ogren, J.A., J. Heintzenberg, and R.J. Charlson, Insitu Sampling of Clouds with a Droplet to Aerosol Converter, *Geophysical Research Letters*, 12 (3), 121-124, 1985.

- Pratt, K.A., P.J. DeMott, J.R. French, Z. Wang, D.L. Westphal, A.J. Heymsfield, C.H. Twohy, A.J. Prenni, and K.A. Prather, In situ detection of biological particles in cloud ice-crystals, *Nature Geoscience*, 2 (6), 397-400, 2009a.
- Pratt, K.A., J.E. Mayer, J.C. Holecek, R.C. Moffet, R.O. Sanchez, T.P. Rebotier, H. Furutani, M. Gonin, K. Fuhrer, Y.X. Su, S. Guazzotti, and K.A. Prather, Development and Characterization of an Aircraft Aerosol Time-of-Flight Mass Spectrometer, *Analytical Chemistry*, 81 (5), 1792-1800, 2009b.
- Rogers, D.C., P.J. DeMott, S.M. Kreidenweis, and Y.L. Chen, A continuous-flow diffusion chamber for airborne measurements of ice nuclei, *Journal of Atmospheric and Oceanic Technology*, 18 (5), 725-741, 2001.
- Russell, S.C., Microorganism characterization by single particle mass spectrometry, *Mass Spectrometry Reviews*, 28 (2), 376-387, 2009.
- Silva, P.J., R.A. Carlin, and K.A. Prather, Single particle analysis of suspended soil dust from Southern California, *Atmospheric Environment*, 34 (11), 1811-1820, 2000.
- White, A.B., J.R. Jordan, B.E. Martner, F.M. Ralph, and B.W. Bartram, Extending the dynamic range of an S-band radar for cloud and precipitation studies, *Journal of Atmospheric and Oceanic Technology*, 17 (9), 1226-1234, 2000.
- White, A.B., P.J. Neiman, F.M. Ralph, D.E. Kingsmill, and P.O.G. Persson, Coastal orographic rainfall processes observed by radar during the California land-falling jets experiment, *Journal of Hydrometeorology*, 4 (2), 264-282, 2003.
- Winker, D.M., J. Pelon, J.A. Coakley, S.A. Ackerman, R.J. Charlson, P.R. Colarco, P. Flamant, Q. Fu, R.M. Hoff, C. Kittaka, T.L. Kubar, H. Le Treut, M.P. McCormick, G. Megie, L. Poole, K. Powell, C. Trepte, M.A. Vaughan, and B.A. Wielicki, THE CALIPSO MISSION A Global 3D View of Aerosols and Clouds, *Bulletin of the American Meteorological Society*, 91 (9), 1211-1229, 2010.